Reaction Engineering in Biocatalytic Reactive Distillation

Vom Promotionsausschuss der
Technischen Universität Hamburg
zur Erlangung des akademischen Grades
Doktor-Ingenieur (Dr.-Ing.)

genehmigte Dissertation

von
Steffen Kühn

aus
Marburg (Lahn)

2018

1st Examiner: Prof. Dr. rer. nat. Andreas Liese
2nd Examiner: Prof. Dr.-Ing. Irina Smirnova

Day of oral examination: 12.10.2018

For Mum, Dad and Elif

ACKNOWLEDGEMENT

The presented and discussed results in this work were generated within the time period of May 2014 and September 2017, in which I worked as a scientific coworker at the Institute of Technical Biocatalysis at the Hamburg University of Technology. At this point, I want to take the chance to express my gratitude to all the people, who supported me during that time and finally helped me to realize and set up this work. It has to be mentioned that without all of you, it would not have been possible to finalize this work.

First of all, I would like to express my sincerest gratitude to my supervisor, *Prof. A. Liese* for offering me the position in his institute. I really appreciated not only your excellent scientific support and inspiration in our fruitful discussions at your office, but also your social dedication to form the 'ITB-family' and offering me a great working atmosphere for the time period in Hamburg. I really want to thank you for a fantastic time!

I would offer my special thanks to *Prof. I. Smirnova* for accepting to take over the position of the 2nd examiner and even more for supporting my scientific work with her excellent knowledge in the field of my research topic. Especially, I want to thank you for your valuable feedback and help to successfully exceed in the process of publishing.

I have additionally greatly benefited from the support and inspiring ideas by *Prof. J.-E. Bäckvall* to substantially drive forward with the topic of dynamic kinetic resolution and get an insight into his extraordinary expertise in organic chemistry. Thanks a lot to *Prof. S. Heinrich* for taking over the lead at the day of examination.

I particularly owe my deepest gratitude to *Dr. J. Kleber* for his excellent support as a group leader, as a friend and his time for intense topic related as well as non-related discussions. I want to thank you for scientific input during proof-reading my thesis, which was pretty important for reflecting writing and to reach the final version. I really appreciate your support!

For your extraordinary encouragement, discussions and help, I want to thank all the *colleagues*, *bachelor & master students* as well as *BTA-applicants & student assistants*, who supported this work. Without you, this work would not have been possible! I would show my greatest appreciation to my friends *G. Sluyter*, *M.-A. Christlieb* and *Dr. R. Heils* for their intense discussions and scientific as well as non-scientific input to the topic. Additionally, it was an honor to participate at conferences together! Besides, I would like to offer my special thanks to *L. Andersen* and *A. Bajat* for their help during their thesis at the ITB. I want to thank *Dr. B. Yang* for his incredible support during his stay at the ITB to allow setting up and performing experiments regarding the topic of dynamic kinetic resolution.

Beside the great support in the scientific environment of this thesis, I want to express my deepest appreciation to my family although words are never enough to show you my gratitude. *Mum and Dad*,

I want to thank you for everything you did for supporting my time in Hamburg, for your encouragement to manage this thesis and your indispensable help in every situation of my life! *Elif*, I would like to thank you for your unconditional love and for being the best wife during all situations of my life. You helped me in uncountable moments to finish this thesis – seni seviyorum!

28th of October, 2018
Steffen Kühn

ABSTRACT

Reactive distillation is a well-established unit operation in chemical industry incorporating reaction and separation in one device for the synthesis of bulk chemicals. Such an integrated process strategy provides economic advantages compared to serially connected unit operations. In a relatively new approach, substitution of chemical catalysts by enantioselective biocatalysts emerges, which allows a broadened scope of reactions. This idea is especially triggered by the growing interest in more valuable chiral molecules for fine chemical or pharmaceutical synthesis. At first glance, the thermal deactivation of a biocatalyst will cause reduced catalyst lifetimes and requires frequently shutdown procedures for replacing the biocatalyst. However, careful selection of relatively thermostable biocatalysts and their fixation on supporting materials enables reasonable process performance.

In this thesis, practicability of *Candida antarctica* lipase B applied as the preparation Novozym435® is evaluated for kinetic resolution reactions in reactive distillation. The defined three step approach, including the theoretical preselection of reactions and their experimental characterization in batch reactors as well as the implementation in a solvent-free reactive distillation column, aims at the isolation of the desired chiral target compound with high purity. In the theoretical preselection step, two different chiral starting materials (*(R/S)*-2-pentanol, *(R/S)*-3-hydroxy ethyl butyrate) were selected for experimental comparison. Main criteria for the feasibility study were the predetermined biocatalyst temperature range (T_{RD} = 30 – 80 °C) and the theoretical operating window of the individual compounds, defined by their boiling points at reduced column pressures. In the second experimental characterization step, both chiral starting materials were investigated in batch reactions for their feasibility in reactive distillation. The investigated parameters comprise the initial catalytic activity, the enantioselectivity, the determination of present equilibrium limitations and the concentration profiles of the starting materials in a batch reactive distillation setup. During the characterization phase, the results for the kinetic resolution of the chiral alcohol *(R/S)*-2-pentanol turned out to be more promising. Therefore in the third step, reactive distillation column experiments were carried out with this starting material aiming at excellent optical purity and high molar fractions of the target compound *(S)*-2-pentanol. In focus of these reactive distillation experiments were the influence of changing the fractional distillation strategy, the spatial distribution of the biocatalyst and the initial molar fractions of the starting material. Finally, successful operation of an integrated batch biocatalytic reactive distillation column is approved by *in situ* isolation of the chiral target compound *(S)*-2-pentanol with high purity ($x_{(S)\text{-2-PeOH}}$ = 0.95 mol·mol^{-1}) and excellent enantiomeric excess ($ee_{(S)\text{-2-PeOH}}$ > 99 %). Moreover, an alternative reaction approach of chemo-enzymatic dynamic kinetic resolution is successfully evaluated in a proof of concept study including a second chemocatalyst.

Based on these results, this thesis underlines the possibility to allow the production of fine chemicals or pharmaceuticals in reactive distillation processes in future times.

KURZZUSAMMENFASSUNG

Der Einsatz von Reaktivrektifikations-Kolonnen repräsentiert einen weltweit etablierten Verfahrensschritt in der chemischen Industrie zur Synthese von *bulk*-Produkten, welcher die Prozessschritte der chemischen Reaktion sowie die anschließende Auftrennung in einem Apparat vereint. Durch diese integrierte Prozessvariante resultieren ökonomische Vorteile gegenüber herkömmlichen sequentiellen Verfahrenskonzepten. Ein neuer Ansatz beschäftigt sich nun mit der Idee ein erweitertes Reaktionsspektrum für die Reaktivrektifikation verfügbar zu machen, indem der chemische Katalysator durch hochselektive Biokatalysatoren ersetzt wird. Der Hauptgrund für die Substitution des chemischen Katalysators liegt insbesondere in dem steigenden Interesse an chiralen Molekülen zur Synthese von Feinchemikalien oder Intermediaten von pharmazeutischen Produkten. Neben dem Vorteil der hohen Selektivität stellt die größte Herausforderung beim Einsatz von Biokatalysatoren in der Reaktivrektifikation dessen Sensitivität gegenüber moderaten Prozesstemperaturen dar. Dadurch wird eine regelmäßige Erneuerung des Katalysators erforderlich, was ein häufiges An- und Abfahren der Kolonne bedingen würde. Die geeignete Auswahl von Biokatalysatoren mit erhöhter thermischer Belastbarkeit und deren Fixierung in Immobilisierungsverfahren ermöglicht wiederum den Einsatz in der Reaktivrektifikation.

Auf dieser Basis wurde im Rahmen der vorliegenden Arbeit der Einsatz von Lipase B aus *Candida antarctica* in der Reaktivrektifikation in lösungsmittelfreien, kinetischen Racematspaltungen untersucht und bewertet. In einem entwickelten dreistufigen Konzept war das Hauptziel die gewünschte chirale Zielkomponente mit hoher Reinheit am Kopf der Kolonne zu isolieren. Im ersten Schritt erfolgte mittels eines aufgebauten *Preselection-Tools* die Auswahl von zwei chiralen Substraten (*(R/S)*-2-Pentanol, *(R/S)*-Ethyl-3-Hydroxybutyrat). Die Hauptkriterien für die theoretische Machbarkeitsstudie der gewählten Substrate waren der vom Biokatalysator definierte Temperaturbereich für die Reaktivrektifikation (T_{RD} = 30 – 80 °C) und das daraus resultierende Prozessfenster, welches die Siedepunkte beim gewählten reduzierten Kolonnendruck umfasst. Im zweiten Schritt erfolgte die experimentelle Charakterisierung der beiden chiralen Substrate, um die Möglichkeit des Einsatzes in der Reaktivrektifikation zu untersuchen. Die gewählten Parameter setzten sich zusammen aus der Anfangsreaktionsgeschwindigkeit des Biokatalysators und vorherrschenden Gleichgewichtslimitierungen der Reaktionen in Batch-Reaktoren sowie der Untersuchung der Konzentrationsprofile in der aufgebauten Batch-Reaktivrektifikation. Während der Charakterisierung zeigte der gewählte chirale Alkohol *(R/S)*-2-Pentanol deutlich vielversprechender Ergebnisse gegenüber dem gewählten chiralen Ester *(R/S)*-Ethyl-3-Hydroxybutyrat. Daher wurde im letzten Schritt in der Reaktivrektifikation ausschließlich *(R/S)*-2-Pentanol in Experimenten eingesetzt, die hinsichtlich der Produktreinheit und des Enantiomerenüberschusses der Zielkomponente *(S)*-2-Pentanol optimiert wurden. Im Fokus standen dabei der Einfluss der Abzugsstrategie am Kopf der Rektifikationskolonne,

die gewählte Verteilung des Biokatalysators und die Anfangszusammensetzung der Reaktanden. So wurden durch gezielte *in situ*-Abtrennung der chiralen Zielkomponente *(S)*-2-Pentanol Produktreinheiten von ($x_{(S)\text{-2-PeOH}} = 0.95\ mol \cdot mol^{-1}$) bei gleichzeitig exzellenten Enantiomerenüberschüssen ($ee_{(S)\text{-2-PeOH}} > 99\ \%$) erreicht. Darüber hinaus wurde in einer alternativen Prozessvariante eine dynamische kinetische Racematspaltung als weiteres Verfahrenskonzept untersucht, welches innerhalb der Machbarkeitsstudie und in *Proof of Concept*-Experimenten die Anwendung eines zusätzlichen Chemokatalysators ermöglichte.

Die in dieser Arbeit herausgearbeiteten Haupteinflussfaktoren auf die biokatalytische Reaktivrektifikation unterstreichen die Möglichkeit zukünftig ein klassisch chemisches Verfahrenskonzept auf die Synthese von höherwertigen chiralen Produkten zu erweitern.

TABLE OF CONTENT

1. INTRODUCTION & STATE OF THE ART

In the sector of chemical industry, permanently improved production processes are required to fulfill the rising demand of economically feasible process performance as well as acceptance in society by ecologically synthesized products. With respect to the *European Commission*, the chemical industry contributed by a percentage of 18 – 19 % to the total energy consumption in Europe between 2009 and 2013 [1]. The concept of integrated process strategies plays a major role to improve production processes and reduce the total energy consumption by merging sequentially connected unit operations to one unit [2]. One of the most prominent examples for this process intensification in industry is reactive distillation [3]. Combining a chemical reaction with thermal separation already affects a proportion of 40 % of the total energy consumption within the chemical industry in Europe [4]. As a result, energy-efficient and sustainable reactive distillation processes have been designed to reduce the caused energy consumption by up to 80 % savings in capital and energy costs compared to sequential reaction performance [3]. Beside cost savings due to a reduced number of unit operations, integrated reactive distillation enables beneficial reaction performance from the engineering point of view. Increased conversion and increased product selectivity as well as less solvent consumption are feasible, because of shifted reaction equilibria in consequence of constantly removed compounds from catalytic sections [5].

Nowadays, more than 150 industrial applications of reactive distillation are realized for the synthesis of bulk chemicals [3]. While the first patents of reactive distillation for homogeneously catalyzed esterification were generated in the 1920s [6] [7], heterogeneous catalyst application in an integrated approach dates back to 1978 for the synthesis of methyl *tert*-butyl ether [8]. The breakthrough of integrated reactive distillation is represented by the *Eastman-Kodak* process in 1984, describing the acid-catalyzed synthesis of highly pure methyl acetate from methanol and acetic acid in a single unit operation [9]. Instead of eight distillation columns to overcome two existing azeotropes between methyl acetate and methanol as well as methyl acetate and water, the performance is achieved in one column by combining the reaction and the thermal separation [10]. This refers to five times less energy consumption, and five times less capital investment costs compared to the sequential process setup [11]. Based on the unique advantages within the intensified methyl acetate synthesis, rising interest on reactive distillation is observed over the following decades illustrated by the continuously increased number of patents and articles published per year (**Figure 1.1**). The presented literature survey refers to the number of results in *google scholar* (Google Inc., California, USA) with respect to the given keywords in the caption of **Figure 1.1**, similar to previous investigations of *Doherty and Malone (2001)* as well as *Gorak and Olujic (2014)* [12] [4]. A broad diversity of approaches is demonstrated in the published articles ranging from continuous [13] to batch [14] and divided wall column operations [15] as well as including modelling strategies for optimization [10] of reactive distillation columns and the

determination of feasible process windows [16]. According to *Rameshwar et al. (2004)*, the major focus of applied reactive distillation is on the synthesis of bulk chemicals via esterifications, etherifications, hydrogenations and hydrodesulfurizations offering flexible process conditions towards temperature (T = 27 – 296 °C) and pressure (p = 0.1 – 30 bar) for chemical catalysts [13]. Up-to-date, the synthesis of more valuable products with chiral centers is still a challenge in reactive distillation for the applied chemical catalysts and their lack in stereoselective synthesis. One simulative study by *Okasinski and Doherty (2003)* already showed the theoretical potential of chiral synthesis in reactive distillation for enantiomerically-pure propylene oxide and propylene glycol [17].

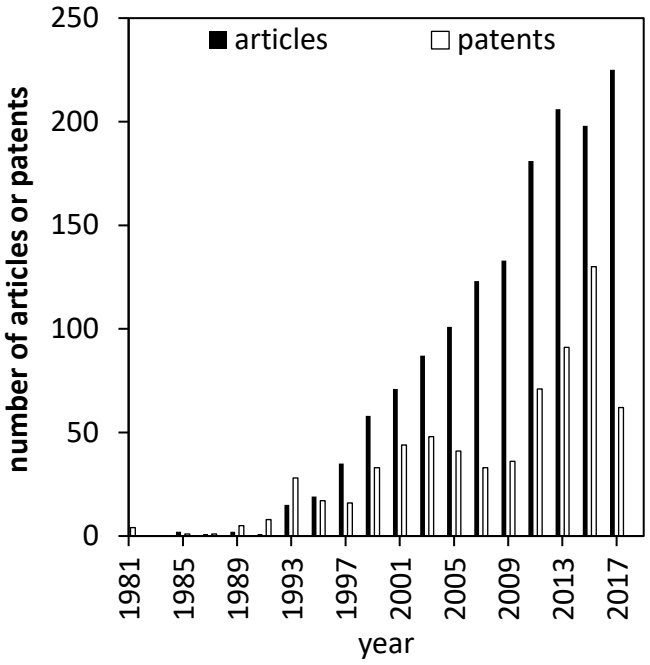

Figure 1.1: Published articles and patents on reactive distillation. The updated literature survey is performed in google scholar with the following keywords similar to published data from *Doherty and Malone (2001)* as well as *Gorak and Olujic (2014)* [12] [4]: reactive distillation, catalytic distillation, catalytic reactive distillation, reaction column, reacting column, reactive packing, catalytic packing.

Beside the classical way of applying chemical catalysts in integrated reactive distillation, another class of catalysts get more and more attractive in the past decades for industrial purposes. Those natural catalysts called biocatalysts or enzymes have the ability of allowing stereoselective or enantioselective synthesis of high-value chiral products for the pharmaceutical industry instead of bulk chemicals [18] [19] [20] [21]. Specific binding of e.g. one enantiomer from a racemic mixture is guaranteed by the unique arrangement of amino acid residues in the active side of the enzyme to preferentially accept one enantiomer [22]. This feature of biocatalysts becomes important for the rising demand of chiral intermediates in the pharmaceutical industry, because nowadays more than 40 % of pharmaceutical compounds include at least one chiral center [23]. A well-known example for highly enantioselective

synthesis by biocatalysts in pharmaceutical industry is a process developed by *Codexis Inc.* (California, USA) involving a NADPH-dependent ketoreductase and a halohydrin dehalogenase to produce chiral intermediates in the atorvastatin synthesis [24]. Beneficial substitution of chemical reaction steps by a biocatalytic route can be represented by a cooperation between *Merck & Co, Inc.* (New Jersey, USA), *Solvias Inc.* (New Jersey, USA) and *Codexis Inc.* in the 3rd generation optimized process for the chiral compound sitagliptin, which is used for the treatment of type-II-diabetes in drugs e.g. Januvia™ [25] [26]. The application of a pyridoxal phosphate-dependent modified transaminase improves the overall yield for sitagliptin from 45 to 75 % and simultaneously reduces the produced waste from 250 $kg \cdot kg^{-1}$ to 41 $kg \cdot kg^{-1}$ [27] [28] [29]. On the other hand, most of the biocatalysts and cofactors exhibit thermal sensitivity even at moderate temperatures [30] as well as high production costs [31]. Thus, thermal stability should be as high as possible to increase the lifetime of expensive biocatalysts especially for the application in reactive distillation approaches. It is stated in literature, that several biocatalysts can be operated at elevated temperatures ranging from lipase catalyzed esterification at T = 60°C to the production of high fructose corn syrup by α-amylases at T = 105-115°C [32] [33] [34]. A useful strategy for further increased thermal stability is the immobilization of the biocatalysts by protecting the protein structure and still allowing activity at in best case reduced mass transfer limitations [35] [36]. Investigations on Lipase B from *Candida antarctica* (CalB) immobilized on polyacrylic resin (Novozym435® manufactured by Novozymes, Bagsvaerd, Denmark) allowed the application without significant loss in residual activity at 80°C after 30 days of operation [37]. Moreover, lipases reveal increased tolerance towards organic solvents [38]. Therefore, changing to biocatalyst application (e.g. immobilized lipases) in integrated processes like reactive distillation can offer the possibility to open accessibility to the production of fine chemicals instead of bulk chemicals by the classical chemically catalyzed reactive distillation.

Applying biocatalysts in reactive distillation approaches is relatively new and recently investigated only in a few research groups. All of them were focusing on kinetic resolution reactions catalyzed by lipases. Initial studies in 2003 are performed by *Paiva et al. (2003)* with lipase from *Mucor miehei*, which is immobilized on anion-exchange resin to catalyze the synthesis of butyl butyrate (BuBu) formed by the starting materials ethyl butyrate (EtBu) and *n*-butanol. Successful biocatalyst implementation is achieved in a batch separation column (h = 230 mm, d = 30 mm) at reduced pressure (p = 150 mbar), while the immobilized lipase is located in 13 inverted pear bulbs over the height of the separation column. During operation, constant removal of the low boiling ethanol (EtOH) is used to improve the reaction conditions [39]. Alternative integration of the biocatalyst in a batch reactive distillation setup (h = 960 mm, d = 45 mm) for the same reaction system is published by *Heils et al. (2012)*. The reaction is catalyzed by CalB in the column height, which is entrapped in a hydrophobic silica coating material covering structured wire gauze packings. Under process conditions (p = 110 mbar, T = 60 °C), removal

of EtOH leads to increased conversion beyond the reaction equilibrium and simultaneously shows the application of the immobilization strategy within silica coating [40]. The same author performed a simulation study based on *Aspen Custom Modeler* (Aspen Technology Inc., Massachusetts, USA), in which the potential of continuous biocatalytic reactive distillation operation is shown as long as a low molar fraction of the model substrate *n*-butanol is present in the reactive section. At simulated process conditions of p = 200 mbar and T = 70 °C, theoretically 90 % conversion can be achieved for *n*-butanol [41]. An extended model validation for butyl butyrate synthesis starting from *n*-butanol by additional experimental investigations in continuous reactive distillation is performed by *Wierschem et al. (2017)* [42]. Beside the examples for batch and continuous operation of biocatalytic reactive distillation, *Egger and Fieg (2017)* introduced the application of immobilized CalB (Novozym435) in a reactive divided wall column at an integrated pilot scale apparatus (h ≈ 5000 mm, d = 65 mm) [43]. For the transesterification of 1-hexanol with *n*-butyl acetate to 1-butanol and *n*-hexyl acetate, a validated model with good agreement to experimental data is presented and the process stability of Novozym435 for at least 100 h accumulated within 8 experiments is proven at T = 60 °C. Independent from the different operation modes and applied reactions, feasibility of immobilized CalB is approved with respect to thermal stability in the given examples. However, the formation of chiral target compounds for the synthesis of pharmaceutical intermediates is not addressed within the selected model reactions. Chiral synthesis in an integrated reactive distillation setup is firstly focused by the work of *Au-Yeung et al. (2013)* in a continuously operated horizontal distillation device with multiple external side reactors connected to subsequent conventional distillation. The external side reactors contain immobilized CalB to increase the liquid phase residence time for an efficient substrate conversion in a multicomponent kinetic resolution reaction [44]. Recently, *Heils et al. (2015)* published a follow-up study applying their developed coating material for the kinetic resolution of *(R/S)*-2-pentanol (*(R/S)*-2-PeOH) with ethyl butyrate (EtBu) in a batch reactive distillation column. Entrapped CalB in the coating material provides high enantioselectivity towards *(R)*-2-PeOH, while residual molecules of the chiral target compound *(S)*-2-PeOH accumulate with high enantiomeric excess at the bottom of the column ($ee_{(S)\text{-2-PeOH}} > 99\%$) and 69% conversion (T = 30-60°C, p = 60-115 mbar). Product inhibition of low boiling EtOH and a shift in the equilibrium limited reaction to the product side is realized by *in situ* removal of the reactants from the reactive section [45]. More recently, an *in situ* coating procedure is developed for the batch reactive distillation approach with CalB coating material in order to replace biocatalytic activity after deactivation [46]. This technology facilitates the replacement of catalyst as long as they are applied entrapped in a silica matrix, but a shutdown of the column setup is still necessary for the new coating layers. Continuous operation of a biocatalytic reactive distillation column is focused by comprehensive studies of *Wierschem et al. (2016, 2017)* involving the CalB catalyzed kinetic resolution of *(R/S)*-1-phenyl ethanol and isopropenyl acetate

to enantiopure *(R)*-1-phenylethyl acetate and low boiling acetone. The validated model allows to predict performed experiments and offers the opportunity of chiral synthesis via biocatalytic reactive distillation by stripping acetone and leftover isopropenyl acetate [47] [48].

Within the given overview on collected articles from literature between 2003 and 2017, feasibility of chiral synthesis in biocatalytic reactive distillation is illustrated by designed validated simulation tools as well as experimental effort in various batch or continuously operated apparatuses. This offers access to a detailed description of biocatalytic reactive distillation and the need for carefully selected biocatalysts with increased thermal stability. The contribution of this work to the growing interest on integrated processes with the application of biocatalysts is the focus on *in situ* isolation of chiral target compounds within an experimental study on biocatalytic batch reactive distillation. By having a look on the well-established classical approach for reactive distillation with chemical catalysts, *in situ* product isolation with high purity is intended to take place at the top of the column setup to prevent impurities and further downstream-processing steps. Based on current literature data, either non-chiral products are aimed to show the successful implementation of biocatalysts or the chiral target compounds are accumulated in the bottom of the setup with additional high boiling reactants. Therefore, reaction engineering and deeper understanding of decisive parameters on the *in situ* isolation is addressed in this study in order to allow an evaluation of the applicability concerning biocatalytic reactive distillation for industrial purposes in future times.

2. THEORETICAL BACKGROUND

Within the following background information, an overview of relevant theories and characteristics on classical reactive distillation approaches with chemical catalysts as well as biocatalytic reactive distillation is presented.

2.1. Reactive Distillation

Performing a chemical reaction and isolating the desired target molecule for its final use in separation steps is the main task for all competing combinations of basic unit operations in process engineering. High flexibility during the phase of selecting proper unit operations in a sequential process comes along with drastically rising investment costs [3] [49]. Beside the approach of connecting several unit operations with each other sequentially, so-called integrated process strategies are available. Reactive distillation is an integrated process approach, in which the specific characteristic is the simultaneous occurrence of a chemical reaction and thermal separation of the involved reactants in one apparatus [50]. The chemical reaction in reactive distillation is generally driven by applying a catalyst in the reactive section, while thermal separation is achieved by different boiling behavior of the pure reactants as well as reactant mixtures in the stripping and rectifying section. Catalyst implementation in integrated reactive distillation processes can either be realized homogeneously or heterogeneously. Homogeneous applications are feasible for autocatalytic reactions, acid or base catalysis [51]. In these cases, feeding the catalyst with the reactants allows increased flexibility in operation concerning varied reaction rates by changing the concentration of the catalyst [52]. However, a continuous feeding of the catalyst should be economically feasible. In heterogeneous application, fixation of solid catalyst during operation results in a well-defined catalytic section. No catalyst recovery is necessary, but long catalyst lifetimes are required to prevent frequent disassembling of the column combined with time-consuming shutdown procedures [10]. While for homogeneous catalyst applications standard column internals allow an increased surface area for separation, specific column internals are developed for the fixation in heterogeneous catalyst applications such as structured packings or trays [4] [53] [54] [55]. For an equilibrium limited chemical reaction including the starting materials *A* and *B*, the sequential and integrated process strategies are exemplary illustrated in **Figure 2.1**. The different positions of the catalyst in both approaches is highlighted by grey boxes. In the majority of conducted processes, the desired target compound represented by *D* is contaminated with at least one side product (e.g. *C*) (**Eq. 1**).

$$A + B \rightleftharpoons C + D \qquad \textbf{Eq. 1}$$

An effective separation technique for getting the products *C* and *D* is the application of multistep distillation, which is used in approximately 90 % of industrial thermal separation tasks [56]. As a rule of thumb, the desired target compound should be isolated at the top of the column to increase the purity.

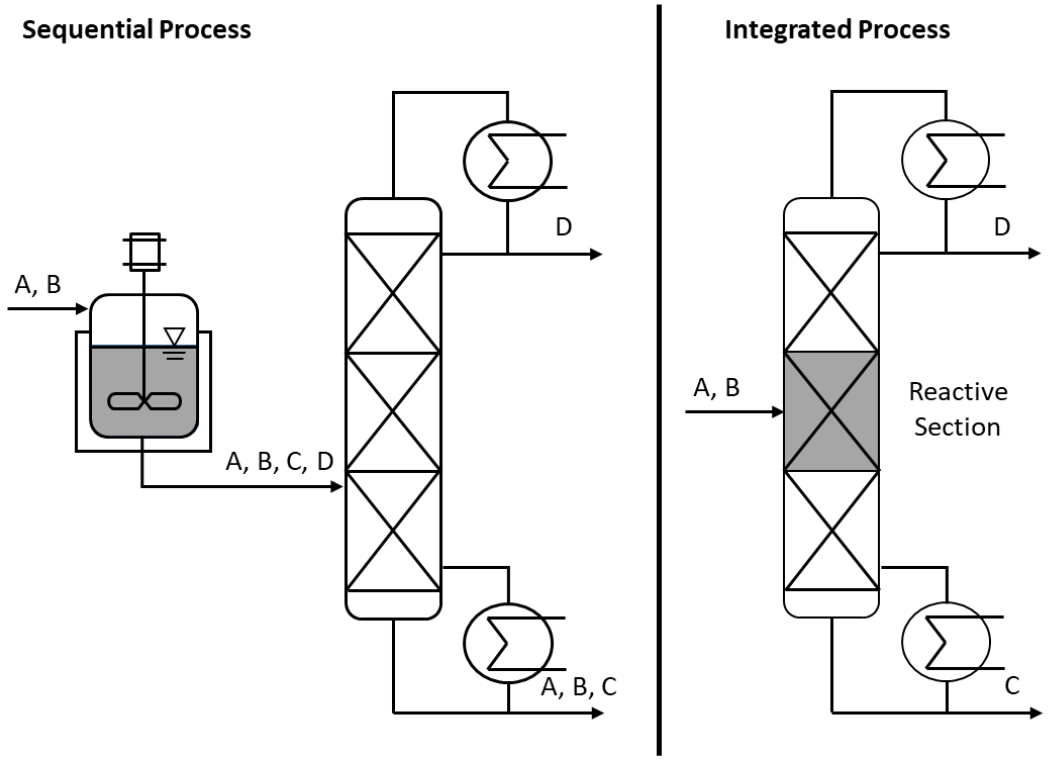

Figure 2.1: Sequential and integrated process for an equilibrium limited reaction. Grey areas indicate the position of the catalyst.

Beside the depicted continuous reactive distillation approach with a single column in **Figure 2.1**, batch equipment or multiple-stage columns in batch or continuous mode can be applied. In some cases, even an externally placed reactive section connected to the column can be beneficial. According to *Schoenmarkers und Bessling (2003)*, the selection of appropriate equipment depends on the degree of difficulty in separation as well as the maximum feasible catalytic reaction rate [52]. At low reaction rates, multiple-stage approaches, external side reactors or batch equipment are preferred to provide increased residence times in the setup. In contrast, high reaction rates allow operation within single column or reactor approaches. For easy separation tasks with increased differences between the boiling points of the products and reactants, reactors or small columns are feasible. On the other hand, longer columns should be considered with rising complexity of the separation boundaries.

2.1.1. Separation Principle

Successful thermal separation in reactive distillation is predominantly dependent on thermodynamic data referring to the ***v**apor-**l**iquid **e**quilibria* (VLE) of component mixtures. Phase change data from the liquid to the vapor aggregate state in a binary component mixture are expressed by temperature - composition diagrams (*T-xy*). Exemplified courses for ideal (**A**) and azeotropic (**B**) behavior (here: temperature minimum azeotrope) of VLE data in a *T-xy* diagram are presented in **Figure 2.2**. Lens-shaped courses are formed by the boiling point curve and the dew point curve with changed mole fractions (*x, y*) of the applied components. The boiling points (T_{boil}) of the pure components (*Pure 1, Pure 2* in **Figure 2.2**) can be determined with the vapor pressure (*p*) and empirical, component-related parameters *A*, *B* and *C* by the Antoine equation (**Eq. 2**) [57].

$$T_{boil} = \frac{B}{A - \log_{10} p} - \mathrm{C} \qquad \textbf{Eq. 2}$$

Within the Antoine equation, dependency of the boiling temperature on the vapor pressure becomes visible. Hence, the *T-xy* diagram is only valid for a specific pressure. Changes in pressure cause a shift of the lenses with respect to the corresponding temperatures as well as result in different shapes of the lenses. As long as the temperature is higher than the dew point curve, the whole mixture is in the vapor phase (*V*). At the same time, temperatures below the boiling point curve represent the area of having both components in the liquid phase (*L*). Consequently, the area enclosed by the lenses involves two phases composed of a vapor and a liquid phase fraction (*V+L*). The corresponding composition of both phases at a specific temperature is accessible by drawing a horizontal line (tie line) and identifying the mole fractions of both components at the intersections of the dew point as well as the boiling point curve (dashed line in **Figure 2.2**, **A**).

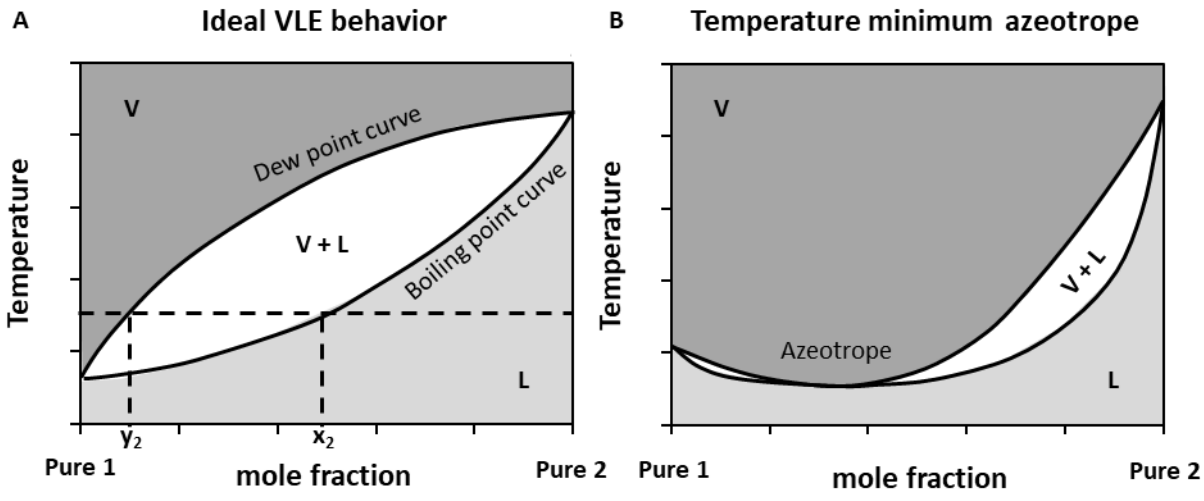

Figure 2.2: Schematic temperature-composition diagrams for vapor-liquid equilibria (VLE) with **A**: ideal behavior and **B**: a temperature minimum azeotrope as one example for non-ideal behavior

In case of ideal as well as non-ideal VLE behavior, the design of the column height for separation of a binary mixture can be achieved graphically by drawing the required number of separating stages according to the *McCabe-Thiele* method [58]. Apart from that, calculating the number of stages is applicable within shortcut methods derived by *Fenske* (minimum number of stages at total reflux) [59], *Underwood* (minimum reflux with infinite number of stages) [60] or *Gilliland* (number of stages with finite reflux) [61]. Generally, the number of stages mainly depends on the shape of the lens, which is influenced by the 'separation factor' or relative volatility *α* [-] of the binary mixture. For a mixture of the components *A* and B, the relative volatility is defined as the fraction of both components in the vapor (*y* [mol·mol^{-1}]) and liquid (*x* [mol·mol^{-1}]) phase (**Eq. 3**).

$$\alpha_{AB} = \frac{y_A / x_A}{y_B / x_B} \qquad \textbf{Eq. 3}$$

The separation task becomes impossible at α ≈ 1, while it becomes more and more feasible at values significantly different to 1 (α > 1 or α < 1). With respect to the dimension of the relative volatility, the effort for separation can be evaluated. Small lenses described by VLE data account for an increased number of stages. Enlarged areas between the dew point curve and the boiling point curve allow easier separation with less number of stages. In a multicomponent mixture, it is necessary to select a light and heavy boiling component in order to determine the relative volatility. Beside ideal behavior, non-ideal behavior occurs for several component mixtures. One specific case of non-ideal behavior is the formation of an azeotrope, e.g. temperature minimum azeotrope (**Figure 2.2**, **B**). The feature of an azeotrope is the intersection of the boiling point curve and the dew point curve (x = y) at molar fractions unequal to 0 and to 1. In dependency of forming a light or high boiling azeotrope, the boiling point of the azeotropic mixture is lower or higher than the boiling points of the pure components forming the binary mixture [62]. Azeotropes are caused by positive or negative deviations of the component related partial pressures in the binary mixture compared to their partial pressures in an ideal mixture according to *Raoult's law* [63]. According to *Ewell et al. (1944)*, temperature minimum azeotropes are detected in the majority of azeotrope occurrences [64]. However, any separation of an azeotropic mixture in multistep distillation is only possible with modifications like changed operating pressures or the application of additives to influence the lens shape. Another strategy is the integration of a chemical reaction in reactive distillation to react the azeotrope away and achieve further separation of the components.

In real separation tasks, further complex mixtures of more than two components may be present. For ternary mixtures consisting of three compounds, deviations of ideal behavior and the formation of azeotropes can be investigated by depicting VLE-data in distillation lines within triangular diagrams [62].

2.1.2. Window of Operation

Based on thermodynamic property data, reactive distillation performance is constrained by reasonable conditions regarding the chemical reaction and the separation task. In particular, both have to be operated under the same conditions as they occur at the same time in the same place. Furthermore, the range of operation can significantly vary with respect to the applied catalyst and the chosen reactive distillation equipment. A useful technique to evaluate the feasible operating range is the design of a process window depending on the decisive parameters temperature and pressure (**Figure 2.3**) [42] [51] [65]). Upper and lower limits of successful RD operation are given by the boiling points of the lowest and highest boiling component ('constraints by reactants', **Figure 2.3**). Operating the column at pressures higher than the pure boiling point of the lowest boiling component, all components will stay in the liquid phase. Reversely, when operating RD at pressures below the boiling point of the highest boiling component, all components will appear in the vapor phase. Besides, temperature limits can be adjusted by the column pressure to ensure reasonable conversion and less side product formation within the catalyzed reaction ('catalytic constraints', **Figure 2.3**). Only for reactions, which can be performed in the resulting operating window are interesting for reactive distillation.

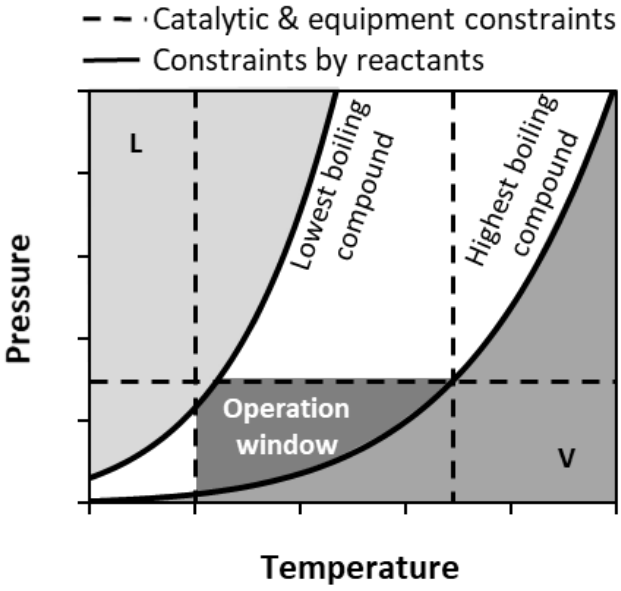

Figure 2.3: Window of operation for reactive distillation processes

2.1.3. Advantages and Challenges

Based on the combined reaction and thermal separation, the following advantages can be pointed out for the reactive distillation approach [4] [51]:

- *Capital and energy savings:* decreasing the number of needed unit operations by an integrated reaction and separation approach reduces the overall plant costs. Generated heat in exothermic reactions can straightforwardly be applied for vaporization to reduce the reboiler duty and circumvent hotspots by evaporating the liquid phase, which leads to less energy consumption [66].
- *Increase in conversion and selectivity:* separation of reactants from the position of the catalyst *in situ* leads to shifted reaction equilibria with considerably rising conversions in limited reaction systems [67]. Simultaneously, consecutive reactions as well as side reactions of the desired target molecule are prevented by the constant removal of reactants [68].
- *Overcoming formed azeotropes:* liquid phase reaction of azeotropic mixtures at the catalyst allows 'reacting away' of the azeotrope to finally increase the separation performance [69].
- *Facilitated separation of close boiling reactants:* provoking a reaction of an entrainer molecule with one of the reactants leads to significantly differed boiling points between the reactants to improve the separation conditions [70].

Among beneficial aspects for the approach of reactive distillation, rising complexity by performing a chemical reaction within a multistep distillation setup brings along challenges and limitations for the successful application. An overview on those limiting issues are presented as follows [4] [51]:

- *Necessity for catalytic long-term stability*: applied heterogeneous catalysts should provide long lifetimes for economical feasible column performance. Thereby, set-up times are reduced and less influence on column operation can be achieved [71].
- *Constraints by volatility:* for successful operation of reactive distillation, significantly different boiling temperatures between the starting materials and the products should be present to increase the starting material concentrations as well as to reduce the product concentrations at the position of the catalyst [72].
- *Feasible operating window required*: selected conditions regarding the operating temperature and pressure have to allow reasonable chemical reaction performance and separation of the reactants at the same time [16] [52].
- *Presence of reactive azeotropes or multiple steady states*: additional boundaries for reactive distillation can arise during the formation of reactive azeotropes, in which benefits in changed concentrations via distillation are neutralized by the performed reaction [73]. Moreover, interacting reaction and separation causes strong nonlinear process performance. These multiple

steady state conditions affect obtained column profiles as well as the resulting target compound specifications within the same column configurations [74] [75].

2.2. Biocatalytic Reactive Distillation

The performance of integrated biocatalytic reactive distillation is mainly based on the same principles as described in **section 2.1** for classical reactive distillation. Substitution of the chemical catalyst by a biocatalyst is the major difference within this relatively new research field. It is driven by the idea of a broadened reaction scope aiming at stereo- or enantioselectively synthesized products in reactive distillation apparatuses [45] [47] [42].

2.2.1. Characteristics of Biocatalysts

Operating reactive distillation with biocatalysts brings along a new set of advantages and challenges beside the previously discussed issues from **section 2.1**. All of them are related to the typical three-dimensional protein structure of the biocatalysts and their origin in predominantly aqueous environment. The three-dimensional structure is composed of a folded polyamide chain, presenting hydrophilic functional groups at the surface. Those hydrophilic functional groups are directing to the outside, while they incorporate lipophilic groups inside the complex molecule. By that, a water layer called 'structural water' (5 - 10 % of the total dry weight) is built up using hydrogen bonds to preserve biocatalytic activity [76]. Resulting from this unique structure, a very efficient reaction performance by factors of 10^8 - 10^{17} compared to non-catalyzed reactions can be achieved under mild conditions (pH 5 – 8, T = 20 – 40 °C) and simultaneously less tendency to perform side reactions is provided [77] [78] [32]. Similar to other catalysts, biocatalysts are able to considerably accelerate a reaction by reducing the activation energy (E_a) between the starting material and the desired target molecule [79]. The driving force for this catalytic acceleration is a stronger binding of the biocatalyst to the transition state of the starting material than to the corresponding ground state, which leads to the formation of a transition-state complex between the biocatalyst and the starting material [80]. At the end, the biocatalyst is released unchanged from the reaction after product formation and therefore does not influence the thermodynamic equilibrium. Hence, limited reactions can be performed in both directions by varying the operation conditions in dependency of the desired target compounds. In contrast to the majority of chemical catalysts, biocatalysts are able to accept specific chiral molecules. This characteristic can be denominated as catalytic flexibility, which allows catalyzing reactions chemoselectively (act on a specific functional group without affecting other reactive groups), regioselectively (distinguish between chemical identical functional groups at different positions in a starting molecule) as well as enantioselectively (recognition of chiral starting materials and convert one enantiomer of a racemic mixture preferentially) [81] [32] [82]. Several mechanisms are developed to understand the uniqueness within the active site of a biocatalyst, all referring to structural-related differences compared to chemical catalysts. Independent from derived theories of induced-fit behavior [83] [84], desolvation [85] or solvation-substitution approaches [86], well-directed

conversion is achieved by the ability of completely enclosing the starting material within the substantially bigger biocatalyst molecule [82].

On the contrary, the complex structure of biocatalysts exhibits challenging aspects involving narrowed operation flexibility, especially with respect to temperature and the used solvent material [82]. Similar to all proteins, a deactivation through thermal sensitivity is observed at temperatures outside their operating range. For operations at elevated temperatures up to T = 105 °C, only a few exceptions are known [87] [88]. Although fixation or entrapment of the biocatalyst by carrier materials offers the opportunity to increase thermal stability through the formation of immobilized biocatalysts, deactivation at elevated temperatures cannot be prevented [36] [35] [89]. Due to their naturally aqueous environment, reaction performance in water allows the highest catalytic activity. By changing to organic solvent materials, which in most cases provide less heat of evaporation and can be adapted to desired reaction conditions, reduced catalytic activity by approximately one order of magnitude is detected [90]. In many biocatalyzed reactions, inhibition phenomena originating from increased starting material concentrations or in consequence of rising product concentrations occur [91] [92]. In such cases, the developed processes should therefore consider strategies for constantly reduced starting material concentrations (e.g. continuous feeding of low starting material concentrations) and *in situ* removal of the products (e.g. evaporation of the product, crystallization).

2.2.2. Impact Factors of Biocatalysts on Reactive Distillation

Based on the overview on the characteristics of biocatalysts, several impact factors on the application in reactive distillation columns can be identified in addition to the aspects discussed in **section 2.1**:

- *Additional decisive parameter = enantioselectivity*: Provision of enantioselective transformations in biocatalysts offers the possibility to synthesize chiral molecules instead of bulk chemicals, which may lead to numerous additional applications of reactive distillation technology.

  For effective synthesis of chiral molecules via biocatalysts, the competition for binding at the active site between two enantiomers (*A*, *B*) can be expressed via the ratio of their reaction rates (v_A, v_B [mol·s^{-1}]) by the dimensionless enantioselectivity (*E* [-]) also called 'enantiomeric ratio' (**Eq. 4**) [93]:

$$E = \frac{v_A}{v_B} \qquad \textbf{Eq. 4}$$

  The corresponding reaction to the products *P* as well as *Q* is presented in **Figure 2.4**, **A**. Both competing enantiomers form a complex consisting of the biocatalyst and the enantiomeric starting material (*[BiocatA], [BiocatB]*), which exhibit different *Gibbs* free energies (*ΔG* [J]) in their transition-states (**Figure 2.4**, **B**). Generally, the system always has the tendency to preferentially convert the enantiomeric starting material with the lowest *ΔG* (here: *A*) due to less effort for

overcoming the activation energy E_a. Hence, a faster reaction rate v_A compared to v_B is present in the given example. The difference between the values of *Gibbs* free energies in the transition-states ($\Delta\Delta G$ [J]) as well as the reaction rates can be referred to the present enantioselectivity of the reaction. Assuming thermodynamic equilibrium conditions, the relation between $\Delta\Delta G$ and the reaction rates (v_A, v_B [mol·s^{-1}]) is defined by the ideal gas constant (R [J·mol^{-1}·K^{-1}]) and the temperature (T [K]) as follows (**Eq. 5**):

$$\Delta\Delta G = -R \cdot T \cdot ln\left(\frac{v_A}{v_B}\right) \qquad \textbf{Eq. 5}$$

For the application in reactive distillation, the enantioselectivity should be as high as possible to achieve the synthesis of optical pure chiral molecules. A detailed discussion on the influence of E on biocatalytic reaction performance in asymmetric synthesis is given in **section 2.2.4**.

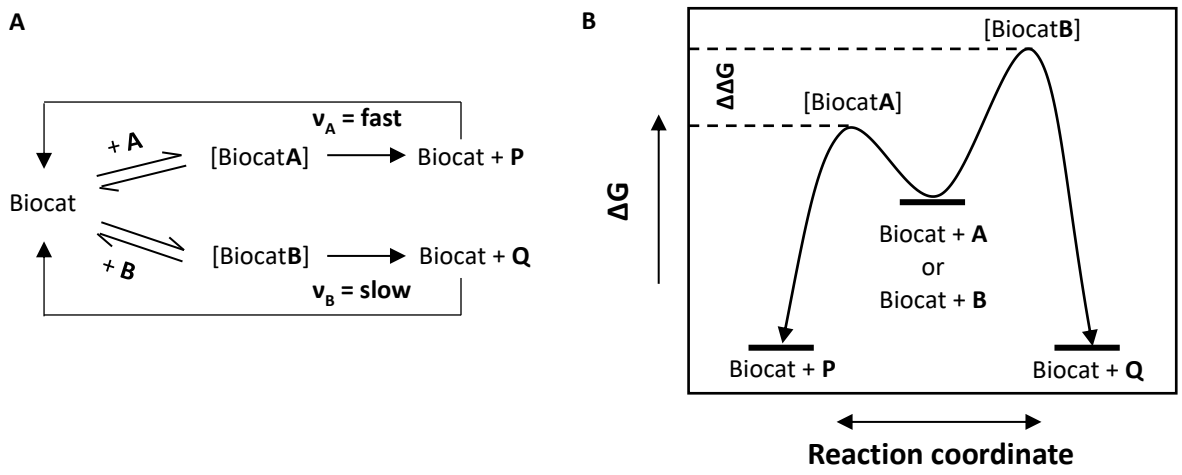

Figure 2.4: Principle of enantiomeric differentiation in a biocatalytic reaction. **A**: Reaction of either enantiomer *A* or *B* with the biocatalyst (*Biocat*) to *P* or *Q* with different reaction rates v_A and v_B. **B**: Energy diagram (transition state *[BiocatA]* is preferred due to less ΔG)

- *Narrowed operating window*: With respect to the feasible operating window in classical reactive distillation (**Figure 2.3**), thermal sensitivity of biocatalysts causes a narrowed temperature constrain for biocatalytic reactive distillation. Basically, the applied temperature is not only influencing the operating window, but determines the accessible catalytic activity according to the principle of *Arrhenius* [94]. In fact, the *Arrhenius*-equation describes the dependency of the reaction rate (k) on the operating temperature (T [K]) involving a pre-exponential factor (k_0), the activation energy (E_a [J·mol^{-1}]) and the ideal gas constant (R [J·mol^{-1}·K^{-1}]). While k_0 represents a reaction-related constant for the frequency of collision between the applied starting materials, E_a is defined as the minimum energy, which is necessary for reaction performance (**Eq. 6**):

$$k = k_0 \cdot e^{-\frac{E_a}{R \cdot T}} \quad \textbf{Eq. 6}$$

With increasing temperature, rising reaction rates *k* are achieved and simultaneously higher catalytic activity is detected (and vice versa). As a rule of thumb going back to *van't-Hoff* (RGT-rule), nearly doubled reaction rates are obtained at a temperature increase of T = 10 K for numerous chemical reactions. However, the RGT-rule does not hold in the case of many biocatalytic reactions [95]. Moreover, the value of the activation energy (E_a) influences the effect on the reaction rate, while typical activation energies range from E_a = 20 – 150 kJ·mol^{-1} [96]. At low activation energies (E_a < 20 kJ·mol^{-1}) an increase in the operating temperature has a lower impact on the reaction rate, whereas higher values for E_a result in an increased effect on the reaction rate. Beside rising reaction rates at increased temperatures, oppositional deactivation with respect to increased temperature reduces the catalytic activity especially for biocatalysts [36] [32]. The effect on the biocatalytic reaction rate (v) can be described by an exponential deactivation term k_d [s^{-1}] within the reaction kinetics, which reduces the initial biocatalytic reaction rate (v_0) in dependency of time (t [s]) (**Eq. 7**):

$$v = v_0 \cdot e^{-k_d \cdot t} \quad \textbf{Eq. 7}$$

One specific case in the deactivation kinetic becomes even more important to compare the behavior of a biocatalyst under changed temperature conditions. The parameter of interest is the half-life time ($\tau_{0.5}$ [s]), describing the time point at which 50 % of initial activity (boundary condition: $v = 0.5 \cdot v_0$) is present in consequence of activity losses (**Eq. 8**):

$$\tau_{0.5} = \frac{\ln(2)}{k_d} \quad \textbf{Eq. 8}$$

It has to be mentioned, that the deactivation term (k_d [s^{-1}]) is not only affected by temperature but involves the sum of multiple impact factors such as the applied solvent material and inhibition phenomena. Independent from the applied biocatalyst, long-term stability represented by increased half-life times should be realized to compete with well-established chemical catalysts. Within biocatalytic reactive distillation, temperature is expected to be the most important influencing factor on k_d. Hence, a tradeoff between reduced catalytic activity in consequence of thermal sensitivity and increased reaction rates at rising temperatures should be focused for biocatalytic reactive distillation approaches.

- *Prevent inhibition phenomena and overcome equilibrium limitations:* Similar to chemical reactions in reactive distillation, shifting the equilibrium to the desired side of reaction needs to be performed in all equilibrium limited reactions to increase the final target compound molar fraction and in this respect the overall yield. Thermodynamically, the equilibrium for an exemplified

equilibrium limited reaction involving the starting materials *A* and *B* as well as the formed products *C* and *D* with the stochiometric factors (ν_i [-]) (**Eq. 9**)

$$|\nu_A|A + |\nu_B|B \rightleftharpoons |\nu_C|C + |\nu_D|D \qquad \textbf{Eq. 9}$$

is expressed by the equilibrium constant K_{eq} [-] (**Eq. 10**). It is composed of the thermodynamic activities (a_i) to the power of the stochiometric factors of the products and the starting materials (ν_i), while the products are placed in the numerator and the starting materials in the denominator.

$$K_{eq} = \prod_i a_i^{\nu_i} = \frac{a_C^{|\nu_C|} \cdot a_D^{|\nu_D|}}{a_A^{|\nu_A|} \cdot a_B^{|\nu_B|}} \qquad \textbf{Eq. 10}$$

Therefore, an equilibrium limitation is present at values of $K_{eq} < 1$, while $K_{eq} > 1$ refers to less equilibrium limited reactions. In real solutions, thermodynamic activity a_i is connected to the molar fraction (x_i [mol·mol^{-1}]) via the following relation (**Eq. 11**).

$$a_i = \gamma_i \cdot x_i \qquad \textbf{Eq. 11}$$

For ideal solutions, intermolecular interactions described by the activity coefficient can be neglected ($\gamma_i \rightarrow 1$) and a_i becomes similar to x_i. The corresponding equilibrium conversion X_{eq} [-] for a stochiometric reaction of the type presented in **Eq. 9** can be calculated with the equilibrium constant K_{eq} according to **Eq. 12**:

$$X_{eq} = \sqrt{\frac{K_{eq}}{1 + K_{eq}}} \qquad \textbf{Eq. 12}$$

As long as an equilibrium limitation in the desired direction of the reaction is defined, it should be modified to allow a successful operation. Useful strategies date back to the principle of *Le Chatelier (1884)*, in which changed pressure, temperature or moles of the reactants mainly influence the equilibrium of the reaction [97]. The possibility to address all those parameters in reactive distillation makes it a powerful approach in handling equilibrium limited reaction systems. Additionally, *in situ* separation of reactants from the position of the catalyst leads to the reduction of inhibition phenomena, which proves biocatalytic reactive distillation to be an interesting alternative concept for chiral synthesis.

2.2.3. Feasible Biocatalysts for Reactive Distillation

Nature provides a broad spectrum of different biocatalysts, which are classified in six categories. They are mainly distinguished on the basis of their catalyzed type of reaction [32] [82]. Biocatalyst implementation in reactive distillation requires increased thermal stability, catalysis of chiral molecules

in equilibrium limited reactions and practicability without additional compounds such as cofactors or solvent material to not further increase complexity in column operation. An evaluation of the previously discussed characteristics within the different classes of biocatalysts toward their feasibility in reactive distillation is presented in **Table 2.1**. The class of hydrolases turned out to be most suitable for reactive distillation as they solely fulfill the stated requirements (*+* indicates fulfilled, - indicates not fulfilled). Catalytically, hydrolytic transformations comprising amide and ester bonds are realized within the scope of hydrolases. They can be subdivided into proteases, esterases and lipases. Roughly, two-thirds of the research within the field of biocatalysis is related to hydrolytic transformations and especially lipases are responsible for around 40 % of their overall applications [21] [98] [82].

Table 2.1: Classification of biocatalysts and evaluation for the applicability in biocatalytic reactive distillation

Class of Biocatalyst [a]	**Catalyzed Type of Reaction**	**Feasibility in Reactive Distillation** [b]
1. Oxidoreductases (25%)	oxidation-reduction	- necessity of T-sensitive cofactors - solvent required + shift in equilibrium to increase conversion
2. Transferases (5%)	transfer of functional groups	- necessity of T-sensitive cofactors - solvent required + shift in equilibrium to increase conversion
3. Hydrolases (60%)	hydrolysis	+ no cofactors needed + solvent-free approach is possible + shift in equilibrium to increase conversion
4. Lyases (7%)	group elimination (double bond formation)	+ no cofactors needed - solvent required - no necessity in shift in equilibrium
5. Isomerases (2%)	isomerization	+ no cofactors needed - solvent required - no necessity in shift in equilibrium
6. Ligases (1%)	bond formation coupled with triphosphate cleavage	- necessity of ATP - plays no role in production of fine chemicals

[a] percentages account for the research performed on the given class of biocatalysts [21] [98] [32]
[b] evaluation is true for the majority of biocatalysts in the different classes

The attention for lipases is mainly related to their unique properties on hydrolyzing triglycerides to fatty acids and glycerol [99] in the food industry [100] [101] [102]. Moreover, their abilities toward hydrolyzing and forming carboxylic ester bonds are useful for the synthesis of chiral intermediates [103] [104] [105]. In particular, the candidate *Candida antarctica* lipase B (CalB) provides the highest

variability with respect to catalytic activity on non-natural esters [106] [107] and is available in bulk quantities [108]. Being catalytically active on non-natural esters, CalB can be applied for kinetic resolution of racemic starting materials such as secondary alcohols (**section 2.2.4**) or dynamic kinetic resolution reactions (**section 2.2.5**). Beside a huge range of accepted starting materials, several beneficial properties compared to other hydrolases can be highlighted to demonstrate the exceptional standing of CalB:

- *Increased thermal stability*: Compared to other biocatalysts, already free CalB is relatively robust toward elevated temperatures of up to T = 50 - 60 °C [108] [82]. In its immobilized configurations, further increased thermal stability up to T = 80 °C is observed [109] [37]
- *No need for interfacial activation:* In contrast to the majority of lipases, CalB does not show considerably increased catalytic activity beyond a critical micellar concentration of the starting material (CMC) in biphasic oil-water systems [110] [111]. The reason for that is the absence of a typical lid-structure, which covers the active site of most of the lipases.
- *Application in organic solvents and solvent-free approaches:* CalB displays high tolerance in organic solvents such as toluene, acetone or *t*-butanol [37] [82] and can even be applied solvent-free [112] [113]. Moreover, water is not needed for the application, which is especially important due to increased energy consumption for its evaporation in reactive distillation processes.
- *No need for cofactors:* Cofactors are generally not needed for hydrolases including CalB, which reduces the complexity and prevents an additional cofactor-regeneration strategy [82]. Furthermore, cofactors usually display thermal sensitivity as well. Exemplary for the cofactor NADH, thermal deactivation significantly increases in a range of T = 4 – 60°C (**Figure 2.5**).

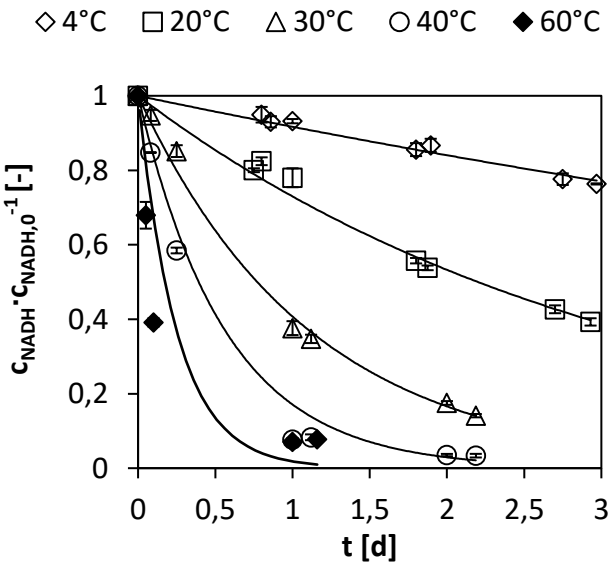

Figure 2.5: NADH deactivation (n = 3) at varied temperature (T = 4 – 60°C) investigated by spectrophotometric assay (according to Lambert-Beer law, λ = 340 nm); c_{NADH} = 20 mM (in 100 mM KP_i buffer, pH = 7)

Expressed by the corresponding half-life time of NADH, $\tau_{0.5}$ < 0.5 d are detected at T = 40 °C. Hence, application of cofactor dependent biocatalysts is not recommended for biocatalytic reactive distillation at the current stage of thermal sensitivity of cofactors.

Based on multiple advantages of applying CalB for accepting chiral starting materials, special interest for its feasibility in reactive distillation is further discussed by focusing on two different types of catalyzed reactions in **section 2.2.4** and **section 2.2.5**.

2.2.4. Kinetic Resolution

In kinetic resolution (KR) reactions, the starting point is a racemic mixture containing equal amounts of two enantiomers. By preferentially converting one of the enantiomers with an increased reaction rate, enriched optical purity of the slower reacting enantiomer is reached with biocatalysts (i.e. CalB) due to their enantioselectivity (**section 2.2.2**) [114]. It has to be distinguished between irreversible KR reactions without the tendency of any back reaction and reversible KR revealing an equilibrium limitation (**Figure 2.6**).

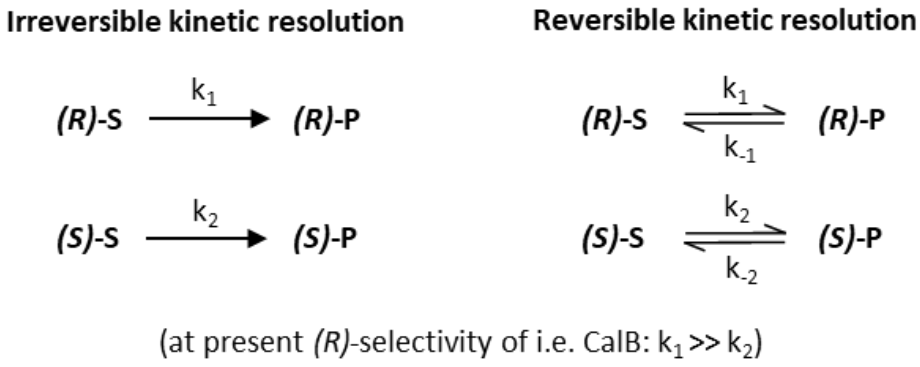

Figure 2.6: Scheme of irreversible and reversible kinetic resolution (KR). Enantioselectivity of the biocatalyst toward the starting materials (*S*) depends on the difference in the reaction rates k_1 and k_2.

In contrast to other asymmetric reactions, the theoretical maximum yield within KR is limited to *Y* = 50 % at ideal conditions. This ideal case will occur, if only the preferential enantiomer is converted and the biocatalyst does not accept the second enantiomer. In reality, at least a small rate of the slower reacting enantiomer will be converted. Thereby, a reduction in the maximum yield is caused, which mainly depends on the enantioselectivity (*E* [-]) of the reaction. Hence, beside the enantioselectivity *E* (**Eq. 4**) the yield (*Y* [-]) as well as the conversion (*X* [-]) and the optical purity of the enantiomers (ee_S, ee_P [-]) are the parameters of interest to describe a KR reaction. Values for *X* (**Eq. 13**) and *Y* (**Eq. 14**) are accessible by the moles of the starting materials (n_S) and the formed products (n_P) at the beginning (t_0 [s]) and at different time points during reaction performance ($t > t_0$). In the KR reactions depicted in

Figure 2.6, n_S consists of the sum of the starting enantiomers (*(R)*-S, *(S)*-S) and n_P is defined by the sum of the products (*(R)*-P, *(S)*-P).

$$X = \frac{n_{S,t_0} - n_{S,t}}{n_{S,t_0}} \quad \textbf{Eq. 13}$$

$$Y = \frac{n_{P,t} - n_{P,t_0}}{n_{S,t_0}} \quad \textbf{Eq. 14}$$

Both, the conversion (*X*) and the yield (*Y*) become equal, if the starting material is transformed to the desired product without side product formation (*X = Y*). The optical purity of the starting materials and the products is expressed by the enantiomeric excess (*ee*), which defines the surplus of one enantiomer toward the other (**Eq. 15**, **Eq. 16**). While racemic mixtures exhibit optical purities of *ee* = 0, the desired target compound should in ideal case provide excellent optical purity of *ee* = 1. In this ideal case, a pure enantiomer is obtained without its undesired counterpart.

$$ee_S = \frac{n_{(S)-S} - n_{(R)-S}}{n_{(S)-S} + n_{(R)-S}} \quad \textbf{Eq. 15}$$

$$ee_P = \frac{n_{(R)-P} - n_{(S)-P}}{n_{(R)-P} + n_{(S)-P}} \quad \textbf{Eq. 16}$$

The enantiomeric ratio *E* within irreversible and reversible KR is connected to the enantiomeric excess of the starting material (ee_S) and the conversion (*X*) by **Eq. 17** and **Eq. 18**. Similarly, **Eq. 19** and **Eq. 20** define *E* in dependency of conversion (*X*) and the enantiomeric excess of the product (ee_P). Those calculations date back to the methods of *Chen et al. (1982)* for irreversible KR and *Chen et al. (1987)* for reversible KR [115] [116]. Based on the established methods, graphical visualization of KR is usually realized by plotting the courses of enantiomeric excess (ee_S, ee_P) over conversion (*X*).

Irreversible KR

$$E = \frac{\ln[(1-X)\cdot(1-ee_S)]}{\ln[(1-X)\cdot(1+ee_S)]} \quad \textbf{Eq. 17}$$

Reversible KR

$$E = \frac{\ln[1-(1+K_{eq})\cdot(X+ee_S(1-X))]}{\ln[1-(1+K_{eq})\cdot(X-ee_S(1-X))]} \quad \textbf{Eq. 18}$$

$$E = \frac{\ln[1-X\cdot(1+ee_P)]}{\ln[1-X\cdot(1-ee_P)]} \quad \text{Eq. 19}$$

$$E = \frac{\ln[1-(1+K_{eq})\cdot X\cdot(1+ee_P)]}{\ln[1-(1+K_{eq})\cdot X\cdot(1-ee_P)]} \quad \text{Eq. 20}$$

For the irreversible case, courses for ee_P and ee_S at rising conversion (*X*) for three different enantiomeric ratios (*E* = 1000, *E* = 35, *E* = 10) are depicted in **Figure 2.7**, **A**. If the faster produced enantiomer of *P* is the desired target compound of KR, the highest possible optical purity is reached in the course of ee_P at X < 50 %. In fact, rising enantiomeric ratios *E* cause increased maximum optical

purities for ee_P in the beginning of the reaction. While the faster reacting enantiomer predominantly forms the target compound *P* at X < 50 %, optical purity of *P* significantly decreases at X > 50 %. This behavior can be referred to the absence of the faster reacting enantiomer and simultaneous acceptance of converting the residual, slower reacting enantiomer at X > 50 %. In order to achieve the highest yield (*Y*) of *P* with excellent optical purity (ee_P = 100) in KR, the reaction should be stopped at X = 50 % in the case of ideal enantioselectivity ($E \geq 1000$). At reduced *E*, the reaction should be stopped at lower *X* to guarantee excellent optical purity for ee_P. Looking at the corresponding trend in optical purity of the slower-reacting starting enantiomer (ee_S), constantly rising ee_S with increasing conversion (*X*) are observed until ee_S = 100 %. With rising enantioselectivities *E*, optically pure ee_S is reached at lower conversion points *X*. In ideal case (*E* = 1000), ee_S = 100 % can be reached at *X* = 50 %. At further increased *X*, optical purity of ee_S stays constantly high due to the absence of the faster reacting starting enantiomer. Thus, the reaction should be stopped at X = 50 % in the case of *E* = 1000 to obtain the slower reacting enantiomer of *S* as the desired target molecule. However, a different operation strategy need to be considered at reduced *E* to get the residual starting enantiomer in high optical purity (ee_S = 100 %). In this case, stopping the reaction is shifted to higher points of conversion *X*, which simultaneously reduces the feasible yield. Hence, the higher the enantioselectivity of the KR reaction, the higher the feasible yield (with a maximum of *Y* = 50 %).

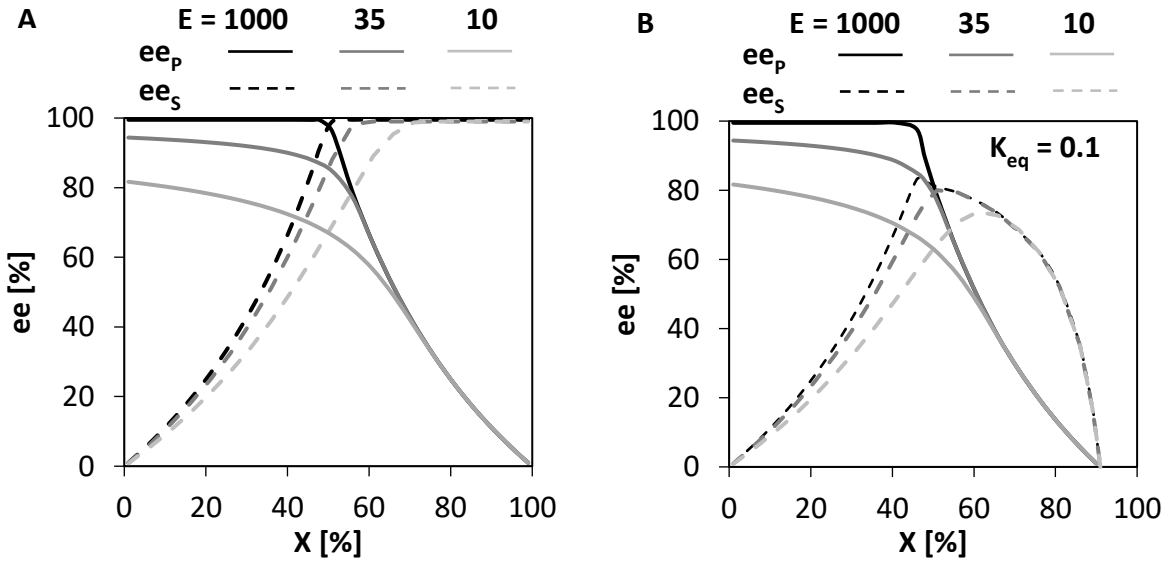

Figure 2.7: Impact of the enantioselectivity *E* on the optical purities (ee_S, ee_P) in reaction performance with rising conversion (*X*). **A**: irreversible KR reaction, **B**: reversible KR reaction (K_{eq} = 0.1).

Following the same procedure with respect to the reversible case of KR reveals similar behavior for ee_P but totally different results for ee_S compared to irreversible KR (**Figure 2.7**, **B**). Instead of ending up in constantly high optical purity for ee_S, a maximum within rising *X* is reached before considerably

decreasing ee_S beyond the maximum. This behavior originates from the preferential conversion of the faster reacting starting enantiomers and their corresponding products. In addition to the desired forward reaction, the undesired backward reaction takes place in reversible KR. Rising ee_S is only observed until the equilibrium of the reaction is reached and the backward reaction becomes dominant due to the formed reaction equilibrium (i.e. at $K_{eq} = 0.1$). The back reaction of the preferentially formed product enantiomer beyond the maximum in ee_S is faster compared to the slower formed product enantiomer, which causes the decrease in ee_S. Moreover, the position of the formed maximum in ee_S depends on the enantioselectivity E of the biocatalyst toward the reactants in KR. Hence, as long as the slower reacting enantiomer of the starting material is the desired target compound, it is not possible to achieve high optical purity of ee_S in reversible KR without shifting the equilibrium, because ee_S is limited by K_{eq}.

Independent from irreversible (**Figure 2.7**, **A**) or reversible KR (**Figure 2.7**, **B**), the decisive parameter for industrial application is the enantiomeric ratio E. At values of $E < 35$, inefficient differentiation between the enantiomers does not allow industrial application. In the range of $35 < E < 100$, the application becomes partly feasible and $E > 100$ refers to a very selective reaction with increased interest for further studies [32].

2.2.5. Dynamic Kinetic Resolution

Dynamic kinetic resolution (DKR) allows the synthesis of chiral target compounds from racemic mixtures through the combination of kinetic resolution (KR) with a simultaneously performed racemization step in one-pot approaches (**Figure 2.8**, **A**). The major benefit compared to KR is the possibility to in principle achieve $Y = 100$ % by *in situ* racemization of the slower reacting starting enantiomer [117]. A powerful strategy to perform DKR with biocatalysts is the combination of a lipase-catalyzed KR combined with a metal-catalyzed racemization step, originating from initial research by *Williams and Bäckvall* [118] [119] [120]. In contrast to KR, the desired target compound has to be the formed product enantiomer of the KR reaction. It cannot be the left-over starting enantiomer due to its racemization. For monitoring a DKR reaction, the courses of enantiomeric excess (ee_S, ee_P) with conversion (X) are essential to understand the desired reaction performance (**Figure 2.8**, **B**). At high enantioselectivities (E), constantly high optical purity for the desired target compound of the KR reaction (ee_P) at low optical purity with respect to the starting material (ee_S) is detected. This behavior can just be achieved as long as both reactions are performed efficiently. In general, high ee_P is related to an efficient KR performance and low ee_S indicates successful performance of the racemization step.

Nowadays, several racemization catalysts are available. They contain complexes of transition metals i.e. rhodium, iridium and ruthenium to perform fast racemization of a broad range of alcoholic starting materials via hydrogen transfer reactions [121]. However, compatibility with enzymes is only approved for some of them. An interference between both catalysts often results in either deactivation of the enzyme or inhibition of the metal catalyst [122]. Therefore, simultaneous operation of both catalysts at least requires to fulfill the following rules [122]:

- *KR has to be at least moderately enantioselective (E > 20)*
- *Racemization step has to be at least 10 times faster than KR step*
- *The metal catalyst must not convert the target compound of KR*
- *KR and racemization have to take place under the same reaction conditions*

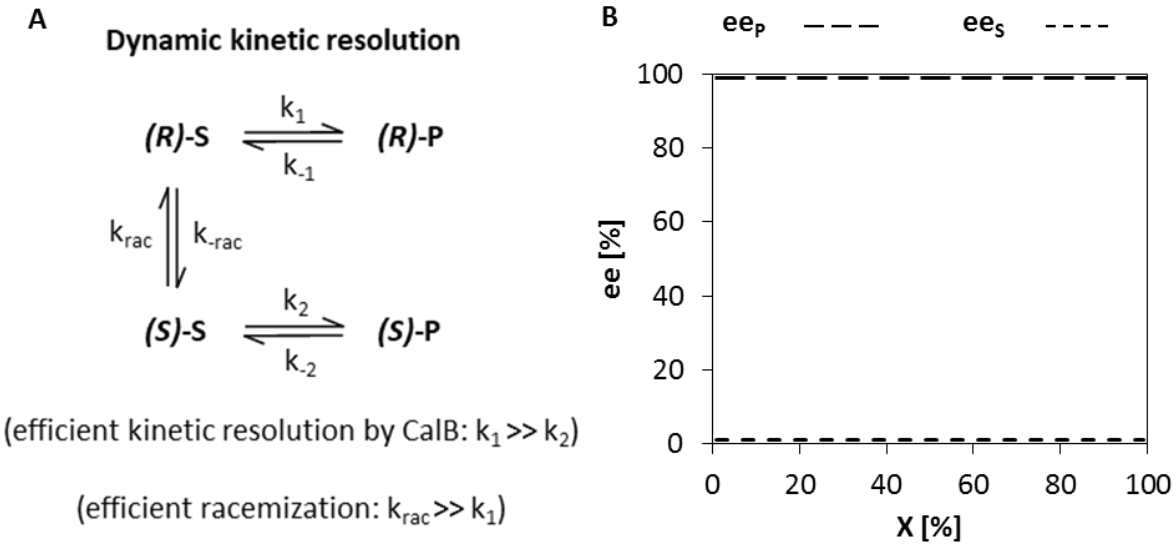

Figure 2.8: Dynamic kinetic resolution (DKR). **A**: Reaction scheme, **B**: Reaction performance with respect to optical purities (ee_S, ee_P) at rising conversion (*X*).

Among a huge variety of investigated DKR reactions and catalyst combinations [117], successfully performed DKR of racemic *sec*-alcohols is reported in *Bäckvall's* group applying CalB for KR and heat-activated Shvo catalyst for the racemization [119] [120]. Shvo catalyst includes a coordinated ruthenium to allow hydrogen transfer between its keto- and alcohol-subunit [123]. For the formation of the subunits, Shvo catalyst needs to be homogeneously dissolved in organic solvent such as toluene. The challenging aspects about metal-complexes used for DKR is the need for high temperatures causing fast deactivation of enzymes as well as their instability in the presence of oxygen species for the majority of designed metal catalysts [124]. However, different configurations of the metal catalysts were investigated. Some of them are even showing practicability at room temperature for the DKR of *sec*-alcohols [125] [126] [127] [128] [129].

2.2.6. Biocatalyst Implementation in Reactive Distillation

For biocatalytic reactive distillation, heterogeneous application is required to prevent contact of the thermal sensitive biocatalyst with the reboiler region of the column. With respect to increased costs of the biocatalyst, it is not recommended to feed the catalyst analogue to homogeneous reactive distillation approaches. Therefore, appropriate fixation of the biocatalyst and simultaneously reasonable separation efficiency of the applied column internals should be guaranteed within the implementation strategy. So far, two different methods are described in literature. Similar to classical reactive distillation with heterogenous chemical catalysts, wire gauze baskets combined with corrugated metal sheets for separation are feasible (**Figure 2.9**, **A**). The biocatalyst can be filled into the baskets to create a catalytic packing. A famous example for this 'sandwich'-procedure is the Katapak-S™ packing developed by *Sulzer Chemtech Ltd.* (Winterthur, Switzerland) [130]. Within a second strategy developed by *Smirnova et al. (2010)* [131], the entrapment of biocatalysts in a silica matrix following the sol-gel process [132] [133] is realized to create a catalytic layer on the surface of standard gauze packings (**Figure 2.9**, **B**). Applicability of the silica-based coating approach is shown by *Heils et al. (2012 & 2015)* [40] [45]. Both strategies depicted in **Figure 2.9** offer the opportunity to fix biocatalysts efficiently in reactive distillation apparatuses.

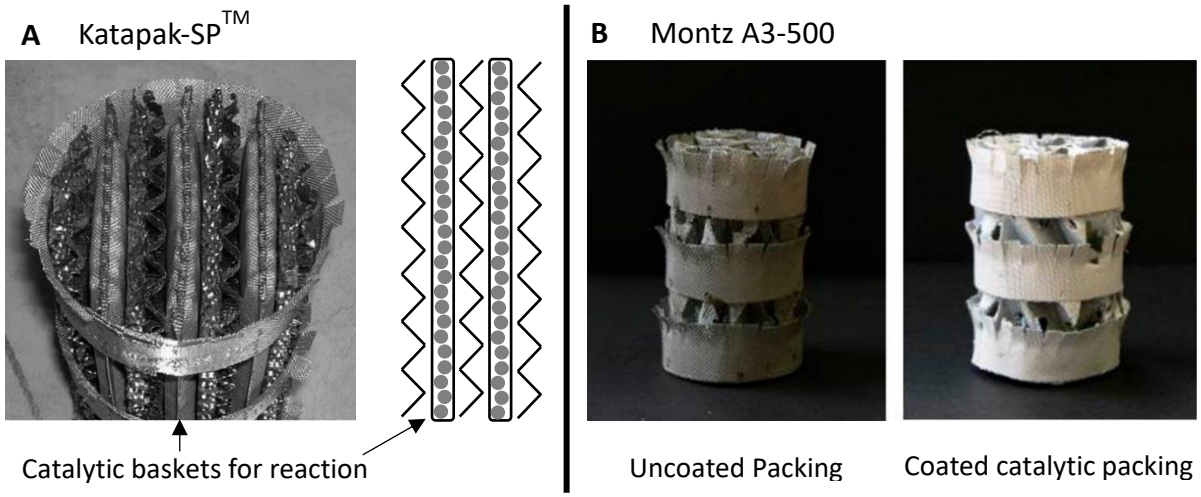

Figure 2.9: Implementation strategies for biocatalysts in reactive distillation columns. **A**: Type Katapak-SP™ following the 'sandwich'-approach by filling the biocatalyst in wire gauze baskets (picture of the packing is taken from [134]); **B**: Type Montz A3-500 following the sol-gel approach by entrapment of the biocatalyst in a silica matrix (picture is taken from [45])

3. MATERIALS & METHODS

In the following part, an overview on the applied reactants and catalysts for reaction performance as well as the corresponding methods and setups is presented.

3.1. Chemicals & Catalysts

Reaction chemicals: *(R/S)*-2-pentanol (≥ 98%), *(R/S)*-3-hydroxy ethyl butyrate (≥ 97%), ethyl butyrate (≥ 98%), propyl butyrate (≥ 98%), *(R/S)*-2-pentyl butyrate (≥ 98%), 1-pentanol (≥ 99%) were purchased from Sigma Aldrich (Merck KGaA, Darmstadt, Germany). 1-propanol (≥ 99.8%) and ethanol (≥ 99.8%) from Carl Roth GmbH & Co. KG (Karlsruhe, Germany).

Additional chemicals: dodecane (≥ 99%), tetramethyl orthosilicate (98%), trimethoxymethyl silane (98%), polyethylene glycol (M_n = 400 g·mol^{-1}), *p*-xylene (≥ 99%) and *p*-nitrophenyl acetate (97%) were purchased from Sigma Aldrich (Merck KGaA, Darmstadt, Germany); methanol (≥ 99.9%), acetonitrile (≥ 99.9%), ethyl acetate (≥ 99.5%), isoamyl alcohol (≥ 98%), acetic anhydride (≥ 99%), pyridine (≥ 99.5%), dichloromethane (≥ 99%), Roti® Nanoquant solution, potassium dihydrogen phosphate (≥ 99%), dipotassium hydrogen phosphate (≥ 99%) and molecular sieve 4 Å (Typ 514, 0.4 nm, Perlform) from Carl Roth GmbH & Co. KG, sodium fluoride from Prolabo (East Grinstead, United Kingdom) and 2-pentanone (≥ 99%) from Fluka (Honeywell Int. Inc., Bucharest, Romania).
For the kinetic resolution reactions, all chemicals were used for experimental investigation without further purification. In dynamic kinetic resolution, further treatment prior to experiments was done under evacuated conditions to avoid impurities by water or different oxidizing molecules. Ethyl butyrate and *p*-xylene were distilled, whereas *(R/S)*-2-pentanol was dried on molecular sieve before use. The storage of pretreated chemicals took place in a vacuum-desiccator at room temperature.

Catalysts: The biocatalyst *Candida antarctica* lipase B (CalB) was applied either on methacrylic carrier available as Novozym435 (CAS: 9001-62-1) or by free Lipozyme CalB L solution, which was kindly provided by Novozymes (Bagsvaerd, Denmark). With respect to the manufacturer, CalB preparation of Novozym435 was produced by a submerged fermentation step of a genetically modified *Aspergillus niger* microorganism and a subsequently adsorption step on macroporous resin material. Activity of porous Novozym435 particles was $v_0 \geq 5000$ U·g^{-1} according to propyl laurate assay. Free Lipozyme CalB L solution showed catalytic activity of $v_0 = 52 \pm 5$ U·ml^{-1} in spectrophotometric measurements by *p*-nitrophenyl acetate assay (50 mM *p*-nitrophenyl acetate in phosphate buffer, T = 30°C, pH 7, λ = 400 nm). The protein content was 0.50 ± 0.01 mass%, obtained in *Bradford* assay [135]. Lipozyme CalB L solution was entrapped in a silica matrix to produce a catalytic xerogel coating. Adjustment of the xerogel composition followed the existing protocol of *Heils et al. (2015)* [45]. In further treatment,

formed xerogel coating material was granulated by a *Gastroback®* cone mill (Hollenstedt, Germany) to get sieve fractions of different particle sizes. An average particle size of d = 450 − 630 µm was applied in the experiments. The storage of all biocatalytic preparations took place in a refrigerator at T < 7°C to preserve activity.

The ruthenium catalyst with the molecular structure of $C_{62}H_{42}O_6Ru_2$ (Shvo catalyst) for racemization in dynamic kinetic resolution reactions was kindly provided by the *Department of Organic Chemistry, Arrhenius Laboratory* (Stockholm, Sweden). It was stored in a vacuum-desiccator at room temperature.

3.2. Sample Analysis & Calibration

Sample analysis for all kinetic resolution (KR) and dynamic kinetic resolution (DKR) experiments was carried out at an *Agilent7890B* gas chromatograph (GC) (Agilent Technologies Inc., Wilmington, Delaware, USA) equipped with a *CP-Chirasil-DEX CB* column (L_{GC} = 25 m, d_{GC} = 0.25 mm) (Agilent Technologies Inc., Amstelveen, Netherlands). Hydrogen served as carrier gas in the column and helium was applied as make-up gas for the flame ionization detector (FID). The sample treatment differed with respect to the investigated reaction system prior to GC-injection.

For KR as well as DKR,starting with the racemic alcohol *(R/S)*-2-PeOH, the samples were diluted in two steps to 1:100 (v/v). While in the first dilution step (100 µL sample, 900 µL solvent), solely ethyl acetate was added as a solvent to the withdrawn sample, ethyl acetate containing the internal standard isoamyl alcohol (internal standard = ISTD, c_{ISTD} = 1 mg·g^{-1}, t = 8.2 min) was used in the second dilution step (100 µL of first dilution step, 900 µL solvent with internal standard). All pipetted sample volumes were weighed to have the exact amount of pipetted volumes. Adjusted parameters and typical retention times in GC analysis for *(R/S)*-2-PeOH with either EtBu (KR and DKR) or PrBu (KR) are presented in **Table 3.1**.

Table 3.1: Sample analysis in gas chromatography (GC) for kinetic resolution (KR) and dynamic kinetic resolution (DKR) reactions of the chiral alcohol *(R/S)*-2-PeOH with either EtBu (KR) or PrBu (KR & DKR)

GC Method		**KR of chiral alcohol (Retention Times)**		**DKR of chiral alcohol (Retention Times)**	
Parameter	**Value**	**Reactant**	**t [min]**	**Reactant**	**t [min]**
$V_{injection}$	1 µL	EtOH	1.3	EtOH	1.3
Flow	1.5 mL·min^{-1}	EtOAC	1.6	EtOAC	1.6
T_{inlet}	250°C	1-PrOH	2.1	2-Pentanone	2.8
T_{start}	50°C	EtBu	5.1	EtBu	5.1
$T_{Ramp\ 1}$	85°C (10°C·min^{-1})	*(R)*-2-PeOH	6.2	*(R)*-2-PeOH	6.2
$T_{Ramp\ 2}$	120°C (30°C·min^{-1})	*(S)*-2-PeOH	6.4	*(S)*-2-PeOH	6.4
$T_{detector}$	300°C	PrBu	7.8	*p*-xylene	6.6
t per sample	10.7 min	*(S)*-2-PeBu	9.5	*(S)*-2-PeBu	9.5
mode	Split (50:1)	*(R)*-2-PeBu	9.7	*(R)*-2-PeBu	9.7

For sample analysis of KR with the racemic starting ester *(R/S)*-3-HEB, additional derivatization became necessary to allow base-line separation of the chiral compounds. Derivatization was realized by the transfer of an acetyl group on the alcohol function of the reactants forming an acetylated ester. While acetic anhydride was the donor of the acetyl group, pyridine served as catalyst to enable the deprotonation of the transition molecule [136]. Within the sample treatment, 1:10 (v/v) dilution in a derivatization agent with subsequent incubation for 3 h (60°C, 600 rpm) took place in the first step. The composition of the derivatization agent is listed in **Table 3.2**.

Table 3.2: Composition of derivatization agent for *(R/S)*-3-HEB sample analysis

Component	Mass fraction (w/w) [%]
Pyridine	8.8
Acetic anhydride	41.4
Dichloromethane	49.3
Dodecane	0.5

The solvent dichloromethane was chosen as it did not affect the derivatization step. Due to its low surface tension and high relative volatility, dichloromethane was stored on ice for improved pipetting conditions. In a second dilution step of 1:10 (v/v), 100 µL of derivatized sample were mixed with 40 µL demineralized water and 860 µL dichloromethane to stop the derivatization reaction by converting residual acetic anhydride into acetic acid. At each step, the sampling mixtures were weighed to have the exact amount of pipetted volumes, respectively. Parameters for GC analysis of the generated samples and typical retention times for KR of *(R/S)*-3-HEB with 1-PeOH are summarized in **Table 3.3**.

Table 3.3: Sample analysis in gas chromatography (GC) for the kinetic resolution (KR) reaction of the chiral ester *(R/S)*-3-HEB with 1-PeOH

GC Method		KR of chiral ester (Retention Times)	
Parameter	**Value**	**Reactant**	**t [min]**
$V_{injection}$	1 µL	EtOH	-
Flow	2 mL·min^{-1}	Dichloromethane	1.6
T_{inlet}	250°C	1-PeOH	2.9
T_{start}	80°C	*(S)*-3-HEB	6.0
$T_{Ramp\ 1}$	5°C·min^{-1} to 120°C	*(R)*-3-HEB	6.2
$T_{Ramp\ 2}$	20°C·min^{-1} to 180°C	Dodecane (ISTD)	7.0
$T_{detector}$	300°C	*(S)*-3-HPB	10.3
t per sample	11 min	*(R)*-3-HPB	10.4
mode	Split (50:1)		

Component calibration of the reactants involved in KR and DKR by the racemic starting alcohol *(R/S)*-2-PeOH was performed by stepwise dilution of stock solutions (n = 10 - 14) to reach a final dilution of 1:100 (v/v). Weighing all pipetted volumes of the calibrated reactants in ethyl acetate as well as ethyl acetate with isoamyl alcohol was performed in the same way to the sample treatment of unknown reactant compositions. The prepared stock solutions covered the whole calibration range up to samples with pure calibrated substance. Accuracy of linear trend lines in calibration was at least $R^2 = 0.95$ (for EtBu). Similar dilution series with additional derivatization (n = 10) was performed for KR of 1-PeOH with the chiral ester *(R/S)*-3-HEB according to previously described sample treatment, which resulted in accuracy of $R^2 = 0.99$. For the calibration of the reaction product (*(R)*- and *(S)*-3-HPB), stochiometric product formation with respect to the conversion of *(R)*- and *(S)*-3-HEB was considered to correlate measured peak areas of *(R)*- and *(S)*-3-HPB. Low boiling ethanol was calibrated by dilution without derivatization to prevent overlapping of the peak areas in derivatized samples. An overview on the accuracy in calibration related to all reactants is given in **Table 3.4**.

Table 3.4: Accuracy of linear regression in the calibration lines of all applied reactants for kinetic resolution (KR) and dynamic kinetic resolution reactions (DKR) expressed by R^2. *n* represents the number of dilution steps for each calibration line.

KR of chiral alcohol			DKR of chiral alcohol			KR of chiral ester		
Reactant	**n [-]**	**R^2 [-]**	**Reactant**	**n [-]**	**R^2 [-]**	**Reactant**	**n [-]**	**R^2 [-]**
EtOH[a]	14	0.99	EtOH[a]	14	0.99	EtOH[a]	10	0.99
1-PrOH[b]	14	0.99	2-pentanone[a]	14	0.99	1-PeOH[a]	10	0.99
(R)-2-PeOH[b]	14	0.99	*(R)*-2-PeOH[b]	14	0.99	*(R)*-3-HEB[a]	10	0.99
(S)-2-PeOH[b]	14	0.99	*(S)*-2-PeOH[b]	14	0.99	*(S)*-3-HEB[a]	10	0.99
EtBu[a]	10	0.95	EtBu[a]	10	0.95	*(S)*-3-HPB[c]	-	0.99
PrBu[b]	14	0.98	*p*-xylene[a]	12	0.99	*(R)*-3-HPB[c]	-	0.99
(S)-2-PeBu[b]	14	0.99	*(S)*-2-PeBu[b]	14	0.99			
(R)-2-PeBu[b]	14	0.99	*(R)*-2-PeBu[b]	14	0.99			

[a]refers to duplicates, [b]refers to triplicates, [c]is iteratively calculated based on *(R)*-3-HEB and *(S)*-3-HEB

3.3. Characterization in Stirred Tank Reactors

Initial activity measurements (v_0) for KR of the chiral starting alcohol *(R/S)*-2-PeOH and the chiral starting ester *(R/S)*-3-HEB took place in jacketed STRs (V = 1 – 7 mL) at varied initial molar ratios ($x_{(R/S)\text{-substrate}}$ = 10 – 90 %) and in a temperature range of T = 30 – 80°C. Solvent-free binary mixtures of the starting materials were preheated to the desired reaction temperature in water baths, in order to avoid temperature differences compared to the batch vessels when starting the experiments. Mixing was achieved by magnetic stir bars at 400 rpm under ambient pressure. The sampling volume of 100 µL was subsequently treated and analyzed in GC according to **section 3.2**. Two different CalB preparations were investigated, including commercially available Novozym435 (NZ435) and entrapment of CalB in

a xerogel coating procedure according to *Heils et al. (2015)* [45]. In all cases, initial activity (v_0) is expressed in $U \cdot mg^{-1}$ wherein 1 U refers to 1 $\mu mol \cdot min^{-1}$. Obtained moles (*n(t)*) of formed product (*(R)*-2-PeBu, *(S)*-2-PeBu, *(R)*-3-HPB or *(S)*-3-HPB) in dependency of the reaction time were fitted by non-linear regression following **Eq. 21**.

$$n(t) = n_{max} \cdot \left(1 - e^{-k \cdot t}\right) \qquad \textbf{Eq. 21}$$

Excel solver® was used to minimize the sum of errors for all data points by varying *k* as parameter in an iteration loop. The parameter n_{max} relates to the maximum moles of product, which are theoretically expected at the end of the reaction at full conversion. Finally, activity was determined by the slope in linear range of **Eq. 21** at conversions $X < 10\,\%$ divided by the applied amount of biocatalyst preparation. The operation conditions for performed experiments with both CalB preparations in the investigated KR reactions are summarized in **Table 3.5**. Additionally, the mean error of the fitting method for catalytic activity is given as the mean standard deviation ($\overline{\sigma}$) of measured and calculated moles with respect to formed *(R)*-2-PeBu or *(R)*-3-HPB.

Based on the same experiments, determination of the **enantioselectivity (*E*)** in the KR reactions was realized by calculating the ratio of the faster reacting enantiomer (*(R)*-2-PeOH or *(R)*-3-HEB) compared to the not preferred enantiomer (*(S)*-2-PeOH or *(S)*-3-HEB) according to **Eq. 4** (**section 2.2.2**).

Table 3.5: Overview on the operation conditions of performed experiments and standard deviations to define the catalytic activity and the enantioselectivity in KR reactions with the chiral alcohol *(R/S)*-2-PeOH as well as the chiral ester *(R/S)*-3-HEB

	KR of chiral alcohol: *(R/S)*-2-PeOH / PrBu		**KR of chiral ester: *(R/S)*-3-HEB / 1-PeOH**	
Applied CalB preparation	gel coating[a]	NZ435[b]	gel coating[a]	NZ435[b]
c_{CalB} [$g_{prep.} \cdot L^{-1}$]	7	7	35	7
T [°C]	60	40 / 60 / 80	60	30 / 40 / 50 / 60 / 70
$x_{(R/S)\text{-substrate},0}$ [$mol \cdot mol^{-1}$]	0.5	0.1 / 0.3 / 0.4 / 0.5 / 0.6 / 0.7 / 0.9	0.5	0.1 / 0.3 / 0.5 / 0.7 / 0.9
$\overline{\sigma}$ [%]	4.5	9.7	5.4	7.5

[a]refers to duplicates, [b]refers to triplicates

Experimental characterization of the **equilibrium constant (K_{eq})** was realized in duplicated batch vessel experiments of V = 1 – 5 mL for KR of the chiral alcohol *(R/S)*-2-PeOH with PrBu and the chiral ester *(R/S)*-3-HEB with 1-PeOH, which were incubated at T = 60 °C with a catalyst concentration of $c_{NZ435} = 35\ g_{.} \cdot L^{-1}$. At varied initial molar fractions of the racemic starting materials

($x_{(R/S)\text{-2-PeOH}}$ = 0.1 / 0.3 / 0.55 / 0.66 / 0.7 / 0.9 mol·mol^{-1}, $x_{(R/S)\text{-3-HEB}}$ = 0.1 / 0.3 / 0.5 / 0.7 / 0.9 mol·mol^{-1}), sampling took place after t = 48 h and t = 72 h in the case of *(R/S)*-2-PeOH and after t = 22 - 23 h in the case of *(R/S)*-3-HEB. Sample treatment and analysis followed the procedures described in **section 3.2**.

Long term stability of Novozym435 (NZ435) was determined in repetitive batch vessel experiments (V = 5 mL). NZ435 was incubated in a drying chamber at defined temperatures in between the different runs. Batch vessel reaction performance of *(R/S)*-2-PeOH with PrBu took place at T = 60°C and T = 80°C with c_{NZ435} = 7 g·L^{-1}, while equimolar initial molar ratios were chosen ($x_{(R/S)\text{-2-PeOH}}$ = 0.5 mol·mol^{-1}). Both temperatures were investigated in duplicates. The residual activity was obtained by referring the initial reaction rate for conversions $X < 10$ % within time intervals of several days to the initial reaction velocity of the first experiment. At the end of every batch reaction, the final reaction mixture was removed from the reactor via syringe.

The **influence of pressure (*p*) on reaction performance** was investigated at ambient as well as reduced pressure in batch vessels (V = 7 mL) under solvent-free environment in duplicates. In contrast to the catalytic activity measurements, the batch vessels were equipped with a vigreux column and a horizontally placed condenser for the separation of low boiling reactants from the reaction mixture. Cooling water of T = 4°C was applied in the jacketed condenser, which was connected to a collection vessel for condensed reactants. Reduced pressures were realized by installing a vacuum pump *PC3001 VARIO^{pro}* (Vacuubrand GmbH & Co. KG, Wertheim, Germany) behind the condenser to prevent the loss of low boiling compounds. Samples of 100 µL were withdrawn through vacuum stable septa via syringe and treated by the same procedure described in **section 3.2**. For KR of *(R/S)*-2-PeOH with EtBu the reduced pressure was adjusted to p = 100 mbar and for KR of *(R/S)*-3-HEB with 1-PeOH to p = 20 mbar. The corresponding initial molar fractions were $x_{(R/S)\text{-substrate}}$ = 0.1 mol·mol^{-1} at T = 60°C and mixing of the reactants at 400 rpm. At ambient pressure, c_{NZ435} = 50 g·L^{-1} (*(R/S)*-2-PeOH) and c_{NZ435} = 35 g·L^{-1} (*(R/S)*-3-HEB) were placed in the batch vessels. Changing to reduced pressures, c_{NZ435} = 50 g·L^{-1} (*(R/S)*-2-PeOH) and c_{NZ435} = 7 g·L^{-1} (*(R/S)*-3-HEB) were applied.

3.4. Batch Reactive Distillation Setup

The **applied batch reactive distillation setup** (Normag, Ilmenau, Germany) within this work was mainly composed of an evaporator, the packing height including a combination of catalytic as well as non-catalytic sections and a condenser (**Figure 3.1**) [137]. In a 4 L round bottom flask, evaporation of the starting materials was induced by a temperature controlled electric heating mantle (TIC, bottom). Constant heating of the starting materials and prevention of delay in boiling in the bottom of the column was guaranteed by magnetic stirring. Evaporated starting materials created a vapor flow through the effective packing height of the column (h = 1200 mm) consisting of four identical glass

cylinders (d_{outer} = 50 mm, h = 300 mm). The glass cylinders were connected to the bottom flask and to each other via detachable flanges and circular silicone seals to allow tightness even at reduced pressure operations. Because of the flange construction, easy assembling and disassembling was possible for a flexible distribution of the column internals. Surrounded by foamed polystyrene, isolated conditions reduce the heat loss through the glass surface of the column. Analogue design of the tubes comprised two radially arranged GL14 side-ports in their lower part for temperature measurements and sampling at different column heights.

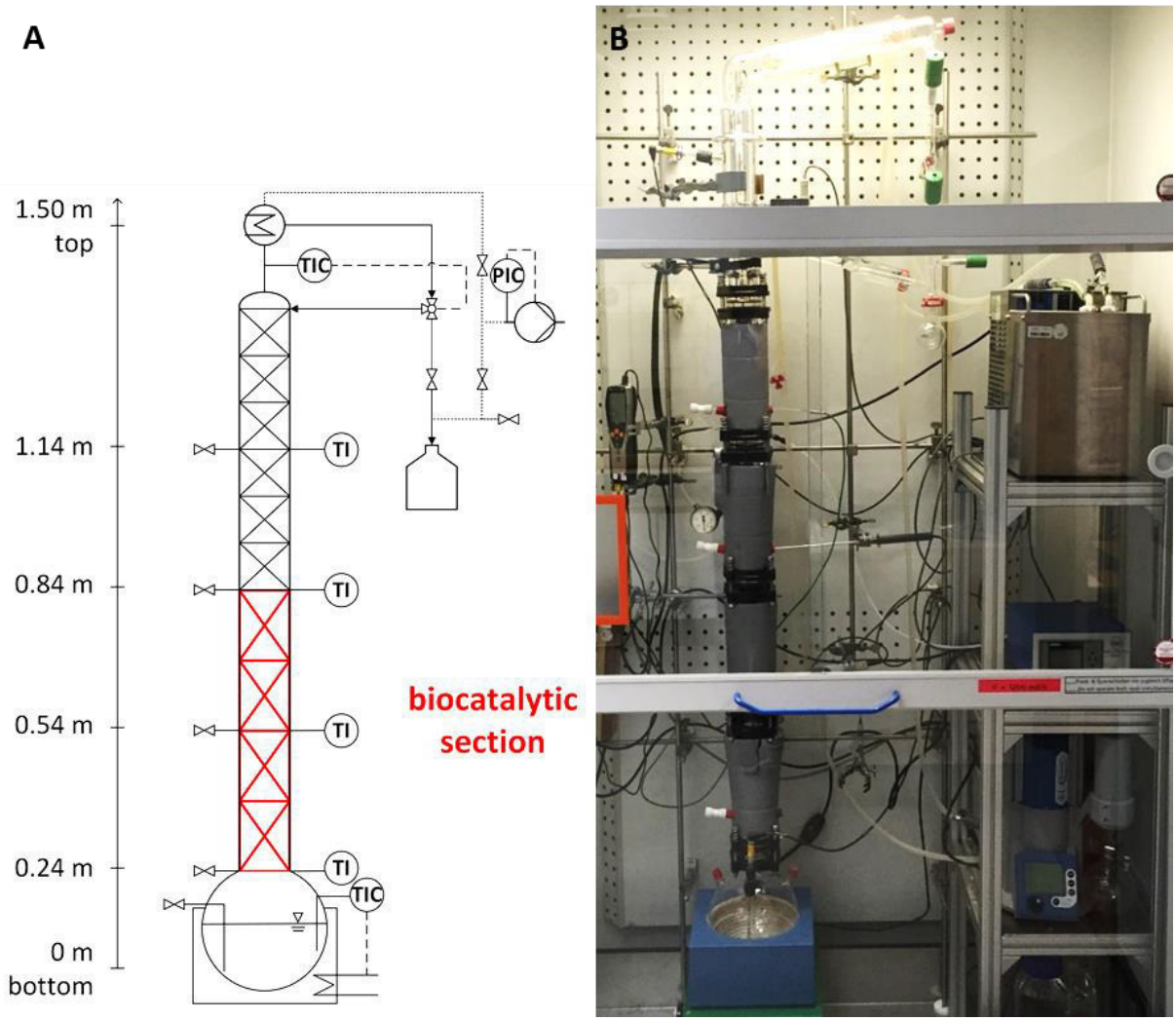

Figure 3.1: Scheme (**A**) and picture (**B**) of the applied batch reactive distillation (RD) setup [137]. The 6 column heights represent the sampling positions during operation as well as the location of temperature measurements (TI), controlled temperature (TIC) and controlled pressure (PIC). An exemplified distribution of the biocatalyst (biocatalytic section) and non-catalytic section (residual part of RD) is presented.

Condensation of the vapor stream took place on top of the column via connection of the condenser to a closed cycle cooling system. The inner part of the condenser was equipped with a swingable glass cylinder containing a magnet for reflux control in dependency of temperature (TIC, top). By controlling the position of the glass cylinder, downcoming liquid was either flushing back into the packing height

or could be automatically withdrawn from the column via a separately cooled sampling tube (Top = 1500 mm). The samples were fractionated in collecting vessels, which could be replaced in variable time intervals for analysis during operation. For the adjustment of reduced pressures, the condenser was connected to a controlled vacuum pump *PC3001 VARIO*^{pro} (Vacuubrand GmbH & Co. KG, Wertheim, Germany) to realize constant pressure during operation (PIC). Sampling in the bottom of the column (Bottom = 0 mm) and in each tube of the packing height (H1 = 240 mm, H2 = 540 mm, H3 = 840 mm, H4 = 1140 mm) was performed manually through silicone septa of vacuum stable sample ports.

For **fractional distillation**, two strategies of adjusting the reflux ratio were applied. Generally, the reflux ratio (*rr* [-]) is defined by the ratio of condensed volumetric liquid flow back into the column ($\dot{V}_L$ [L·s^{-1}]) and the withdrawn distillate flow at the top of the column ($\dot{V}_D$[L·s^{-1}]) (**Eq. 22**).

$$rr = \frac{\dot{V}_L}{\dot{V}_D} \qquad \textbf{Eq. 22}$$

Both strategies for the reflux ratio in this work were characterized by a split in the liquid flow via magnet induced switching of a glass funnel, which was placed in the condenser of the RD setup. The funnel could be in an *OFF*-position or an *ON*-position, while its movement was either adjusted manually or temperature controlled. In the case of manual operation, a fixed algorithm with respect to time could have been started at any point of operation to enable a change in the position of the funnel. If a reflux ratio of *rr* = 10 was adjusted, liquid was flushing back into the column for *t* = 10 s in the *OFF*-position followed by *t* = 1 s in *ON*-position in order to strip accumulated compounds at the column top (**Figure 3.2**, **A**). In contrast, the temperature-controlled operation initiated funnel movement in dependency of a fixed temperature value (T_{border}), measured by a resistance thermometer PT100 at Top position (**Figure 3.2**, **B**). Hence, the same algorithm with respect to time was started for *rr* = 10, if the measured column temperature was lower than T_{border}. Otherwise, the funnel was constantly in the *OFF*-position.

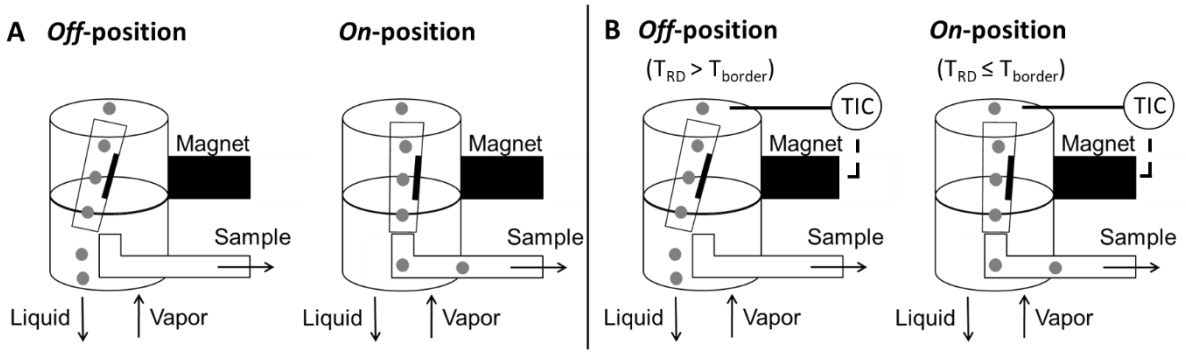

Figure 3.2: Reflux strategies for fractional distillation by magnet induced switching of a glass funnel. **A**: manual reflux operation, **B**: automated temperature-controlled reflux operation. T_{RD} = temperature in the top of the reactive distillation setup, T_{border} = given limiting value for temperature to initiate funnel movement.

Catalyst integration in RD: In all presented and discussed RD experiments, a combination of catalytic and non-catalytic packing elements is applied in flexible arrangements to allow reaction performance of kinetic resolution. Catalytic packing elements (h = 100 mm, d = 43 mm, $a_{spec.}$ = 210 $m^2 \cdot m^{-3}$) were created by placing NZ435 in baskets of Katapak-SP-like wire gauze structures provided by Sulzer Chemtech (Winterthur, Switzerland). Biocatalytic capacity of one catalytic packing element is up to m_{NZ435} = 8 g. As long as less amounts of NZ435 were applied per catalytic packing element, increased catalyst distribution was achieved by adding glass beads to the wire gauze baskets. A loss of NZ435 through the wire gauze baskets during preparation of catalytic packing elements is prevented by sieving the particles to a diameter of $d_p \geq 630$ µm. Additional preparation and fixation of self-made mesh funnels (d = 50 mm) at the bottom of the catalytic packing elements caused increased liquid flows through the catalytic baskets by collecting downcoming liquid from the column wall. Preparation of the catalytic packing elements is depicted in **Figure 3.3**.

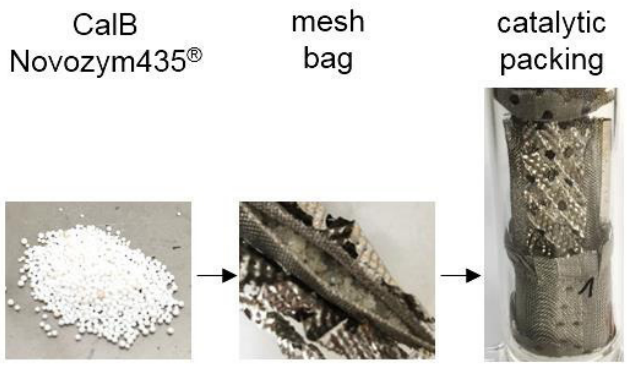

Figure 3.3: Procedure to create catalytic packing elements with NZ435 placed in baskets of Katapak-SP-like wire gauze packing elements (taken from Kühn et al. (2017) [137])

Non-catalytic regions in the column were equipped with Montz A3-500 (Julius Montz GmbH, Hilden, Germany) wire gauze column internals (h = 60 mm, d = 43 mm, $a_{spec.}$ = 500 $m^2 \cdot m^{-3}$). In those regions, increased separation efficiency of the non-catalytic packings was realized by exhibiting a larger surface area compared to the catalytic packing elements. The applied distributions and amounts of NZ435 for the RD column experiments, which will be discussed in **section 5.3** and **5.4**, are summarized in **Table 3.6** and **Table 3.7**.

Table 3.6: Equipped distribution of column internals for batch reactive distillation experiments

	***(R/S)*-2-PeOH / EtBu**		***(R/S)*-2-PeOH / PrBu**									
x_0 [%]	**10:90**		**10:90**		**60:40 (A)**		**60:40 (B)**		**65:35**		**67:33**	
Packing	n_{CP}	n_P	n_{CP}	n_P	n_{CP}	n_P	n_{CP}	n_P	n_{CP}	n_P	n_{CP}	n_P
H4	-	3	-	3	1	2	-	3	1	2	1	2
H3	-	3	-	3	1	2	-	4	1	2	1	2
H2	2	-	-	3	1	2	2	1	2	1	2	1
H1	2	-	2	-	1	2	2	1	2	1	2	1
Sum	4	6	2	9	4	8	4	9	6	6	6	6

H_i = column height divided into the glass tubes in the reactive distillation setup
n_{CP} = number of catalytic packing elements (Katapak-SP-like)
n_P = number of non-catalytic packing elements (Montz A3-500)
x_0 = initial molar fraction of the starting materials

Table 3.7: Amount and distribution of NZ435 per catalytic column internal in batch reactive distillation experiments

	***(R/S)*-2-PeOH / EtBu**	***(R/S)*-2-PeOH / PrBu**				
x_0 [%]	**10:90**	**10:90**	**60:40 (A)**	**60:40 (B)**	**65:35**	**67:33**
Catalyst	m_{NZ435} [g]	m_{NZ435} [g]	m_{NZ435} [g]	m_{NZ435} [g]	m_{NZ435} [g]	m_{NZ435} [g]
H4	-	-	7.54	-	6.85	6.85
H3	-	-	7.03	-	8.08	8.08
H2	3.46	-	7.98	14.57	14.57	14.57
H1	3.04	6.15	7.81	15.79	15.79	15.79
Sum	6.50	6.15	30.36	30.36	45.29	45.29

F-factor calculation within RD experiments: The vapor load in the applied column setup expressed by the **F-factor (F_V)** was estimated via the following **Eq. 23**. It involves the gas velocity (u_V [m·s^{-1}]) in the column and the vapor density (ρ_V [kg·m^{-3}]). While the gas velocity was accessible by the ratio of the vapor mass flow ($\dot{m}_V$ [kg·s^{-1}]) through the cross-sectional column area, an average density between the bottom and top of the column was assumed to determine a constant ρ_V. The mean density in the column was calculated by the obtained molar fractions in stationary column experiments without catalyst at the bottom and the top of the column, assuming ideal gas behavior for binary mixtures of the starting materials.

$$F_V = u_V \cdot \sqrt{\rho_V} = \frac{\dot{m}_V}{\sqrt{\rho_V} \cdot \frac{\pi}{4} \cdot d^2} \qquad \textbf{Eq. 23}$$

For the determination of the vapor mass flow ($\dot{m}_V$ [kg·s^{-1}]), an energy balance at the reboiler stage of the column was performed according to **Eq. 24**:

$$\dot{m}_V = \frac{\dot{Q}_{heat}}{h_V} \qquad \textbf{Eq. 24}$$

The introduced heat flow $\dot{Q}_{heat}$ [W] into the column was calculated based on experimentally determined vapor mass flows. They are referred to water evaporation at various adjusted temperatures within the heating device, monitoring a time dependent temperature increase in the round bottom flask of the reactive distillation setup. Transferring the obtained values for $\dot{Q}_{heat}$ to the mass flow ($\dot{m}_V$) of the starting materials *(R/S)*-2-PeOH and PrBu was done via substitution of the vaporization enthalpies (h_v [J·mol^{-1}]). Final determination of h_v accounted for the mean enthalpy calculated with literature data and considering the initially applied molar fractions of *(R/S)*-2-PeOH and PrBu [138] [139]. An overview on the correlation data for $\dot{Q}_{heat}$ in dependency of the temperature difference between the electric heating device and the mean column temperature is given in **appendix section A**, while the final F-Factors for the column experiments are integrated in **Table 3.8**.

Calculation of reaction performance in RD experiments: Evaluation of experimental data in reactive distillation equipped with catalytic packing elements was performed by expressing the course of enantiomeric excess (*ee*) with increased conversion (*X*). In contrast to single-phase experiments in standard batch vessels, the additional vapor phase in reactive distillation caused a liquid hold-up of reactants in the packing height and the condenser stage. Therefore, the conversion (*X*) became a function of the liquid hold-up in the column, which reduced the moles in the bottom of the column. The stationary **liquid hold-up ($V_{HU,stat}$ [mL])** of the applied Katapak-SP-like packing elements and the Montz A3-500 column internals was specified within the weight difference under wet and dry conditions. Wet conditions were created by an artificial liquid flow of EtOH, which was sprayed on top of the structured packings. After draining, a liquid hold-up volume for experimental evaluation of $V_{HU,stat}$ = 14.7 mL for Katapak-SP-like packing elements and $V_{HU,stat}$ = 5.0 mL for Montz A3-500 was determined. For the condenser, $V_{HU,stat}$ = 9 mL was estimated consisting of the liquid hold-up at the inner surface area as well as in the swingable glass cylinder. In dependency of the equipment regarding catalytic and non-catalytic packing elements, the liquid hold-up for the performed experiments was defined for the different column sections comprising each glass tube of the packing height as well as the condenser stage. In fact, it was assumed to have a significantly higher stationary liquid hold-up compared to dynamic hold-up volumes in the column. For the dynamic hold-up in presence of Katapak-SP-like packing elements, $V_{HU,dyn}$ = 5 - 10 mL per glass tube was estimated within the packing height. The sum of all partial stationary and dynamic liquid hold-up volumes resulted in the overall column

hold-up (V_{HU}), which is summarized together with the operation conditions for the performed experiments in **Table 3.8**.

Table 3.8: Operation conditions for batch reactive distillation experiments

	KR of chiral alcohol: *(R/S)*-2-PeOH / EtBu	**KR of chiral alcohol: *(R/S)*-2-PeOH / PrBu**				
x_0 [%]	**10:90**	**10:90**	**60:40 (A)**	**60:40 (B)**	**65:35**	**67:33**
m_0 [g]	800	800	800	800	800	800
p [mbar][a]	100	80	80	80	80	80
rr	manually	controlled	controlled	controlled	controlled	controlled
F [$Pa^{0.5}$][b]	-	2.4	1.8	1.8	1.8	1.9
V_{HU} [mL]	117.8	93.4	127.8	132.8	157.2	157.2
T_{heat} [°C][c]	280 - 300	290 - 300	250	240 - 250	250 - 260	250 - 270
T_{cool} [°C][c]	2	2	2	2	2	2

[a]given numbers account for mean values over the whole time of experiment
[b]estimated on the basis of a binary mixture of the starting materials
[c]values refer to the adjusted temperature conditions

Beside the liquid hold-up, sampling at different column positions and stripping of low boiling components at the top of the column were considered in a mole balance over the whole column to calculate the actual number of moles for all present reactants within the different column sections at any time during operation. Thereby, partial terms of moles (*n*) were obtained at the investigated sampling ports (*j = Bottom, H1, H2, H3, H4, Top*), of which the sum was used to calculate the **overall conversion (*X*)** in the column at any time point $t > t_0$ (**Eq. 25**). It was assumed to have the same molar fractions present in the whole glass tube of the packing height as measured in the corresponding sampling port (H1, H2, H3, H4).

$$X = \frac{n_{(R)-2-PeOH,0} + n_{(S)-2-PeOH,0} - \sum_j (n_{(R)-2-PeOH,t,j} + n_{(S)-2-PeOH,t,j})}{n_{(R)-2-PeOH,0} + n_{(S)-2-PeOH,0}} \qquad \textbf{Eq. 25}$$

Similar calculation by the sum of partial terms with respect to the column sections was performed for the **enantiomeric excess (*ee*)** of the chiral starting material (*(R/S)*-2-PeOH, **Eq. 26**) and the formed product (*(R/S)*-2-PeBu, **Eq. 27**).

$$ee_S = \frac{\sum_j n_{(S)-2-PeOH,t,j} - \sum_j n_{(R)-2-PeOH,t,j}}{\sum_j (n_{(S)-2-PeOH,t,j} + n_{(R)-2-PeOH,t,j})} \qquad \textbf{Eq. 26}$$

$$ee_P = \frac{\sum_j n_{(R)-2-PeBu,t,j} - \sum_j n_{(S)-2-PeBu,t,j}}{\sum_j (n_{(R)-2-PeBu,t,j} + n_{(S)-2-PeBu,t,j})} \quad \textbf{Eq. 27}$$

As long as the applied biocatalyst NZ435 does not form any side-products in the investigated kinetic resolution reactions, the conversion (*X*) becomes equal to the yield (*Y*) (**section 2.2.4**) and in this case both equations become valid to generate the presentation of data in an enantiomeric excess - conversion diagram (**Eq. 25** or **Eq. 28**).

$$X = Y = \frac{\sum_j n_{(R)-2-PeBu,t,j} - \sum_j n_{(S)-2-PeBu,t,j}}{n_{(R)-2-PeOH,0} + n_{(S)-2-PeOH,0}} \quad \textbf{Eq. 28}$$

Reproducibility in reactive distillation experiments: All experimental errors for the conversion (*X*), the enantiomeric excess (ee_S) and the molar fractions of the reactants (x_i) in batch reactive distillation account for their maximum errors ($\triangle z$) according to **Eq. 29**. The maximum error Δz consists of *m* variable dependent or independent terms, which are equal to the number of influencing factors on the parameter *x*. Each individual term is formed by the product of the first derivative and the corresponding standard deviation (Δx_j).

$$\Delta z = \sum_{j=1}^{m} \left| \frac{\partial f}{\partial x_j} \cdot \Delta x_j \right| \quad \textbf{Eq. 29}$$

In this work, the influencing factors were represented by the moles of the participating reactants. Predominantly, deviations in gas chromatography (GC) analysis, in the mass balance of the experiment and in the hold-up volume were expected. Standard deviations in GC account for twice performed sample analysis. The mass balance at the start and the end of an experiment considered sampling during operation at different column heights, residual liquid amounts in the packing height and collected liquid in cooling traps beyond the vacuum pump (1.3 – 5.5 %). With respect to the column hold-up, deviations during operation of up to 10 % were assumed. In dependency of the investigated parameter (*X*, *ee*, x_i), different combinations of those error sources were applied to determine reasonable errors. For the conversion (*X*), all three error sources are considered, while for errors in the mole fractions (x_i) a combination of deviations in gas chromatography (GC) analysis and the mass balance were involved (changed hold-up volumes did not influence the fraction of a compound). The error of the enantiomeric excess (*ee*) only depended on gas chromatography (GC) analysis, which was referred to the involved relation of identically boiling compounds within the determination of *ee.* The corresponding mean errors ($\overline{\Delta z}$) within reactive distillation experiments are listed in **Table 3.9**.

Table 3.9: Calculated errors in reactive distillation experiments with respect to maximum error determination. Numbers for the mean deviation ($\overline{\Delta z}$), the lowest deviation ($\triangle z_{min}$) and the highest deviation ($\triangle z_{max}$) are given for the parameters conversion (X), enantiomeric excess ($ee_{(S)\text{-}2\text{-}PeOH}$) and the molar fractions of applied reactants (x_i).

	***(R/S)*-2-PeOH / EtBu**	***(R/S)*-2-PeOH / PrBu**				
x_0 [%]	**10:90**	**10:90**	**60:40 (A)**	**60:40 (B)**	**65:35**	**67:33**
deviation	$\overline{\Delta z}$ ($\triangle z_{min}$, $\triangle z_{max}$) [%]	$\overline{\Delta z}$ ($\triangle z_{min}$, $\triangle z_{max}$) [%]				
$ee_{(S)\text{-}2\text{-}PeOH}$[a]	0.2 (0.1, 0.2)	0.9 (0.1, 4.8)	0.1 (0.1, 0.5)	0.1 (0.1, 0.2)	0.1 (0.1, 0.2)	0.1 (0.1, 0.2)
X[a]	3.2 (0.6, 4.7)	2.7 (0.8, 6.4)	2.8 (0.1, 5.7)	3.4 (0.8, 1.7)	2.6 (0.3, 7.0)	1.9 (0.1, 3.6)
$x_{(S)\text{-}2\text{-}PeOH}$[b]	9.6 (9.2, 10.4)	7.2 (3.3, 9.0)	7.8 (1.9, 9.3)	7.8 (2.3, 10.9)	3.7 (0.4, 6.6)	2.5 (0.4, 5.0)
$x_{(R)\text{-}2\text{-}PeOH}$[b]	9.5 (9.5, 9.5)	9.4 (8.9, 9.8)	9.4 (8.2, 9.8)	10.9 (11.3, 12.5)	5.7 (5.6, 7.1)	3.3 (2.5, 10.3)
$x_{(S)\text{-}2\text{-}PeBu}$[a]	10.2 (9.6, 11.5)	10.8 (9.6, 17.9)	9.8 (9.0, 11.4)	11.1 (9.6, 13.0)	2.8 (0.7, 5.5)	2.9 (2.5, 3.6)
$x_{(R)\text{-}2\text{-}PeBu}$[a]	9.4 (9.1, 9.9)	9.9 (8.8, 16.5)	5.8 (2.5, 9.8)	6.6 (2.7, 11.5)	5.6 (5.2, 6.3)	1.6 (0.2, 3.1)
x_{EtBu}, x_{PrBu}[b]	4.4 (1.0, 7.5)	7.3 (1.1, 9.3)	9.4 (8.8, 9.9)	10.7 (10.0, 11.3)	6.0 (5.5, 7.3)	3.4 (2.7, 5.4)
x_{EtOH}, $x_{1\text{-}PrOH}$[b]	5.6 (2.4, 9.3)	4.2 (1.6, 9.2)	2.8 (0.8, 8.7)	4.2 (0.9, 9.7)	3.0 (0.9, 10.0)	1.4 (0.5, 4.1)

[a]referred to the bottom of the reactive distillation column
[b]referred to the top of the reactive distillation column

3.5. Setup for Dynamic Kinetic Resolution

Integrated chemo-enzymatic dynamic kinetic resolution with separated catalysts was conducted in an evacuated Soxhlet reactor setup (h = 600 mm, **Figure 3.4**). At the bottom of the setup, a batch vessel surrounded by an oil bath represented the reboiler region to evaporate applied reactants and generate a vapor stream. The batch vessel was filled with the pretreated starting materials (*(R/S)*-2-PeOH and EtBu), the solvent material (*p*-xylene) as well as the chemocatalyst for racemization at the beginning of each experiment. It was connected to a Soxhlet-extractor, which typically consists of a vertical glass tube with two separate lines. The 'vapor line' was empty and let the vapor stream rise to the top of the setup. During operation, uprising vapor was condensed by a reflux condenser at the top of the setup, which caused a liquid flow through the second line of the extractor unit. In the second line, the immobilized biocatalyst (NZ435) was placed either in the upper part or in the lower part, while the

residual volume was filled with glass beads (d = 2 -3 mm). This 'liquid line' contained a valve for liquid reflux in the lower part to allow circulation of reactants back to the batch vessel and simultaneously prevented a contact of both applied catalysts. Due to the cooling effect in the condenser, a reduced temperature was present in the condensed droplets of the liquid flow and consequently at the position of the biocatalyst as well. Overpressure in the evacuated system was prevented by the connection of a balloon at the top of the reflux condenser. At the same position, either nitrogen flow or vacuum was applied via a flexible shifted valve in a connected Schlenk-line to evacuate the system and reduce deactivation of the racemization catalyst by molecular oxygen.

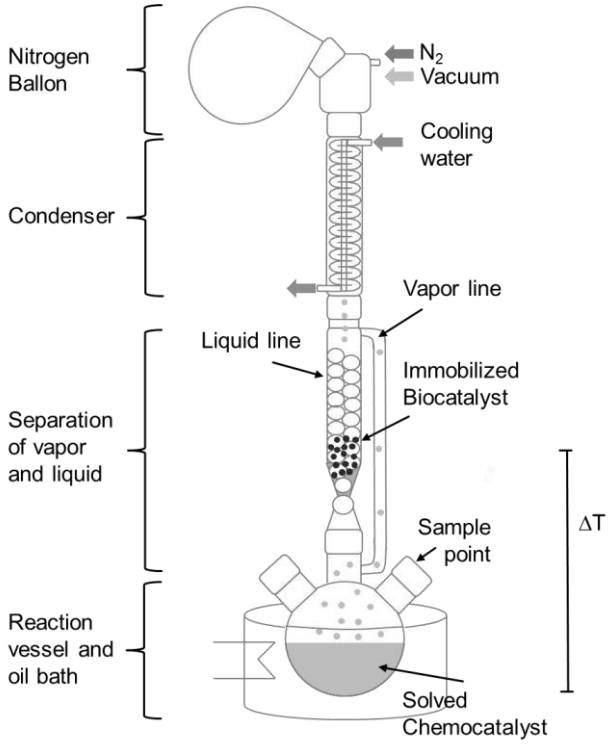

Figure 3.4: Integrated soxhlet reactor setup for chemo-enzymatic dynamic kinetic resolution with separated catalysts

For each experiment, three evacuation intervals were done. Additionally, all connection parts were sealed with Teflon tape and applied glassware was flamed prior to use to get rid of moisture. In the batch vessel, m = 1 g dried sodium carbonate (Na_2CO_3) supported the absence of oxidizing species during operation. All reactants and the racemization catalyst were added under evacuated conditions at room temperature and mixing within the batch vessel was realized by a magnetic stir bar to circumvent delays in boiling. Sampling during operation was performed through silicone septa and temperature was monitored in the reboiler region (resistance thermometer) as well as in the 'liquid line' (infrared thermometer) to analyze the temperature at the position of both catalysts. With respect

to promising results of *Bogar et al. (2007)* in classical chemo-enzymatic DKR, the weight ratio of NZ435 to Shvo catalyst for DKR was adjusted to 1.56 $g_{NZ435} \cdot g_{Shvo}^{-1}$ [124].

Operation in the **classical DKR approach by adding both catalysts in batch vessels** was performed with reactor volumes of V = 2 mL in standard batch vessels, which were evacuated similar to the conditions described in the section of the Soxhlet reactor setup. In contrast to the Soxhlet reactor setup, both catalysts were operated at the same temperature in this classical DKR approach.
The operation conditions for chemo-enzymatic DKR with spatially separated and not separated catalysts are summarized in **Table 3.10**.

Table 3.10: Overview on operation conditions in chemo-enzymatic dynamic kinetic resolution of *(R/S)*-2-PeOH with EtBu in *p*-xylene.

	Soxhlet reactor setup (spatially separated catalysts)		**Batch vessel (not separated catalysts)**	
x_0 [%] (EtBu : *(R/S)*-2-PeOH : *p*-xylene)	**54 : 23 : 23**	**54 : 23 : 23**	**56 : 24 : 20**	**82 : 11 : 7**
p [mbar]	1013	1013	1013	1013
m_o [g]	13	13	2.2	1.5
m_{NZ435} [g]	0.25	0.25	0.035	0.035
m_{Shvo} [g]	0.16	0.16	0.022	0.022
T_{NZ435} [°C]	31 ± 2	57	32	65
T_{Shvo} [°C]	183 ± 5	183 to 193	32	65
$\Delta T_{Catalysts}$ [°C]	152 ± 4	135	0	0
p [mbar]	1013	1013	1013	1013
n [-]	2	1	1	1

4. SCOPE OF WORK

The aim of the present study will be the development of an approach for feasible reaction performance with biocatalysts in an integrated batch reactive distillation (RD) setup (**Figure 4.1**). Within the biocatalytic RD setup, it will be of special interest to realize *in situ* separation and isolation of chiral target compounds in contrast to the well-established case of non-chiral compounds in course of RD with chemical catalysts. Hence, a new set of target compounds should be addressed for RD resulting from the application of biocatalysts. On the other hand, challenging aspects such as thermal deactivation of biocatalysts should be overcome in biocatalytic RD to be attractive for industrial application in future times. With respect to economic evaluation, increased amounts of chiral target compounds can theoretically be achieved by solvent-free application of the starting materials and well-chosen reactants to generally allow their *in situ* isolation within the RD setup.

Therefore, a preselection (**A**) and characterization (**B**) part will be performed to select theoretically feasible candidates and verify them experimentally with respect to their implementation in biocatalytic batch RD. While the preselection phase should be supported by property data from literature, stirred tank reactors (STR) will be taken into account for experimental studies.

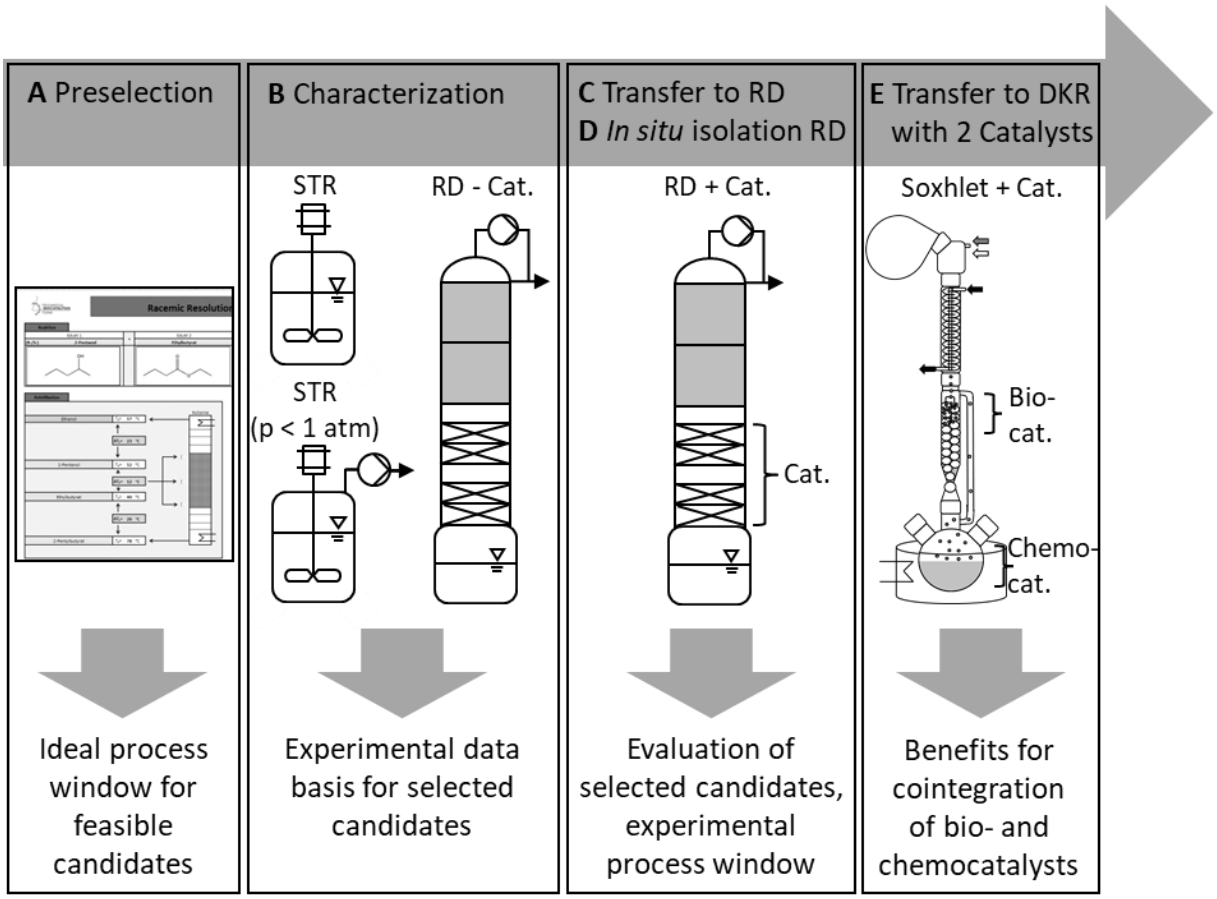

Figure 4.1: Approach of the present work

The experiments in stirred tank reactors (STR) should provide influencing parameters of a selected starting material combination such as biocatalytic activity, enantioselectivity, and the identification of equilibrium limitations as well as the thermal stability of the biocatalyst. Furthermore, application of STRs at reduced pressures compared to ambient conditions of p = 1 atm = 1013 mbar (STR p < 1 atm) will be performed to evaluate the necessity of shifting equilibrium limited reactions to the product side. In addition to that, reactive distillation (RD) performance needs to be established and applied without catalyst (RD - Cat.) during the characterization phase. Thereby, the availability of chosen starting materials at different operating conditions can be proven to select a proper position of the biocatalyst for further studies. Based on generated experimental data, interesting starting material combinations ideally will be transferred to RD with catalyst (RD + Cat.) (**C**). As long as a transfer to RD is successful, the major aim will be to identify a strategy for the possibility of *in situ* target compound isolation. This strategy should comprise the variation of influencing parameters (i.e. fractional distillation, position of the biocatalyst, racemic starting molar fraction) to determine a process window for an interesting candidate with *in situ* target compound isolation (**D**) and perform economic evaluation of this reaction system. In the case of a achieving the *in situ* isolation and demonstrating the feasibility of biocatalytic RD, the application of a cointegrated approach by a biocatalyst and a chemocatalyst in a Soxhlet reactor setup (Soxhlet + Cat.) will be considered and investigated (**E**) to evaluate the feasibility of broadening the application of biocatalytic batch RD to dynamic kinetic resolution (DKR).

The working packages **A** - **E** of the developed approach depicted in **Figure 4.1** will be discussed in detail in the following sections of **chapter 5**:

A Selection of Applicable Reactions for Biocatalytic Reactive Distillation (**section 5.1**)
B Characterization of Kinetic Resolution Reactions for Biocatalytic Reactive Distillation (**section 5.2**)
C Implementation of Selected Reactions in Biocatalytic Reactive Distillation (**section 5.3**)
D Chiral Target Compound Isolation in Biocatalytic Reactive Distillation (**section 5.4**)
E Combination of Chemo- and Biocatalysts by Dynamic Kinetic Resolution (**section 5.5**)

5. RESULTS & DISCUSSION

5.1. Selection of Applicable Reactions for Biocatalytic Reactive Distillation

For the successful application of biocatalysts in an integrated batch reactive distillation column (RD), the selection of starting materials prior to experimental studies is focused in the first part of the result section. The investigated type of catalyzed reaction is the kinetic resolution (KR) of short chain racemic alcohols with non-chiral esters (**section 2.2.4**). In **Figure 5.1**, the generated interface in Microsoft Excel for comparing different starting materials is presented.

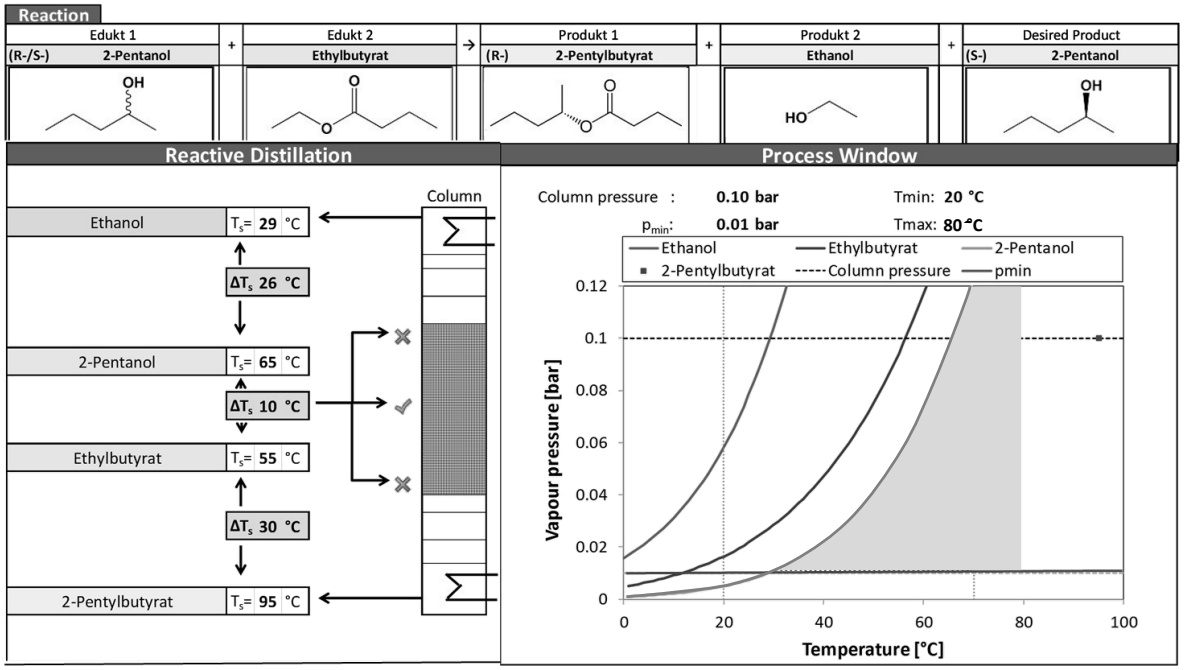

Figure 5.1: Implemented preselection tool to identify feasible starting material combinations for biocatalytic reactive distillation

Implemented racemic starting alcohols comprise butyl-, pentyl- and hexyl-alcohols with one chiral center and their derivatives including additional methyl or dimethyl sidechains (10 different molecules). The corresponding starting esters range from (iso)-butyrates over (meth)-acrylates to isovalerates with methyl-, ethyl- or propyl moiety (12 different molecules). An overview on the starting materials is given in **appendix section B** (**Table B.1**). With respect to its unique properties, lipase B from *Candida antarctica* (CalB) is the selected catalyst throughout the whole work (**section 2.2.3**). In this part, theoretical application of the 120 different combinations for KR in RD is evaluated by literature data on the implemented reactants taken from the *National Institute of Standards and Technology* (NIST) database [140].In particular, the boiling temperatures of the reactants at varied operating pressures are of interest for biocatalytic RD due to thermal deactivation of CalB at elevated temperatures. Hence, the major criterion is to

a) operate RD in a feasible temperature range for the chosen biocatalyst CalB (T_{RD}).

At batch RD column temperatures up to $T_{RD} \leq 80$ °C, theoretical feasibility of CalB is expected [37]. Thus, fixed column temperature constrains the boiling points of investigated starting materials. To allow evaporation of the starting materials, reduced pressures in the RD column are considered for decreasing the boiling points according to the corresponding Antoine parameters from *NIST* [140]. For the calculation of the boiling points at varied operating pressures via the Antoine equation (**Eq. 2**, **section 2.1.1**) pure reactants are considered. Simultaneously, batch RD operation is expected to depend on the availability of the starting materials at the position of the biocatalyst as well as the separation of the low and high boiling reactants to overcome reaction equilibria of KR reactions. Therefore, theoretical feasibility of starting material combinations comprises criteria for

b) similar boiling points of the pure starting materials ($\Delta T_{evaporation}$) in the bottom of RD

and

c) separation of low boiling as well as high boiling reactants ($\Delta T_{separation}$) in the column height.

The applied criterion for evaporation ($\Delta T_{evaporation}$) is restricted by a maximum boiling point difference between the pure reactants at varied operating pressures, whereas the border of the separation criteria is given by a minimum boiling point difference. A limiting maximum boiling point difference for evaporation is chosen, because no reaction will take place without the availability of both starting materials at the position of the biocatalyst at high temperature differences. On the other hand, a limiting minimum boiling point difference is necessary for the separation of reactants ($\Delta T_{separation}$).
As long as the three described preselection criteria are fulfilled for a specific combination of starting materials, RD operation is theoretically feasible. In a second step, the selected combination of starting materials should be investigated more in detail with respect to property data (e.g. VLE data) as well as experimental characterization. The described approach is discussed within the following subchapters to select candidates for biocatalytic batch RD:

1. Influence of preselection criteria on the number of feasible combinations (**section 5.1.1**)
2. Selected kinetic resolution reactions and property data (**section 5.1.2**)

5.1.1. Influence of Preselection Criteria on the Number of Feasible Combinations

The influence of the temperature differences between the reactants in KR ($\Delta T_{separation}$ & $\Delta T_{evaporation}$) on the theoretical feasible number of reactions (n_{Reac}) at varied operating temperature of the batch RD column (T_{RD}) was investigated for an operating pressure of p = 100 mbar. Both discussed temperature criteria account for the boiling point differences between the pure compounds. The aim of those

temperature criteria is to serve as an initial decision parameter for evaluating further investigation on a specific starting material combination. The criterion for separation includes the temperature differences between the low boiling reactants as well as the high boiling reactants and is represented by $\Delta T_{separation}$ in **Figure 5.2**, **A**. Evaporation of the starting materials is taken into consideration by $\Delta T_{evaporation}$ in **Figure 5.2**, **B**. For both criteria, the temperature difference ranges from $\Delta T = 2 – 15$ °C while in each case the second criterion is kept constant. Presented lines are implemented for visual aid of the trend.

Figure 5.2, **A** demonstrates a slight decrease in the number of theoretically feasible reactions (n_{Reac}) with rising $\Delta T_{separation}$ at a constant T_{RD} and fixed $\Delta T_{evaporation} < 15$ °C. Moreover, a strong increase in n_{Reac} was observed at rising column temperatures in the range of $T_{RD} = 60 – 80$ °C. While only $n_{Reac} = 44$ were reached for $\Delta T_{separation} > 15$ °C (filled diamonds), stepwise increased reactions of $n_{Reac} = 48$ at $\Delta T_{separation} > 10$ °C (filled squares), $n_{Reac} = 53$ at $\Delta T_{separation} > 5$ °C (filled triangles) and $n_{Reac} = 54$ at $\Delta T_{separation} > 2$ °C (filled squares) were detected to be feasible at a column temperature of $T_{RD} = 80$ °C. At reduced column temperatures of $T_{RD} = 60$ °C, less flexibility in the number of feasible reactions was observed by $n_{Reac} = 6$ ($\Delta T_{separation} > 15$ °C) up to $n_{Reac} = 8$ ($\Delta T_{separation} > 2$ °C).

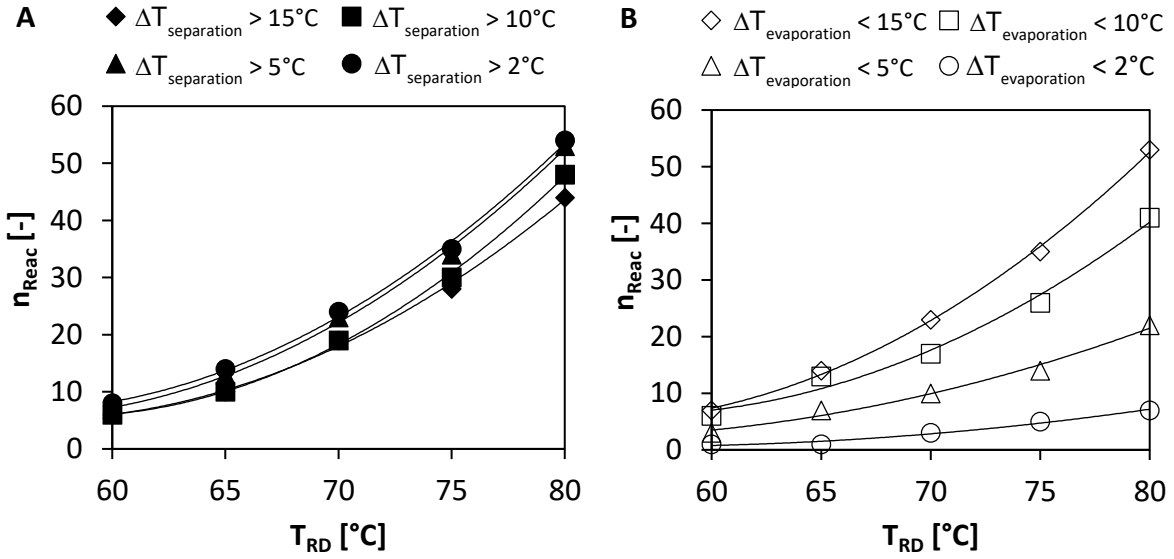

Figure 5.2: Theoretically feasible number of reactions (n_{Reac}) in batch reactive distillation at varied temperature criteria and column temperatures ($T_{RD} = 60 – 80$ °C). **A**: Criterion for separation by boiling point differences between the low and high boiling reactants ($\Delta T_{separation} > 2$ / 5 / 10 / 15 °C) at fixed $\Delta T_{evaporation} < 15$ °C. **B**: Criterion for evaporation by boiling point differences between the starting materials ($\Delta T_{evaporation} < 2$ / 5 / 10 / 15 °C) at fixed $\Delta T_{separation} > 5$ °C.

Hence, the main influencing factor on n_{Reac} with respect to the separation criteria $\Delta T_{separation}$ was T_{RD}, which is determined by the thermal stability of the biocatalyst. Besides, minor effects of a changed separation efficiency in the range of $\Delta T_{separation} > 2$ - 15 °C on n_{Reac} were detected at a fixed T_{RD}. This

observation can be explained by the boiling temperatures of the formed lowest and highest boiling compounds. In the presented case of KR reactions with short chain racemic alcohols and non-chiral esters, the lowest boiling product alcohols are formed by cleavage of the ester compound. Within the investigated reactants, the esters comprise methyl, ethyl or propyl moiety. That is why the low boiler is either methanol, ethanol or 1-propanol, which provides significant decreased boiling temperatures compared to the starting esters. Only if the applied racemic starting alcohol has a low boiling temperature, $\Delta T_{separation}$ is not fulfilled in the preselection tool. Same is true for the highest boiling compound, which is formed by adding the faster reacting enantiomer of the racemic starting material with a butyl, pentyl or hexyl structure on the residual part of the ester compound. By that, considerably increased boiling temperatures for the formed esters are obtained compared to the starting materials. Thus, the separation criterion showed a minor influence on the feasibility of KR in biocatalytic RD.

The results for rising temperature differences between the starting materials ($\Delta T_{evaporation}$) revealed a strong increase in n_{Reac} with rising T_{RD} = 60 – 80 °C in the range of $\Delta T_{evaporation}$ < 15 – 2 °C (**Figure 5.2**, **B**). Moreover, an increased number of reactions was observed with rising $\Delta T_{evaporation}$ at a fixed T_{RD}. Within the presented data on $\Delta T_{evaporation}$, a fixed separation criterion of $\Delta T_{separation}$ > 5 °C is considered. The lowest number of reactions was revealed at low temperature differences between the starting materials of $\Delta T_{evaporation}$ < 2 °C in the range of n_{Reac} = 1 at T_{RD} = 60 °C up to n_{Reac} = 7 at T_{RD} = 80 °C (open circles). At $\Delta T_{evaporation}$ < 5 °C, the number of reactions was increased to n_{Reac} = 3 (T_{RD} = 60 °C) up to n_{Reac} = 22 at T_{RD} = 80 °C (open triangles). A further increase was detected to n_{Reac} = 6 at T_{RD} = 60 °C up to n_{Reac} = 41 at T_{RD} = 80 °C for $\Delta T_{evaporation}$ < 10 °C (open squares). Finally, the highest number of reactions was present at $\Delta T_{evaporation}$ < 15 °C with n_{Reac} = 7 (T_{RD} = 60 °C) up to n_{Reac} = 53 at T_{RD} = 80 °C (open diamonds).

In contrast to the observations for $\Delta T_{separation}$ in **Figure 5.2**, **A**, the evaporation criterion ($\Delta T_{evaporation}$) showed an increased influence on n_{Reac} at a fixed T_{RD} in **Figure 5.2**, **B**. This can be explained by less flexibility toward the boiling points of the starting materials in the preselection approach. While the lowest and highest boiling compounds are predetermined by the length of the applied alcohol residue in the reactants and the reaction mechanism (**Figure 5.2**, **A**), similar boiling points of the starting materials are not present by selecting a random combination of racemic alcohols and an ester compound (e.g. *(R/S)*-3-hexanol and methyl butyrate). If higher $\Delta T_{evaporation}$ were allowed, an increased number of randomly chosen combinations became theoretically feasible. But anyway, only the combined effect of increased thermal stability of the catalyst (T_{RD}) and high $\Delta T_{evaporation}$ resulted in the maximum number of feasible KR reactions in the preselection tool.

Finally, for both temperature criteria ($\Delta T_{separation}$ and $\Delta T_{evaporation}$), T_{RD} was the main influencing factor on n_{Reac}. Therefore, the highest number of reactions can be reached for increased T_{RD} equivalent to

increased thermal stability of the biocatalyst. In fact, thermal stability is predefined by the catalyst preparation applied in RD. Thus, preferably increased $\Delta T_{evaporation}$ and reduced $\Delta T_{separation}$ should be adjusted by the column setup to allow an additional increase in n_{Reac} beside the main influencing criterion of T_{RD}. However, during real evaporation of a binary reactant mixture, actually only one boiling point is present instead of a temperature difference. The application of the preselection criteria of $\Delta T_{separation}$ and $\Delta T_{evaporation}$ was addressed due to a lack of information on vapor liquid equilibria (VLE data) for the investigated starting material combinations. Hence, the performed preselection study simplifies the real behavior by temperature differences between the pure compounds to obtain feasible candidates for reactive distillation. But anyway, experimental investigations should be performed in a second step for promising candidates.

As an additional parameter for an increase in the number of feasible starting material combinations (n_{Reac}), further reduced operating pressure of p = 10 mbar is taken into account to decrease the boiling temperatures of the reactants in accordance to Antoine dependency (**section 2.1.1**). Below pressures of p = 10 mbar, sampling within the applied batch reactive distillation setup described in **section 3.4** becomes challenging. Thus, beside the influence of T_{RD} on the temperature differences $\Delta T_{separation}$ as well as $\Delta T_{evaporation}$, the impact of T_{RD} on the varied operating pressure was investigated in the range of T_{RD} = 60 – 80 °C. In **Figure 5.3**, the feasible number of reactions (n_{Reac}) is presented at virtual reduced pressures of p = 10 mbar (filled bars) and p = 100 mbar (open bars). The criteria for the previously discussed temperature differences were kept constant at $\Delta T_{separation}$ > 5 °C and $\Delta T_{evaporation}$ < 15 °C.
At p = 10 mbar, constant values for n_{Reac} = 44 were observed independent from T_{RD} = 60 – 80 °C. On the contrary, a rising number of n_{Reac} = 7 at T_{RD} = 60 °C up to n_{Reac} = 53 at T_{RD} = 80 °C was present at p = 100 mbar, respectively (see **Figure 5.2**, **B**).

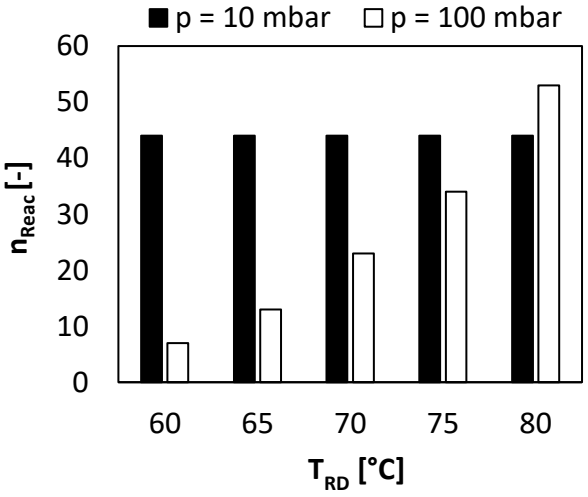

Figure 5.3: Theoretically feasible number of reactions (n_{Reac}) in batch reactive distillation at varied operating pressure (p = 10 mbar, p = 100 mbar) and column temperatures (T_{RD} = 60 – 80 °C). Fixed criteria for $\Delta T_{separation}$ > 5 °C and $\Delta T_{evaporation}$ < 15 °C were considered.

According to the results, a strict reduction of the operating pressure in batch RD was required for all starting material combinations to fulfill theoretical feasibility at reduced T_{RD}. If the virtual operating pressure was reduced to p = 10 mbar, 6 times increased n_{Reac} with respect to the investigated KR were feasible at T_{RD} = 60 °C in comparison to p = 100 mbar. This behavior clearly demonstrates the operating pressure to be the major design variable for increasing n_{Reac} at lower thermal stability of the biocatalyst. Derived from the observations at different operating pressures, highly reduced pressures should be applied to achieve application of biocatalysts with lowered thermal stability. For the investigated KR reactions, at maximum n_{Reac} = 44 (at p = 10 mbar and T_{RD} = 60 °C) and n_{Reac} = 53 (at 100 mbar and T_{RD} = 80 °C) of initially 120 different options were determined to be feasible for further work. Overviews on the feasible combinations at the discussed temperature constraints at p = 10 mbar (T_{RD} = 60 °C) and p = 100 mbar (T_{RD} = 80 °C) are given in **appendix section B** (**Table B.2**, **Table B.3**). The observed reduction in n_{Reac} (**Figure 5.3**) to 37 – 44 % of the theoretical maximum of 120 options was mainly caused by high boiling temperatures of the reactants, which were not evaporating at reduced T_{RD} and the chosen operating pressure. However, increased thermal stability of the biocatalyst allows a constant increase in feasible n_{Reac}. At T_{RD} = 80 °C, it becomes more efficient to operate the column at p = 100 mbar with respect to the resulting number of reactions due to increased n_{Reac} compared to an operating pressure of p = 10 mbar. Therefore, it is always a question of thermal stability of the biocatalyst to get the optimal flexibility with respect to n_{Reac}. Hence, the adjusted operating pressure should be optimized for selected starting materials, individually.

Concise summary of section 5.1.1:

- Increased thermal stability of the biocatalyst allows higher number of feasible kinetic resolution (KR) reactions n_{Reac} in reactive distillation (RD): n_{Reac} = 7 at T = 60 °C, n_{Reac} = 53 at T = 80 °C (p = 100 mbar)
- The lower the thermal stability of the biocatalyst, the lower the pressure that should be applied in RD: p = 100 mbar (n_{Reac} = 7 at T = 60 °C), p = 10 mbar (n_{Reac} = 44, T = 60 °C)

5.1.2. Selected Kinetic Resolution Reactions and Property Data

In order to evaluate the presented preselection tool described and discussed in **section 5.1.1**, two chiral starting materials were selected for a detailed study on their property data.

In the first case, racemic 2-pentanol (*(R/S)*-2-PeOH) and either the non-chiral butyric ester compound ethyl butyrate (EtBu) or propyl butyrate (PrBu) were selected to be the starting materials for kinetic

resolution (KR) with CalB (**Figure 5.4**). The involved substitution of the non-chiral ester should give detailed information on the influence of varied starting materials aiming at the same target compound. This target compound is the less preferentially converted enantiomer *(S)*-2-PeOH of the racemic starting material *(R/S)*-2-PeOH. In both reactions, CalB forms either *(R)*-2-pentyl butyrate (*(R)*-2-PeBu) or *(S)*-2-PeBu within a transesterification. In dependency of the present enantioselectivity for CalB, only the faster reacting enantiomer of *(R/S)*-2-PeOH (here: *(R)*-2-PeOH) is converted under cleavage of low boiling ethanol (EtOH) or 1-propanol (1-PrOH) from the starting ester. Both reactions are part of the preselection tool (**section 5.1.1**).

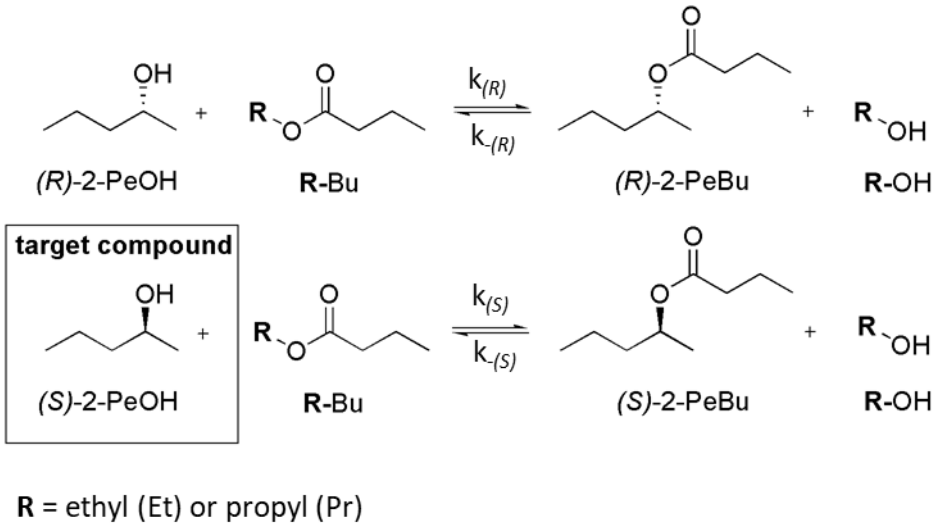

Figure 5.4: Selected kinetic resolution reactions of the racemic starting alcohol *(R/S)*-2-pentanol (*(R/S)*-2-PeOH) with **A:** ethyl butyrate (EtBu) or **B:** propyl butyrate (PrBu) catalyzed by *Candida antarctica* lipase B (CalB). Target compound: *(S)*-2-PeOH, $k_{(R)} >> k_{(S)}$.

In the second case, racemic *(R/S)*-3-hydroxy ethyl butyrate (*(R/S)*-3-HEB) was selected in combination with the non-chiral primary alcohol 1-pentanol (1-PeOH) (**Figure 5.5**).

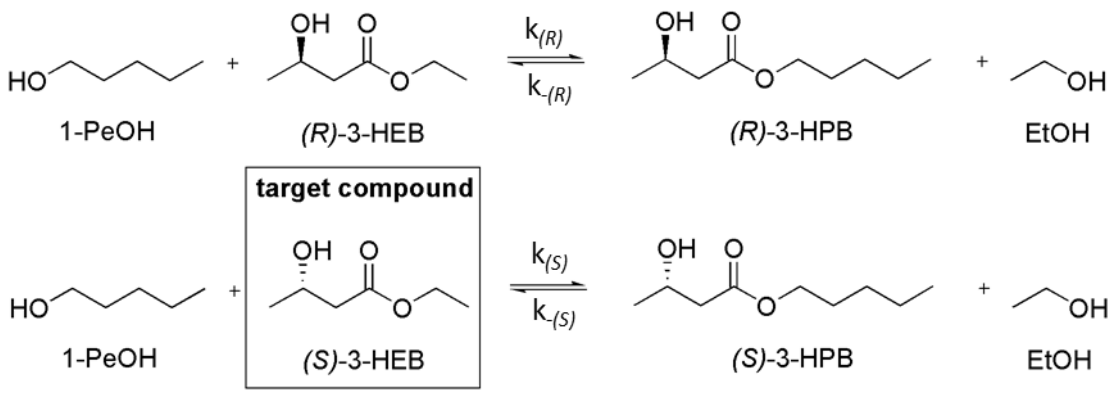

Figure 5.5: Selected kinetic resolution reaction of the racemic starting ester *(R/S)*-3-hydroxy ethyl butyrate (*(R/S)*-3-HEB) with 1-pentanol (1-PeOH) catalyzed by *Candida antarctica* lipase B (CalB). Target compound: *(S)*-3-HEB is the target compound, $k_{(R)} > k_{(S)}$.

Similar to the first case, the residual enantiomer of the starting material (*(S)*-3-HEB) is the target compound and the corresponding pentyl esters *(R)*- or *(S)*-3-hydroxy pentyl butyrate (*(R)*-, *(S)*-3-HPB) are formed in dependency of the enantioselectivity of the applied biocatalyst CalB. Additionally, the low boiler ethanol (EtOH) is produced. The main differences in comparison to the KR of the racemic starting alcohol *(R/S)*-2-PeOH is the switch of chirality to the ester compound. This reaction represents a randomly chosen starting material combination, which is of interest for pharmaceutical industry as an intermediate molecule [141].

To evaluate the feasibility of the selected KR reactions, the Antoine behavior for the pure compounds was used to determine the resulting theoretical operating window. Therefore, the calculated boiling points of the pure compounds (T) are displayed in dependency of the applied column pressure (p) for the selected KR reactions starting either with the racemic alcohol *(R/S)*-2-PeOH (**Figure 5.6**, **A**) or the racemic ester *(R/S)*-3-HEB (**Figure 5.6**, **B**). Experimental data from literature (data points) and parameter estimation calculated by Antoine equation (lines) (**Eq. 2**, **section 2.1.1**) were compared to each other for the starting materials (*(R/S)*-2-PeOH, *(R/S)*-3-HEB, EtBu, PrBu, 1-PeOH) as well as the formed low boiling alcohols (EtOH, 1-PrOH). The boiling points of the formed high boiling pentyl esters (*(R/S)*-2-PeBu, *(R/S)*-3-HPB) were estimated differently, because no information on the Antoine parameters of those compounds was available. For *(R/S)*-2-PeBu (dashed line, **Figure 5.6**, **A**), the estimation was performed based on linear extrapolation of the behavior for methyl, ethyl, propyl and butyl butyrate (R^2 = 0.99). In the case of *(R/S)*-3-HPB (dashed line, **Figure 5.6**, **B**), the group contribution method of Joback was applied to estimate the boiling temperature in dependency of the pressure [142]. For this method, an error in the estimation of 7.2 % was present with respect to the comparison of the available boiling temperature for *(R/S)*-3-HEB (p = 1 bar) and the derived Joback data for *(R/S)*-3-HEB [143] [142]. Furthermore, reasonable operating range of CalB is expected between T = 30 - 80 °C. At T = 80°C, the highest feasible operating temperature with respect to thermal stability of CalB is highlighted by a dotted line.

Independent from the reactant, typical trends of rising vapor pressures were observed at increased temperatures. In **Figure 5.6**, **A**, the theoretical feasible operating range of batch RD for *(R/S)*-2-PeOH with PrBu is represented by a light grey box within T = 30 - 80 °C, whereas the sum of the dark and the light grey box represents the theoretical operating window for KR of *(R/S)*-2-PeOH with EtBu. Those areas are feasible, because any binary mixture of the starting materials can be evaporated and the highest boiling reaction product will not evaporate simultaneously (see **section 2.1.2**). Additionally, changing from ethyl to propyl moiety in the applied ester compound (EtBu or PrBu) resulted in a different boiling point order of the starting materials over the complete range of the operating pressure. While *(R/S)*-2-PeOH (filled diamonds) has an increased boiling point compared to the starting

ester EtBu (filled triangles), *(R/S)*-2-PeOH has a lower boiling point compared to the starting ester PrBu (open triangles). Similarly, the resulting operating window for *(R/S)*-3-HEB with 1-PeOH in **Figure 5.6**, **B** is visualized by a grey box. Obviously, a reduced operating range is theoretically feasible for evaporation of *(R/S)*-3-HEB.

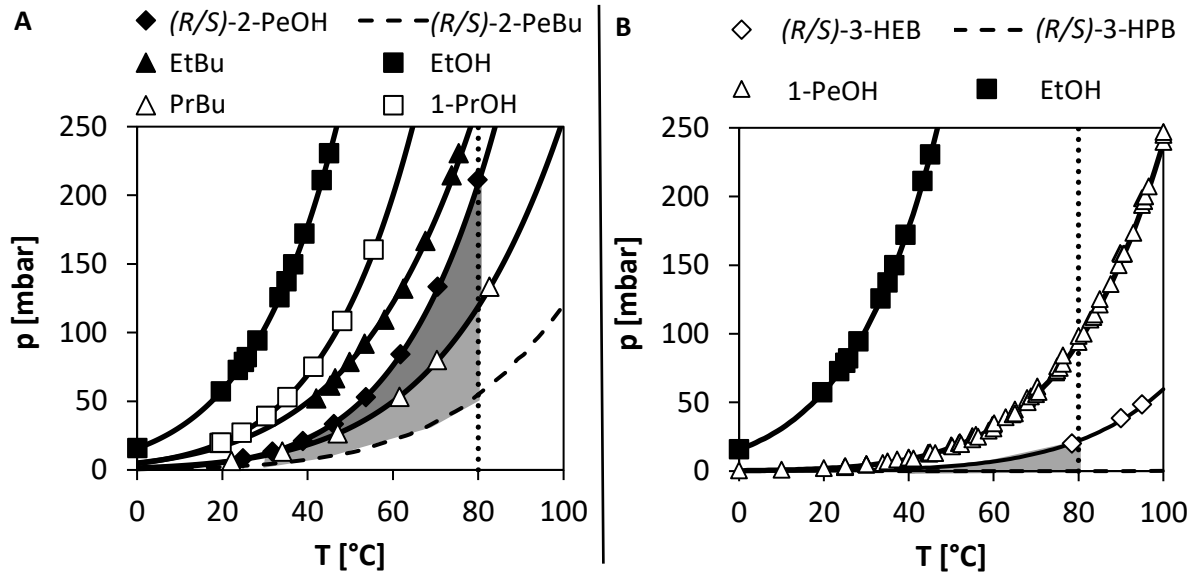

Figure 5.6: Theoretical operating window of the selected kinetic resolution reactions for biocatalytic batch reactive distillation with CalB. **A**: *(R/S)*-2-PeOH with either EtBu (dark + light grey box) or PrBu (light grey box), **B**: *(R/S)*-3-HEB with 1-PeOH (grey box). Dotted line at T = 80°C: limit for thermal stability of CalB, filled lines: calculated Antoine behavior, data points: experimental data from literature (*(R/S)*-2-PeOH [144], EtBu [145], EtOH [146] [147], PrBu [148] [149], 1-PrOH [150], *(R/S)*-3-HEB and 1-PeOH [140]), dashed lines: estimated Antoine behavior for *(R/S)*-2-PeBu by linear extrapolation of methyl-/ethyl-/propyl- & butyl-butyrate, estimated Antoine behavior for *(R/S)*-3-HPB by group contribution method of Joback.

In fact, comparing experimental data from literature (data points) and calculated Antoine behavior (lines) for the starting materials and the low boiling reaction products are in good agreement. Moreover, changing the racemic starting material from *(R/S)*-2-PeOH to *(R/S)*-3-HEB showed a strict influence on the theoretically feasible operating window in the applicable temperature range of the biocatalyst (T_{RD}). This is caused by the substantially increased boiling temperature of *(R/S)*-3-HEB ($T_{boil,(R/S)\text{-3-HEB}}$ = 181 °C) compared to *(R/S)*-2-PeOH ($T_{boil,(R/S)\text{-2-PeOH}}$ = 119 °C). Thus, the racemic starting alcohol *(R/S)*-2-PeOH can be operated in a broader range with respect to the applied column pressure. Furthermore, even slight changes in the moiety of the non-chiral starting material from EtBu to PrBu revealed a different boiling point order of the reactants for the racemic starting alcohol *(R/S)*-2-PeOH. A changed boiling point order of the reactants in principle allows *in situ* separation of the chiral target compound at the top of the RD column by fractional distillation which will be addressed in **section 5.3** and **5.4** of this work.

Beside the operating window with respect to the thermal stability of CalB by feasible T_{RD}, fulfilling the criteria for the temperature differences regarding evaporation ($\Delta T_{evaporation}$) and separation ($\Delta T_{separation}$) at different virtual column pressures can be extracted from the given data in **Figure 5.6**, **A** & **B**. Therefore, the boiling temperatures of the reactants in the investigated starting material combinations are presented at three different column pressures in **Table 5.1**. A successful batch RD operation is expected to be feasible at $\Delta T_{evaporation} < 15$ °C and $\Delta T_{separation} > 5$ °C as long as the boiling temperatures of the starting materials are within the range of $T < 80$ °C.

In the case of *(R/S)*-2-PeOH and EtBu behaving as the starting materials, the preselection criteria are fulfilled at p = 80 mbar ($\Delta T_{evaporation} = 10$ °C, $\Delta T_{separation} > 26$ °C) and 100 mbar ($\Delta T_{evaporation} = 11$ °C, $\Delta T_{separation} > 25$ °C) as well as a maximum boiling temperature for evaporation of up to $T_{boil,(R/S)\text{-2-peOH}} = 65$ °C at p = 100 mbar. At strictly reduced column pressures of p = 10 mbar, the evaporation criterion is not fulfilled ($\Delta T_{evaporation} = 17$ °C). Substituting the ester compound by PrBu revealed theoretical feasibility at all three reduced pressures between p = 10 - 100 mbar. However, increased temperatures of up to $T_{boil,PrBu} = 76$ °C will be necessary for evaporation, which is close to the maximum temperature for $T_{RD} = 80$ °C. Hence, the operating pressure cannot be randomly chosen for changed starting material combination and for further work on *(R/S)*-2-PeOH with EtBu column pressures of p = 100 mbar are selected. To be more flexible in operation of *(R/S)*-2-PeOH with PrBu, a pressure of p = 80 mbar is selected for further parts of this work, which will allow evaporation of the binary mixtures of the starting materials at least at $T_{RD} = 70$ °C. Therefore, similar temperature differences of $\Delta T_{evaporation} = 9$ - 10 °C for the two selected starting material combinations with *(R/S)*-2-PeOH are generated.

In contrast to the selected combinations with *(R/S)*-2-PeOH, starting with *(R/S)*-3-HEB and 1-PeOH gives a temperature difference apart from the feasible range for $\Delta T_{evaporation} < 15$ °C ($\Delta T_{evaporation} = 24$ - 30 °C) at p = 10 - 100 mbar. Additionally, $T_{RD} < 80$ °C can only be achieved at p = 10 mbar for the higher boiling starting ester *(R/S)*-3-HEB ($T_{boil,(R/S)\text{-3-HEB}} = 66$ °C). Only $\Delta T_{separation} > 5$ °C ($\Delta T_{separation} > 48$ -52 °C) is fulfilled within the theoretical operating window for *(R/S)*-3-HEB with 1-PeOH. Hence, feasibility of *(R/S)*-3-HEB and 1-PeOH due to the fixed temperature criteria of the preselection tool is not given.

In order to verify these observations within the preselection criteria, experimental investigation on both racemic starting materials will be performed (**section 5.2**). Moreover, it has to be mentioned that the worst-case scenario was implemented for the preselection criteria with respect to estimated Antoine parameters. In contrast to the pure boiling temperature of the higher boiling starting material, real boiling temperatures of applied starting material mixtures will be in most cases lower than the boiling temperature of the higher boiling starting material. The only exception is the formation of a temperature maximum azeotrope, which does only occur in minor cases [64]. In all other cases, the

pure higher boiling starting material could be evaporated at a given column temperature as long as the preselection criteria are fulfilled.

Table 5.1: Boiling temperatures ($T_{b,i}$) of the reactants and criteria for separation ($\Delta T_{separation}$) as well as evaporation ($\Delta T_{evaporation}$) at varied pressures (p) for the selected kinetic resolution reactions with either *(R/S)*-2-PeOH or *(R/S)*-3-HEB.

	***(R/S)*-2-PeOH / EtBu**			***(R/S)*-2-PeOH / PrBu**			***(R/S)*-3-HEB / 1-PeOH**		
p_{RD} [mbar]	100	80	10	100	80	10	100	80	10
$T_{b,(R/S)\text{-2-PeOH}}$ [°C]	65	61	28	65	61	28			
$T_{b,EtBu}$ [°C]	55	50	11						
$T_{b,PrBu}$ [°C]				76	70	29			
$T_{b,(R/S)\text{-2-PeBu}}$ [°C]	95	89	45	95	89	45			
$T_{b,EtOH}$ [°C]	29	25	-6				29	25	-6
$T_{b,1\text{-PrOH}}$ [°C]				46	42	10			
$T_{b,(R/S)\text{-3-HEB}}$ [°C]							112	107	66
$T_{b,1\text{-PeOH}}$ [°C]							81	76	42
$T_{b,(R/S)\text{-3-HPB}}$ [°C]							172	170	151
$\Delta T_{evaporation}$ [°C]	10	11	17	11	9	1	31	31	24
$\Delta T_{separation}$ [°C]	> 26	> 25	> 17	> 18	> 18	> 16	> 52	> 51	> 48

Previously discussed restrictions by the application of Antoine parameters for pure reactants instead of using VLE data for binary reaction mixtures are exemplary discussed for *(R/S)*-2-PeOH with PrBu. With respect to literature, experimental data on the behavior of binary mixtures are only available for the involved non-chiral ester PrBu with either isopropanol or the racemic starting alcohol *(R/S)*-2-BuOH [151] and mixtures of PrBu with the formed low boiling alcohol 1-PrOH at ambient pressure [152]. Due to strictly reduced availability of experimental VLE data, the non-ideal binary behavior was estimated by the software Aspen properties V8.0 (Aspen Technology, Bedford, Massachusetts, USA) applying the universal quasi-chemical UNIQUAC equation as a g^E model [153]. For the calculation of activity coefficients based on group contribution methods in the UNIQUAC equation, UNIFAC Dortmund parameters (UNIFAC DMD) were used [154].

The results for estimated VLE behavior of binary mixtures of 1-PrOH and PrBu or *(R/S)*-2-PeOH and PrBu at ambient pressure as well as reduced pressure of p = 80 mbar are presented in **Figure 5.7**, **A** - **D**. In **Figure 5.7**, **A**, experimental data from literature are displayed by diamond shaped data points for the vapor mole fraction of low boiling 1-PrOH ($y_{1\text{-PrOH}}$) and squares for the liquid mole fraction of 1-PrOH ($x_{1\text{-PrOH}}$) [152]. The corresponding estimated VLE behavior of the vapor mole fractions ($y_{1\text{-PrOH}}$ / $y_{(R/S)\text{-2-PeOH}}$) are represented by dashed lines and for the liquid mole fractions ($x_{1\text{-PrOH}}$ / $x_{(R/S)\text{-2-PeOH}}$) by filled lines, which are in good agreement with the experimental data.

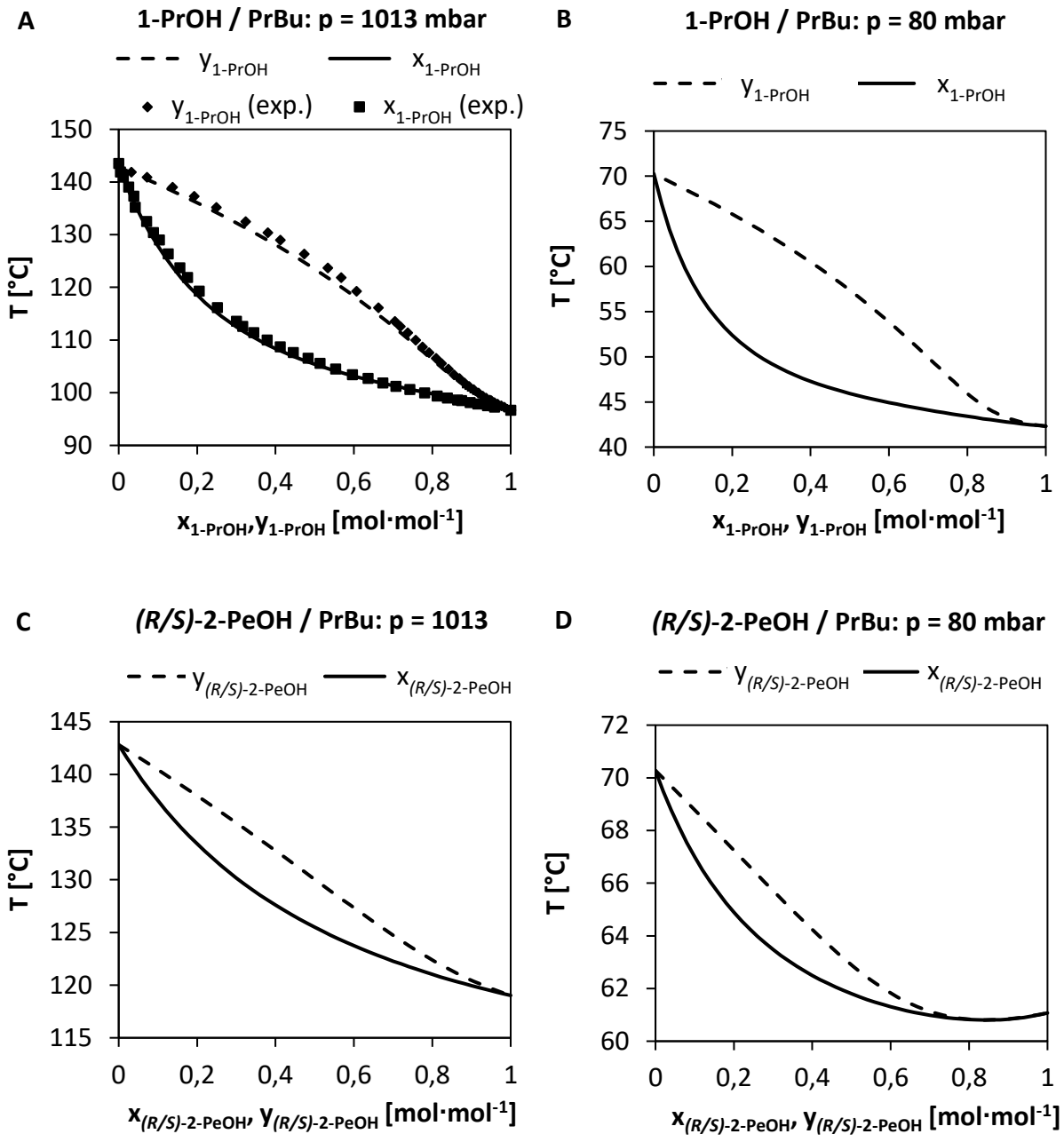

Figure 5.7: Estimated vapor liquid equilibria (VLE) by the software Aspen properties V8.0 for binary mixtures of 1-PrOH and PrBu (**A**: p = 1013 mbar, **B**: p = 80 mbar) as well as *(R/S)*-2-PeOH and PrBu (**C**: p = 1013 mbar, **D**: p = 80 mbar). Filled lines: liquid molar fraction (x_i), dashed lines: vapor molar fraction (y_i), data points: experimental data taken from *Ortega et al. (1995)* [152].

For binary mixtures of 1-PrOH and PrBu at ambient (**Figure 5.7**, **A**) and the desired reduced pressure of p = 80 mbar (**Figure 5.7**, **B**), no azeotropic behavior was detected, although almost similar molar fractions were observed at T = 42.4 °C ($x_{1\text{-PrOH}}$ = 0.99 mol·mol^{-1}, $y_{1\text{-PrOH}}$ = 0.98 mol·mol^{-1}). Therefore, full separation of 1-PrOH and PrBu is feasible according to the estimated VLE data. Similar results of theoretically feasible full separation were obtained for the estimated binary VLE data of *(R/S)*-2-PeOH and PrBu (**Figure 5.7**, **C**). In contrast, estimated *(R/S)*-2-PeOH and PrBu in **Figure 5.7**, **D** revealed

azeotropic behavior at p = 80 mbar, T = 60.8 °C and $x_{(R/S)\text{-2-PeOH}} = y_{(R/S)\text{-2-PeOH}} = 0.84$ mol·mol^{-1} ($x_{PrBu} = y_{PrBu} = 0.16$ mol·mol^{-1}). Hence, *(R/S)*-2-PeOH and PrBu can not easily be fully separated in RD. For all other estimated binary VLE data including the reactants of the KR by *(R/S)*-2-PeOH with PrBu, azeotrope formation is not observed. The corresponding additional VLE data are depicted in **appendix section B** (**Figure B.1**).

By the detection of an azeotrope, the importance of investigating non-ideal behavior between the applied reactants became clear in the preselection phase of a starting material combination for RD application. However, comparing the boiling temperatures of pure reactants to the estimated binary reactant mixture of *(R/S)*-2-PeOH and PrBu within the VLE data revealed a reduced boiling temperature of the formed temperature minimum azeotrope. According to *Ewell et al. (1944)* [64], this temperature minimum azeotrope is present in the majority of cases. Therefore, applicability of the established preselection tool based on temperature criteria for pure compounds is still feasible in the case of temperature minimum azeotropes, because evaporation of the azeotropic mixture with a reduced boiling point is still possible in the range of the presented preselection criteria. Consequently, the number of feasible reactions can be increased if VLE data for all starting material combinations would be available but no restriction for selected starting material combinations occurs for a temperature minimum azeotrope. Only in the case of a temperature maximum azeotrope and a desired operation of RD near to the temperature constraints can cause false theoretical preselection. Furthermore, the desired reaction performance in a biocatalytic batch RD column in principle allows overcoming the azeotropic behavior (**section 5.4**). Finally it can be stated, that the presented approach for preselection takes into account available data for the Antoine parameters to roughly give information on theoretical performance by ideal estimation of pure boiling temperatures, which can be extended by VLE estimation as well as RD column experiments to monitor the real column behavior for interesting candidates.

Concise summary of section 5.1.2:

- Property data need to be considered for the selection of candidates in the preselection phase to identify azeotropic mixtures and adjust the boiling point order of the reactants
- *(R/S)*-2-PeOH with PrBu shows azeotropic behavior during binary VLE-data estimation (azeotropic mixture: p = 80 mbar, T = 60.8 °C and $x_{(R/S)\text{-2-PeOH}} = 0.84$ mol·mol^{-1})

5.1.3. Interim Summary: Selection of Applicable Reactions

- Successfully established preselection tool allows simple comparison with available data from literature (Antoine) and first decision on feasible starting material combinations by discarding many inacceptable combinations at an early stage of investigation
- Preselection is demonstrated for KR reactions of short chain racemic alcohols and non-chiral ester compounds, which can be extended to further reactions (37 - 44 % are feasible according to the applied preselection criteria for the implemented KR reactions)
- Two racemic starting materials are selected for detailed investigation of CalB catalyzed kinetic resolution:

  (R/S)-2-PeOH: with either EtBu or PrBu

  (R/S)-3-HEB: with 1-PeOH
- Their theoretical feasibility ranges can be identified using the applied preselection criteria for evaporation in the column ($\Delta T_{evaporation} < 15$ °C), separation of the reactants ($\Delta T_{separation} > 5$ °C) and the biocatalyst stability ($T_{RD} < 80$ °C):

  (R/S)-2-PeOH with EtBu: all three fulfilled at p = 80 mbar and p = 100 mbar

  (R/S)-2-PeOH with PrBu: all three fulfilled at p = 10 mbar, p = 80 mbar and p = 100 mbar

  (R/S)-3-HEB with 1-PeOH: only $\Delta T_{separation} > 5$ °C fulfilled at p = 10 - 100 mbar

5.2. Characterization of Kinetic Resolution Reactions for Application in Biocatalytic Reactive Distillation

This part deals with the experimental characterization of the selected CalB catalyzed solvent-free kinetic resolution (KR) reactions from **section 5.1** in terms of their feasibility in biocatalytic reactive distillation (RD). In addition to the theoretical feasibility proven in **section 5.1**, performed experiments and their results have to prove the application in small scale approaches within stirred tank reactors (STR) at ambient and reduced pressure. The aim of this part is to generate an experimental data basis for the selected KR reactions to allow a comparison with RD experiments afterwards. In the selected reactions, chirality is either present in the racemic starting alcohol *(R/S)*-2-PeOH or the racemic starting ester *(R/S)*-3-HEB, respectively. A comparison of both chiral starting materials is performed focusing on the following parameters:

1. Influence of catalyst preparation and starting molar fraction on catalytic activity (**section 5.2.1**)
2. Influence of operating temperature on catalyst stability and catalytic activity (**section 5.2.2**)
3. Influence of operating pressure on reaction performance (**section 5.2.3**)
4. Availability of starting materials in reactive distillation experiments (**section 5.2.4)**

5.2.1. Influence of Catalyst Preparation and Starting Molar Fraction on Catalytic Activity

Biocatalytic activity for the selected biocatalyst CalB was investigated within two different catalyst preparations applied in stirred tank reactor (STR) experiments. On the one hand, gel coating procedure was applied in which the biocatalyst is entrapped in a silica matrix following the sol-gel process by *Reetz et al. (1996)* [132] [133] (open bars, **Figure 5.8**). The gel coating material was produced according to the method of *Heils et al. (2015)* and can be implemented in RD via coated Montz A3-500 wire gauze column internals [45]. On the other hand, CalB adsorbed on poly acrylic carrier material known as commercially available Novozym435 (NZ435) was investigated (filled bars, **Figure 5.8**). NZ435 particles can be applied in RD by filling mesh baskets of Katapak-SP-like wire gauze column internals to create catalytic packing elements. In contrast to the application of free biocatalysts, those immobilization techniques can guarantee sufficient fixation within RD column height during operation and allow increased thermal stability compared to the application of free biocatalysts [37] [132] [45].

Measured initial activities for particles produced by the gel coating procedure and NZ435 depicted in **Figure 5.8** showed an 12 - 16 times increase for NZ435 at T = 60 °C comparing the amount of applied catalyst preparation ($U \cdot mg_{NZ435}^{-1}$ and $U \cdot mg_{gel\ coating}^{-1}$). Independent from chirality either in the racemic starting alcohol *(R/S)*-2-PeOH or in the racemic hydroxy ester *(R/S)*-3-HEB, initial activities of NZ435 were $v_0 = 1.97 \pm 0.04\ U \cdot mg^{-1}$ (*(R/S)*-2-PeOH) and $v_0 = 1.89 \pm 0.16\ U \cdot mg^{-1}$ (*(R/S)*-3-HEB) for $c_{NZ435} = 7\ mg \cdot mL^{-1}$ and equimolar initial molar fractions ($x_{i,0} = 0.5\ mol \cdot mol^{-1}$). At the same initial molar

fraction and increased catalyst concentration for the gel coating material ($c_{gel\ coating}$ = 35 mg·mL^{-1}), initial activities of v_0 = 0.07 ± 0.01 U·mg^{-1} (*(R/S)*-2-PeOH) and v_0 = 0.12 ± 0.02 U·mg^{-1} (*(R/S)*-3-HEB) were detected for both reactions.

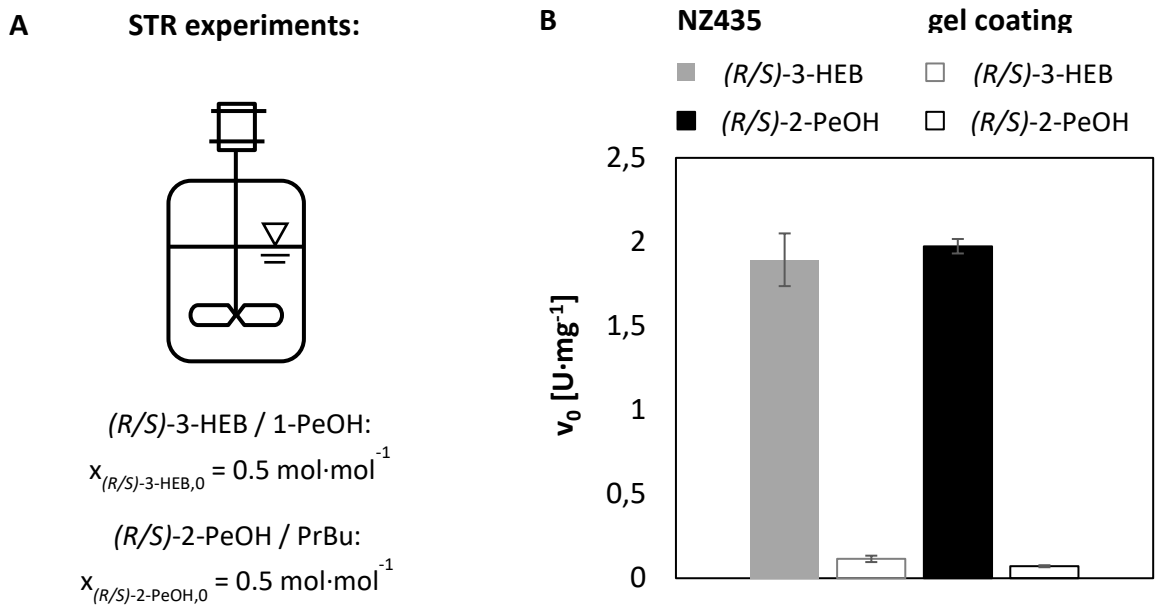

Figure 5.8: Initial activity (v_0) for two biocatalyst preparations of CalB comprising gel coating applied as particles and Novozym435 (NZ435) for the selected kinetic resolution reactions of *(R/S)*-3-HEB with 1-PeOH or *(R/S)*-2-PeOH with PrBu. **A**: Scheme of STR, **B**: experimental data. **Operation conditions**: p = 1 bar, T = 60°C, 400 rpm, c_{NZ435} = 7 mg·mL^{-1}, $c_{gel\ coating}$ = 35 mg·mL^{-1}, *(R/S)*-2-PeOH: $x_{(R/S)\text{-2-PeOH},0}$ = 0.5 mol·mol^{-1}, $x_{PrBu,0}$ = 0.5 mol·mol^{-1}, *(R/S)*-3-HEB: $x_{(R/S)\text{-3-HEB},0}$ = 0.5 mol·mol^{-1}, $x_{1\text{-PeOH},0}$ = 0.5 mol·mol^{-1}. SD: n = 2 for gel coating (*(R/S)*-2-PeOH, *(R/S)*-3-HEB) and NZ435 in (*(R/S)*-2-PeOH), n = 3 for NZ435 (*(R/S)*-3-HEB).

Beside the visible increased catalytic activity for NZ435, the theoretically applicable catalytic activity per column section is calculated for both catalyst preparations to allow a proper selection. For NZ435 placed in Katapak-SP-like catalytic packing elements, at maximum a capacity of m_{NZ435} = 8 g per packing element is possible. In one part of the column height (h = 300 mm), implementation of two Katapak-SP-like catalytic packing elements ($m_{NZ435,max}$ = 16 g) can be realized (**section 3.4**). This refers to initial activities of v_0 = 31520 ± 640 U (*(R/S)*-2-PeOH) and v_0 = 30240 ± 2560 U (*(R/S)*-3-HEB) per column part for equimolar initial molar fractions in both selected KR reactions based on the presented initial catalytic activities and their corresponding errors in **Figure 5.8**. Additionally, the capacity for gel coating is calculated assuming similar conditions by published data of *Heils et al. (2015)* [45]. With a provided $m_{gel\ coating}$ = 3.43 g per packing element and having the possibility to place three Montz A3-500 packing elements in one part of the column (h = 300 mm), initial activities of v_0 = 720 ± 103 U (*(R/S)*-2-PeOH) and v_0 = 1235 ± 206 U (*(R/S)*-3-HEB) per column part can be realized at $x_{i,0}$ = 0.5 mol·mol^{-1}. Hence, beside 12 - 16 times increased catalytic activity of NZ435, 1.6-fold increased mass of NZ435 can theoretically be integrated into one part of the RD setup. Therefore, NZ435 offers the opportunity of

increased flexibility in the position of the reactive zone and allows higher initial activities in RD experiments, which leads to the decision of using NZ435 for further experiments.

In the next step, the initial activity (v_0) of the selected catalyst preparation NZ435 was investigated at varied initial molar fractions of *(R/S)*-2-PeOH as well as *(R/S)*-3-HEB in a range of $x_{(R/S)\text{-substrate},0}$ = 0.1 - 0.9 mol·mol^{-1} in STR's at T = 60 °C (**Figure 5.9**). This is particularly important with respect to the selection of initial molar fractions for the aimed RD experiments, because in the column changed composition of the molar fractions over the column height and in the bottom of the setup are expected during RD operation. This is referred to the separation of the reactant mixtures according to their phase change behavior described in the corresponding vapor-liquid equilibria (**section 2.1.1**). Therefore, the information of initial activity at varied initial molar fractions of the starting materials which may consist at different RD column heights, is necessary to evaluate the RD process.

For low initial molar fractions of the racemic starting alcohol *(R/S)*-2-PeOH ($x_{(R/S)\text{-2-PeOH},0}$ = 0.1 - 0.4 mol·mol^{-1}) with PrBu, similar initial activities of v_0 = 2.33 ± 0.02 U·mg^{-1} were observed for the faster reacting *(R)*-2-PeOH (filled diamonds, **Figure 5.9**). A further increase in the initial molar fraction of *(R/S)*-2-PeOH showed a constant decrease of the initial activity. The lowest initial activity of v_0 = 0.60 ± 0.03 U·mg^{-1} was obtained at $x_{(R/S)\text{-2-PeOH},0}$ =0.9 mol·mol^{-1}. For the corresponding *(S)*-enantiomer, no initial activity was detected at varied initial molar fractions of *(R/S)*-2PeOH (filled squares, **Figure 5.9**).

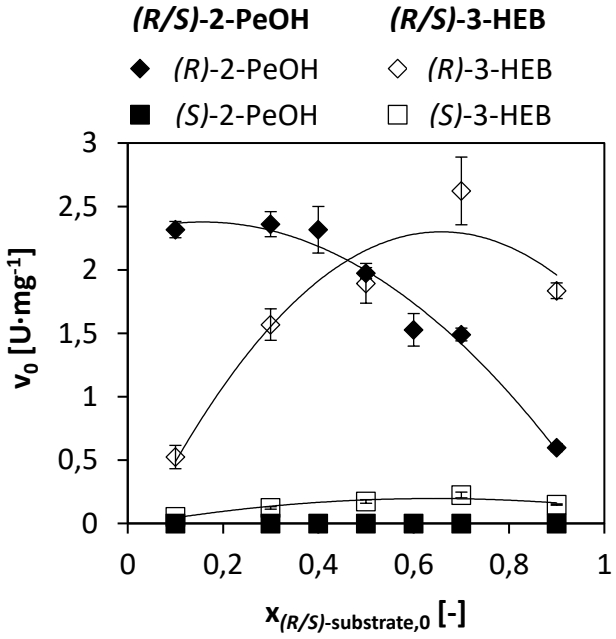

Figure 5.9: Dependency of initial activity (v_0) on the applied racemic initial molar fraction ($x_{(R/S)\text{-substrate},0}$) for the kinetic resolution reaction of *(R/S)*-2-PeOH with PrBu and *(R/S)*-3-HEB with 1-PeOH. **Operation conditions**: p = 1 bar, T = 60 °C, 400 rpm, c_{NZ435} = 7 mg·mL^{-1}, lines serve as visual aid, SD: n = 2 (*(R/S)*-2-PeOH) and n = 3 (*(R/S)*-3-HEB).

On the contrary, an increase in initial activity was identified for *(R)*-3-HEB at rising initial molar fractions with 1-PeOH up to v_0 = 2.62 ± 0.27 U·mg^{-1} at $x_{(R/S)\text{-3-HEB},0}$ = 0.7 mol·mol^{-1} (open diamonds, **Figure 5.9**). At higher starting molar fractions of $x_{(R/S)\text{-3-HEB},0}$ = 0.9 mol·mol^{-1}, decreased initial activity of v_0 = 1.83 ± 0.06 U·mg^{-1} was detected for *(R)*-3-HEB. Similar behavior was observed for the corresponding *(S)*-enantiomer, although highest initial activity was present at a lower level of v_0 = 0.22 ± 0.02 U·mg^{-1} at $x_{(R/S)\text{-3-HEB},0}$ = 0.7 mol·mol^{-1} (open squares, **Figure 5.9**). All described trends are highlighted by visual aid lines in **Figure 5.9**.

The observed trend of reduced initial activities for preferentially reacting *(R)*-2-PeOH with PrBu can be explained by the effect of substrate surplus inhibition of the racemic starting alcohol *(R/S)*-2-PeOH. Thus, $x_{(R/S)\text{-2-PeOH},0}$ = 0.1 - 0.4 mol·mol^{-1} showed the most promising results for the aimed RD application focusing only on high initial activity (v_0). At the same time, reduced mass of the target compound *(S)*-2-PeOH can be reached in KR at low initial molar fractions of *(R/S)*-2-PeOH due to an excess of the corresponding initial molar fraction of the non-chiral ester PrBu. Additionally, the feature of ideally having X = 50 % in KR at an excellent enantioselectivity of the applied biocatalyst toward the starting materials causes a further reduction in the mass of the target compound at low initial molar fractions of *(R/S)*-2-PeOH (**section 2.2.4**). This means to achieve 0.05 mol·mol^{-1} of the desired target compound *(S)*-2-PeOH in the case of excellent enantioselectivity at a starting molar fraction of $x_{(R/S)\text{-2-PeOH},0}$ = 0.1 mol·mol^{-1}. Simultaneously, the starting ester PrBu will be present with an unreacted residual molar fraction of 0.85 mol·mol^{-1} at the end of the kinetic resolution. Excellent enantioselectivity of E >> 100 was proven over the complete range of the initial molar fraction of the racemic starting alcohol *(R/S)*-2-PeOH due to the absence of undesired formation of *(S)*-2-PeBu. Hence, increasing the initial molar fractions of *(R/S)*-2-PeOH in the range of $x_{(R/S)\text{-2-PeOH},0} \leq$ 0.4 - 0.66 mol·mol^{-1} will theoretically allow higher mass of the target compound in RD although the initial activity is reduced by up to 36 % at $x_{(R/S)\text{-2-PeOH},0}$ = 0.66 mol·mol^{-1}. Referring to the increase in the starting molar fraction up to $x_{(R/S)\text{-2-PeOH},0}$ = 0.66 mol·mol^{-1}, 0.33 mol·mol^{-1} of the desired target compound *(S)*-2-PeOH can be realized at excellent enantioselectivity while almost full conversion of the applied starting ester PrBu ($x_{PrBu,0}$ = 0.34 mol·mol^{-1}) takes place. At increased starting molar fractions of $x_{(R/S)\text{-2-PeOH},0} >$ 0.66 mol·mol^{-1}, initial activity is further reduced and the present excess of the faster reacting starting enantiomer *(R)*-2-PeOH compared to PrBu prevents full KR performance. If a starting molar fraction of $x_{(R/S)\text{-2-PeOH},0}$ = 0.9 mol·mol^{-1} is applied, only 0.05 mol·mol^{-1} are converted at excellent enantioselectivity and the target compound can never reach high optical purity under those conditions. Therefore, finally a reasonable trade-off between inhibition phenomena causing reduced initial activity and the possibility of an increased mass of the target compound at full KR performance needs to be adjusted for successful RD operation. Both of the discussed regions of initial molar

fractions are addressed in **section 5.4** by operating RD at initial molar fractions of $x_{(R/S)\text{-2-PeOH},0}$ = 0.1, 0.6 and 0.66 mol·mol^{-1} with the corresponding starting ester PrBu.

For the KR reaction performance of the racemic starting ester *(R/S)*-3-HEB, the opposite trend in initial activity is referred to the substituted chirality in the ester compound instead of the alcohol (*(R/S)*-2-PeOH).

At regions with low initial molar fractions of the racemic ester *(R/S)*-3-HEB ($x_{(R/S)\text{-3-HEB},0} \leq 0.5$ mol·mol^{-1}), substrate surplus inhibition of the non-chiral starting alcohol 1-PeOH was present causing reduced initial activities. With increasing initial molar fractions of *(R/S)*-3-HEB, inhibiting effects by the reactant 1-PeOH were reduced due to its lowered initial molar fraction. However, the revealed maximum at $x_{(R/S)\text{-3-HEB}}$ = 0.7 mol·mol^{-1} cannot be explained only by inhibition through the reactant 1-PeOH. Thus, an influence of stochastic binding to the active side of CalB is assumed within the applied catalyst preparation NZ435. Stochastically, less probability of simultaneous presence of both starting materials *(R/S)*-3-HEB and 1-PeOH at the active side of CalB is expected for reaction performance at high initial molar fractions of $x_{(R/S)\text{-3-HEB},0}$ = 0.9 mol·mol^{-1} ($x_{1\text{-PeOH},0}$ = 0.1 mol·mol^{-1}). That is why small initial molar fractions of either the racemic ester *(R/S)*-3-HEB or the starting non-chiral alcohol 1-PeOH caused decreased initial activities. However, initial molar fractions of $x_{(R/S)\text{-3-HEB},0}$ = 0.66 mol·mol^{-1} as mentioned in the case of the racemic starting alcohol *(R/S)*-2-PeOH theoretically allow full KR at excellent enantioselectivity. But indeed, reduced enantioselectivity is observed for the racemic starting ester *(R/S)*-3-HEB due to the formation of undesired *(S)*-3-HPB. Therefore, a reduced molar fraction of $x_{(R/S)\text{-3-HEB},0} < 0.66$ mol·mol^{-1} should be applied to realize full KR. As an example, at $x_{(R/S)\text{-3-HEB},0}$ = 0.5 mol·mol^{-1} enough 1-PeOH ($x_{1\text{-PeOH},0}$ = 0.5 mol·mol^{-1}) is present for the conversion of *(R)*- as well as *(S)*-3-HEB with a starting molar fraction for both enantiomers of 0.25 mol·mol^{-1}. However, this strictly reduces the theoretical mass of the desired target compound (S)-3-HEB in the KR in comparison to the case with excellent enantioselectivity.Finally, for *(R/S)*-3-HEB a synergistic effect of increased initial activity and an increased mass of the target compound could be formed, while a compromise between lowered initial activity and increased mass of the target compound became necessary for *(R/S)*-2-PeOH. On the other hand, the formation of undesired product *(S)*-3-HPB by converting *(S)*-3-HEB beside the preferential *(R)*-3-HEB, less enantioselectivity of E = 10 – 13 was detected for the racemic starting ester *(R/S)*-3-HEB with 1-PeOH. Hence, CalB was not able to distinguish between the enantiomers of the racemic starting ester *(R/S)*-3-HEB as good as for the racemic starting alcohol *(R/S)*-2-PeOH.

As a conclusion, a strong influence of the applied initial molar fraction of the starting materials on the initial activity is observed for both tested KR reactions with *(R/S)*-2-PeOH or *(R/S)*-3-HEB. Additionally, the corresponding enantioselectivity was strictly decreased by changing from *(R/S)*-2-PeOH to *(R/S)*-3-HEB.

The observed differences in the initial activities of the *(R)*- and *(S)*-enantiomers of both racemic starting materials in **Figure 5.9** were further investigated by comparing the relative reaction velocity over the course of the conversion (X) at a specific racemic initial molar fraction of $x_{(R/S)\text{-substrate},0}$ = 0.1 mol·mol^{-1} (**Figure 5.10**). Calculation of the relative reaction velocity was done by dividing the obtained reaction velocity for the formation of either the *(R)*- or *(S)*-pentyl ester at different points of conversion with the initial reaction velocity of the preferably reacting *(R)*-enantiomer. The ratio of the relative reaction velocity is abbreviated by $v_{(R)}{\cdot}v_{(R),0}^{-1}$ for the formation of *(R)*-2-PeBu and *(R)*-3-HPB (filled and open diamonds) as well as $v_{(S)}{\cdot}v_{(R),0}^{-1}$ for the formation of *(S)*-2-PeBu and *(S)*-3-HPB (filled and open squares). In both cases, the trends of the relative reaction velocities are shown by visual aid lines.
Independent from the applied racemic starting material, the relative reaction velocity of the faster reacting *(R)*-enantiomers strictly decreased (diamonds, **Figure 5.10**).

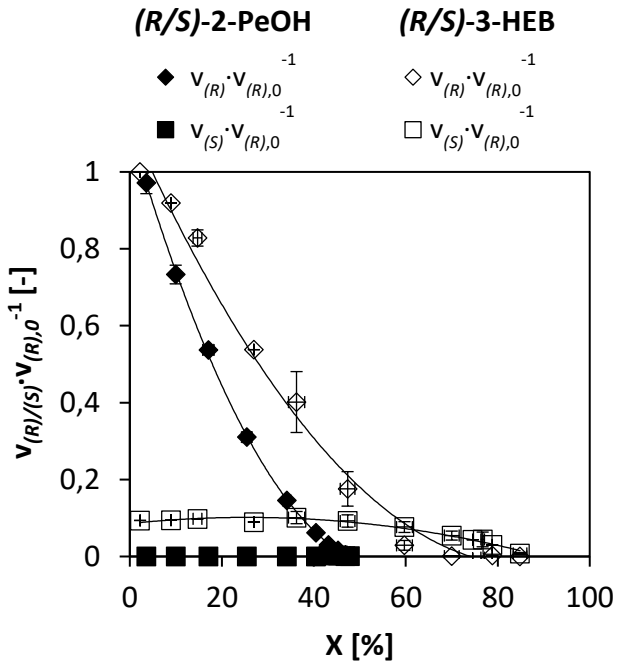

Figure 5.10: Comparison of the relative reaction velocities ($v_{(R)}{\cdot}v_{(R),0}^{-1}$, $v_{(S)}{\cdot}v_{(R),0}^{-1}$) for the kinetic resolution reactions of *(R/S)*-2-PeOH with PrBu and *(R/S)*-3-HEB with 1-PeOH. **Operation conditions**: p = 1 bar, T = 60 °C, SD: n = 2. *(R/S)*-2-PeOH: $x_{(R/S)\text{-2-PeOH}}$ = 0.1 mol·mol^{-1}, x_{PrBu} = 0.9 mol·mol^{-1}, c_{NZ435} = 7 mg·mL^{-1}, *(R/S)*-3-HEB: $x_{(R/S)\text{-3-HEB}}$ = 0.1 mol·mol^{-1}, $x_{1\text{-PeOH}}$ = 0.9 mol·mol^{-1}, c_{NZ435} = 35 mg·mL^{-1}.

For KR of *(R/S)*-2-PeOH with PrBu, at X = 47 ± 1 % an extremely low relative reaction velocity of $v_{(R)}{\cdot}v_{(R),0}^{-1} = v_{(S)}{\cdot}v_{(R),0}^{-1}$ = 0.14 ± 0.03 % was detected. In the case of *(R/S)*-3-HEB with 1-PeOH, a similar low relative reaction velocity of $v_{(R)}{\cdot}v_{(R),0}^{-1}$ = 0.10 ± 0.01 % for the *(R)*-enantiomer was reached at substantially increased conversions of X = 70 ± 2 %. Comparing both trends revealed higher $v_{(R)}{\cdot}v_{(R),0}^{-1}$ for the racemic starting ester *(R/S)*-3-HEB. Simultaneously, the corresponding relative reaction velocities of the *(S)*-enantiomers in both KR reactions were lower indicated by $v_{(S)}{\cdot}v_{(R),0}^{-1}$ (squares,

Figure 5.10). However, increased $v_{(S)} \cdot v_{(R),0}^{-1}$ = 10.12 ± 1.59 % was observed within KR of *(R/S)*-3-HEB with 1-PeOH, whereas at maximum $v_{(S)} \cdot v_{(R),0}^{-1}$ = 0.11 ± 0.1 % was detected for KR of *(R/S)*-2-PeOH with PrBu.

Thus, *(R)*-selectivity of CalB was detected by increased reaction velocities of $v_{(R)} \cdot v_{(R),0}^{-1}$ and by that faster conversion of *(R)*-2-PeOH as well as *(R)*-3-HEB. Moreover, increased relative reaction velocity was present for both enantiomers in the KR by *(R/S)*-3-HEB with 1-PeOH. This is related to the previously described reduced enantioselectivity, which caused increased $v_{(R)} \cdot v_{(R),0}^{-1}$ until *(R)*-3-HEB was either fully converted or reaching the reaction equilibrium at higher conversion points at X = 70 ± 2 %. Low enantioselectivity for KR of *(R/S)*-3-HEB with 1-PeOH could be supported by simultaneous conversion of *(S)*-3-HEB represented by increased $v_{(S)} \cdot v_{(R),0}^{-1}$ compared to the absence of any reaction with *(S)*-2-PeOH. On the other hand, excellent enantioselectivity in the KR of *(R/S)*-2-PeOH with PrBu was proven by fast depletion of *(R)*-2-PeOH up to X = 47 ± 1 % indicated by a strict decrease in $v_{(R)} \cdot v_{(R),0}^{-1}$. Additionally, high enantioselectivity was underlined by prevented conversion of *(S)*-2-PeOH indicated by $v_{(S)} \cdot v_{(R),0}^{-1}$ = 0.14 ± 0.03 %. Finally, changing the racemic starting material influences not only the initial activity (**Figure 5.9**) but affects the relative reaction velocity as well (**Figure 5.10**).

Furthermore, the influence of the initial molar fraction on the reaction equilibrium was investigated for the racemic starting alcohol *(R/S)*-2-PeOH and the racemic starting ester *(R/S)*-3-HEB to identify the point of equilibrium conversion. Therefore, the equilibrium constant (K_{eq}) was determined at varied initial molar fractions ($x_{(R/S)\text{-substrate},0}$ = 0.1 – 0.9 mol·mol^{-1}) at T = 60 °C and p = 1 bar (**Figure 5.11**).

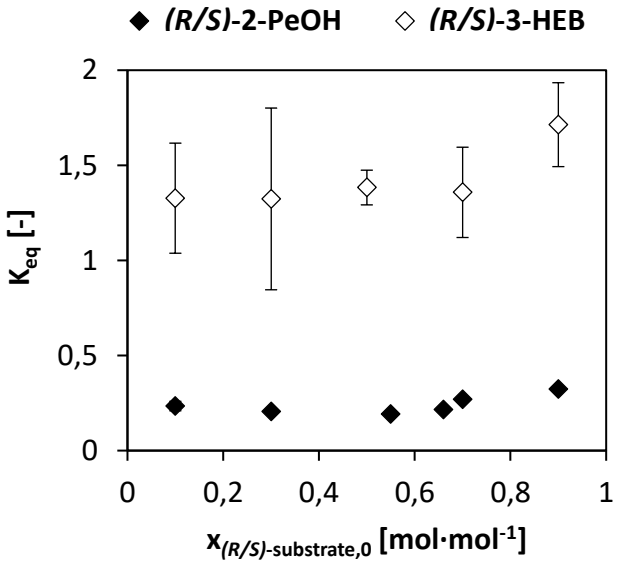

Figure 5.11: Experimentally determined equilibrium constant (K_{eq}) in dependency of the racemic initial molar fraction ($x_{(R/S)\text{-substrate},0}$) for the kinetic resolution reactions of *(R/S)*-2-PeOH with PrBu and *(R/S)*-3-HEB with 1-PeOH. **Operation conditions**: p = 1 bar, T = 60°C, c_{NZ435} = 35 mg·mL^{-1}, SD: n = 2.

Rather constant values of K_{eq} = 0.24 ± 0.04 were obtained for KR of *(R/S)*-2-PeOH with PrBu in the range of $x_{(R/S)\text{-2-PeOH},0}$ = 0.1 – 0.9 mol·mol^{-1} (filled diamonds). This refers to an equilibrium conversion of X_{eq} = 44 ± 3 % for the racemic starting alcohol *(R/S)*-2-PeOH. The equilibrium conversion is calculated by **Eq. 12** in **section 2.2.2**. For KR of *(R/S)*-3-HEB with 1-PeOH, strong fluctuations were observed in the determined equilibrium constants (open diamonds). So far, there is no explanation for the big deviations in the equilibrium constants with *(R/S)*-3-HEB. They resulted in a mean value of K_{eq} = 1.42 ± 0.15 within the investigated range of initial molar fractions ($x_{(R/S)\text{-3-HEB},0}$ = 0.1 – 0.9 mol·mol^{-1}). The corresponding equilibrium conversion was calculated to be X_{eq} = 77 ± 8 % for the racemic starting ester *(R/S)*-3-HEB.

Hence, the KR of *(R/S)*-2-PeOH with PrBu showed strong equilibrium limitation at $K_{eq} << 1$ and did not allow full KR at $x_{(R/S)\text{-2-PeOH},0}$ = 0.1 – 0.9 mol·mol^{-1} even at excellent enantioselectivity due to $X_{eq} < 50$ %. This observation can be supported by the previously described low detected relative reaction velocities at a conversion of X = 47 ± 1 % (**Figure 5.10**). Therefore, a shift in equilibrium for the selected racemic alcohol *(R/S)*-2-PeOH is necessary in the feasible range of $x_{(R/S)\text{-2-PeOH},0}$. This issue will be further addressed by operating STRs (**section 5.2.3**) and the RD column at reduced pressure (**section 5.3.1**). In the procedure of *in situ* product removal, the equilibrium is shifted by reducing the moles on the product side according to the principle of *Le Chatelier* [97].

With respect to the reaction equilibrium for the KR of *(R/S)*-3-HEB with 1-PeOH, $K_{eq} > 1$ implied the equilibrium to be on the product side. However, less enantioselectivity of E = 10 – 13 requires increased conversions of $X_{eq} \geq 75$ % instead of $X_{eq} \geq 50$ % for a reaction with excellent enantioselectivity (**section 2.2.4**). Although high standard deviations within experimental data were detected for *(R/S)*-3-HEB with 1-PeOH, the reaction was not as strictly equilibrium limited as the KR of *(R/S)*-2-PeOH with PrBu. This can be underlined by experimental data, in which X_{eq} = 85 ± 2 % was obtained (**Figure 5.10**). Finally, comparing both selected KR reactions with respect to the equilibrium constant K_{eq} revealed the necessity of shifting the equilibrium clearly in the case of the KR of *(R/S)*-2-PeOH with PrBu.

Concise summary of section 5.2.1:

- Both selected starting materials reveal successful performance of solvent-free KR in stirred tank reactors (STR) with the biocatalyst preparation NZ435 (*(R/S)*-2-PeOH with PrBu: v_0 = 1.97 ± 0.04 U·mg^{-1}, *(R/S)*-3-HEB with 1-PeOH: v_0 = 1.89 ± 0.16 U·mg^{-1})
- Full KR can be achieved in STRs at initial molar fractions of $x_{(R/S)\text{-substrate},0} \leq 0.66$ mol·mol^{-1}
- Significant changes in the enantioselectivity (E) are detected in dependency of the applied starting material (*(R/S)*-2-PeOH with PrBu: excellent E >> 100, *(R/S)*-3-HEB with 1-PeOH: low E = 10 - 13)

- A strong equilibrium limitation is identified at T = 60 °C and p = 1 bar for KR of *(R/S)*-2-PeOH with PrBu (K_{eq} = 0.24 ± 0.04, X_{eq} = 44 ± 3 %), while *(R/S)*-3-HEB with 1-PeOH is not equilibrium limited (K_{eq} = 1.42 ± 0.15, X_{eq} = 77 ± 8 %)

5.2.2. Influence of Operating Temperature on Catalyst Stability and Catalytic Activity

The thermal stability of NZ435 was investigated for the KR of the racemic starting alcohol *(R/S)*-2-PeOH with PrBu in STR experiments at operating temperatures of T = 60 °C and T = 80 °C (**Figure 5.12**). Equimolar starting molar fractions of $x_{(R/S)\text{-2-PeOH},0}$ = 0.5 mol·mol^{-1} were used for both temperatures. The time dependent courses of residual activity were determined by the ratio of the initial activity in each experiment to the initial activity in the first experiment (**section 3.3**). Independent of temperature, decreased residual activity is depicted by open diamonds in the case of T = 60 °C and filled diamonds at T = 80 °C (**Figure 5.12**). Both experiments showed the expected exponential decrease in residual activity. The experiment at T = 80 °C was carried out for t = 21 d, which resulted in a decrease of 46 ± 6 % after this time period. In comparison, a significantly increased residual activity of 62 ± 5 % after t = 58 d was obtained at T = 60 °C. Those observed exponential trends correspond to the deactivation constants k_{des} = 0.036 ± 0.005 d^{-1} at T = 80 °C and k_{des} = 0.008 ± 0.001 d^{-1} at T = 60 °C (**Eq. 7**, **section 2.2.2**). The calculated half-life times are $\tau_{0.5}$ = 19 ± 3 d (T = 80 °C) and $\tau_{0.5}$ = 87 ± 11 d (T = 60 °C) for CalB applied as NZ435 (**Eq. 8**, **section 2.2.2**).

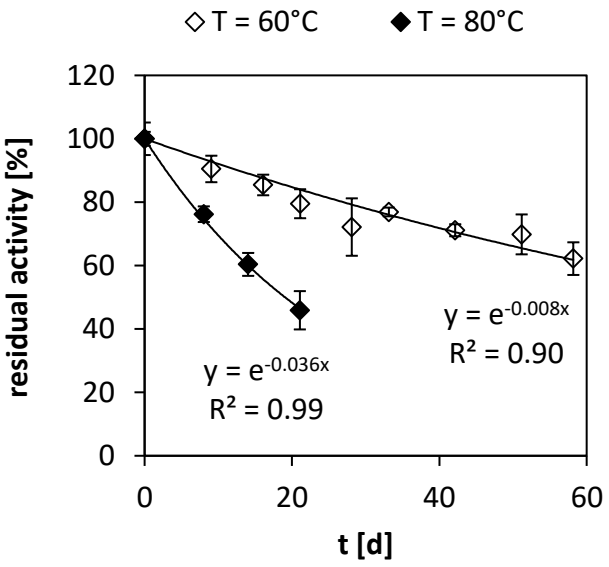

Figure 5.12: Thermal stability of the selected biocatalyst preparation NZ435 at varied operating temperatures of T = 60 °C and T = 80 °C. **Operation conditions**: p = 1 bar, $x_{(R/S)\text{-2-PeOH},0}$ = 0.5 mol·mol^{-1}, $x_{PrBu,0}$ = 0.5 mol·mol^{-1}, c_{NZ435} = 7 mg·mL^{-1}, 400 rpm, n = 2

The observed time-dependent decrease in residual activity at both temperatures is referred to thermal deactivation of CalB (**section 2.2.2**). Therefore, this effect became stronger at an increased operating temperature of T = 80 °C. However, NZ435 was robust enough toward elevated temperatures of T = 60 °C – 80 °C for the investigated solvent-free KR reaction. In fact, the detected thermal stability of CalB in the presented results of T = 60 °C – 80 °C can be supported by literature. While *Heils et al. (2012)* determined similar residual activity of 58 % after t = 50 d and at T = 60 °C applying CalB in gel coating material [40], *Poojari et al. (2013)* stated no significant activity loss for NZ435 at T = 80 °C after t = 30 d with incubation in toluene [37].

Thus, the application of NZ435 in biocatalytic reactive distillation as well as numerous reuse of the same NZ435 particles is expected to be feasible according to the detected half-life times. Clearly, a reduction in the applied temperature resulted in a substantially longer lifetime of NZ435. Although the results were obtained in STR experiments, similar behavior with respect to the temperature is assumed to be present in the RD setup. Additionally, stirring may cause disruptive effects within the collision of NZ435 particles as well as the abrasion by the stirrer itself to increase deactivation of CalB within STR experiments. Even more, reduced operating temperatures (T ≤ 60 °C) in RD by guaranteed evaporation of the starting materials can be realized by reduced pressure and would further increase the lifetime of NZ435 (**section 2.2.3**). Although in reactive distillation processes in chemical industry, catalyst lifetimes of up to several years are preferred for the synthesis of bulk chemicals [3], the main difference is the synthesis of fine chemicals by the application of highly enantioselective but less thermal stable biocatalysts. However, economic evaluation of the reusability of the catalyst and the value of the target compounds should always be considered.

Beside the influence of two operating temperatures on catalyst stability, the effect of the operating temperature on initial activity and enantioselectivity at fixed racemic initial molar fractions of $x_{(R/S)\text{-substrate},0}$ = 0.5 mol·mol^{-1} was investigated. According to Arrhenius, rising temperatures are known to result in increased catalytic activity for chemical reactions [94].

Figure 5.13, **A** shows the results of Arrhenius dependency for the selected KR reactions in STR experiments. Within this Arrhenius dependency, comparing the logarithmic initial activity ($\ln(v_0)$) to reciprocal temperature (T^{-1}) allows calculation of the activation energy E_a by linear regression (**section 2.2.2**). In addition to T^{-1}, the corresponding temperature (T) is given in **Figure 5.13**, **A**. For *(R/S)*-2-PeOH with PrBu, temperatures of T = 40 °C, 60 °C and 80 °C (filled data points) were investigated and for *(R/S)*-3-HEB with 1-PeOH temperatures of T = 30 °C, 40 °C, 50 °C, 60 °C and 70 °C were applied (open data points). The corresponding activation energy was calculated for the formation of either *(R)*- and *(S)*-2-PeBu or *(R)*- and *(S)*-3-HPB. Diamond shaped data points represent the results for *(R)*-2-PeBu and *(R)*-3-HPB, whereas data for *(S)*-3-HPB are depicted by squares in **Figure 5.13**, **A**.

Similar activation energies of E_a = 14.0 ± 0.1 kJ·mol^{-1} for *(R)*-2-PeBu in KR of *(R/S)*-2-PeOH with PrBu and E_a = 18.1 ± 0.1 kJ·mol^{-1} for *(R)*-3-HPB in KR of *(R/S)*-3-HEB with 1-PeOH were obtained. The experiments indicated a 1.9-fold increased initial activity from T = 40 °C to T = 80 °C (ΔT = 40 °C) for *(R/S)*-2-PeOH with PrBu.

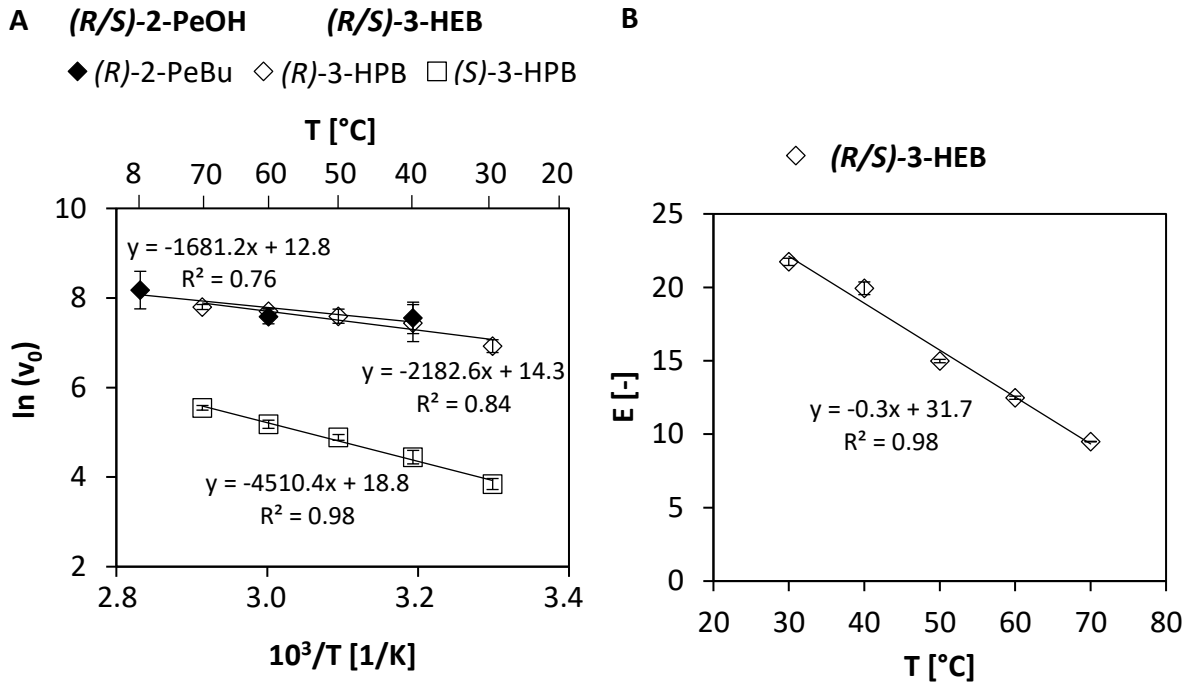

Figure 5.13: Effect of operating temperature on kinetic resolution of *(R/S)*-2-PeOH with PrBu and *(R/S)*-3-HEB with 1-PeOH. **A**: Arrhenius dependency (ln(v_0) over 1/T) for varied temperatures (T). **B**: Effect on enantioselectivity *E*. **Operation conditions**: p = 1 bar, 400 rpm, c_{NZ435} = 7 mg·mL^{-1}, *(R/S)*-2-PeOH with PrBu (n = 2): $x_{(R/S)\text{-2-PeOH},0}$ = 0.5 mol·mol^{-1}, $x_{PrBu,0}$ = 0.5 mol·mol^{-1}, T = 40°C, 60°C, 80°C. *(R/S)*-3-HEB with 1-PeOH (n = 3): $x_{(R/S)\text{-3-HEB},0}$ = 0.5 mol·mol^{-1}, $x_{1\text{-PeOH},0}$ = 0.5 mol·mol^{-1}, T = 30°C, 40°C, 50°C, 60°C, 70°C

For detailed information on the corresponding numbers for initial activity, it is referred to **appendix section C** (**Table C.1** (*(R/S)*-3-HEB), **Table C.2** (*(R/S)*-2-PeOH)). Regarding the same temperature difference within T = 30 – 70 °C (ΔT = 40 °C) for KR performance of *(R/S)*-3-HEB with 1-PeOH, 2.4 times increased initial activities were observed. For the corresponding *(S)*-enantiomers, significant differences between the racemic starting materials occurred. In the case of starting with *(R/S)*-2-PeOH, no formation of *(S)*-2-PeBu was detected at the three investigated temperatures between T = 40 - 80 °C and therefore is missing in **Figure 5.13**, **A**. If *(R/S)*-3-HEB was applied, simultaneous formation of *(S)*-3-HPB took place. In fact, doubled activation energy of E_a = 37.5 ± 0.1 kJ·mol^{-1} for formed *(S)*-3-HPB was calculated compared to *(R)*-3-HPB. At the same time, 5.6-fold increased initial activity was present for the formation of *(S)*-3-HPB. Moreover, the dependency of enantioselectivity (E) on the operating temperature is visualized for the racemic starting ester *(R/S)*-3-HEB with 1-PeOH at the same temperature range between T = 30 – 70 °C in **Figure 5.13**, **B**. The calculation of *E* was done

on the basis of **Eq. 4** (**section 2.2.2**). Assuming linear behavior resulted in decreased E-values at rising temperatures. While an enantioselectivity of E = 20 is detected at T = 30 °C, it is reduced by more than 50 % to E = 9 at T = 70 °C.

Thus, faster conversion of the *(R)*-enantiomers was present independent from the applied racemic starting material. In the case of *(R/S)*-2-PeOH with PrBu, excellent enantioselectivity was present at the investigated temperature range between T = 40 – 80 °C, because no formation of *(S)*-2-PeBu was detected (E >> 100). Similar results about the enantioselectivity of KR by *(R/S)*-2-PeOH with PrBu were obtained for varied starting molar fractions in **section 5.2.1**. Even for the less enantioselective KR performance of *(R/S)*-3-HEB with 1-PeOH, slightly faster reaction was detected for the *(R)*-enantiomer. All those observations are in accordance to literature, wherein CalB is known to be *(R)*-selective [155]. Comparing both racemic starting materials, the initial activity is roughly doubled (1.9 to 2.4-fold) for a temperature difference of ΔT = 40 °C. As a rule of thumb, doubled initial activities are already assumed at a temperature difference of ΔT = 10 °C for chemical reactions [94]. Within the presented results, at a temperature gradient of ΔT = 10°C just a reduced increase of 1.2-fold in initial activity was detected. Hence, in combination with observed low activation energies of E_a < 20 kJ·mol^{-1} for the *(R)*-reactions, the impact of temperature on the initial activity in both selected KR reactions is lower in the investigated operating temperature range of NZ435. Even for increased E_a = 37.5 ± 0.1 kJ·mol^{-1} with respect to the *(S)*-enantiomer in KR of *(R/S)*-3-HEB with 1-PeOH, the increase in initial activity was not doubled but 1.5-fold at a temperature gradient of ΔT = 10°C. In fact, the observed reduced temperature influence in principle allows catalyst distribution even in regions with low temperature as well as a reduced overall column temperature for aimed RD experiments. Based on previously discussed results, reducing the overall column temperature will decrease biocatalyst deactivation of NZ435 and allow increased lifetime of the catalyst in column operation (**Figure 5.12**). Beside increased lifetime of NZ435 at reduced temperatures, an increase in enantioselectivity was detected for the KR reaction of *(R/S)*-3-HEB with 1-PeOH. The increase in E is caused by different E_a for both enantiomers. As long as different behavior for both enantiomers is present, integration of reactions with not excellent enantioselectivities may become feasible in RD due to adjusting the operating temperatures and therefore the enantioselectivity of the reaction as well.

Concise summary of section 5.2.2:

- High thermal stability of NZ435 with $\tau_{0.5}$ = 19 d (T = 80 °C) and $\tau_{0.5}$ = 87 d (T = 60 °C) is obtained
- Less influence of rising temperatures on v_0 at ΔT = 10 ° is observed in Arrhenius dependency (*(R/S)*-2-PeOH with PrBu: 1.2-fold increase, *(R/S)*-3-HEB with 1-PeOH: 1.2-fold increase)

5.2.3. Influence of Operating Pressure on Reaction Performance

The influence of pressure on the reaction performance of the two selected racemic starting molecules *(R/S)*-2-PeOH and *(R/S)*-3-HEB is addressed by the progress of enantiomeric excess (ee) with rising conversions (X) at a racemic initial molar fraction of $x_{(R/S)\text{-substrate},0}$ = 0.1 mol·mol^{-1} (**Figure 5.14**). Both, experimental data for the enantiomeric excess of the target compounds *(S)*-2-PeOH or *(S)*-3-HEB as well as the enantiomeric excess of the formed pentyl esters were compared to calculated data by the method of *Chen et al. (1982)* [115] (**section 2.2.4**).

For KR of the racemic starting alcohol *(R/S)*-2-PeOH with EtBu, the course of $ee_{(S)\text{-2-PeOH}}$ is depicted in **Figure 5.14**, **A** at ambient pressure (p = 1 bar, open diamonds) and reduced pressure of p = 0.1 bar (filled diamonds). At a reduced pressure of p = 0.1 bar, full KR with $ee_{(S)\text{-2-PeOH}}$ > 98 % was reached at X = 58.6 ± 0.7 %. Further increased conversion points up to X = 78.8 ± 1.9 % (p = 0.1 bar) showed constantly high values for $ee_{(S)\text{-2-PeOH}}$. On the other hand, KR at ambient pressure stopped at $ee_{(S)\text{-2-PeOH}}$ = 81.8 ± 1.5 % and X = 48.5 ± 0.4 %. Simultaneously, the enantiomeric excess of formed *(R)*-2-PeBu was observed to be constant at $ee_{(R)\text{-2-PeBu}}$ > 98 % up to X = 48.5 ± 0.4 % (p = 1 bar, open squares) and X = 45.9 ± 0.4 % (p = 0.1 bar, filled squares) followed by a decrease in $ee_{(R)\text{-2-PeBu}}$. Finally, $ee_{(R)\text{-2-PeBu}}$ = 94.2 ± 2.0 % at p = 1 bar (X = 48.5 ± 0.4 %) and $ee_{(R)\text{-2-PeBu}}$ = 30.7 ± 3.3 % at p = 0.1 bar (X = 78.8 ± 1.9 %) were detected before stopping the experiments.

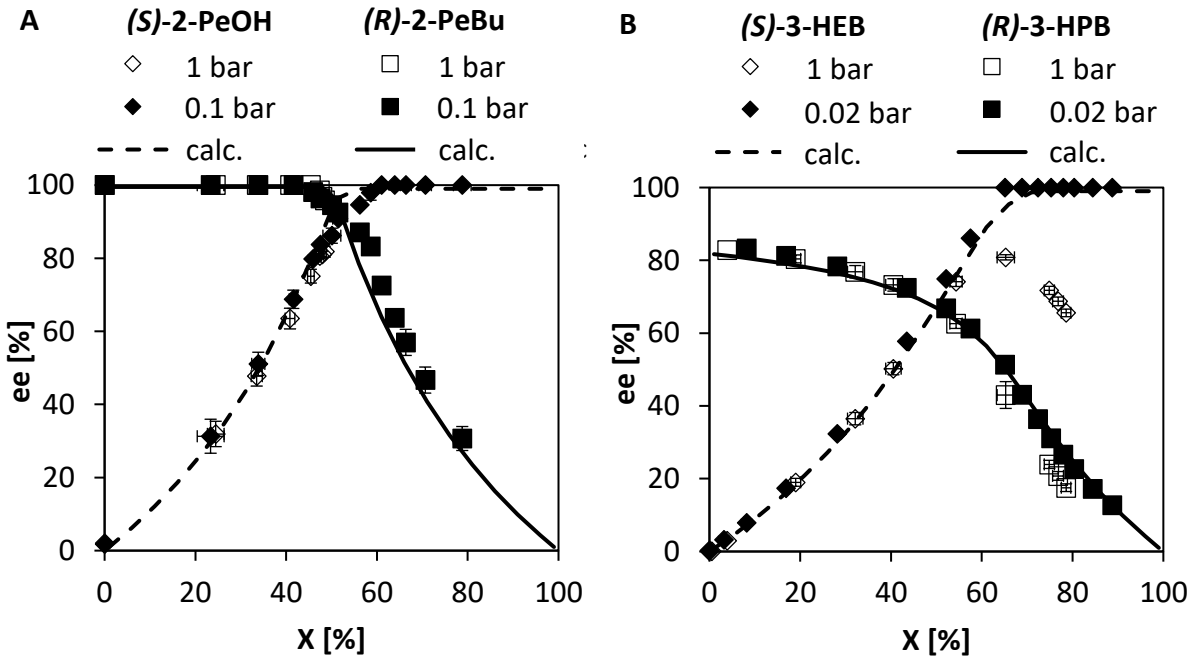

Figure 5.14: Reaction performance of kinetic resolution reactions at varied operating pressures. **A**: *(R/S)*-2-PeOH with EtBu, **B**: *(R/S)*-3-HEB with 1-PeOH. **Operation conditions**: $x_{(R/S)\text{-substrate},0}$ = 0.1 mol·mol^{-1}, T = 60 °C, 400 rpm, SD: n=2, *(R/S)*-2-PeOH: p = 1 bar and 0.1 bar, c_{NZ435} = 50 mg·mL^{-1}, lines: calculated behavior at E ≥ 100, *(R/S)*-3-HEB: p = 1 bar, c_{NZ435} = 35 mg·mL^{-1}, p = 0.02 bar, c_{NZ435} = 7 mg·mL^{-1}, lines: calculated behavior at E = 10.

The presented results are in good agreement with calculated data by the method of *Chen et al. (1982)* [115] assuming an irreversible KR reaction for *(R/S)*-2-PeOH with EtBu (filled and dashed line, **Figure 5.14**, **A**). In addition, experimental data for KR of *(R/S)*-2-PeOH with the corresponding starting ester PrBu at ambient pressure showed the same trends (**appendix section C**, **Figure C.1**). Rising enantiomeric excess values with respect to the target compound *(S)*-2-PeOH up to $ee_{(S)\text{-2-PeOH}}$ = 79.9 ± 0.3 % were detected while the formed pentyl ester was constantly at $ee_{(R)\text{-2-PeBu}}$ > 98.0 ± 0.1 % up to X = 46.4 ± 0.3 % for starting with PrBu (**appendix section C**, **Figure C.1**). With respect to the previously discussed equilibrium conversion of X_{eq} = 44 ± 3 % in **Figure 5.11** (**section 5.2.1**), the reaction of *(R/S)*-2-PeOH with PrBu clearly was at its equilibrium state. According to the results for *(R/S)*-2-PeOH with EtBu at ambient pressure, the same reason can explain the incomplete KR reaction at p = 1 bar. Comparing experimental data of KR by *(R/S)*-2-PeOH with either EtBu or PrBu represented excellent enantioselectivities at ambient (with EtBu or PrBu) as well as reduced pressure (EtBu) by initially obtained $ee_{(R)\text{-2-PeBu}}$ > 98 % up to X ≤ 46 ± 1 %. Hence, mainly the preferentially reacting starting enantiomer *(R)*-2-PeOH was converted by CalB (provided as NZ435) as long it is present in the reaction mixture. Especially at increased conversions beyond equilibrium conversion, reaction velocity was enhanced by *in situ* separation of EtOH at reduced pressures, which is displayed by substantially rising conversion up to X = 78.8 ± 1.9 % (p = 0.1 bar) compared to X = 48.5 ± 0.4 % at ambient pressure (p = 1 bar) within similar operation times of t = 300 min. The driving force for increased conversion at reduced pressure was a shift in the equilibrium via *in situ* product removal of low boiling EtOH. In fact, shifting the equilibrium of KR is required for PrBu applied as starting ester due to lower K_{eq} = 0.24 ± 0.04 and an equilibrium conversion of X_{eq} = 44 ± 3 % (**section 5.2.1**). As the same behavior is detected for the starting ester EtBu, full KR in the case of *(R/S)*-2-PeOH can only be achieved at reduced pressures and by shifting the equilibrium. Hence, the design opportunity by the operation at reduced pressures can be beneficial for the application of KR in RD.

Similar experiments for the determination of the dependency of enantiomeric excess from conversion at two different operating pressures of p = 1 bar (open data points) and p = 0.02 bar (filled data points) were performed for KR of the racemic starting ester *(R/S)*-3-HEB with 1-PeOH (**Figure 5.14**, **B**). In contrast to the racemic starting alcohol, reduced enantiomeric excess of the formed pentyl ester *(R)*-3-HPB was observed in the beginning of the experiments for both investigated pressures due to low *E*-values (**section 5.2.1**). While $ee_{(R)\text{-3-HPB}}$ = 82.9 % at X = 3.9 % and p = 1 bar was detected (open squares), $ee_{(R)\text{-3-HPB}}$ = 83.3 ± 0.3 % at X = 8.2 ± 0.6 % was present at reduced pressure of p = 0.02 bar (filled squares). Over the course of conversion, similar reduction in the enantiomeric excess of *(R)*-3-HPB took place for both pressures. At the end of the experiment an $ee_{(R)\text{-3-HPB}}$ = 17.5 ± 1.1% at p = 1 bar (X = 78.6 ± 1.1 %) and $ee_{(R)\text{-3-HPB}}$ = 12.7 % at p = 0.02 bar (X = 88.8 %) was obtained. In respect

to the enantiomeric excess of the target compound *(S)*-3-HEB, experimental data at ambient pressure are passing through a maximum at $ee_{(S)\text{-3-HEB}}$ = 80.8 ± 0.7 % and X = 65.3 ± 1.9 % before decreasing again at further increased X to reduced $ee_{(S)\text{-3-HEB}}$ = 65.6 ± 1.1 % (X = 78.6 ± 1.1 %). At a reduced pressure of p = 0.02 bar, contradictory behavior of rising $ee_{(S)\text{-3-HEB}}$ ending up at constantly high $ee_{(S)\text{-3-HEB}}$ > 99 % at 65.1 ± 0.1 % ≤ X ≤ 88.8 % were detected.

Hence, full KR was only achieved at reduced operating pressure (p = 0.02 bar) indicated by $ee_{(S)\text{-3-HEB}}$ >99 %, whereas it was prevented at ambient pressure ($ee_{(S)\text{-3-HEB}}$ = 80.8 ± 0.7 %). Assuming an ideally performed irreversible KR reaction with less enantioselectivity (filled and dashed line, **Figure 5.14**, **B**) showed the same behavior for calculated $ee_{(S)\text{-3-HEB}}$ compared to the presented experimental data at reduced pressure. Moreover, within the results at ambient pressure, a typical reversible reaction described in **section 2.2.4** is indicated by the point of inflexion at X = 65.3 ± 1.9 % [116]. Hence, desired formation of the pentyl esters as well as low boiling EtOH was the preferred direction of KR at conversions of X < 65.3 ± 1.9 %. In this part of the reaction, the faster reacting enantiomer *(R)*-3-HEB was preferably converted and increased $ee_{(S)\text{-3-HEB}}$ were detected. Afterwards at X > 65.3 ± 1.9 %, the corresponding back reaction to the starting materials was preferentially taking place. This behavior is referred to the presence of formed *(R)*-3-HPB, which can be converted faster by CalB due to the same chirality as it is present in *(R)*-3-HEB [82]. At the same time, the undesired second reaction takes place by converting *(S)*-3-HEB to the corresponding pentyl ester *(S)*-3-HPB. This is caused by less ability of CalB to distinguish between the enantiomers of the racemic starting ester *(R/S)*-3-HEB indicated by E = 10 at $x_{(R/S)\text{-3-HEB},0}$ = 0.1 mol·mol^{-1} (**section 5.2.1**). Therefore, the observed behavior in the course of $ee_{(R)\text{-3-HPB}}$ providing a maximum at X = 65.3 ± 1.9 % is expected to be an overlaying effect of equilibrium characteristics and low enantioselectivity of the KR reaction. In fact, this reversible reaction with a decrease in $ee_{(S)\text{-3-HEB}}$ could be circumvented by performing the reaction at reduced pressures (p = 0.02 bar).

To conclude, the operating pressure shows increased impact on the reaction performance of KR with the racemic starting alcohol *(R/S)*-2-PeOH as well as the racemic starting ester *(R/S)*-3-HEB. At reduced pressures, two main parameters allow an optimized reaction performance. On the one hand, the equilibrium conversion can be overcome by removal of low boiling products (here: EtOH or 1-PrOH). On the other hand, the back reaction especially for a less enantioselective KR reaction represented by *(R/S)*-3-HEB with 1-PeOH can be achieved to realize full KR with excellent $ee_{(S)\text{-3-HEB}}$. This feature of removing reactants *in situ* can be applied in RD as well. Additionally, the performance of KR reactions at reduced pressures in RD may offer the opportunity for direct separation of the chiral target compound at the top of the column.

Concise summary of section 5.2.3:

- Equilibrium of the limited KR reaction with *(R/S)*-2-PeOH can be shifted to the product side in stirred tank reactors at reduced pressures (p = 0.1 bar) by *in situ* product removal to exceed full KR ($ee_{(S)\text{-2-PeOH}}$ > 98 %, X = 58.6 ± 0.7 %)
- Back reaction is prevented at reduced pressures (p = 0.02 bar) for the investigated KR of the chiral starting ester *(R/S)*-3-HEB to exceed full KR ($ee_{(S)\text{-3-HEB}}$ > 99 %, X = 65.1 ± 0.1 %)

5.2.4. Availability of Starting Materials in Reactive Distillation Experiments as Function of the Column Height

Based on the theoretical feasibility study in the preselection tool (**section 5.1**) and experimental characterization of KR by *(R/S)*-2-PeOH with PrBu as well as *(R/S)*-3-HEB with 1-PeOH (**section 5.2.1– 5.2.3**), their behavior in RD was investigated by performing column experiments without the presence of CalB. The addressed parameters were the substrate availability in different column heights to define the position of the catalytic section and the separation efficiency of the column setup.

Two binary mixtures for *(R/S)*-2-PeOH with PrBu (**Figure 5.15**, **A**) as well as *(R/S)*-3-HEB with 1-PeOH (**Figure 5.15**, **B**) were investigated in RD with infinite reflux ratio (rr = ∞) to evaluate their distribution over the column height. At infinite reflux, no fractional distillation takes place by total condensation at the column top and returning the complete stream of evaporated reactants back into the column. The column pressure was adjusted to p = 80 mbar in the case of operating the RD setup with two binary mixture of *(R/S)*-2-PeOH and PrBu ($x_{(R/S)\text{-2-PeOH},0}$ = 0.4 mol·mol^{-1}, $x_{(R/S)\text{-2-PeOH},0}$ = 0.6 mol·mol^{-1}) (**Figure 5.15**, **A**). For *(R/S)*-3-HEB and 1-PeOH, further reduced column pressures of p = 10 – 20 mbar were applied due to an increased boiling temperature of the binary reactant mixture (**section 5.1.2**). The investigated initial molar fractions for the racemic starting ester were $x_{(R/S)\text{-3-HEB},0}$ = 0.5 mol·mol^{-1} and $x_{(R/S)\text{-3-HEB},0}$ = 0.8 mol·mol^{-1} (**Figure 5.15**, **B**). Final distribution of the reactants over the column heights are presented in stationary state, which refers to at least two samples at a specific column height during constant column temperatures. A column height of H = 0 m refers to the bottom of the batch RD setup, whereas H = 0.72 m (for *(R/S)*-3-HEB) or H = 1.5 m (for *(R/S)*-2-PeOH) corresponds to the condenser stage at the top of the column. For separation of the reactants, RD is either equipped with a combination of Katapak-SP-like packing elements and Montz A3-500 wire gauze structures in the case of *(R/S)*-2-PeOH or just by Montz A3-500 in the case of *(R/S)*-3-HEB. A combination of column internals in the case of *(R/S)*-2-PeOH was applied to imitate catalyst integration in the mesh baskets of

Katapak-SP-like packings by packing glass beads inside and profit from increased separation efficiency within Montz A3-500 structures (**section 3.4**). With respect to literature, the separation efficiency of Katapak-SP like packings (HETP = 0.4 – 0.5 m at p = 100 mbar and F_V = 1.2 - 2.8 $Pa^{0.5}$) is reduced compared to Montz A3-500 column internals (HETP = 0.2 – 0.3 m at p = 100 mbar and F_V = 1.2 - 2.5 $Pa^{0.5}$) [156] [157] [45]. The presented experimental data show the mean values of obtained molar fractions over the column height for varied F-Factors in a range of F_V = 0.9 – 2.6 $Pa^{0.5}$. Calculation of the F-Factors is based on an energy balance in the evaporator of RD by the procedure described in **section 3.4** and additional data are given in **appendix section A** (**Figure A.1**, **Table A.1**).
In **Figure 5.15**, **A**, the height dependent column profiles of the initial material molar fractions of *(R/S)*-2-PeOH (diamonds) and PrBu (squares) at six different sampling positions within the column setup are visualized. Independent from the applied initial molar fractions in the bottom of the column, $x_{(R/S)\text{-2-PeOH}}$ increased with rising column heights at a simultaneous decrease of x_{PrBu}.

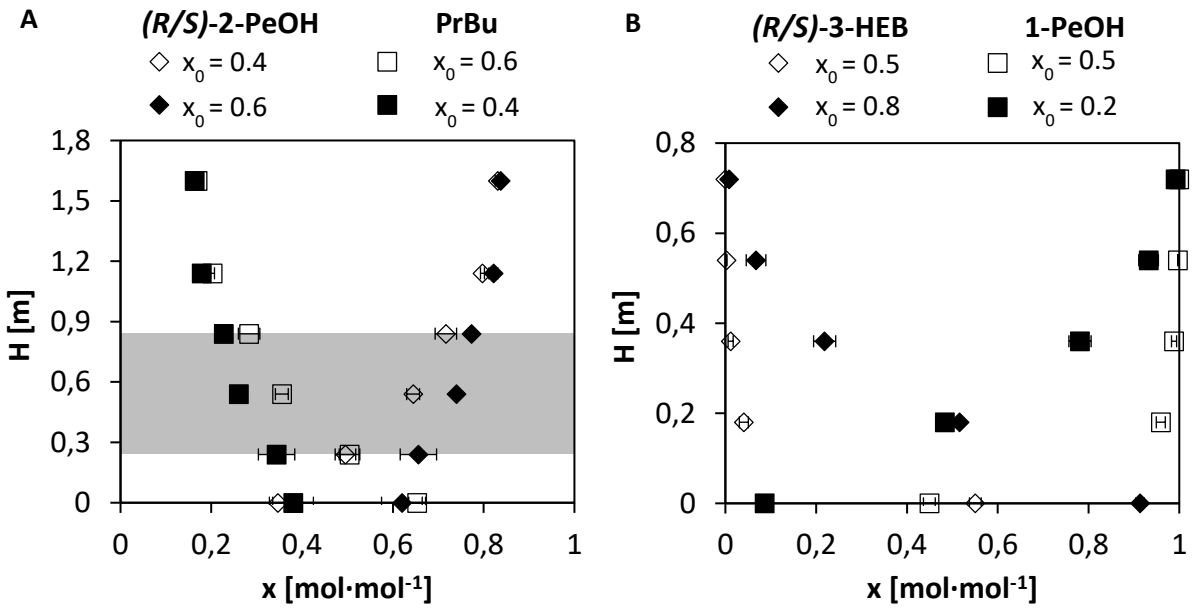

Figure 5.15: Stationary column profiles in reactive distillation without biocatalyst for the distribution of binary mixtures. **A**: *(R/S)*-2-PeOH and PrBu, the grey box indicates the feasible region for performing full KR at decreased temperatures; **B**: *(R/S)*-3-HEB and 1-PeOH. **Operation conditions: A**: p = 80 mbar, $m_{Bottom,0}$ = 800 g, total reflux (rr = ∞); $x_{(R/S)\text{-2-PeOH},0}$ = 0.4 mol·mol^{-1}: $T_{stat,\,top}$ = 59 ± 2°C, $T_{stat,\,bottom}$ = 64 ± 1°C (n = 3); $x_{(R/S)\text{-2-PeOH},0}$ = 0.6 mol·mol^{-1}: $T_{stat,\,top}$ = 56 ± 4°C, $T_{stat,\,bottom}$ = 63 ± 1°C (n = 4); **B:** $m_{Bottom,0}$ = 800 g, total reflux (rr = ∞) $x_{(R/S)\text{-3-HEB},0}$ = 0.5 mol·mol^{-1}: p = 20 mbar, $T_{stat,\,top}$ = 59°C, $T_{stat,\,bottom}$ = 69°C, SD: 4 samples at stationary conditions; $x_{(R/S)\text{-3-HEB},0}$ = 0.8 mol·mol^{-1}: p = 10 mbar, $T_{stat,\,top}$ = 43°C, $T_{stat,\,bottom}$ = 64°C, total reflux (rr = ∞), SD: 4 samples at stationary conditions

In the case of starting with $x_{(R/S)\text{-2-PeOH},0}$ = 0.4 mol·mol^{-1} (open diamonds), up to $x_{(R/S)\text{-2-PeOH}}$ = 0.83 ± 0.01 mol·mol^{-1} were detected at the column top (H = 1.5 m) at stationary column conditions. At the same time, a slight shift from $x_{(R/S)\text{-2-PeOH},0}$ = 0.4 mol·mol^{-1} to

$x_{(R/S)\text{-2-PeOH}}$ = 0.35 ± 0.02 mol·mol^{-1} was observed at the bottom of the column (H = 0 m). This decrease at H = 0 m was caused by an increased tendency for evaporation of the lower boiling reactant *(R/S)*-2-PeOH in the applied binary mixture (**section 2.1.1**). Within the lowest sampling position of the packing height at H = 0.24 m, an intersection of the molar fractions occurred with molar fractions of $x_{(R/S)\text{-2-PeOH}}$ = 0.50 ± 0.01 mol·mol^{-1}. In the experiments with an increased racemic initial molar fraction of $x_{(R/S)\text{-2-PeOH},0}$ = 0.6 mol·mol^{-1} (filled diamonds) was applied, similar $x_{(R/S)\text{-2-PeOH}}$ = 0.84 ± 0.01 mol·mol^{-1} were obtained at the column top (H = 1.5 m) under stationary conditions. In contrast to the previously discussed results, no intersection along the column height was observed for an initial molar fraction of $x_{(R/S)\text{-2-PeOH},0}$ = 0.6 mol·mol^{-1}.

Hence, for both investigated racemic initial molar fractions, separation over the RD column height ended up in similar $x_{(R/S)\text{-2-PeOH}}$ = 0.83 – 0.84 mol·mol^{-1} and x_{PrBu} = 0.16 - 0.17 mol·mol^{-1} at the top of the column. This behavior of similar molar fractions at the top of the column for varied initial molar fractions indicated the formation of an azeotropic mixture. In fact, this is in accordance with previously discussed results in **section 5.1.2**, in which a temperature minimum azeotrope at similar conditions of $x_{(R/S)\text{-2-PeOH}}$ = 0.84 mol·mol^{-1}, x_{PrBu} = 0.16 mol·mol^{-1}, T = 60.8 °C and p = 80 mbar was estimated by VLE-data in Aspen properties V8.0. Theoretically, overcoming the azeotrope is possible by shifting $x_{(R/S)\text{-2-PeOH}}$ in an additional performed KR reaction in the RD setup with the application of biocatalysts. Within the reaction, the molar fractions of the starting materials will be decreased and at carefully adjusted initial molar fractions full separation should be feasible. For offering advantageous conditions to catalyze the reaction sufficiently, availability of both starting materials at different column heights becomes particularly important. Therefore, the catalyst should at least be placed at the column sections containing *(R/S)*-2-PeOH and PrBu. According to the investigated binary mixtures of $x_{(R/S)\text{-2-PeOH},0}$ = 0.4 mol·mol^{-1} and $x_{(R/S)\text{-2-PeOH},0}$ = 0.6 mol·mol^{-1} in **Figure 5.15**, **A**, both starting materials can be detected along the whole column height and catalyst placement is theoretically sufficient in all column sections. In view of rather similar molar fractions of the starting materials in lower column sections, the catalyst should be preferably in RD column heights of H = 0.24 – 0.84 m (grey box, **Figure 5.15**, **A)**. Although the option of placing the catalyst in the bottom of the setup allows similar molar fractions of the starting materials, thermal deactivation of the biocatalyst preparation will be significantly increased due to formation of the high boiling pentyl ester *(R)*-2-PeBu (**section 5.2.2**). Hence, placement of the biocatalyst preparation at column sections with decreased temperatures is focused (H > 0 m). Besides, increased RD column heights of H > 0.84 m would allow further decreased temperatures at the position of the biocatalyst, but formed low boiling 1-PrOH will accumulate at those column positions. That is why in uppermost position of RD biocatalyst placement will not be as efficient as in lower positions of the column. The effects on the reaction performance of varied biocatalyst placement along the column height is discussed in detail for RD experiments with NZ435 in **section 5.4**.

For binary mixtures of *(R/S)*-3-HEB with 1-PeOH (**Figure 5.15**, **B**), their height dependent distribution in RD without catalyst at equimolar initial molar fractions of $x_{(R/S)\text{-3-HEB},0}$ = 0.5 mol·mol^{-1} and $x_{1\text{-PeOH},0}$ = 0.5 mol·mol^{-1} were compared to increased racemic starting molar fractions of $x_{(R/S)\text{-3-HEB},0}$ = 0.8 mol·mol^{-1} ($x_{1\text{-PeOH},0}$ = 0.2 mol·mol^{-1}). As a result, pure low boiling $x_{1\text{-PeOH}}$ was detected at the top of the column (H = 0.72 m) for both starting molar fractions at stationary conditions, whereas no *(R/S)*-3-HEB was present. Initial molar fractions of $x_{(R/S)\text{-3-HEB},0}$ = 0.5 mol·mol^{-1} (open diamonds) revealed a considerably decrease from $x_{(R/S)\text{-3-HEB}}$ = 0.55 ± 0.01 mol·mol^{-1} in the bottom of RD to $x_{(R/S)\text{-3-HEB}}$ = 0.05 ± 0.01 mol·mol^{-1} at the lowest sampling position within the packing height (H = 0.18 m). At initial molar fractions of $x_{(R/S)\text{-3-HEB},0}$ = 0.8 mol·mol^{-1} (filled diamonds), constantly decreasing molar fractions of *(R/S)*-3-HEB were observed with an intersection of both reactants at H = 0.18 m $x_{(R/S)\text{-3-HEB}}$ = 0.51 ± 0.01 mol·mol^{-1} (filled squares).

In contrast to the results in **Figure 5.15**, **A**, full separation for two binary mixtures of *(R/S)*-3-HEB and 1-PeOH over the applied RD column height was achieved (**Figure 5.15**, **B)**. This is indicated by pure 1-PeOH at the top of the column. Hence, no azeotrope formation was observed for the racemic starting ester, which would allow less challenging separation compared to the results of *(R/S)*-2-PeOH and PrBu. However, the placement of the biocatalyst becomes challenging due to less availability of the starting materials at $x_{(R/S)\text{-3-HEB},0}$ = 0.5 mol·mol^{-1}. Only in the bottom and at H = 0.18 m, higher boiling *(R/S)*-3-HEB was detected. A broadened column section for placing the biocatalyst can only be realized by increasing the molar fraction of *(R/S)*-3-HEB. Although placement of the biocatalyst at $x_{(R/S)\text{-3-HEB},0}$ = 0.8 mol·mol^{-1} would be feasible in a range of H = 0.18 – 0.54 m in the investigated setup, the reaction performance at $x_{(R/S)\text{-3-HEB},0}$ > 0.66 mol·mol^{-1} prevents full KR with optical pure *(S)*-3-HEB due to a deficit in $x_{1\text{-PeOH},0}$ (**section 5.2.1**). The main reason for reduced availability of both starting materials in the packing height of the column is the increased difference in the boiling temperatures of *(R/S)*-2-PeOH and 1-PeOH of $\Delta T_{evaporation}$ = 24 °C (**section 5.1.2**). Indeed, the observed challenges in column operation without catalyst proves previously discussed feasibility based on the preselection criteria in **section 5.1.1** and **section 5.1.2**.

Finally, the presented results in **Figure 5.15**, **A** & **B** clearly demonstrated no feasibility of the starting materials *(R/S)*-3-HEB and 1-PeOH for biocatalytic RD, supported by initially determined preselection criteria. On the other hand, feasibility of KR by *(R/S)*-2-PeOH with PrBu detected by the preselection criteria was successfully proven for biocatalytic RD in column experiments without catalyst. Those results underline the importance of establishing a preselection basis prior to experimental investigations, which will be discussed in the following chapters of this work.

Concise summary of section 5.2.4:

- Distribution of the starting materials along the RD column height without catalyst shows availability of both starting materials over the whole column height in the case of *(R/S)*-2-PeOH with PrBu and confirms the estimated azeotropic mixture
- Less availability of *(R/S)*-3-HEB in the whole column height is detected

5.2.5. Interim Summary: Characterization of Kinetic Resolution Reactions

- The biocatalyst preparation NZ435 is selected for the implementation in RD in this work due to 12 – 16 times increased catalytic activity compared to gel coating material and high thermal stability up to T = 80 °C
- Several requirements for biocatalytic reactive distillation can be derived from the obtained results in stirred tank reactors (STR) during the characterization phase:
    a. Starting molar fractions should be adjusted to $x_{(R/S)\text{-substrate},0} \leq 0.66$ mol·mol^{-1} to theoretically allow full KR performance
    b. Excellent enantioselectivity ($E \geq 100$) is needed
    c. As long as an equilibrium limited reaction is present ($K_{eq} < 1$), the feature of *in situ* separation in RD can be used to shift the equilibrium to the product side and to reach full KR under vacuum conditions
    d. Back reactions are avoided under vacuum conditions
    e. Placement of NZ435 should be realized at least in lower column sections of the packing height ($H \geq 0.24$ m) despite the bottom to allow availability of both starting materials and simultaneously increase the catalyst lifetime by decreased column temperature at the position of the catalyst
    f. KR with the chiral starting alcohol *(R/S)*-2-PeOH fulfills the stated requirements and is therefore selected for investigations in a reactive distillation setup

5.3. Implementation of Selected Reactions in Biocatalytic Reactive Distillation

On the basis of the selected and characterized CalB catalyzed kinetic resolution (KR) reactions of *(R/S)*-2-pentanol (*(R/S)*-2-PeOH) with either ethyl butyrate (EtBu) or propyl butyrate (PrBu) from the described and discussed results within stirred tank reactors (STR) in the previous **sections 5.1** and **5.2**, this part will focus transferring and comparing this results to biocatalytic reactive distillation (RD) application. The major aim of this part is the implementation of NZ435 in the RD column setup as well as the focus on reaction performance of two different reactions in RD. The following sections address the transfer and comparison of the results from STR experiments at reduced pressures (VAC = vacuum) to biocatalytic RD:

1. Comparison of the reaction performance in stirred tank reactors at reduced pressure and in biocatalytic reactive distillation (**section 5.3.1**)
2. Influence of the boiling point order on reaction performance (**section 5.3.2**)

5.3.1. Comparison of the Reaction Performance in Stirred Tank Reactors at Reduced Pressure and in Biocatalytic Reactive Distillation

For the transfer of obtained characteristics in STR experiments at reduced pressure (VAC) in **section 5.2.3** (**Figure 5.14**, **A**) to the batch biocatalytic RD column setup, the KR experiments at similar starting molar fractions of the racemic mixture *(R/S)*-2-PeOH ($x_{(R/S)\text{-2-PeOH},0}$ = 0.1 mol·mol^{-1}) and the starting ester EtBu ($x_{EtBu,0}$ = 0.9 mol·mol^{-1}) at p = 100 mbar and T = 60 °C were performed. Schemes of the applied reactor setups are depicted in **Figure 5.16**, **A**. The main differences between both reactors were the position of the catalyst preparation NZ435 and the multistep separation along the column height in RD. While NZ435 was placed in the liquid volume in VAC experiments, it is distributed in four Katapak-SP-like catalytic packing elements at the bottommost column heights (H1 – H2) in the RD setup. A higher separation efficiency in the RD setup was generated by non-catalytic wire gauze structures (Montz A3-500) at increased column heights of H3 – H4 (grey area: **Figure 5.16**, **A**).

In **Figure 5.16**, **B**, the enantiomeric excess of *(S)*-2-PeOH and *(R)*-2-PeBu for both experimental setups is shown over the conversion. In the RD setup, manually enabled fractional distillation at the top of the column was performed with a reflux ratio of rr = 20 (20 : 1) during the range of 43.4 ± 4.1 % ≤ X ≤ 53.3 ± 4.5 % (grey area, **Figure 5.16**, **B**). Presented standard deviations (SD) for the RD experiment refers to the maximum error estimation according to **section 3.4**. The performed manual reflux strategy corresponds to a liquid side stream at the column top, which is switched on and off by the operator at specific time points. For a detailed description of this manual reflux strategy, it is referred to **section 3.4**. The enantiomeric excess in both reactor setups (VAC, open data points & RD, filled data points) are compared to each other as well as to theoretical calculated data based on

the method of *Chen et al. (1982)* (calc., lines in **Figure 5.16**, **B**) [115]. Within the experiments of stirred tank reactors, the enantiomeric excess as well as the conversion can directly be calculated by the withdrawn samples. For the RD experiment the situation becomes more complex and the samples at different height positions were considered to calculate the parameters in the RD experiment. Therefore, presented data for $ee_{(R)\text{-2-PeBu}}$ and $ee_{(S)\text{-2-PeOH}}$ are referred to the mean values including all sampling positions in the RD column to allow a consideration of the liquid column hold-up. The corresponding conversion was calculated based on the sum of changed moles of the racemic starting material *(R/S)*-2-PeOH at all sampling positions related to the initially applied moles of *(R/S)*-2-PeOH. An overview on the calculation procedure is given in **section 3.4**.

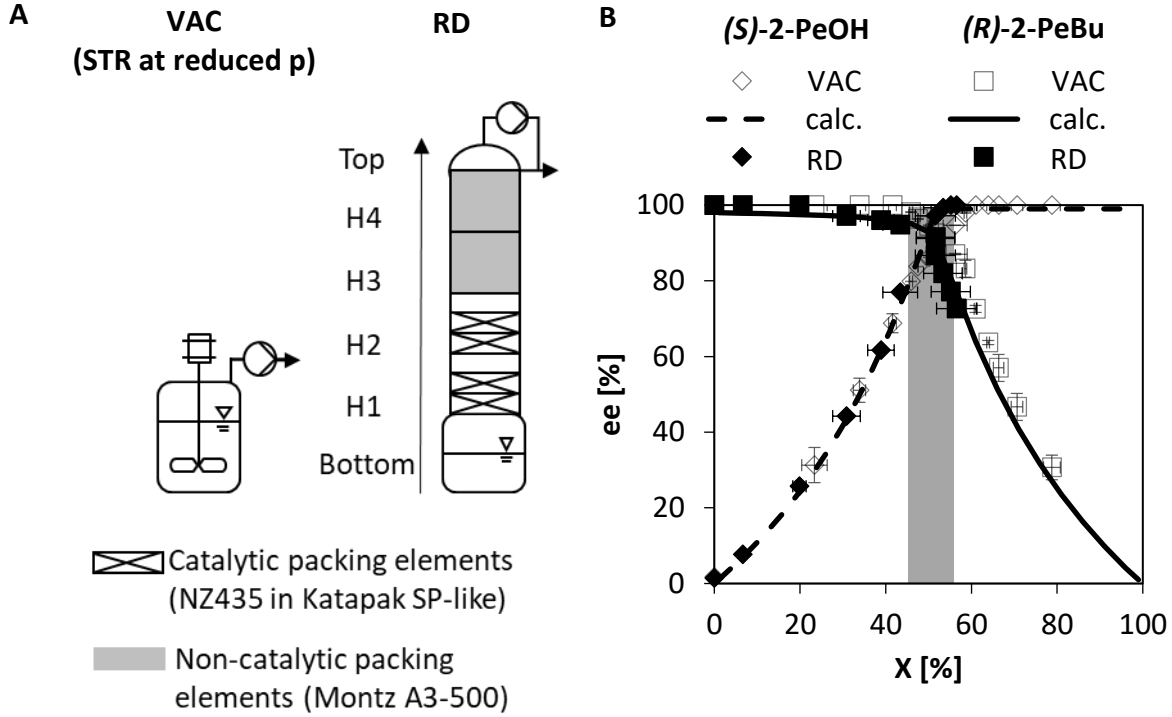

Figure 5.16: Comparison of kinetic resolution performance for *(R/S)*-2-PeOH with EtBu in a stirred tank reactor operated at reduced pressure (VAC) and biocatalytic batch reactive distillation (RD). **A**: Applied reactor setups with NZ435 either placed in the liquid volume (VAC) or in catalytic packing elements (RD). **B**: Experimentally and calculated data for the enantiomeric excess ($ee_{(S)\text{-2-PeOH}}$, $ee_{(R)\text{-2-PeBu}}$) at rising conversion (X). **Operation conditions**: $x_{EtBu,0}$ = 0.9 mol·mol^{-1}, $x_{(R/S)\text{-2-PeOH},0}$ = 0.1 mol·mol^{-1}, p = 100 mbar; **VAC** (n=2): T = 60 °C, m_{NZ435} = 0.35 g (c_{NZ435} = 50 mg·mL^{-1}, c_{NZ435} = 500 mg·g$_{(R/S)\text{-2-PeOH},0}^{-1}$); **RD** (n = 1): $m_{Bottom,0}$ = 800 g, grey box: area of manually adjusted fractional distillation with rr = 20 (20 : 1), T_{Bottom} = 58 – 64 °C, m_{NZ435} = 6.5 g (c_{NZ435} = 104 mg·g$_{(R/S)\text{-2-PeOH},0}^{-1}$), SD: refers to maximum error estimation according to **section 3.4**.

During RD operation, constantly increasing enantiomeric excess of the desired target compound *(S)*-2-PeOH to $ee_{(S)\text{-2-PeOH}}$ > 99 % was observed with rising conversion up to X = 53.3 ± 4.5 %. A further increase in conversion to X = 56.5 ± 4.7 % had no effect on $ee_{(S)\text{-2-PeOH}}$ due to total consumption of the faster reacting enantiomer *(R)*-2-PeOH. At the same time, high enantioselectivity of the reaction was

confirmed by high enantiomeric excess values of the preferably formed ester *(R)*-2-PeBu ($ee_{(R)\text{-2-PeBu}}$ > 94.8 ± 0.2 %) until X = 43.4 ± 4.1 %. Same trends were true for previously discussed results in stirred tank reactors at reduced pressure (VAC) indicating high values for the enantiomeric excess of $ee_{(S)\text{-2-PeOH}}$ > 98 % in a range of 58.6 ± 0.7 % ≤ X ≤ 78.8 ± 1.9 % and high $ee_{(R)\text{-2-PeBu}}$ > 98 % at X ≤ 45.9 ± 0.4 %. For detailed discussion on the presented data within VAC experiments, it is referred to **section 5.2.3**.

Within presented experimental data in **Figure 5.16**, **B**, good agreement is observed for the two compared setups in VAC and RD experiments as well as the theoretical calculated values by revealed identical reaction performance for $ee_{(R)\text{-2-PeBu}}$ as well as $ee_{(S)\text{-2-PeOH}}$ with increasing conversion. Thus, it is obvious to see the successful implementation of NZ435 in Katapak-SP-like catalytic packings for full KR in the batch biocatalytic RD setup. Hence, the validation of similarities between VAC experiments and the RD column used in this work can be stated due to consistent data for enantiopure formation of *(S)*-2-PeOH.

Concise summary of section 5.3.1:

- Identical behavior with respect to $ee_{(S)\text{-2-PeOH}}$ and X in STRs at reduced pressure as well as in batch reactive distillation is achieved at p = 100 mbar and $x_{(R/S)\text{-2-PeOH},0}$ = 0.1 mol·mol^{-1}
- Experimental results are in good agreement with calculated ideal courses of $ee_{(S)\text{-2-PeOH}}$ and X

5.3.2. Influence of the Boiling Point Order on Reaction Performance

Changes in the boiling point order of the starting materials in CalB catalyzed KR are considered by substituting the applied chain length of the starting ester from an ethyl- to a propyl-side chain in EtBu and PrBu (**section 5.1.2**). In both reactions, *(R/S)*-2-PeOH served as the racemic starting alcohol. For experiments in biocatalytic batch RD, the same column conditions were chosen with respect to the starting molar fractions of *(R/S)*-2-PeOH ($x_{(R/S)\text{-2-PeOH},0}$ = 0.1 mol·mol^{-1}) and the varied starting ester EtBu or PrBu ($x_{Ester,0}$ = 0.9 mol·mol^{-1}). Schemes of the two RD experiments with varied starting esters are depicted in **Figure 5.17**, **A**. Moreover, operating the RD column at reduced pressures of p = 100 mbar for the application of EtBu and p = 80 mbar for PrBu indicates similar temperature differences between the pure boiling points of the starting materials of $\Delta T_{evaporation}$ = 9 - 10 °C according to the presented preselection approach (**section 5.1**). By this reduced temperature differences, any binary mixture of the starting materials should guarantee the availability of the reactants in the biocatalytic section of the column setup. While a similar mass of NZ435 of m_{NZ435} = 6.2 - 6.5 g was implemented within

Katapak-SP-like catalytic packing elements at the bottommost column height, distribution took place either in two (PrBu, only in H1) or four catalytic packing elements (EtBu, H1 - H2). The preparation of catalytic packing elements is described in **section 3.4** and is depicted in **Figure 5.17**, **A** by crosses for each catalytic packing element. Residual parts of the RD column were equipped with non-catalytic Montz A3-500 wire gauze packing elements (grey area, **Figure 5.17**, **A**). Fractional distillation at the top of RD was performed with reflux ratios of rr = 20 (20 : 1) for EtBu and rr = 7.5 (15 : 2) for PrBu in dependency of the applied starting ester. For PrBu, automated temperature controlled fractional distillation was applied within the RD experiment. This temperature controlled strategy comprises a liquid side stream at the top of the column independent from the operator but induced by a set temperature value (**section 3.4**).

In **Figure 5.17**, **B**, the results of the two experiments for KR performance with varied starting esters of EtBu and PrBu in biocatalytic RD are shown.

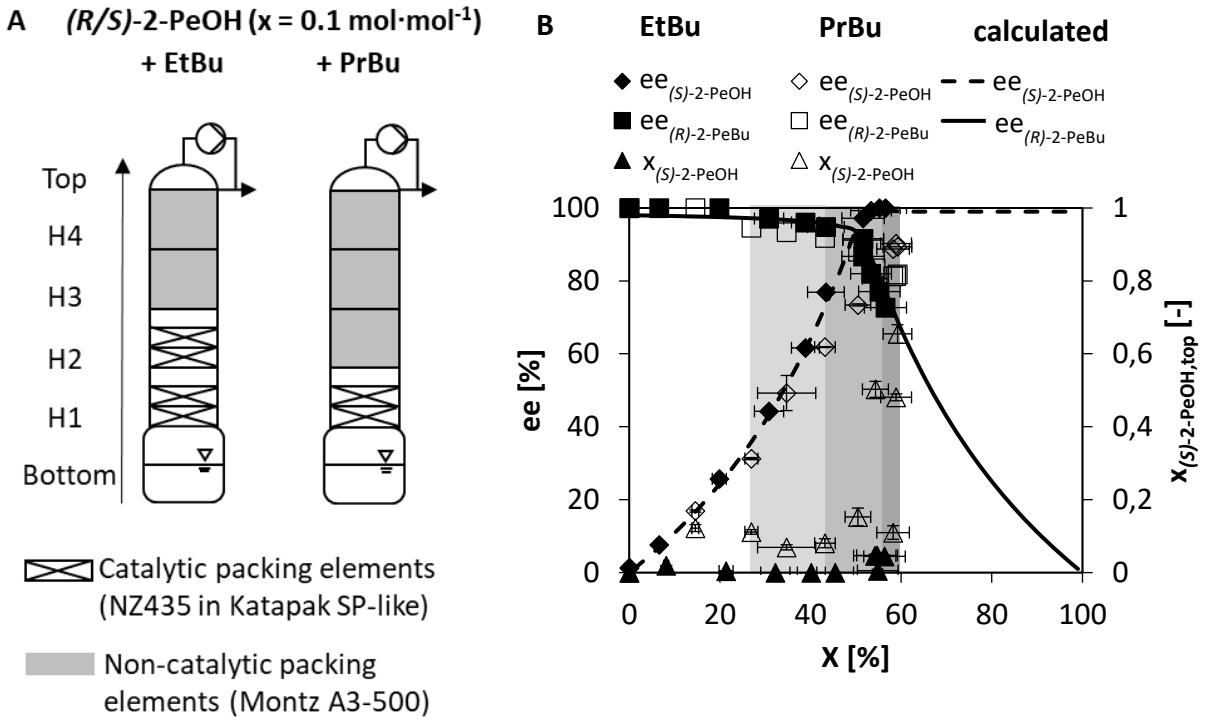

Figure 5.17: Investigation of a changed boiling point order in kinetic resolution performance of *(R/S)*-2-PeOH with either EtBu or PrBu in biocatalytic batch reactive distillation (RD). **A**: Equipment of the two RD experiments. **B**: Reaction performance by enantiomeric excess ($ee_{(S)\text{-2-PeOH}}$ and $ee_{(R)\text{-2-PeBu}}$) as well as molar fraction at the top of the column ($x_{(S)\text{-2-PeOH,top}}$) at rising conversion (X). **Operation conditions**: $x_{(R/S)\text{-2-PeOH},0}$ = 0.1 mol·mol^{-1}, $m_{Bottom,0}$ = 800 g, SD: refers to maximum error estimation according to **section 3.4**. **EtBu**: $x_{EtBu,0}$ = 0.9 mol·mol^{-1}, p = 100 mbar, at 43.4 ± 4.1 % ≤ X ≤ 53.3 ± 4.5 %: manually adjusted fractional distillation (rr = 20), T_{Bottom} = 58 – 64 °C, m_{NZ435} = 6.5 g (c_{NZ435} = 104 mg·g$_{(R/S)\text{-2-PeOH},0}^{-1}$), **PrBu**: $x_{PrBu,0}$ = 0.9 mol·mol^{-1}, p = 80 mbar, $m_{Bottom,0}$ = 800 g, grey areas: automated temperature controlled fractional distillation (rr = 7.5), set temperature value: T ≤ 43 °C (lightest grey), T ≤ 46 °C (light grey), T ≤ 60 °C (dark grey), T_{Bottom} = 70 - 74°C, m_{NZ435} = 6.15 g (c_{NZ435} = 110 mg·g$_{(R/S)\text{-2-PeOH},0}^{-1}$).

Hence, the focus is to investigate the influence of a changed boiling point order of the starting materials for the racemic starting alcohol *(R/S)*-2-PeOH (**section 5.1.2**). Beside the courses of enantiomeric excess for the target compound *(S)*-2-PeOH ($ee_{(S)\text{-2-PeOH}}$) and the formed pentyl ester *(R)*-2-PeBu ($ee_{(R)\text{-2-PeBu}}$), obtained molar fraction of the target compound at the top of the column ($x_{(S)\text{-2-PeOH}}$) are presented in dependency of conversion (X). Additionally, the theoretical calculated courses of the enantiomeric excess for *(S)*-2-PeOH (dashed line) and *(R)*-2-PeBu (filled line) are shown. The stepwise increased set temperature values for fractional distillation in the experiment with PrBu were adjusted from $T \leq 43$ °C at $27.0 \pm 1.4\ \% \leq X \leq 43.2 \pm 2.3\ \%$ to $T \leq 46$ °C at $43.2 \pm 2.3\ \% \leq X \leq 54.3 \pm 2.9\ \%$ and $T \leq 60$ °C at $54.3 \pm 2.9\ \% \leq X \leq 58.2 \pm 3.6\ \%$. Those areas are visualized by light to dark grey boxes for rising set temperature values in **Figure 5.17**, **B**. By this procedure, condensed liquid was stripped out of the top of the column automatically at the defined set temperature values, which behaved as temperature constraints.

Regarding the molar fraction of the target compound *(S)*-2-PeOH at the top of the column ($x_{(S)\text{-2-PeOH}}$), $x_{(S)\text{-2-PeOH}} < 0.05 \pm 0.01\ mol \cdot mol^{-1}$ was detected over the complete course of reaction in the case of applying EtBu (filled triangles, **Figure 5.17**, **B**). However, the composition of the reactants at the top of the column was shifted by manually applied fractional distillation between $43.4 \pm 4.1\ \% \leq X \leq 53.3 \pm 4.5\ \%$. An additional figure with respect to the molar fractions of all reactants in the top of the column is placed in **appendix section D** (**Figure D.1**, **A**). While EtOH was the dominant compound due to its accumulation at the top of the column at $X \leq 43.4 \pm 4.1\ \%$ with molar fractions up to $x_{EtOH} = 0.75 \pm 0.02\ mol \cdot mol^{-1}$, it was decreased by manual fractional distillation to $x_{EtOH} = 0.05 \pm 0.01\ mol \cdot mol^{-1}$ at $X = 53.3 \pm 4.5\ \%$. At the same time, EtBu became the major compound at the top of the column as it was the second lowest boiling component. An increase from $x_{EtBu} = 0.25 \pm 0.02\ mol \cdot mol^{-1}$, to $x_{EtBu} = 0.90 \pm 0.01\ mol \cdot mol^{-1}$ was observed within the period of $43.4 \pm 4.1\ \% \leq X \leq 53.3 \pm 4.5\ \%$. Within the courses of $ee_{(R)\text{-2PeBu}}$ (filled squares) and $ee_{(S)\text{-2-PeOH}}$ (filled diamonds) over conversion (X), the presented results of RD with EtBu showed typical behavior for an enantioselective KR reaction similar to the calculated behavior ($ee_{(R)\text{-2-PeBu}}$ = filled line and $ee_{(S)\text{-2-PeOH}}$ = dashed line), respectively. For a detailed description on the results of enantiomeric excess over conversion for applying EtBu as the starting ester, it is referred to the previously discussed results in **section 5.3.1** (**Figure 5.16**, **B**).

If the same initial molar fractions with the starting ester PrBu were applied, an increased molar fraction of the target compound *(S)*-2-PeOH up to $x_{(S)\text{-2-PeOH}} = 0.65 \pm 0.02\ mol \cdot mol^{-1}$ at $X = 59.2 \pm 3.2\ \%$ was realized at the top of the column (open triangles, **Figure 5.17**, **B**). Residual components in this sample at $X = 59.2 \pm 3.2\ \%$ were $x_{(R)\text{-2-PeOH}} = 0.04 \pm 0.01\ mol \cdot mol^{-1}$, $x_{1\text{-PrOH}} = 0.07 \pm 0.01\ mol \cdot mol^{-1}$ and $x_{PrBu} = 0.24 \pm 0.02\ mol \cdot mol^{-1}$. The corresponding molar fractions of all reactants in the top of the column experiment with PrBu over the whole course of the experiment are depicted in **appendix**

section D (**Figure D.1**, **B**). Within the first part of the reaction ($X \leq 43.2 \pm 2.3$ %), low molar fractions of up to $x_{(S)\text{-2-PeOH}} = 0.12 \pm 0.01$ mol·mol^{-1} were detected at the top of the column due to formation and separation of low boiling 1-PrOH in the column setup. This leads to increased molar fractions of low boiling 1-PrOH up to $x_{1\text{-PrOH}} = 0.83 \pm 0.01$ mol·mol^{-1} at the top of the column in the range of $X \leq 43.2 \pm 2.3$ %. In consequence of automated temperature controlled fractional distillation with a set temperature value of $T \leq 46$ °C, stripping of the low boiling 1-PrOH allowed an accumulation of *(S)*-2-PeOH at the top of the column in the second part of the reaction. This was indicated by the increase in its molar fraction up to $x_{(S)\text{-2-PeOH}} = 0.65 \pm 0.02$ mol·mol^{-1} at $X = 59.2 \pm 3.2$ %. Afterwards, no change in conversion was detected until the end of the experiment at simultaneously decreased molar fractions to $x_{(S)\text{-2-PeOH}} = 0.11 \pm 0.01$ mol·mol^{-1} and increased molar fractions of PrBu to $x_{PrBu} = 0.88 \pm 0.01$ mol·mol^{-1}. Additionally, $x_{(R)\text{-2-PeOH}} = 0.01 \pm 0.01$ mol·mol^{-1} were detected in the same sample. The behavior of substantially reduced molar fractions of *(S)*-2-PeOH can be explained by the low initial molar fractions of $x_{(R/S)\text{-2-PeOH},0} = 0.1$ mol·mol^{-1}, which was fully stripped over the top of the column in the end of the experiment. The expected course of enantiomeric excess with conversion for PrBu is presented by open squares for $ee_{(R)\text{-2-PeBu}}$ and open diamonds for $ee_{(S)\text{-2-PeOH}}$. In the period of $X \leq 43.2 \pm 2.3$ %, the enantiomeric excess of preferably formed *(R)*-2-PeBu was observed to be $ee_{(R)\text{-2-PeBu}} > 91.8 \pm 0.3$ %. At further increased conversion up to $X \leq 59.2 \pm 3.2$ %, $ee_{(R)\text{-2-PeBu}}$ was reduced to 81.3 ± 0.2 %. At the same time, constantly increasing enantiomeric excess of the target compound was detected up to $ee_{(S)\text{-2-PeOH}} = 90.3 \pm 0.3$ % at $X = 59.2 \pm 3.2$ %.

Comparing the obtained molar fractions of *(S)*-2-PeOH for the two RD experiments at the top of the column revealed successful accumulation and stripping of this target compound with molar fractions of $x_{(S)\text{-2-PeOH}} = 0.65 \pm 0.02$ mol·mol^{-1} in the case of PrBu as the applied starting ester. In contrast, it is prevented in the case of starting with EtBu ($x_{(S)\text{-2-PeOH}} \leq 0.05 \pm 0.01$ mol·mol^{-1}) due to a different boiling point order of the starting materials. Hence, instead of the target compound *(S)*-2-PeOH, EtBu had a lower boiling point and was enriched at the top of the column in consequence of stripping the lowest boiling compound EtOH. Changing this behavior by applying PrBu with a higher boiling temperature compared to the racemic starting alcohol *(R/S)*-2-PeOH lead to successful stripping of *(S)*-2-PeOH at the top of the column. In particular, the adjusted set temperature values for automated temperature controlled fractional distillation of $T \leq 46$ °C and $T \leq 60$ °C in the experiment with PrBu allowed a stepwise increase of the target compound *(S)*-2-PeOH at the top of the column. Finally, 13 times increased molar fractions of *(S)*-2-PeOH were detected at the column top operating the column with PrBu instead of EtBu as the starting ester and initial starting molar fractions of $x_{(R/S)\text{-2-PeOH},0} = 0.1$ mol·mol^{-1}. This substantial increase of a chiral target compound molar fraction in

biocatalytic batch RD demonstrates the need for a careful preselection of the starting materials, if an *in situ* isolation of the chiral target molecule is desired.

With respect to the courses of enantiomeric excess as function of conversion, high enantioselectivity in RD was observed for both column experiments due to high $ee_{(S)\text{-2-PeOH}}$ = 90.3 ± 0.3 % at X = 59.2 ± 3.2 % (PrBu) and excellent $ee_{(S)\text{-2-PeOH}}$ > 99 % at X = 53.3 ± 4.7 % (EtBu). While the results for *(R/S)*-2-PeOH and EtBu show good agreement until the end of the experiment at X = 56.5 ± 4.7 % between experimental data and calculated behavior with the assumption of an enantioselectivity of E = 100, the results for starting with *(R/S)*-2-PeOH and PrBu, fit the calculated values only at X ≤ 43.2 ± 2.3 %. At further increased conversions, deviations to the calculated behavior occurred. While $ee_{(R)\text{-2-PeBu}}$ gave higher values compared to calculated behavior, $ee_{(S)\text{-2-PeOH}}$ was reduced (**Figure 5.17**, **B**). Obtained experimental data of $ee_{(S)\text{-2-PeOH}}$ in RD were rather similar to the course of reduced enantioselectivity of E = 10 (for comparison see **Figure 2.7**, **A** in **section 2.2.4**), which would indicate an apparent behavior of low enantioselectivity. However, high enantioselectivity of E > 100 is expected due to previously discussed results in stirred tank reactors (**section 5.2.1**) for the starting ester PrBu. Looking at the course of the preferably formed pentyl ester *(R)*-2-PeBu (open squares in **Figure 5.17**, **B**), $ee_{(R)\text{-2-PeBu}}$ > 99 % were still detected in the beginning of the experiment. In fact, drastically reduced $ee_{(R)\text{-2-PeBu}}$ should be present at E = 10. Therefore, the reason for observed decreased $ee_{(S)\text{-2-PeOH}}$ in KR with PrBu has to be a feature of changed reaction performance in RD operation compared to the application of EtBu. The main difference of both reactions was the opportunity for *in situ* separation of the target compound *(S)*-2-PeOH caused by a changed boiling point order of the reactants, respectively. Hence, this should be the main influencing factor for the reduced $ee_{(S)\text{-2-PeOH}}$ in KR with PrBu. Especially during the period of fractional distillation at conversions of X > 43.2 ± 2.3 %, stripping of 1-PrOH lead to accumulation of *(S)*-2-PeOH as well as not reacted *(R)*-2-PeOH ($x_{(R)\text{-2-PeOH}}$ = 0.03 ± 0.01 mol·mol^{-1}) at the top of the column (**appendix section D**, **Figure D.1**, **B**). Simultaneously, no *(R)*-2-PeOH ($x_{(R)\text{-2-PeOH}}$ = 0 mol·mol^{-1}) was left in the bottom of the column and at the position of NZ435 in H1 (**appendix section D**, **Figure D.1**, **C** & **D**). Thereby, the low starting molar fraction of $x_{(S)\text{-2-PeOH}}$ = 0.10 mol·mol^{-1} prevented constant availability of *(R)*-2-PeOH at the position of NZ435 for increased conversions (X > 43.2 ± 2.3 %) and its simultaneous accumulation at the top of the column caused a reduced $ee_{(S)\text{-2-PeOH}}$ in the biocatalytic batch RD experiment.

To draw a conclusion, as long as small molar fractions of *(R)*-2-PeOH and *(S)*-2-PeOH were present in the column, optical pure *(S)*-2-PeOH at the top of RD were prevented at the applied fractional distillation strategy and a lowered boiling temperature of pure racemic *(R/S)*-2-PeOH compared to the non-chiral starting ester PrBu. On the contrary, availability of the racemic starting alcohol was achieved in the reactive section at the position of NZ435 at H1 – H2 for the lower boiling ester EtBu compared to *(R/S)*-2-PeOH even after fractional distillation of the low boiling product EtOH and the starting ester

EtBu. But in this case, *in situ* separation of *(S)*-2-PeOH during column operation is not possible at an applied initial molar fraction of $x_{(R/S)\text{-2-PeOH},0}$ = 0.1 mol·mol^{-1}. Therefore, the selection of a proper starting molar fraction, reasonable distribution of NZ435 along the column height and adjustment of the temperature constraint for fractional distillation should be addressed in further experiments to achieve *in situ* separation of the target compound with increased enantiomeric excess and purity at the top of the column (**section 5.4**).

Moreover, the influence of the applied boiling point order on the reaction performance of the two selected KR reactions is investigated by monitoring the temperature profiles over the course of conversion at four different column heights (Bottom, H2, H3, Top) in the same RD experiments (EtBu in **Figure 5.18**, **A** and PrBu in **Figure 5.18**, **B**). Horizontal lines represent the boiling points of the pure reactants (*(R/S)*-2-PeOH = filled line, EtBu or PrBu = dashed line, EtOH or 1-PrOH = dotted line) at the applied operating pressure for each experiment (p = 100 mbar (EtBu), p = 80 mbar (PrBu)). Within the grey shaded areas, the periods of fractional distillation are highlighted.

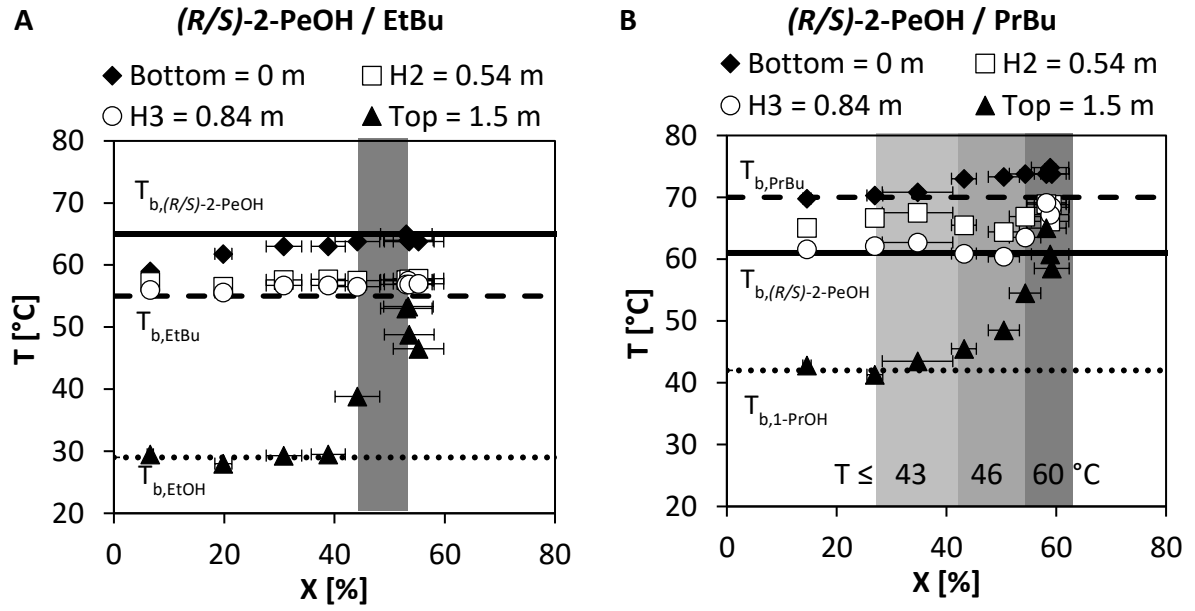

Figure 5.18: Temperature profiles within a changed boiling point order in kinetic resolution performance of *(R/S)*-2-PeOH with either EtBu or PrBu in biocatalytic batch reactive distillation (RD). **A**: EtBu ($x_{EtBu,0}$ = 0.9 mol·mol^{-1}), **B**: PrBu ($x_{PrBu,0}$ = 0.9 mol·mol^{-1}). **Operation conditions**: $m_{Bottom,0}$ = 800 g**,** $x_{(R/S)\text{-2-PeOH}}$ = 0.1 mol·mol^{-1} (detailed in caption of **Figure 5.16**).

In both experiments, the highest column temperature was measured in the bottom of the column displayed by diamond-shaped data points. Starting with a 9-fold molar excess of EtBu (**Figure 5.18**, **A**), this was dominating the initial boiling temperature of the reactant mixture of T_{Bottom} = 59 °C, which was slightly increased compared to the pure boiling temperature of EtBu (T_b = 55°C) at an operating

pressure of p = 100 mbar. This observed slight increase in the boiling temperature of the reactant mixture can be referred to the vapor-liquid binary interaction of both reactants during evaporation (**section 2.1.1**). Indeed, less molecules from the higher boiling racemic starting alcohol *(R/S)*-2-PeOH (T_b = 65°C) of the binary mixture change from the liquid to the vapor phase than of the lower boiling starting ester EtBu (**appendix section D**, **Figure D.2**, **A**). With proceeding conversion, an increase in the bottom temperature up to T_{Bottom} = 64 °C was detected because of formed high boiling *(R)*-2-PeBu. The same trend was present at the bottom of RD for a 9-fold molar excess of PrBu, in which an increase in the boiling temperature of the reactant mixture from T_{Bottom} = 70 °C to T_{Bottom} = 74 °C occurred (**Figure 5.18**, **B**). In contrast to the application of EtBu, the initial boiling temperature of the reactant mixture was similar to the boiling temperature of the higher boiling starting ester PrBu (T_b = 70 °C). This is referred to the changed boiling point order of the starting materials, of which *(R/S)*-2-PeOH is the lower boiling reactant and therefore evaporating in a higher extent compared to PrBu (**appendix section D**, **Figure D.1**, **C**). At increased X > 43.2 ± 2.3 % in the experiment with PrBu, the RD column temperature in the bottom became even higher than the boiling point of PrBu. This behavior occurred based on the formation of high boiling *(R)*-2-PeBu, which accumulated at the bottom of RD and simultaneously increased the boiling temperature of the reactant mixture (**appendix section D**, **Figure D.1**, **C**). Finally, this temperature increase clearly indicated successful biocatalytic reaction performance and supported the results in the offline samples.

At the column positions H2 (squares) and H3 (circles), decreased temperatures of the reactant mixtures were observed compared to the temperature in the bottom with values in between the boiling temperatures of the pure starting materials. Those temperatures showed the availability of both starting materials within the column height. In **Figure 5.18**, **A**, almost constant temperatures of $T_{H2,H3}$ = 57 ± 1 °C at H2 and H3 were monitored over the complete course of reaction including mainly EtBu with molar fractions of x_{EtBu} = 0.92 ± 0.02 mol·mol^{-1} (**appendix section D**, **Figure D.2**, **B** & **C**). Therefore, the temperatures at H2 and H3 were not affected by the applied manual fractional distillation strategy in the range of 43.4 ± 4.1 % ≤ X ≤ 53.3 ± 4.5 %. However, the experiment with PrBu demonstrated fluctuating column temperatures at H2 and H3 (**Figure 5.18**, **B**). While the temperature at position H2 ranged from T_{H2} = 65 °C to T_{H2} = 69 °C, slightly decreased values of T_{H3} = 62 °C were detected in the beginning of the reaction at H3 up to similar temperatures of T_{H3} = 69 °C at the end of the experiment. Some fluctuations can be referred to the automated temperature controlled fractional distillation strategy. Until the set temperature value was adjusted to T ≤ 60 °C, temperature at H3 stayed rather constant at T_{H3} = 61 ± 1 °C and afterwards it increased up to T_{H3} = 69 °C.

At the top of the column, the lowest temperature was detected (triangles in **Figure 5.18**, **A** & **B**). During reaction performance, the temperature at the top of the column is similar to the formed and accumulating low boiling compounds EtOH (**Figure 5.18**, **A**) or 1-PrOH (**Figure 5.18**, **B**). In the periods

of different fractional distillation strategies, drastically increased temperatures were detected. In the case of performing KR with EtBu, the temperature increased up to T_{Top} = 53 °C. This temperature almost referred to the pure boiling temperature of EtBu, as it was the dominating compound at the top of the column after stripping low boiling EtOH (**appendix section D**, **Figure D.1**, **A**). Moreover, decreased temperatures were observed after applied fractional distillation X > 53.3 ± 4.5 %, which was indicating further reaction and accumulation of EtOH (**appendix section D**, **Figure D.1**, **A**). The course of temperature at the top of the column for PrBu showed a constant temperature increase from T_{Top} = 42 °C to T_{Top} = 65 °C due to stepwise performed fractional distillation (**Figure 5.18**, **B**).

Finally, the obtained temperature profiles within the two KR reactions operated in RD and its interpretation clearly visualize the dependency of column operation on the applied boiling point order of the starting materials. Independent from the applied fractional distillation strategy, *in situ* separation of the formed low boiling product (EtOH or 1-PrOH) lead to increased temperatures at the top of the column. Due to an excess of the varied starting ester, the temperature at the top of the column after *in situ* separation was similar to the pure boiling points of the corresponding starting esters. Therefore, the temperature profiles support the results of molar fraction analysis discussed in **Figure 5.16**, **B** and allow evaluation of the reaction performance. Moreover, the column temperatures did not exceed T = 64 °C (EtBu) and T = 74 °C (PrBu) for both experiments. With respect to thermal deactivation of NZ435 (**section 5.2.2**), the results confirm feasible operation with NZ435 for both selected KR reactions with initial starting molar fractions of $x_{(R/S)\text{-2-PeOH},0}$ = 0.1 mol·mol^{-1}.

Concise summary of section 5.3.2:

- Changing the boiling point order of the starting materials has major impact on RD column experiments and allows *in situ* isolation of the target compound *(S)*-2-PeOH with $x_{(S)\text{-2-PeOH,top}}$ = 0.65 mol·mol^{-1} at $ee_{(S)\text{-2-PeOH}}$ = 90.3 ± 0.3 % (X = 59.2 ± 3.2 %) during operation of KR by *(R/S)*-2-PeOH with PrBu
- Applicability of NZ435 is proven by monitored temperatures staying constantly below T = 80 °C

5.3.3. Interim Summary: Implementation of Selected Reactions

- Experimental results for the chiral starting alcohol *(R/S)*-2-PeOH are successfully transferred from stirred tank reactors at reduced pressures to batch reactive distillation at starting molar fractions of $x_{(R/S)\text{-2-PeOH},0} = 0.1\ \text{mol}\cdot\text{mol}^{-1}$
- Predicted changes in the boiling point order within the preselection phase lead to 13 times increased chiral target compound molar fractions of $x_{(S)\text{-2-PeOH,top}} = 0.65\ \text{mol}\cdot\text{mol}^{-1}$ for KR of *(R/S)*-2-PeOH with PrBu compared to *(R/S)*-2-PeOH with EtBu
- The KR of *(R/S)*-2-PeOH with PrBu is selected for further work

5.4. Chiral Target Compound Isolation in Biocatalytic Reactive Distillation

Previously described and discussed results revealed the feasibility of kinetic resolution (KR) in biocatalytic reactive distillation (RD) with a solvent-free mixture of *(R/S)*-2-PeOH with PrBu. Successful *in situ* isolation of the target compound *(S)*-2-PeOH in consequence of adjusting the boiling point order and availability of starting materials in the reactive section was achieved in the batch RD column setup. However, in this subchapter improved reaction performance in batch RD column operation was addressed and further investigations were made to obtain isolated target compound with increased purity. Therefore, the following influencing parameters were investigated to achieve a better reaction performance in biocatalytic batch RD:

1. Influence of catalyst distribution (**section 5.4.1**)
2. Influence of temperature controlled fractional distillation (**section 5.4.2**)
3. Influence of initial molar fractions of the starting materials (**section 5.4.3**)
4. Economic evaluation of chiral target compound isolation (**section 5.4.4**)

5.4.1. Influence of Catalyst Distribution

Distribution of NZ435 in the batch RD setup was investigated by two different strategies for the arrangements of Katapak-SP-like catalytic packing elements over the column height. The catalytic packings were either placed alternately with two non-catalytic Montz A3-500 wire gauze elements (NZ435 in H1 - H4) or by applying a larger reactive section only in the bottommost positions of the RD setup (NZ435 in H1 - H2) (**Figure 5.19**, **A**). Residual sections in RD with the catalyst only in bottommost column positions were also equipped with non-catalytic Montz A3-500 wire gauze elements. Independent from the two different catalyst arrangements, similar catalyst amounts (m_{NZ435} = 30.36 g) as well as initial starting molar fractions of $x_{(R/S)\text{-2-PeOH},0}$ = 0.6 mol·mol^{-1} and $x_{PrBu,0}$ = 0.4 mol·mol^{-1} were applied. Detailed information on the number of catalytic and non-catalytic column internals and the corresponding amounts of NZ435 per packing element in the experiments are given in **section 3.4** (**Table 3.6** and **Table 3.7**). Stepwise fractional distillation was performed to strip low boiling 1-PrOH at T ≤ 46 °C in a first step and in a second step the higher boiling target compound *(S)*-2-PeOH by switching to T ≤ 60°C at high values for enantiomeric excess of *(S)*-2-PeOH. The temperature controlled reflux ratio was adjusted to rr = 9 (18 : 2) for stripping 1-PrOH and changed to rr = 3 (15 : 5) in the end of the experiment for faster stripping of *(S)*-2-PeOH in the case of alternately distribution of catalytic packing elements (NZ435 in H1 - H4). In the experiment with NZ435 in H1 - H2, a constant reflux ratio of rr = 9 (18 : 2) was applied over the whole reaction time.

Figure 5.19, **B** demonstrates the behavior of enantiomeric excess ($ee_{(S)\text{-2-PeOH}}$, diamonds) and purity ($x_{(S)\text{-2-PeOH}}$, triangles) with respect to the target compound *(S)*-2-PeOH over the course of conversion (X),

whereas $ee_{(S)\text{-2-PeOH}}$ represents the arithmetic mean over the whole RD column height and $x_{(S)\text{-2-PeOH}}$ the molar fraction only in the uppermost sampling position at the top of batch RD. Filled data points correspond to the first experiment with NZ435 placed in H1 - H4 and open data points represent the second experiment with NZ435 placed in H1 - H2. Additionally, the theoretical calculated course of $ee_{(S)\text{-2-PeOH}}$ for an enantioselective reaction (E = 100) is depicted by a dashed line. Presented standard deviations (SD) for $ee_{(S)\text{-2-PeOH}}$, $x_{(S)\text{-2-PeOH}}$ and X were calculated by maximum error estimation according to the procedure in **section 3.4**. An overview on those determined maximum errors is summarized in **Table 3.9** (**section 3.4**). For the discussion, SD between both experiments are given. Similar fractional distillation at the corresponding temperature constraint ($T \leq 46$ °C, $T \leq 60$ °C) is depicted by filled vertical lines and arrows for NZ435 placed in H1 - H4 as well as dashed vertical lines and arrows for NZ435 placed in H1 - H2 (**Figure 5.19**, **B**).

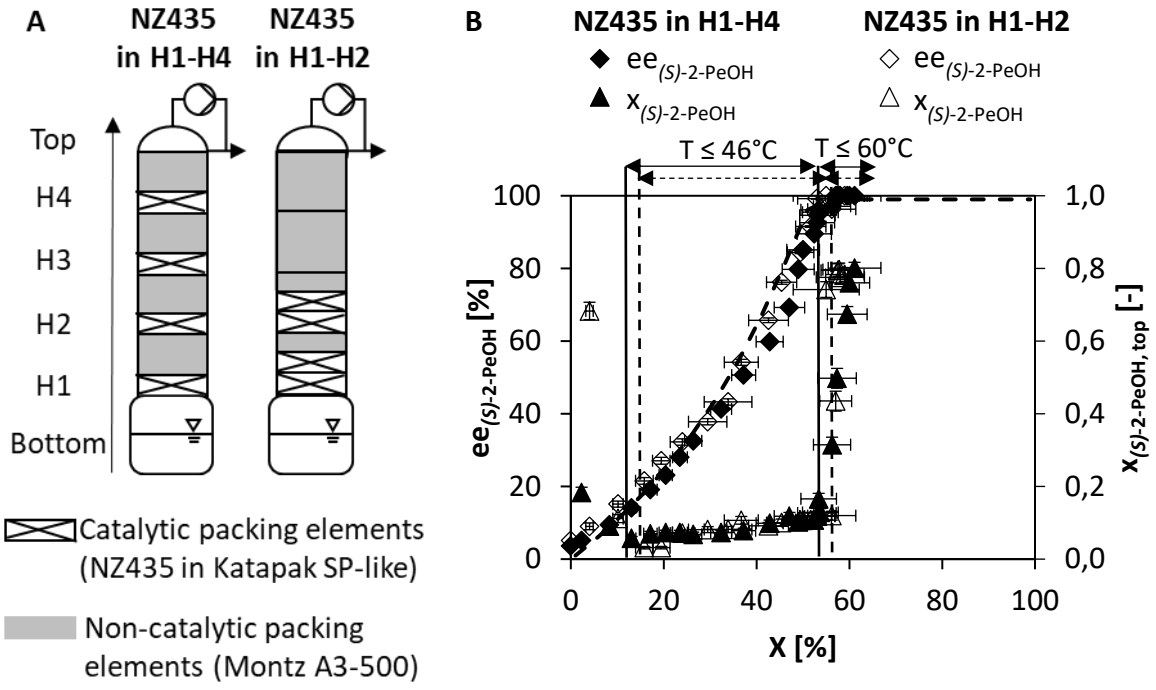

Figure 5.19: Catalyst distribution of NZ435 in batch reactive distillation (RD). **A**: Scheme of two distribution strategies. **B**: Influence of the distribution strategies on the enantiomeric excess ($ee_{(S)\text{-2-PeOH}}$) over the whole column and the purity ($x_{(S)\text{-2-PeOH,top}}$) at the top of RD. **Operation conditions**: $x_{PrBu,0} = 0.4$ mol·mol^{-1}, $x_{(R/S)\text{-2-PeOH},0} = 0.6$ mol·mol^{-1}, p = 80 mbar, $m_{Bottom,0} = 800$ g, $m_{NZ435} = 30.36$ g ($c_{NZ435} = 75$ mg·g$_{(R/S)\text{-2-PeOH},0}^{-1}$), dashed line: calculated behavior of $ee_{(S)\text{-2-PeOH}}$, temperature induced fractional distillation at $T \leq 46$ °C and $T \leq 60$ °C: vertical lines and horizontal arrows (filled: NZ435 in H1 - H4, dashed: NZ435 in H1 - H2), SD: maximum error according to **section 3.4**.

In the beginning of both experiments, an increase of $x_{(S)\text{-2-PeOH,top}}$ was observed at the top of the column setup followed by a strong decrease up to a conversion of X = 14 ± 1 % and $x_{(S)\text{-2-PeOH,top}} < 0.05 \pm 0.01$ mol·mol^{-1}. This behavior can be explained by initially low concentrations of

the lowest boiling reaction product 1-PrOH, which was increasing afterwards due to constantly proceeding reaction and accumulation at the top of the column. Present differences in $x_{(S)\text{-2-PeOH,top}}$ between both experiments in the beginning of the reaction were related to evaporation of residual reaction compounds in the catalytic packing elements as they are reused for the second experiment. As the dominant compound in the column at the end of the experiments was *(S)*-2-PeOH, an increase from $x_{(S)\text{-2-PeOH,top}} = 0.2\ \text{mol·mol}^{-1}$ to $x_{(S)\text{-2-PeOH,top}} = 0.7\ \text{mol·mol}^{-1}$ occurred at the top of the column after starting a new experiment. Within the range of fractional distillation at $T \leq 46°C$ in between $14 \pm 1 < X < 55 \pm 2$ %, a continuous increase in $ee_{(S)\text{-2-PeOH}}$ up to 97 ± 2 % at slightly increasing $x_{(S)\text{-2-PeOH,top}}$ up to $0.13 \pm 0.01\ \text{mol·mol}^{-1}$ can be noted. In this part of the reaction, faster conversion of *(R)*-2-PeOH resulted in increased $ee_{(S)\text{-2-PeOH}}$ while $x_{(S)\text{-2-PeOH,top}}$ was constantly low with respect to continuous formation and accumulation of low boiling 1-PrOH. In the last part of the experiment ($X > 55 \pm 2$ %, $ee_{(S)\text{-2-PeOH}} > 99$ %), temperature induced fractional distillation was set to $T \leq 60$ °C to gain the target compound *(S)*-2-PeOH with increased purity at the top of the column. Immediately after changing the temperature for fractional distillation, strongly increased $x_{(S)\text{-2-PeOH}}$ can be observed. Finally, similar purities of at maximum $x_{(S)\text{-2-PeOH,top}} = 0.8\ \text{mol·mol}^{-1}$ with $ee_{(S)\text{-2-PeOH}} > 99$ % and $X = 61 \pm 4$% were reached within the top samples independent from the catalyst distribution. Those samples additionally contained molar fractions of $x_{1\text{-PrOH,top}} = 0.11 \pm 0.01\ \text{mol·mol}^{-1}$ and $x_{PrBu,top} = 0.09 \pm 0.01\ \text{mol·mol}^{-1}$. A comparison between the theoretical and experimental process of $ee_{(S)\text{-2-PeOH}}$ with conversion in **Figure 5.19**, **B** revealed good agreement for NZ435 distributed in H1 - H4 as well as NZ435 in H1 - H2. This indicates reproducibility of RD column operation even though NZ435 distribution is varied.

Hence, flexible arrangements of catalytic and non-catalytic packing elements seem to have no effect on the purity of *(S)*-2-PeOH ($x_{(S)\text{-2-PeOH}}$) and thereby on the separation efficiency. This result stays in contrast to the literature, in which an increased separation efficiency of Montz A3-500 is obtained compared to the application of Katapak-SP-like column internals [45]. It is stated to have a height equivalent to a theoretical plate (HETP) of HETP = 0.12 – 0.15 m at F-Factors in a range of 0.39 – 1.02 $Pa^{0.5}$ for Montz A3-500, while separation efficiency is reduced by HETP = 0.4 – 0.47 m for Katapak-SP-like packings in the same F-Factor range. One reason for similar behavior regarding the purity of *(S)*-2-PeOH in the performed experiments with differently distributed NZ435 (**Figure 5.19**, **B**) is the presence of azeotropic behavior at p = 80 mbar, T = 60.8 °C and $x_{(R/S)\text{-2-PeOH}} = 0.84\ \text{mol·mol}^{-1}$, which is discussed for a binary mixture of *(R/S)*-2-PeOH and PrBu in **section 5.1.2** (**Figure 5.6**, **D**). Therefore, an increased separation efficiency cannot result in preferable or full separation of *(R/S)*-2-PeOH and PrBu. To overcome the binary azeotrope, reduced molar fractions of PrBu should be addressed at the top of the column by varying the initial molar fraction of PrBu. If the reaction performance allows a shift to higher molar fractions than azeotropic composition, full separation of the reactants will be possible or the amount of formed azeotrope can at least be reduced. The second

reason for similar purities of *(S)*-2-PeOH in RD operation is the effect of the applied reflux ratio for temperature induced fractional distillation. Further increased purities might be feasible by stripping the residual molar fraction of low boiling 1-PrOH, which is still detected in the final top samples ($x_{1\text{-PrOH,top}}$ = 0.11 ± 0.01 mol·mol^{-1}). It has to be mentioned, that this procedure will only work for the detected binary azeotrope between *(R/S)*-2-PeOH and PrBu. As long as more complex azeotropic mixtures (i.e. ternary azeotropes) occur, it will not be possible to significantly increase the purity of *(S)*-2-PeOH by changing the starting molar fractions. However, the presence of ternary azeotropes is not investigated within this study. Both, the influence of varied starting molar fractions and different temperature controlled fractional distillation approaches is described and discussed in **section 5.4.2** and **section 5.4.3**.

As discussed above for **Figure 5.19**, **B**, the mean enantiomeric excess of *(S)*-2-PeOH over the whole column with respect to the different sampling positions is not affected by different arrangements of NZ435 in batch RD experiments. To get a more detailed view on the behavior of $ee_{(S)\text{-2-PeOH}}$ and detect differences or similarities between the varied catalyst arrangements, it was additionally investigated space-resolved at various column heights (**Figure 5.20**, **A** & **B**). The evaluation of space-resolved $ee_{(S)\text{-2-PeOH}}$ takes into consideration two comparable conversion points, one in an earlier stage of the reaction (X = 16.7 ± 0.9 %, **Figure 5.20**, **A**) and one in an increased stage of the reaction (X = 42.7 ± 0.1 %, **Figure 5.20**, **B**).

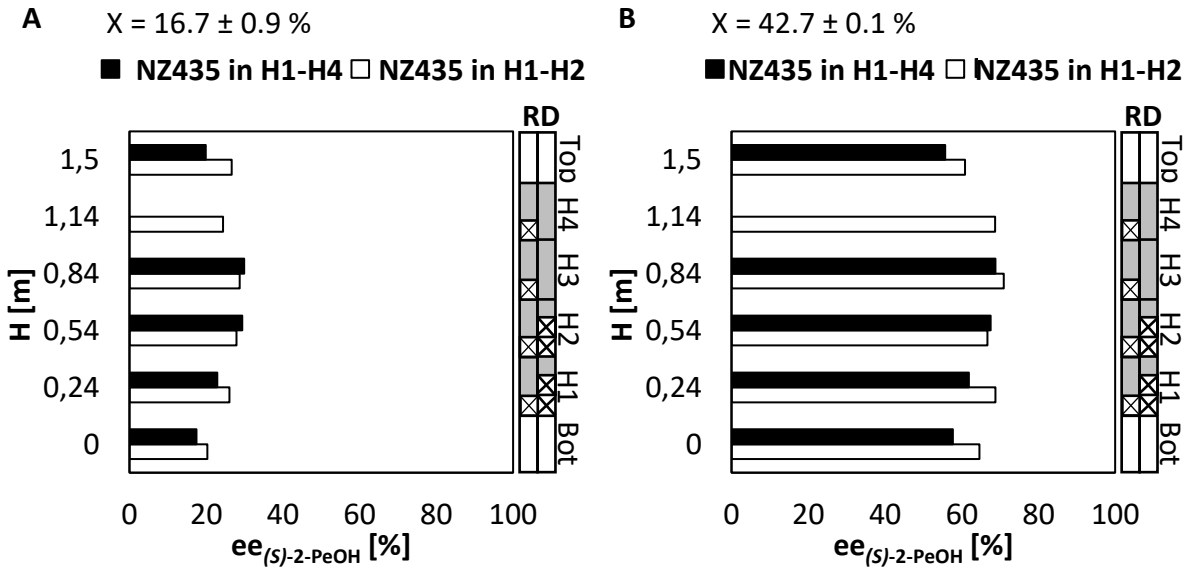

Figure 5.20: Spatially-resolved enantiomeric excess ($ee_{(S)\text{-2-PeOH}}$) at similar conversion points (**A**: X = 16.7 ± 0.9 %, **B**: X = 42.7 ± 0.1 %) for NZ435 either distributed in H1 - H4 or in H1 - H2 in batch reactive distillation. **Operation conditions**: $x_{PrBu,0}$ = 0.4 mol·mol^{-1}, $x_{(R/S)\text{-2-PeOH},0}$ = 0.6 mol·mol^{-1}, p = 80 mbar, $m_{Bottom,0}$ = 800 g, m_{NZ435} = 30.36 g (c_{NZ435} = 75 mg·g$_{(R/S)\text{-2-PeOH},0}^{-1}$), SD of X is referred to mean values of compared conversions points in both RD experiments (n = 2).

For the experiment with NZ435 in H1 - H2 (non-filled bars), the results refer to sampling carried out at six different column positions (Bottom, H1, H2, H3, H4, Top). In the experiment of NZ435 in H1 - H4 (filled bars), five sampling positions are considered (Bottom, H1, H2, H3, Top).

At both conversion points and investigated distributions of NZ435, similar $ee_{(S)\text{-2-PeOH}}$ were detected showing the highest $ee_{(S)\text{-2-PeOH}}$ in the middle of the RD column at sampling position H3 = 0.84 m. Same is true for conversions points at X = 24.1 ± 0.1 % and X = 33.1 ± 0.7 % depicted in **appendix section E** (**Figure E.1**, **A** & **B**). For NZ435 in H1 - H4, $ee_{(S)\text{-2-PeOH}}$ slightly increased stepwise from the bottom of the column (Bottom = 0 m) up to the height position H3 (H3 = 0.84 m) followed by reduced $ee_{(S)\text{-2-PeOH}}$ in the upper part at the top of the column (Top = 1.50 m). In contrast, results obtained within the experiment of placing NZ435 in H1 - H2 showed a more constant column profile.

Therefore, obtained $ee_{(S)\text{-2-PeOH}}$ at all investigated column positions was similar in both tested catalyst distribution strategies. This supports the possibility of applying flexible catalyst arrangements in batch RD operation indicated by the similar courses of enantiomeric excess with rising conversion in **Figure 5.19**, **B**.

Beside the behavior of enantiomeric excess and purity of *(S)*-2-PeOH with rising conversion, the temperature profile is mandatory to evaluate the different catalyst distribution strategies with respect to their influence on thermal deactivation of NZ435. Therefore, the temperature profile (T) is monitored within the course of reaction time (t) over the column height (Bottom, H2 – H4, Top) in **Figure 5.21**. It is referred to the same batch RD experiments from **Figure 5.19** with distribution of NZ435 either in H1 - H4 depicted by filled data points or in H1 - H2 illustrated by open data points. Temperature measurements were realized at similar positions to the sampling ports for all column heights despite H1. In addition to the temperature in the bottom (filled and open diamonds) and the top of the column (filled and open circles), mean temperature at the positions H2 – H4 (filled and open squares) is shown in **Figure 5.21**. Changes in the applied temperature for controlled reflux from T ≤ 46 °C to T ≤ 60 °C are visualized by vertical lines and horizontal arrows for the experiment with NZ435 in H1 - H4 and by dashed lines and arrows for NZ435 in H1 - H2. Given standard deviations in the discussion (SD) are referred to the mean value of both experiments, respectively.

In **Figure 5.21**, a similar decrease in the temperature from the bottom of the column to the top took place within both experiments over the complete reaction time. While only slight differences in the column temperature ΔT = 5 ± 1 °C occurred in the beginning of the experiments (t = 0 – 80 min) comparing the temperature in the bottom and the investigated positions along the column height (H2 – H4), a continuous increase to ΔT = 28 ± 2 °C is detected at the end of the experiments (t = 855 – 913 min). Increased temperature differences between those column sections were observed

due to almost constant temperatures of T = 60 ± 4 °C within the column sections of H2 – H4 and simultaneously rising temperatures from T = 65 ± 1 °C to T = 88 ± 2 °C in the bottom of the column.

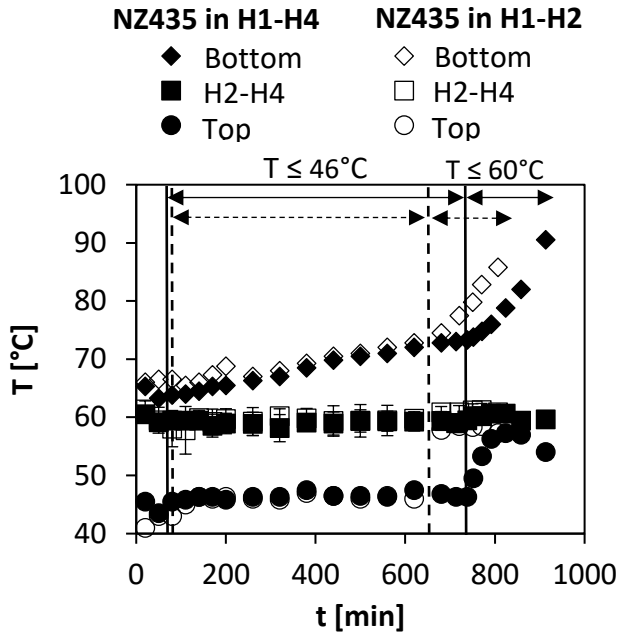

Figure 5.21: Temperature profile in batch reactive distillation for differently distributed NZ435 either in H1 – H4 or in H1 – H2. Operation conditions: $x_{PrBu,0}$ = 0.4 mol·mol^{-1}, $x_{(R/S)\text{-2-PeOH},0}$ = 0.6 mol·mol^{-1}, p = 80 mbar, $m_{Bottom,0}$ = 800 g, m_{NZ435} = 30.36 g (c_{NZ435} = 75 mg·g$_{(R/S)\text{-2-PeOH},0}^{-1}$), SD for temperature in H2-H4 refers to 3 positions in RD column height, vertical lines and arrows: temperature induced fractional distillation at T < 46 °C and T < 60 °C.

This trend is referred to the reactant composition within the column bottom and the column height, which is dominated by the starting materials in the beginning of the reaction with simultaneously low molar fractions of the high boiling reaction product (at t = 0 – 80 min: $x_{(R/S)\text{-2-PeBu}}$ < 0.10 ± 0.01 mol·mol^{-1}). The time dependent trends of the molar fractions with respect to all reactants within the RD column setup are depicted in **appendix section E** (**Figure E.2**, **A** - **E** for NZ435 in H1 - H4 and **Figure E.3**, **A** – **F** for NZ435 in H1 - H2). During operation, formation and accumulation of high boiling *(R/S)*-2-PeBu up to 0.90 ± 0.01 mol·mol^{-1} at t = 855 – 913 min at the bottom of the column caused an increased temperature compared to the column height and the column top with mainly *(S)*-2-PeOH ($x_{(S)\text{-2-PeOH,top}}$ = 0.80 ± 0.01 mol·mol^{-1}) and PrBu ($x_{PrBu,top}$ = 0.09 ± 0.01 mol·mol^{-1}). The effect of increased temperature differences is even enhanced after changing the temperature of controlled reflux to T ≤ 60 °C due to a faster stripping of lower boiling reactants such as 1-PrOH, *(R/S)*-2-PeOH and PrBu (vertical lines at t = 646 min and t = 730 min **Figure 5.21**). In contrast, a strictly decreased temperature difference of ΔT = 2 ± 1 °C is obtained between the mean temperature at H2 – H4 (T = 60 ± 4 °C) and the top of the column (T = 46 ± 1 °C) within the time period of a temperature for controlled reflux of T ≤ 60 °C (t > 646 min and t > 730 min). The observed decrease

can be related to the stripping of low boiling 1-PrOH from $x_{1\text{-PrOH,top}}$ = 0.83 ± 0.01 mol·mol^{-1} at the point of adjusting T ≤ 60 °C for fractional distillation to $x_{1\text{-PrOH,top}}$ = 0.11 ± 0.01 mol·mol^{-1}, which induced rising temperatures in the end of the experiment even at the top of the column. Beforehand, the temperature difference between H2 – H4 and the top of the column is nearly constant at ΔT = 14 ± 3 °C due to a constant temperature for controlled reflux at T ≤ 46 °C and concurrent high molar fractions of 1-PrOH at the column top ($x_{1\text{-PrOH,top}}$ = 0.86 ± 0.04 mol·mol^{-1} between t = 80 min and t = 646 - 730 min). Based on the described temperature profiles, less effects of deactivation concerning NZ435 can be guaranteed in the regions H2 - H4 by constant T = 60 ± 4 °C and in the top of the applied batch RD setup with T < 58 ± 2 °C (depending on the adjusted temperature for fractional distillation). In the bottom of the setup, constantly rising temperatures prevent application of the biocatalyst due to increased thermal deactivation. Although the temperature at H1 was not investigated within the RD experiments, NZ435 is placed at this position in the column height at which slightly higher temperatures compared to H2 - H4 can be expected. However, the temperature is definitely reduced compared to the bottom of the column. With respect to the temperature influence on the reaction performance with differently distributed NZ435, an increased temperature influence on the reaction velocity could have been assumed at the column top or bottom because of strong changes in the temperatures over the course of the experiments. But, according to obtained Arrhenius data discussed in **section 5.2.2** (**Figure 5.13**, **A**), a reduced impact of 1.2 times increased reaction speed in the chosen kinetic resolution reaction of *(R/S)*-2-PeOH with PrBu for deviations in temperature of ΔT < 10 °C was observed. That is why the reaction performance of the RD experiments was not affected by differently distributed NZ435, which was indicated by reduced effects on the enantiomeric excess and conversion behavior in **Figure 5.19**.

Concise summary of section 5.4.1:

- Reproducible batch RD performance is achieved for two varied distributions of NZ435 along the column height at starting molar fractions of $x_{(R/S)\text{-2-PeOH,0}}$ = 0.6 mol·mol^{-1}
- Full KR for the chiral target compound *(S)*-2-PeOH with $ee_{(S)\text{-2-PeOH}}$ > 99 % (X = 61 ± 4%) and increased purities up to $x_{(S)\text{-2-PeOH,top}}$ = 0.80 ±0.01 mol·mol^{-1} are obtained
- Monitored temperature profile proves the applicability of NZ435 in the column height with T = 60 ± 4 °C, while bottom temperature was significantly higher (up to T = 88 ± 2 °C)

5.4.2. Influence of Temperature Controlled Fractional Distillation

Previously discussed results in batch reactive distillation experiments with initial starting molar fractions of $x_{(R/S)\text{-2-PeOH},0}$ = 0.10 mol·mol^{-1} (**section 5.3.2**, **Figure 5.17**, **B**) as well as $x_{(R/S)\text{-2-PeOH},0}$ = 0.60 mol·mol^{-1} (**section 5.4.1**, **Figure 5.19**, **B**) showed the possibility of *in situ* separation of the chiral target compound *(S)*-2-PeOH at the top of the column by fractional distillation with purities up to $x_{(S)\text{-2-PeOH,top,max}}$ = 0.8 mol·mol^{-1}. The applied fractional distillation was based on an automated temperature controlled operation to adjust the reflux ratio according to the procedure described in **section 3.4**. In order to investigate the influence of this fractional distillation at the top of the reactive distillation column on the purity of *(S)*-2-PeOH, identical catalyst amounts as well as identical distribution of the catalyst were applied at initial starting molar fractions of $x_{(R/S)\text{-2-PeOH},0}$ = 0.65 mol·mol^{-1} and $x_{(R/S)\text{-2-PeOH},0}$ = 0.67 mol·mol^{-1} (**Figure 5.22, A**). While the same reflux ratio was applied (rr = 9 (18:2) at t < 1035 min, rr = 0 at t > 1035 min), time points for changing the top temperature for fractional distillation is varied during column operation. The fractional distillation strategy is divided into the following steps. Initially, reflux was adjusted to take place at T ≤ 46 °C in the top of the column. This allows separation of formed low boiling 1-PrOH from RD with a boiling point of T_b = 42 °C at the applied operating pressure of p = 80 mbar. During the experiment, the temperature constraint is increased stepwise up to T ≤ 60 °C to obtain the target compound *in situ* at the column top.

The sum of fractional distillate samples in mass stripped at the column top ($m_{sum,top}$, filled and open triangles) and the measured temperature at the column top (T_{top}, filled and open diamonds) are compared for the two experiments with $x_{(R/S)\text{-2-PeOH},0}$ = 0.65 mol·mol^{-1} (open data points) and $x_{(R/S)\text{-2-PeOH},0}$ = 0.67 mol·mol^{-1} (filled data points) over their proceeded reaction time (**Figure 5.22, B**). Changing the time intervals of applying the individual temperatures at the top of the column is the major difference in operation between the two experiments. Stepwise adjustment of the temperature setting for fractional distillation is visualized by full lines operating the column with $x_{(R/S)\text{-2-PeOH},0}$ = 0.67 mol·mol^{-1} and dashed lines in the case of $x_{(R/S)\text{-2-PeOH},0}$ = 0.65 mol·mol^{-1}. Starting with the sum of stripped sample mass at the column top at $x_{(R/S)\text{-2-PeOH},0}$ = 0.67 mol·mol^{-1} (filled diamonds), a constant temperature controlled reflux at T ≤ 46 °C was applied for the fractional distillation up to t = 680 min. After an initially observed continuous increase of the sum of stripped sample mass at the column top up to $m_{sum,top}$ = 147.2 g, a plateau is detected in between t = 440 - 680 min ($m_{sum,top}$ = 147.9 ± 0.5 g). In this time period, the distillate was mainly composed of low boiling 1-PrOH ($x_{1\text{-PrOH,top}}$ = 0.77 ± 0.03 mol·mol^{-1}) and *(S)*-2-PeOH ($x_{(S)\text{-2-PeOH,top}}$ = 0.16 ± 0.02 mol·mol^{-1}). Residual compounds in the distillate samples were the faster reacting *(R)*-2-PeOH ($x_{(R)\text{-2-PeOH,top}}$ = 0.04 ± 0.01 mol·mol^{-1}) and PrBu ($x_{PrBu,top}$ = 0.03 ± 0.01 mol·mol^{-1}). The corresponding time dependent course of the molar fractions in the top of the column are depicted in **appendix**

section E (**Figure E.4**, **A**). Immediately after increasing the temperature for controlled reflux to T ≤ 49 °C, stripping of accumulated reactants at the RD column top started again. This effect was even enhanced by further increased temperature for controlled reflux up to T ≤ 60 °C resulting in $m_{sum,top}$ = 367.2 g at the end of the experiment. Within the corresponding time interval between t = 680 – 1050 min at adjusted temperatures for controlled reflux of T ≤ 46 - 60 °C, a significant increase in the molar fraction of *(S)*-2-PeOH was observed from $x_{(S)\text{-2-PeOH,top}}$ = 0.19 mol·mol^{-1} to $x_{(S)\text{-2-PeOH,top}}$ = 0.93 mol·mol^{-1}. Simultaneously, considerable decreasing molar fraction of low boiling 1-PrOH were detected from $x_{1\text{-PrOH,top}}$ = 0.72 mol·mol^{-1} to $x_{1\text{-PrOH,top}}$ = 0.01 mol·mol^{-1} (**appendix section E**, **Figure E.4**, **A**). A similar trend over the course of the experiment can be observed in the measured temperature at the column top (T_{top}, filled triangles). Before and during the plateau of the sum of fractional distillate samples, temperature stays nearly constant at a level of T = 46 °C. After changing the temperature for controlled reflux, the column temperature increased stepwise to the set temperature values.

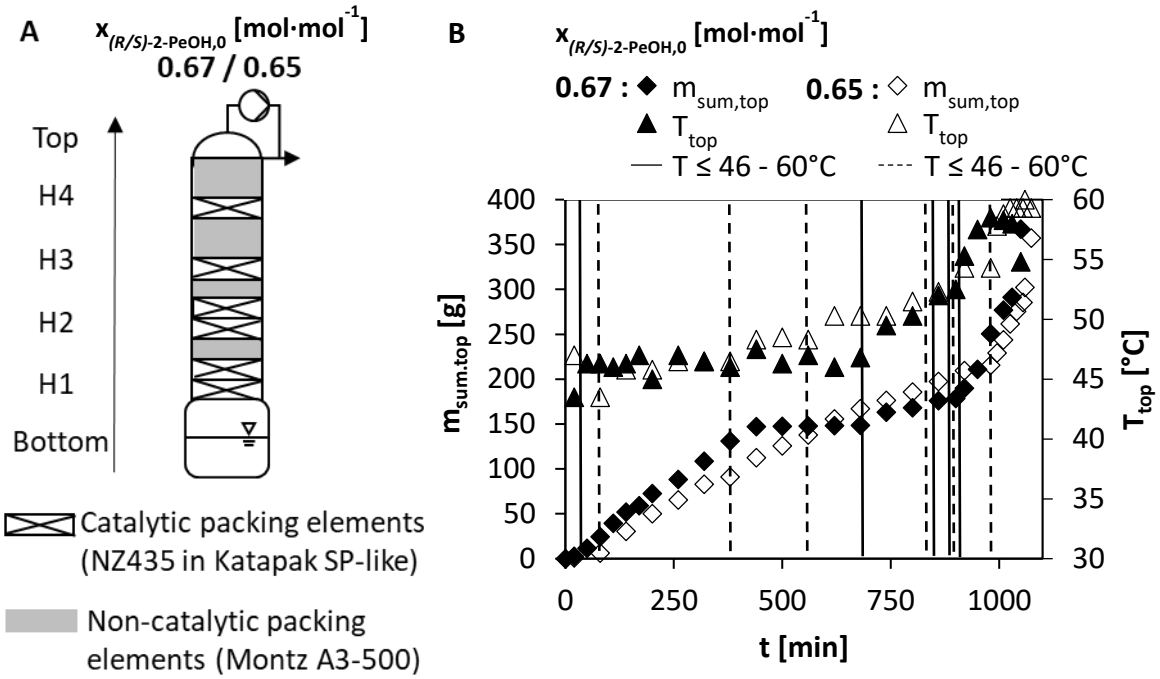

Figure 5.22: Automated temperature controlled fractional distillation in reactive distillation experiments **A**: Scheme of reactive distillation equipment for experiments with $x_{(R/S)\text{-2-PeOH,0}}$ = 0.67 mol·mol^{-1} and 0.65 mol·mol^{-1}. **B**: Influence of changed time intervals of adjusted temperature constraints for fractional distillation on the sum of fractional distillate samples in mass ($m_{sum,top}$) and the temperature at the top of the column (T_{top}). **Operation conditions**: p = 80 mbar, $m_{Bottom,0}$ = 800 g, m_{NZ435} = 45.3 g (c_{NZ435} = 98 - 104 mg·g$_{(R/S)\text{-2-PeOH,0}}^{-1}$), rr = 9 (18 : 2) at t < 1035 min, rr = 0 at t > 1035 min, T constrains: $x_{(R/S)\text{-2-PeOH,0}}$ = 0.67 mol·mol^{-1} (= filled vertical lines): 46°C (40 – 680 min), 49°C (680 – 830 min), 52°C (830 – 900 min), 55°C (900 – 920 min), 60°C (920 – 1050 min); $x_{(R/S)\text{-2-PeOH,0}}$ = 0.65 mol·mol^{-1} (= dashed vertical lines): 46°C (80 – 380 min), 48°C (380 – 560 min), 50°C (560 – 830 min), 52°C (830 – 900 min), 54°C (900 – 980 min), 60°C (980 – 1074 min).

For the sum of stripped sample mass at the column top in the second experiment with $x_{(R/S)\text{-2-PeOH},0}$ = 0.65 mol·mol^{-1} (open diamonds), reduced time intervals between the changes in temperature for controlled reflux in the range of T ≤ 46 °C up to T ≤ 54 °C resulted in almost constant amounts fractionated at the column top up to $m_{sum,top}$ = 215.7 g at t = 980 min. The corresponding molar fraction of the target compound *(S)*-2-PeOH at t = 980 min was $x_{(S)\text{-2-PeOH},top}$ = 0.50 mol·mol^{-1}, including $x_{1\text{-PrOH},top}$ = 0.45 mol·mol^{-1}, $x_{(R)\text{-2-PeOH},top}$ = 0.02 mol·mol^{-1} and $x_{PrBu,top}$ = 0.03 mol·mol^{-1} (**appendix section E**, **Figure E.4**, **B**). Afterwards, further increase in the temperature constraint to T ≤ 60 °C allowed a fast removal of reactants from RD with a final $m_{sum,top}$ = 357.3 g. This can be noted in the composition of the final fractionated top sample at t = 1074 min, wherein the target compound molar fraction is $x_{(S)\text{-2-PeOH},top}$ = 0.95 mol·mol^{-1} ($x_{1\text{-PrOH},top}$ = 0.01 mol·mol^{-1}, $x_{PrBu,top}$ = 0.04 mol·mol^{-1}). With respect to the monitored temperature at the top of the column, stepwise increase in the column temperature in consequence of adjusting the temperature for fractional distillation is clearly visible in **Figure 5.22**, **B** in the course of open triangles.

In fact, the results of both experiments in **Figure 5.22**, **B** demonstrated the effect of automated temperature controlled fractional distillation during RD operation. As long as the temperature constraint for temperature controlled fractional distillation is below the boiling point of the desired target compound *(S)*-2-PeOH (T ≤ 46 - 55 °C), mainly low boiling 1-PrOH was withdrawn at the top of the column at rr = 9 (18 : 2). Simultaneously, this supports the KR reaction by constant removal of 1-PrOH and less removal of higher boiling compounds (i.e. *(S)*-2-PeOH). Generally, in a first step high enantiomeric excess of the target compound *(S)*-2-PeOH should be obtained by either constant or stepwise increasing the temperature for controlled fractional distillation prior to the adjustment of the temperature constraint to the boiling temperature of the target compound in the presented reaction case of kinetic resolution. Moreover, an observed plateau within the data points of initial molar fractions of $x_{(R/S)\text{-2-PeOH},0}$ = 0.67 mol·mol^{-1} (filled diamonds in **Figure 5.22**, **B**) indicated the point of changing the temperature constraint. At an observed constant temperature at the top of the column, which is similar to the adjusted temperature constraint, an increased temperature constraint should be adjusted to prevent the formation of a plateau. This is successfully demonstrated for initial molar fractions of $x_{(R/S)\text{-2-PeOH},0}$ = 0.65 mol·mol^{-1} by constantly increasing $m_{sum,top}$. In a second step, adjusting the temperature constraint near to the boiling point of the target compound *(S)*-2-PeOH (T ≤ 60 °C) generated fast stripping of reactant mixtures containing *(S)*-2-PeOH. This fast stripping procedure was applied for both experiments only in the end of the reaction for t > 1035 min to enhance reactant removal and to withdraw nearly pure *(S)*-2-PeOH *in situ* at the column top by operating without any reflux back into the column at rr = 0 (**Figure 5.22, B**).

Additionally, the discussed influence of the automated temperature controlled fractional distillation on the reaction performance ($ee_{(S)\text{-2-PeOH,top}}$, $x_{(S)\text{-2-PeOH,top}}$) at the top of the column was investigated for the initial starting molar fractions of $x_{(R/S)\text{-2-PeOH},0}$ = 0.65 mol·mol^{-1} (**Figure 5.23**, **A**) and $x_{(R/S)\text{-2-PeOH},0}$ = 0.67 mol·mol^{-1} (**Figure 5.23**, **B**). Chosen parameters were the enantiomeric excess of the target compound *(S)*-2-PeOH ($ee_{(S)\text{-2-PeOH,top}}$, open and filled diamonds) and the corresponding purity ($x_{(S)\text{-2-PeOH,top}}$, open and filled triangles) in dependency of the isolated yield ($Y_{(S)\text{-2-PeOH,isolated,top}}$). All three parameters were investigated in withdrawn sample fractions at the column top. For the calculation of the isolated yield, the moles of *(S)*-2-PeOH in the withdrawn top samples are referred to the moles of *(R/S)*-2-PeOH in the beginning of the experiment. During the experiments, withdrawn samples at the top of the column were directly analyzed in gas chromatography to allow a fast response on conditions in the temperature constraint at different levels of $ee_{(S)\text{-2-PeOH,top}}$. Hence, the shown isolated yield represents the analyzed samples at the top of the column without further purification steps.

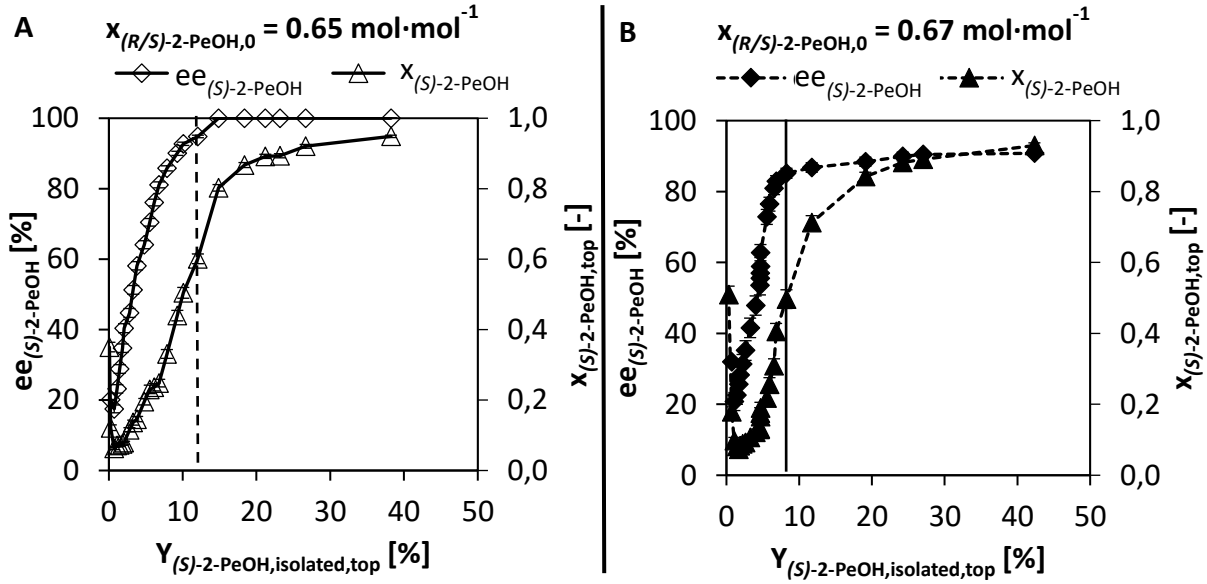

Figure 5.23: Influence of varied temperature constraints for automated temperature controlled fractional distillation on the reaction performance in biocatalytic reactive distillation with **A**: $x_{(R/S)\text{-2-PeOH},0}$ = 0.65 mol·mol^{-1} and **B**: $x_{(R/S)\text{-2-PeOH},0}$ = 0.67 mol·mol^{-1}. Vertical lines: adjustment of temperature constraint to T ≤ 60 °C. Operation conditions: similar to **Figure 5.22**. SD refers to maximum error estimation according to **section 3.4**.

In the first part of the reaction, $ee_{(S)\text{-2-PeOH,top}}$ was the decisive parameter for changing the temperature constraint in view of chiral compound synthesis. The reason for being the decisive parameter is, that a high $ee_{(S)\text{-2-PeOH,top}}$ indicates full kinetic resolution reaction, respectively. During this time period, the temperature constraint for fractional distillation was adjusted to T ≤ 46 - 54 °C ($x_{(R/S)\text{-2-PeOH},0}$ = 0.65 mol·mol^{-1}) and T ≤ 46 - 55 °C ($x_{(R/S)\text{-2-PeOH},0}$ = 0.67 mol·mol^{-1}). At an adjusted temperature constraint of T ≤ 60 °C, the corresponding purity becomes the essential parameter.

Thereby, increased purities of *(S)*-2-PeOH ($x_{(S)\text{-2-PeOH,top}}$) were focused by changed composition of the reactant mixture at the column top. This change is caused by fractional distillation, which results in reduced molar fractions of PrBu and 1-PrOH besides the desired target compound *(S)*-2-PeOH. The point of changing the decisive parameter is indicated by a vertical line for both experiments ($x_{(R/S)\text{-2-PeOH},0}$ = 0.65 mol·mol^{-1}, **Figure 5.23**, **A** and $x_{(R/S)\text{-2-PeOH},0}$ = 0.67 mol·mol^{-1}, **Figure 5.23**, **B**). In both cases, high values for $ee_{(S)\text{-2-PeOH,top}}$ were reached at this specific point, although full kinetic resolution was only achieved for the experiment with starting molar fractions of $x_{(R/S)\text{-2-PeOH},0}$ = 0.65 mol·mol^{-1}. However, this effect can be related to the varied initial starting molar fraction and it is addressed and discussed in **section 5.4.3**. With respect to the isolated yield of the target compound, the applied fractional distillation strategy was able to increase the target compound fractions with high $ee_{(S)\text{-2-PeOH,top}}$ (≥ 90 %) and high purity ($x_{(S)\text{-2-PeOH,top}}$ ≥ 0.93 mol·mol^{-1}). In the presented data, the isolated yield in the period of the process with reduced enantiomeric excess was $Y_{isolated,top}$ = 12.1 % for $x_{(R/S)\text{-2-PeOH},0}$ = 0.65 mol·mol^{-1} and $Y_{isolated,top}$ = 8.2 % for $x_{(R/S)\text{-2-PeOH},0}$ = 0.67 mol·mol^{-1}.

Hence, application of automated temperature controlled fractional distillation allowed successful column operation with respect to a well-timed change in the temperature constraint to withdraw nearly pure *(S)*-2-PeOH *in situ* at the column top. Similarly, previously discussed RD experiments in **Figure 5.19**, **B** with differently distributed NZ435 were performed with this fractional distillation strategy.

Concise summary of section 5.4.2:

- Stepwise fractional distillation by given temperature constraints at the top of the column results in further increased purities up to $x_{(S)\text{-2-PeOH,top}}$ = 0.93 – 0.95 mol·mol^{-1} at starting molar fractions of $x_{(R/S)\text{-2-PeOH},0}$ = 0.65 – 0.67 mol·mol^{-1}
- Two-step approach for fractional distillation allows *in situ* isolation of *(S)*-2-PeOH:
  1st part: enantiomeric excess is decisive parameter until high $ee_{(S)\text{-2-PeOH}}$ > 90 % is reached
  2nd part: purity is decisive parameter as long as high $ee_{(S)\text{-2-PeOH}}$ > 90 % is present

5.4.3. Influence of Initial Molar Fractions of the Starting Materials

For a possible future application of the studied batch biocatalytic reactive distillation (RD) in chiral synthesis, an efficient *in situ* isolation of the desired target compound *(S)*-2-PeOH at the top of the column is required with high purity and excellent enantiomeric excess. Therefore, column experiments with varied initial molar fractions of the racemic starting material *(R/S)*-2-PeOH ($x_{(R/S)\text{-2-PeOH},0}$ = 0.1, 0.6,

0.65, 0.67 mol·mol^{-1}) and PrBu ($x_{PrBu,0}$ = 0.9, 0.4, 0.35, 0.33 mol·mol^{-1}) were performed to evaluate the influence on the purity of *(S)*-2-PeOH in the RD column top ($x_{(S)\text{-2-PeOH,top,max}}$) and the corresponding $ee_{(S)\text{-2-PeOH,top,max}}$.

The applied catalyst distribution in RD at the corresponding initial molar fraction of *(R/S)*-2-PeOH is depicted in **Figure 5.24**, **A**. According to previously discussed results on the catalyst distribution in RD (**section 5.4.1**), NZ435 is at least placed in the bottommost position of the column height (H1). Moreover, the catalyst amount of NZ435 per initially applied amount of the starting materials was in the range of c_{NZ435} = 75 - 110 mg·g$_{(R/S)\text{-2-PeOH},0}^{-1}$. Further details on the equipment for the column experiments are summarized in **section 3.4** (**Table 3.6** – **Table 3.8**).

Resulting purities ($x_{(S)\text{-2-PeOH,top,max}}$) at different initial molar fractions of the starting materials are presented in **Figure 5.24**, **B**, wherein a strong increase in purity (triangles) was obtained for an increase in the starting molar fraction up to $x_{(R/S)\text{-2-PeOH},0}$ = 0.65 mol·mol^{-1}.

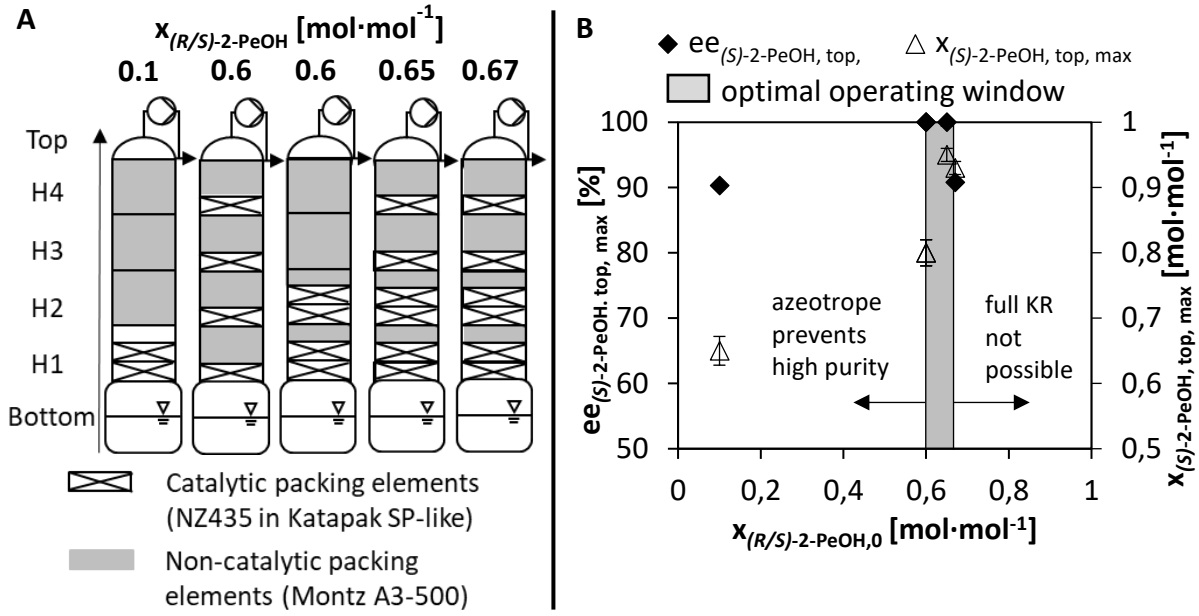

Figure 5.24: Operating range of batch biocatalytic reactive distillation at varied initial molar fractions of *(R/S)*-2-PeOH. **A**: Distribution of NZ435, **B**: Operating window in dependency of the enantiomeric excess ($ee_{(S)\text{-2-PeOH,top,max}}$) and purity ($x_{(S)\text{-2-PeOH,top,max}}$). Grey box: optimal operation window for kinetic resolution. **Operation conditions**: p = 80 mbar, $m_{Substrates,0}$ = 800 g, c_{NZ435} = 75 - 110 mg·g$_{(R/S)\text{-2-PeOH},0}^{-1}$, SD in $ee_{(S)\text{-2-PeOH}}$ and $x_{(S)\text{-2-PeOH}}$ refers to maximum error estimation (**section 3.4**)

While starting with low molar fractions of $x_{(R/S)\text{-2-PeOH},0}$ = 0.1 mol·mol^{-1} resulted in a purity of $x_{(S)\text{-2-PeOH,top,max}}$ = 0.65 mol·mol^{-1}, up to $x_{(S)\text{-2-PeOH,top,max}}$ = 0.95 mol·mol^{-1} was achieved by starting with increased molar fractions of $x_{(R/S)\text{-2-PeOH},0}$ = 0.65 mol·mol^{-1}. Furthermore, enantiopure *(S)*-2-PeOH ($ee_{(S)\text{-2-PeOH,top,max}}$ > 99 %) was reached by operating the column within the range of 0.6 mol·mol^{-1} < $x_{(R/S)\text{-2-PeOH},0}$ < 0.65 mol·mol^{-1}. At significantly lower ($x_{(R/S)\text{-2-PeOH},0}$ = 0.1 mol·mol^{-1}) and

slightly higher initial molar fractions ($x_{(R/S)\text{-2-PeOH},0}$ = 0.67 mol·mol^{-1}), a maximum enantiomeric excess of $ee_{(S)\text{-2-PeOH,top,max}}$ = 90 % was present for the target compound (diamonds, **Figure 5.24**, **B**). Although a reduced $ee_{(S)\text{-2-PeOH,top,max}}$ was detected at $x_{(R/S)\text{-2-PeOH},0}$ = 0.67 mol·mol^{-1}, similar purity at the top of the column of $x_{(S)\text{-2-PeOH,top,max}}$ = 0.93 mol·mol^{-1} was realized compared to the results of $x_{(R/S)\text{-2-PeOH},0}$ = 0.65 mol·mol^{-1}. The main difference of both RD experiments with $x_{(S)\text{-2-PeOH,top,max}}$ > 0.93 mol·mol^{-1} was the composition of present residual starting ester PrBu and formed low boiling 1-PrOH. Starting with $x_{(R/S)\text{-2-PeOH},0}$ = 0.65 mol·mol^{-1} of the racemic mixture, the additional compounds beside *(S)*-2-PeOH (x = 0.05 mol·mol^{-1}) could be identified as $x_{PrBu,top,max}$ = 0.04 mol·mol^{-1} and $x_{1\text{-PrOH,top,max}}$ = 0.01 mol·mol^{-1} (**appendix section E**, **Figure E.4**, **B**). On the contrary, residual reactant composition beside *(S)*-2-PeOH for starting with $x_{(R/S)\text{-2-PeOH},0}$ = 0.67 mol·mol^{-1} (x = 0.07 mol·mol^{-1}) was $x_{PrBu,top,max}$ = 0.01 mol·mol^{-1}, $x_{1\text{-PrOH,top,max}}$ = 0.01 mol·mol^{-1} and $x_{(R)\text{-2-PeOH,top,max}}$ = 0.05 mol·mol^{-1} (**appendix section E**, **Figure E.4**, **A**). Within the presented data it became visible, that reduced molar fractions of PrBu ($x_{PrBu,0}$ = 0.33 mol·mol^{-1}) at initial starting molar fractions of $x_{(R/S)\text{-2-PeOH},0}$ = 0.67 mol·mol^{-1} prevented full kinetic resolution reaction. On the other hand, RD operation with an excess of PrBu ($x_{PrBu,0}$ = 0.4 mol·mol^{-1}) compared to the preferentially converted enantiomer *(R)*-2-PeOH ($x_{(R)\text{-2-PeOH},0}$ = 0.3 mol·mol^{-1}) ended up in reduced purities of $x_{(S)\text{-2-PeOH,top,max}}$ = 0.8 mol·mol^{-1} while full kinetic resolution was performed successfully ($ee_{(S)\text{-2-PeOH,top,max}}$ > 99 %). The major reason for a maximum purity of $x_{(S)\text{-2-PeOH,top,max}}$ = 0.8 mol·mol^{-1} in those experiments was the presence of an azeotrope between the starting materials *(R/S)*-2-PeOH and PrBu (**section 5.1.2**). According to this azeotropic behavior, no further separation was possible at initial molar fractions of $x_{(R/S)\text{-2-PeOH},0}$ = 0.6 mol·mol^{-1}. To overcome the azeotrope by reaction was not feasible at $x_{(R/S)\text{-2-PeOH},0}$ = 0.6 mol·mol^{-1} due to observed slow reaction rates for the residual enantiomer *(S)*-2-PeOH with PrBu. Surprisingly, at $x_{(R/S)\text{-2-PeOH},0}$ = 0.1 mol·mol^{-1} an $ee_{(S)\text{-2-PeOH,top,max}}$ = 90 % was not exceeded although in principle full KR performance should be feasible at the selected starting molar fraction of *(R/S)*-2-PeOH. This phenomenon is expected to be referred to an accumulation of unreacted molar fractions of *(R)*-2-PeOH at the top of the column, which did not get into contact with the biocatalyst at position H1 and thereby reduced the final $ee_{(S)\text{-2-PeOH,top,max}}$ (**section 5.3.2**, **Figure 5.17**, **B**).

Comparing the performed column experiments, beneficial operation conditions with respect to the initial molar fractions of *(R/S)*-2-PeOH and PrBu need to be adjusted to allow a reasonable tradeoff between high enantiomeric excess ($ee_{(S)\text{-2-PeOH,top,max}}$ > 99 %) and high purity ($x_{(S)\text{-2-PeOH,top,max}}$ = 0.95 mol·mol^{-1}), which is shown within the results of **Figure 5.24**, **B** for $x_{(R/S)\text{-2-PeOH},0}$ = 0.65 mol·mol^{-1}. On the one hand, high enantiomeric excess values have been reached due to the presence of the starting ester PrBu until the faster reacting enantiomer of the racemic starting alcohol (*(R)*-2-PeOH) was fully converted. On the other hand, low molar fractions of PrBu ($x_{PrBu,top,max}$ = 0.04 mol·mol^{-1}) were left after full conversion of *(R)*-2-PeOH, which allowed further

separation in the column. Therefore, high purities were feasible containing small amounts of the azeotrope in the column top if the initial molar fractions were carefully adjusted to $x_{(R/S)\text{-2-PeOH},0}$ = 0.65 mol·mol^{-1} and $x_{PrBu,0}$ = 0.35 mol·mol^{-1}. Consequently, an optimal operation window of a starting molar fraction in the range of 0.6 mol·mol^{-1} < $x_{(R/S)\text{-2-PeOH},0}$ < 0.67 mol·mol^{-1} was obtained for the kinetic resolution of *(R/S)*-2-PeOH with PrBu (grey box: **Figure 5.24**, **B**).

Concise summary of section 5.4.3:

- An experimental operating window for full KR in biocatalytic batch reactive distillation is derived: it ranges from starting molar fractions of 0.6 mol·mol^{-1} < $x_{(R/S)\text{-2-PeOH},0}$ < 0.67 mol·mol^{-1}
- At $x_{(R/S)\text{-2-PeOH},0}$ ≤ 0.6 mol·mol^{-1}: azeotrope formation prevents high purity
- At $x_{(R/S)\text{-2-PeOH},0}$ ≥ 0.67 mol·mol^{-1}: full KR is not feasible and decreased $ee_{(S)\text{-2-PeOH}}$ are obtained

5.4.4. Economic Evaluation of Chiral Target Compound Isolation

As stated in **section 5.4.3**, the highest purities of $x_{(S)\text{-2-PeOH,top,max}}$ = 0.93 - 0.95 mol·mol^{-1} were realized within batch biocatalytic RD experiments for the kinetic resolution of *(R/S)*-2-PeOH with PrBu at initial molar fractions of $x_{(R/S)\text{-2-PeOH},0}$ = 0.65 mol·mol^{-1} and 0.67 mol·mol^{-1}. Therefore, economic evaluation for those two experiments was performed. Within the experimental results, total masses of $m_{(S)\text{-2-PeOH}}$ = 55.1 g and 76.0 g were achieved with corresponding isolated yields of $Y_{(S)\text{-2-PeOH,isolated}}$ = 11.6 % and 15.3 % at the maximum reached purities and enantiomeric excess values of the target compound *(S)*-2-PeOH (**Table 5.2**). The isolated yields in the batch RD experiments were determined by the percentage of the total moles of *(S)*-2-PeOH in the fractionated top sample with highest purity of $x_{(S)\text{-2-PeOH,top,max}}$ = 0.95 mol·mol^{-1} and 0.93 mol·mol^{-1} referred to the initially applied total moles of *(R/S)*-2-PeOH. Reduced isolated yields to theoretically feasible values of $Y_{(S)\text{-2-PeOH,isolated}}$ = 50 % were obtained due to fractionated samples at the top of the column with $ee_{(S)\text{-2-PeOH,top,max}}$ < 99 % in the first part of the reaction. For both experiments, the batch RD was identically equipped with NZ435 over the complete column height (**section 5.4.2**, **Figure 5.22**, **A**).

Final economic evaluation was performed by calculating the productivity of *(S)*-2-PeOH per the applied mass of NZ435 within the batch RD experiments. In addition, the profit based on the prices for the starting materials and desired target compounds at the chemical supplier Sigma-Aldrich (Merck, Darmstadt, Germany) was calculated.

The resulting productivity per batch RD experiment ranged from 1.2 - 1.7 $kg_{(S)\text{-2-PeOH}}{\cdot}kg_{NZ435}^{-1}$. Considering obtained half-life times of $\tau_{0.5}$ = 87 d for NZ435 at T = 60 °C (**section 5.2.2, Figure 5.12**) and assuming one batch per day (t_{batch} = 17.5 – 17.9 h referring to $x_{(R/S)\text{-2-PeOH},0}$ = 0.65 mol·mol^{-1} and

0.67 mol·mol^{-1}), the estimated overall productivity can be increased to 104.4 – 147.9 $kg_{(S)\text{-2-PeOH}}\cdot kg_{NZ435}^{-1}$ in biocatalytic batch RD. According to literature, a productivity range of 50 - 100 $kg_{Product}\cdot kg_{Biocatalyst}^{-1}$ for product costs > 100 €·kg^{-1} is at least required for the application of an immobilized biocatalyst [31]. Hence, repetitive batch operation in RD theoretically allows to fulfill this required range of productivity. However, the calculated productivity value will be affected by having only 50% retained activity in the case of operating the RD column for t = 87 d. But simultaneously, the selected column equipment involves two different design opportunities having an impact on the retained activity of NZ435. On the one hand, an increased mass of catalyst can be applied in the column by increasing the number of Katapak-SP-like catalytic packing elements. While in the experiments 45.3 g of NZ435 distributed in six catalytic packing elements were applied (71 % of the maximum capacity of 64 g), there is room for 18.7 g (29 %) of additional catalyst amounts. This would be possible by incorporating the whole column height only with Katapak-SP-like packing elements. Within the same strategy, reduced batch run times can be achieved to allow an increased number of batches in a similar time period (e.g. 87 d). On the other hand, reduced productivities of the process of 50 $kg_{Product}\cdot kg_{Biocatalyst}^{-1}$ still fulfill the requirements according to *Tufvesson et al. (2011)* [31]. This minimum productivity of 50 $kg_{Product}\cdot kg_{Biocatalyst}^{-1}$ can theoretically be reached with the applied mass of NZ435 (45.3 g), after operation times of t = 42 d at retained activities of 71 % for $x_{(R/S)\text{-2-PeOH},0}$ = 0.65 mol·mol^{-1} and t = 29 d at retained activities of 79% for $x_{(R/S)\text{-2-PeOH},0}$ = 0.67 mol·mol^{-1}. Calculation of the percentages were done on the basis of the results regarding thermal stability of NZ435 in **section 5.2.2 (Figure 5.12)** as well as the determined productivities (1.2 - 1.7 $kg_{(S)\text{-2-PeOH}}\cdot kg_{NZ435}^{-1}$) for the batch runs in RD from **Table 5.2**. Thereby, operation in batch RD even gives room for reacting on fluctuations in the deactivation rate of NZ435 and achieve required productivities.

Table 5.2: Obtained product specifications for *(S)*-2-PeOH and *(R)*-2-PeBu in batch biocatalytic reactive distillation experiments with initial starting molar fractions of $x_{(R/S)\text{-2-PeOH},0}$ = 0.65 mol·mol^{-1} and $x_{(R/S)\text{-2-PeOH},0}$ = 0.67 mol·mol^{-1}

	***(S)*-2-PeOH**[a]		***(R)*-2-PeBu**[b]	
$x_{(R/S)\text{-2-PeOH},0}$ [mol·mol^{-1}]	**0.65**	**0.67**	**0.65**	**0.67**
x_i [mol·mol^{-1}]	0.95	0.93	0.91	0.93
ee_i [%]	> 99	90	83.6	86.4
X [%]	54.6	51.5	54.6	51.5
m_{NZ435} [g]	45.3	45.3	45.3	45.3
m_i [g]	55.1	76.0	393.8	331.1
$Y_{i,isolated}$ [%]	11.6	15.3	47.2	36.5
Productivity per RD [$kg_i\cdot kg_{NZ435}^{-1}$]	1.2	1.7	8.7	7.3
Productivity [$kg_i\cdot kg_{NZ435}^{-1}$][c]	104.4	147.9	756.9	635.1

[a] referred to the top sample of the batch reactive distillation column with highest product specifications

[b] referred to the bottom of the batch reactive distillation column with highest product specifications

[c] at t = 87 d due to stability tests performed with NZ435 at T = 60 °C ($\tau_{0.5}$ = 87 ± 11 d, **section 5.2.2**)

Calculation of the profit is performed based on available prices for the applied starting materials at the chemical supplier *Sigma-Aldrich* (Merck, Darmstadt, Germany) of 70 €·kg^{-1} for *(R/S)*-2-PeOH (≥ 98 %) and 205.50 € for 500 mg of *(S)*-2-PeOH (≥ 98 %) (= 411 k€·kg^{-1}) [158]. This results in a value increasing factor of $5.87 \cdot 10^3$ for the enantiomerically pure target compound *(S)*-2-PeOH after full kinetic resolution. Assuming the same price for purities of $x_{(S)\text{-2-PeOH}}$ = 0.93 mol·mol^{-1} and 0.95 mol·mol^{-1}, 22.6 – 31.2 k€ of profit was achieved within the performed batch RD experiments with respect to obtained isolated masses of *(S)*-2-PeOH in **Table 5.2**. This profit is slightly reduced by the catalyst costs, which account for 1.2 k€ with respect to the applied amounts of NZ435 in the discussed experiments (calculated by the price of 77 € per 3 g_{NZ435} [158]). At an expected catalyst half-life times of $\tau_{0.5}$ = 87 d for NZ435, 1966.2 – 2714.4 k€ of profit is theoretically possible for one set of catalytic packing elements. In fact, those numbers for economic evaluation of the process already indicate the potential of biocatalytic batch RD for valuable compounds in chiral synthesis, although the corresponding isolated yields ($Y_{(S)\text{-2-PeOH,isolated}}$ = 11.6 % and 15.3 %) can substantially be improved in future times.

Furthermore, productivity and profit of the biocatalytic batch RD process is enhanced, if the chiral ester compound formed during the kinetic resolution reaction is considered in the evaluation as a second valuable product. In the specific case of the kinetic resolution of *(R/S)*-2-PeOH with PrBu, the chiral ester *(R)*-2-PeBu accumulates in the bottom of the column, while the target compound *(S)*-2-PeOH is separated at the top of the column via fractional distillation. Therefore, evaluation of *(R)*-2-PeBu takes place in the bottom of RD similar to previously presented data for *(S)*-2-PeOH at the top of the column. In contrast to the target compound, high isolated yields of $Y_{(R)\text{-2-PeBu,isolated}}$ = 47.2 % for $x_{(R/S)\text{-2-PeOH,0}}$ = 0.65 mol·mol^{-1} and $Y_{(R)\text{-2-PeBu,isolated}}$ = 36.5 % for $x_{(R/S)\text{-2-PeOH,0}}$ = 0.67 mol·mol^{-1} were obtained at the end of the experiments. The corresponding purity was $x_{(R)\text{-2-PeBu,bottom,max}}$ = 0.91 mol·mol^{-1} ($x_{(R/S)\text{-2-PeOH,0}}$ = 0.65 mol·mol^{-1}) and 0.93 mol·mol^{-1} ($x_{(R/S)\text{-2-PeOH,0}}$ = 0.67 mol·mol^{-1}). The substantially increased isolated yield compared to *(S)*-2-PeOH is referred to neglectable removal of *(R)*-2-PeBu during operation due to its high boiling point. In contrast, the target compound *(S)*-2-PeOH was removed at the top of the column during the applied fractional distillation strategy. Thus, only the withdrawn sample amounts and residual amounts in catalytic packing elements in lower column sections reduced the isolated yield of *(R)*-2-PeBu. Observed differences in isolated yields for both experiments are referred to unequal overall sampling amounts and additional amounts of residual reactants from previous column operation due to the reuse of the same catalytic packing elements. The corresponding enantiomeric excess of *(R)*-2-PeBu was 83.6 % ($x_{(R/S)\text{-2-PeOH,0}}$ = 0.65 mol·mol^{-1}) and 86.4 % ($x_{(R/S)\text{-2-PeOH,0}}$ = 0.67 mol·mol^{-1}). In fact, in industry only the racemic pentyl ester (*(R/S)*-2-PeBu) is used as a flavoring additive and does therefore not have to be enantiopure in contrast to the desired target compound *(S)*-2-PeOH in the discussed example. However, it is pointed out for the presented

case to have the possibility of gaining two chiral compounds with high purity in batch RD by performing kinetic resolution with excellent enantioselectivity.

The obtained 'bottle on the table'-amounts of the target compound *(S)*-2-PeOH and the reaction product *(R)*-2-PeBu are depicted in **Figure 5.25**.

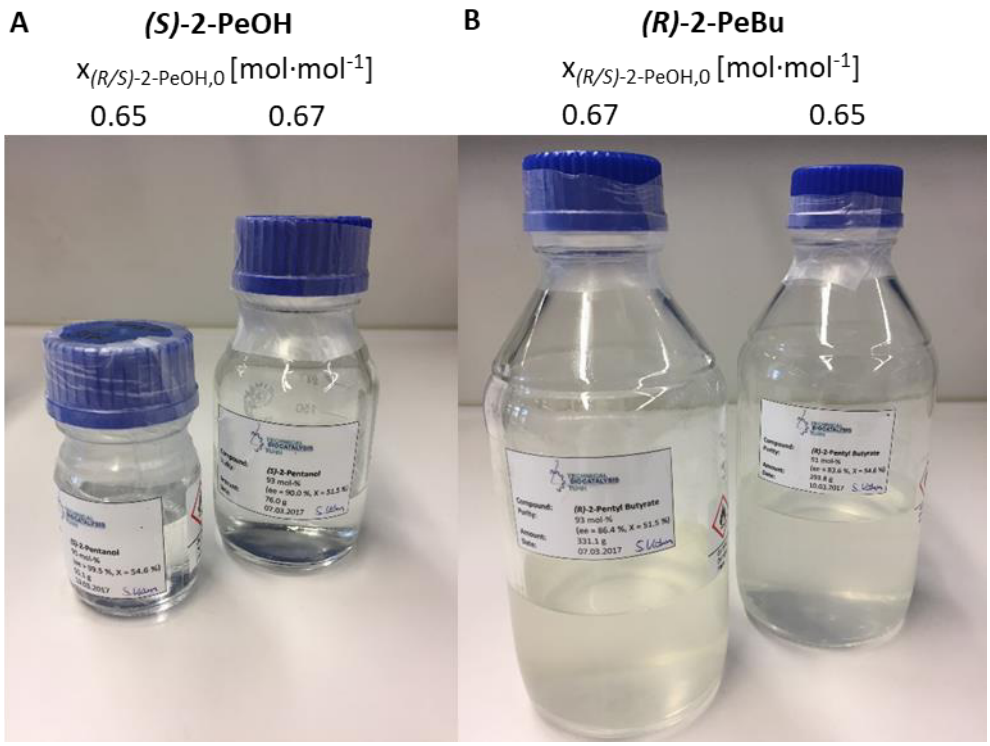

Figure 5.25: "Bottle on the table" obtained in biocatalytic batch reactive distillation experiments with initial starting molar fractions of $x_{(R/S)\text{-2-PeOH},0}$ = 0.65 mol·mol^{-1} and $x_{(R/S)\text{-2-PeOH},0}$ = 0.67 mol·mol^{-1} and the reactant specifications summarized in **Table 5.2**. **A**: *(S)*-2-PeOH, **B**: *(R)*-2-PeBu.

All in all, performed economic evaluation clearly demonstrates feasibility of kinetic resolution in biocatalytic batch RD at carefully chosen reaction conditions. *In situ* separation of the target compound *(S)*-2-PeOH with high purity of $x_{(S)\text{-2-PeOH,top,max}}$ = 0.93 - 0.95 mol·mol^{-1} was obtained for the first time for a chiral target compound in a biocatalytic RD setup to the best of our knowledge. However, it has to be mentioned, that the carried out experiments were mainly focusing feasible application of NZ435 in biocatalytic batch RD to provide the opportunity of an additional concept to produce chiral compounds biocatalytically in an integrated process. Further studies are needed to investigate competitive reactor concepts (i.e. sequential setup with batch vessels and subsequent distillation) and their efficiency in the performance of the chosen kinetic resolution reaction.

Concise summary of section 5.4.4:

- 'Bottle on the table' of the chiral target compound *(S)*-2-PeOH is generated ($m_{(S)\text{-2-PeOH,top}}$ = 55.1 g, $ee_{(S)\text{-2-PeOH,top,max}}$ > 99 %, X = 54.6 %, $x_{(S)\text{-2-PeOH,top,max}}$ = 0.95 mol·mol^{-1})
- Productivity of a single batch RD run with 1.2 $kg_{(S)\text{-2-PeOH}}$·kg_{NZ435}^{-1} is below industrial value, but considering the half-life time of NZ435 theoretically allows high productivities 104.4 $kg_{(S)\text{-2-PeOH}}$·kg_{NZ435}^{-1} within the industrial range

5.4.5. Interim Summary: Chiral Target Compound Isolation

- High purity and high enantiomeric excess are achieved in KR of *(R/S)*-2-PeOH with PrBu in a batch biocatalytic RD column
- The following rules can be derived by the investigated influencing parameters on the operation of a batch biocatalytic reactive distillation setup:
    a. Distribution of NZ435 is flexible in the column height despite the bottom position to enable KR performance within the thermal stability range of the biocatalyst preparation
    b. Predominant position of NZ435 should be the lowest section of the column height
    c. Stepwise fractional distillation is necessary to achieve *in situ* isolation of the second lowest boiling target compound *(S)*-2-PeOH (1. Stripping of lowest boiling compound to shift equilibrium, 2. Stripping of target compound with high ee)
    d. Increasing the starting molar fraction of *(R/S)*-2-PeOH allows higher purity of *(S)*-2-PeOH at the top of the column at starting molar fractions $x_{(R/S)\text{-2-PeOH},0}$ < 0.67 mol·mol^{-1}
    e. High potential for biocatalytic RD is given for the investigated KR reaction of *(R/S)*-2-PeOH with PrBu

5.5. Combination of Chemo- and Biocatalysts by Dynamic Kinetic Resolution[1]

The performance of a kinetic resolution (KR) and the main influencing factors on this operation in a biocatalytic batch reactive distillation (RD) were successfully investigated and demonstrated in the previous section of this work. In the following part, the main focus is to broaden the reaction spectrum of the biocatalytic RD approach by evaluating a combination of a biocatalytic reaction with a chemically catalyzed reaction to overcome the main performance limitation of KR. This limitation of KR is its maximum theoretical yield of 50 %. Increased yields are not feasible, because full conversion of one enantiomer of the racemic starting material to the corresponding product enantiomer is reached at 50 % overall conversion assuming ideal enantioselectivity. Therefore, it is tried to enhance the theoretical yields to 100 % by performing a chemo-enzymatic dynamic kinetic resolution (DKR) including a KR and an additional racemization step in a Soxhlet reactor setup (**section 3.5**). A similar approach was applied by *Mavrynsky et al. (2014)* for chemo-enzymatic DKR of chiral amines [159]. Especially, the proof of concept study for the feasibility within this developed integrated setup will be addressed by focusing the following aspects:

1. Selection of a suitable model reaction for chemo-enzymatic DKR (**section 5.5.1**)
2. Influence of spatial catalyst separation on chemo-enzymatic DKR (**section 5.5.2**)
3. Reaction performance of chemo-enzymatic DKR (**section 5.5.3**)

5.5.1. Selection of a Suitable Model Reaction

For the chemo-enzymatic approach, DKR is divided into two simultaneously performed reactions (**Figure 5.26**). The biocatalytic part of the reaction is a highly selective KR of the starting materials *(R/S)*-2-pentanol (*(R/S)*-2-PeOH) with ethyl butyrate (EtBu) to the favored reaction products *(R)*-2-pentyl butyrate (*(R)*-2-PeBu) and ethanol (EtOH). In an additional reaction step, chemo-catalyzed racemization of residual *(S)*-2-PeOH takes place. So, in contrast to KR, the desired target compound is the high boiling reaction product *(R)*-2-PeBu. In detail, NZ435 is applied to catalyze the KR step efficiently. As already described in **section 5.2.1**, it shows high enantioselectivity towards *(R)*-2-PeOH. The racemization step is catalyzed by Shvo catalyst, which is a metal catalyst consisting of an alcoholic- and keto-subunit with a coordinated ruthenium (**section 2.2.5**) [123]. Only in absence of molecular oxygen and water, the residual *(S)*-2-PeOH of KR is unspecifically converted to 2-pentanone in a transition step to yield *(S)*- or *(R)*-2-PeOH in a final step. As long as the racemization step is performed at least 10 times faster than KR, residual *(S)*-2-PeOH becomes racemized [122].

[1] The results in this chapter were obtained in cooperation with the working group of Prof. J.-E. Bäckvall, Stockholm University, Sweden

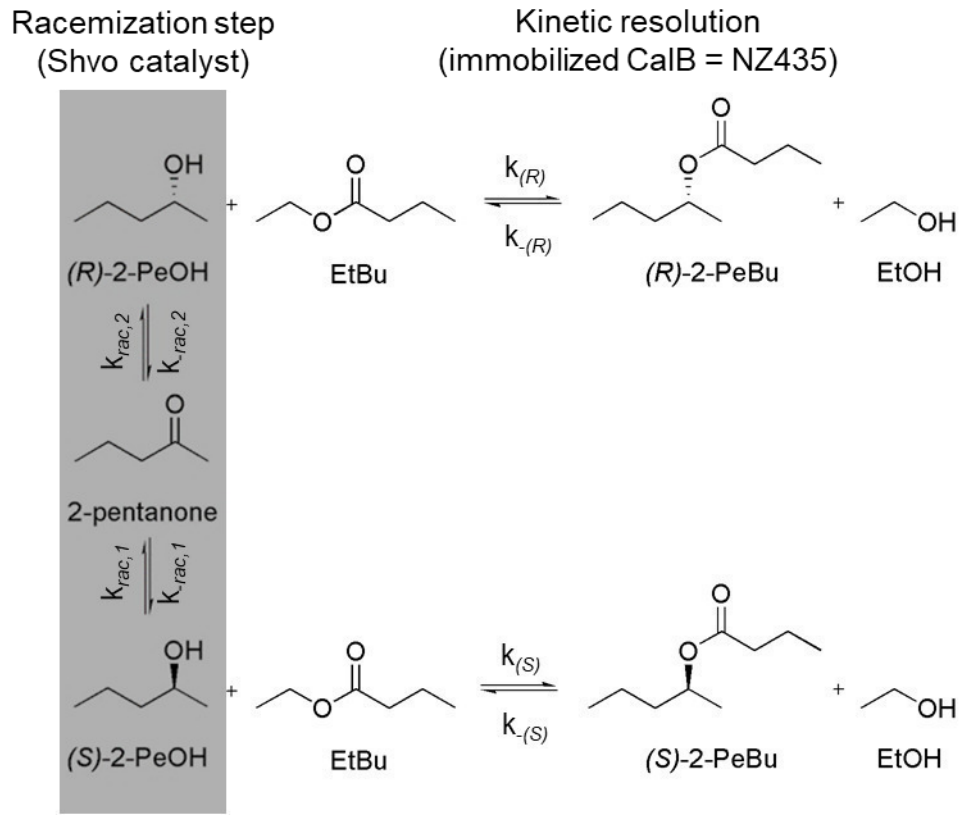

Figure 5.26: Scheme of chemo-enzymatic dynamic kinetic resolution (DKR). Enzymatic reaction step: CalB (NZ435) catalyzed kinetic resolution (KR) of *(R/S)*-2-PeOH with EtBu ($k_{(R)} >> k_{(S)}$). Chemocatalytic reaction step: racemization of residual *(S)*-2-PeOH by Shvo catalyst ($k_{rac,1}$ and $k_{rac,2} \geq 10 \cdot k_{(R)}$). The corresponding intermediate product of the racemization step is 2-pentanone.

The choice on the starting materials *(R/S)*-2-PeOH and EtBu was done based on the application of the preselection tool discussed in **section 5.1.1 - 5.1.2**. **Figure 5.27** presents literature data (data points) on boiling point measurements (T) in dependency of the pressure (p) for the pure compounds. Those data points are compared to calculated Antoine parameters (lines) taken from the *National Institute of Standards and Technology* (NIST) database [140]. By means of estimated parameters for all reactants, determination of a theoretical operating window for DKR application in the Soxhlet reactor setup can be evaluated. With respect to required evaporation of the starting materials, similar boiling points (T_b) at ambient conditions allow availability of *(R/S)*-2-PeOH ($T_{b,(R/S)\text{-2-PeOH}}$ = 119 °C) and EtBu ($T_{b,EtBu}$ = 121 °C) at the position of the biocatalyst (*(R/S)*-2-PeOH = diamonds, EtBu = triangles in **Figure 5.27**). Moreover, increased boiling point differences of ΔT = 18 – 53 °C between the starting materials and the formed reaction product *(R)*-2-PeBu ($T_{b,(R)\text{-2-PeBu}}$ = 174 °C, dashed line in **Figure 5.27**) as well as the formed side products 2-pentanone ($T_{b,2\text{-pentanone}}$ = 101°C, crosses in **Figure 5.27**) and EtOH ($T_{b,EtOH}$ = 78 °C, squares in **Figure 5.27**) are present at ambient conditions to theoretically allow separation in the Soxhlet reactor setup. Additionally, a solvent material is required to homogeneously dissolve the Shvo catalyst. This solvent material should not evaporate in higher amounts than the

starting materials. Therefore, *p*-xylene with a boiling point of $T_{b,p\text{-xylene}}$ = 138 °C at ambient pressure was chosen (circles in **Figure 5.27**).

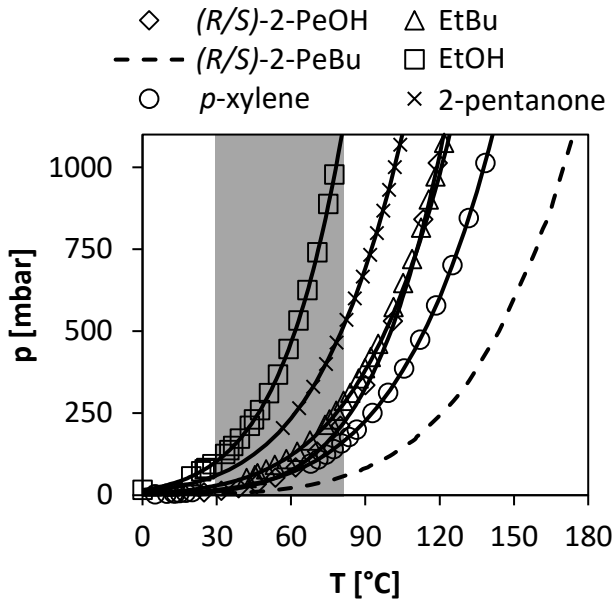

Figure 5.27: Boiling points of pure reactants (T) at varied column pressures (p) for chemo-enzymatic dynamic kinetic resolution (DKR). Grey box indicates the operating range of the enzymatic preparation NZ435. The whole temperature range is feasible for Shvo catalyst. Lines: calculated Antoine parameters, data points: experimental data taken from literature: *(R/S)*-2-PeOH [144], EtBu [145], EtOH [146] [147], 2-pentanone [160], *p*-xylene [161], *(R/S)*-2-PeBu is estimated based on linear extrapolation of methyl, ethyl, propyl & butyl butyrate

The resulting theoretical operation window is mainly restricted by limited thermal stability of the biocatalyst at T > 80 °C. Therefore, feasible operation of chemo-enzymatic DKR with NZ435 can only be guaranteed in the range of T = 30 - 80 °C indicated by the grey box in **Figure 5.27**. In principle, NZ435 will perform at T < 30 °C as well, but at substantially reduced activities. Thus, reaction temperatures below T = 30 °C are not taken into consideration for DKR performance with NZ435. On the other hand, the application of the chemocatalyst is suitable at least up to T = 180 °C. To overcome thermal restrictions of NZ435, two different strategies are taken into account to allow operation of chemo-enzymatic DKR. On the one hand, reduced pressure (i.e. 100 mbar) is feasible to operate the Soxhlet reactor setup at decreased boiling temperatures of the reactants (T < 80 °C). Thereby, the lifetime of NZ435 is increased by a decreased deactivation rate. This procedure was addressed in previously discussed KR performance in biocatalytic batch reactive distillation. Alternatively, spatial separation of the catalysts can be addressed by generating two temperature zones. While the biocatalyst is placed in a temperature zone of T < 80 °C in upper parts of the Soxhlet reactor setup to perform KR, the more robust chemocatalyst can be applied in the zone of increased temperature T >> 80 °C in the batch vessel at the bottom of the setup to catalyze the racemization step. In contrast to simultaneous

application of both catalysts in a batch vessel, which is the state of the art procedure for DKR performance [117] [122] [129], the application of a Soxhlet reactor setup allows the spatial separation of the chemocatalyst and the biocatalyst in different temperature zones.

Concise summary of section 5.5.1:

- A model reaction for chemo-enzymatic DKR is selected:
  Enzymatic part: NZ435 catalyzed KR of *(R/S)*-2-PeOH with EtBu, reaction product: *(R)*-2-PeBu
  Chemocatalytic part: Shvo catalyst dissolved in *p*-xylene for racemization of *(R/S)*-2-PeOH

5.5.2. Influence of Spatial Catalyst Separation

For the proof of concept study (**Figure 5.28**), the integrated Soxhlet reactor setup (**section 3.5**) was equipped with spatially separated catalysts involving 0.5 mol% Shvo catalyst (m_{Shvo} = 0.16 g, M_{Shvo} = 1085 g·mol^{-1}) in the bottom.

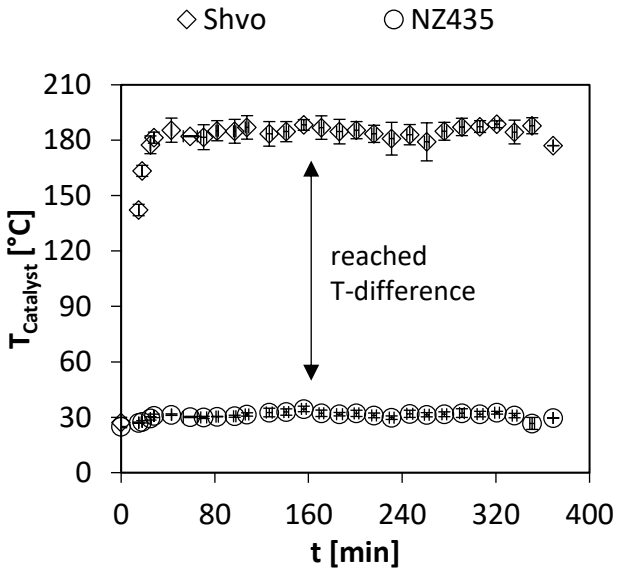

Figure 5.28: Chemo-enzymatic DKR in an integrated Soxhlet reactor setup with spatially separated catalysts. Temperatures refer to the position of the chemocatalyst (Shvo) and the biocatalyst (NZ435). Operation conditions: p = 1013 mbar, x_{EtBu} = 0.54 (64 mmol), $x_{(R/S)\text{-2-PeOH}}$ = 0.23 (28 mmol), $x_{p\text{-xylene}}$ = 0.23 (28 mmol), m_{NZ435} = 0.25 g, m_{Shvo} = 0.16 g, m_0 = 13.0 g (n = 2), position of Shvo catalyst: bottom of the setup, position of NZ435: lower part of liquid line in the setup.

By evaporation of the reactants in the reboiler region, a vapor flow is generated passing through the vapor line. This vapor flow is cooled down at the condenser and the reactants flush back through the liquid line. In the liquid line, NZ435 (m_{NZ435} = 0.25 g) was incorporated to ensure moderate

temperatures at the position of the biocatalyst. For the selected reaction conditions, 3-fold increased moles of the racemic starting material ($n_{(R/S)\text{-2-PeOH}}$ = 28 mmol) and up to 50 % reduced concentrations of both catalysts (0.5 mol% Shvo catalyst, 8.9 mg·mmol^{-1} NZ435) were adjusted compared to the study of *Mavrynsky et al. (2014)* ($n_{(R/S)\text{-amine}}$ = 10 mmol, 1 mol% Shvo catalyst, 20 mg·mmol^{-1} NZ435) [159]. Over the course of reaction, temperature at the position of both catalysts was monitored. While temperatures of T_{Shvo} = 183 ± 5 °C were obtained in the bottom of the setup containing homogeneously dissolved Shvo catalyst (diamonds in **Figure 5.28**), reduced temperatures of T_{NZ435} = 31 ± 2 °C were observed in the liquid line at the position of NZ435 (circles in **Figure 5.28**). Finally, a temperature difference of ΔT = 152 ± 4 °C between the spatially separated catalysts is achieved.

This demonstrated temperature difference for the chemo-enzymatic DKR with the racemic starting alcohol *(R/S)*-2-PeOH and EtBu behaves as a design opportunity, because reached operation conditions are feasible for both catalysts. Thereby, the thermal induced deactivation rate of the biocatalyst can be reduced according to lowered temperatures in the liquid line. At the same time, increased temperature at the position of the chemocatalyst results in accelerated reaction rates due to Arrhenius dependency [94]. Moreover, spatial separation prevents interference of the chemo- and the biocatalyst. Hence, the successfully applied temperature difference in chemo-enzymatic DKR enables operation of both catalysts at preferred temperature conditions. In comparison to the study operating a similar Soxhlet apparatus for chemo-enzymatic DKR of chiral amines by *Mavrynsky et al. (2014)*, spatial separation of CalB and Shvo's catalyst resulted in temperature differences of ΔT = 50 – 65 °C at reduced pressures in the range of p = 0.5 mbar to p = 130 mbar [159]. The feasibility in this study shows operation of the chiral secondary alcohol *(R/S)*-2-PeOH at ambient pressure with a 3-fold increased temperature difference.

Concise summary of section 5.5.2:

- Spatial catalyst separation enables a temperature differences between NZ435 and Shvo catalyst of ΔT = 152 ± 4 °C in the Soxhlet-approach for chemo-enzymatic DKR

5.5.3. Reaction Performance in a Soxhlet Reactor Setup

For evaluation of the reaction performance with spatially separated catalysts in the Soxhlet reactor setup, the enantiomeric excess of the residual starting material *(R/S)*-2-PeOH and the formed reaction product *(R)*-2-PeBu is plotted against the proceeding analytical yield ($Y_{analytical}$) in **Figure 5.29**, **A**. Two experiments were performed with a temperature difference of ΔT = 152 ± 4 °C (filled and open

diamonds) and one experiment with ΔT = 135 °C (filled and open squares). At ΔT = 152 ± 4 °C, NZ435 was placed in the lower part of the liquid line in the Soxhlet reactor setup, while it was placed in the upper part of the liquid line for ΔT = 135 °C. Changes within the resulting temperature difference originate from the position of NZ435. According to the hot rising vapor passing through the upper part of the liquid line on the way to the condenser, an increased temperature is present at this position. This results in a decrease in the temperature difference of both catalysts compared to less affected zones in the lower part of the liquid line. In the ideal case, $Y_{analytical}$ = 100 % can be achieved for *(R)*-2-PeBu, respectively. DKR becomes beneficial compared to KR, if $Y_{analytical}$ > 50 % is reached towards *(R)*-2-PeBu for the chosen reaction systems. In the presented results, $Y_{analytical}$ is referred to the sum of formed moles of the reaction product *(R)*-2-PeBu and the formed intermediate product 2-pentanone in the bottom of the setup. An indicator for efficient operation of the KR reaction step catalyzed by NZ435 is a constantly high enantiomeric excess of the reaction product *(R)*-2-PeBu, which is ideally constant at $ee_{(R)\text{-2-PeBu}}$ = 100 %. This behavior was observed in the two performed reactions with an $ee_{(R)\text{-2-PeBu}}$ > 99 % up to overall analytical yields of $Y_{analytical}$ = 43.4 ± 0.1 % at an applied temperature difference of ΔT = 152 ± 4 °C depicted by open diamonds and $Y_{analytical}$ = 64.5 % at ΔT = 135 °C depicted by open squares in **Figure 5.29**, **A**.

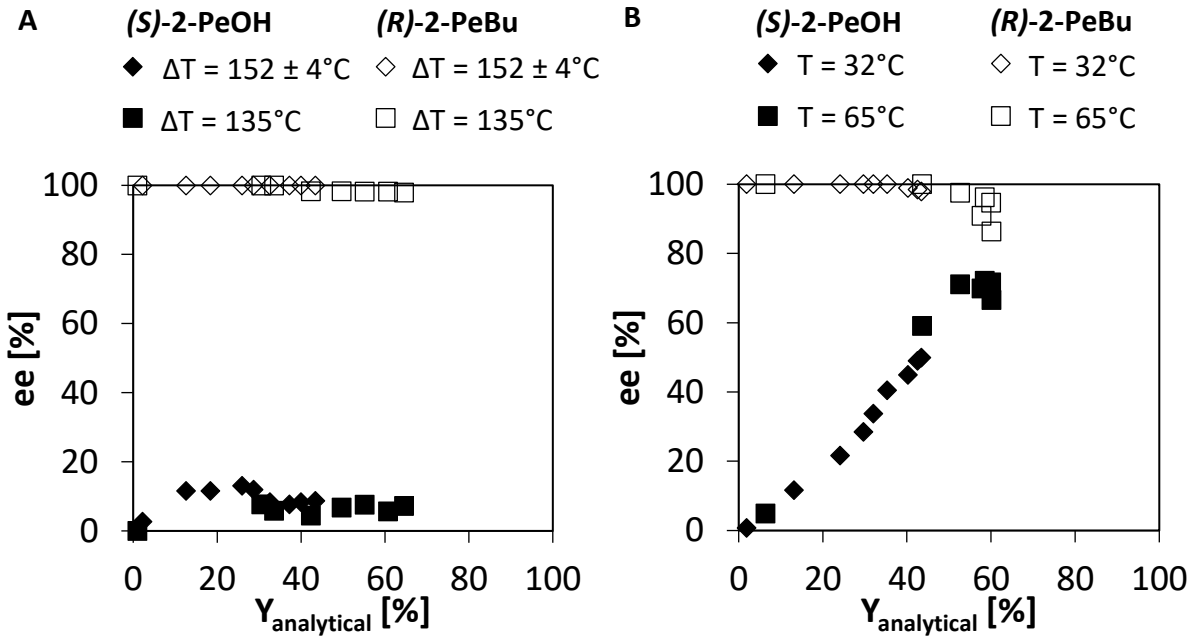

Figure 5.29: Reaction performance of chemo-enzymatic DKR monitored by enantiomeric excess (ee) of *(R)*-2-PeBu and *(S)*-2-PeOH with increasing analytical yields ($Y_{analytical}$). **A**: In Soxhlet reactor setup with spatially separated catalysts, operation conditions: p = 1013 mbar, x_{EtBu} = 0.54, $x_{(R/S)\text{-2-PeOH}}$ = 0.23, $x_{p\text{-xylene}}$ = 0.23, m_{NZ435} = 0.25 g, m_{Shvo} = 0.16 g, m_0 = 13.0 g, ΔT = 152 ± 4 °C (n = 2): position of Shvo catalyst: bottom of the setup, position of NZ435: lower part of liquid line in the setup. ΔT = 135 °C (n = 1): position of Shvo catalyst: bottom of the setup, position of NZ435: upper part of liquid line in the setup. **B**: In batch vessel with both catalysts operated at the same temperature, operation conditions: p = 1013 mbar, m_{NZ435} = 0.035 g, m_{Shvo} = 0.022 g, T = 32 °C: x_{EtBu} = 0.56, $x_{(R/S)\text{-2-PeOH}}$ = 0.24, $x_{p\text{-xylene}}$ = 0.20, m_0 = 2.2 g, T = 65 °C: x_{EtBu} = 0.82, $x_{(R/S)\text{-2-PeOH}}$ = 0.11, $x_{p\text{-xylene}}$ = 0.07, m_0 = 1.5 g

Hence, selective formation of *(R)*-2-PeBu with respect to high enantioselectivity of NZ435 was successfully established in the chemo-enzymatic DKR reaction with spatial separation of the catalysts. Simultaneously, low $ee_{(S)\text{-2-PeOH}} < 13 \pm 0.05$ % were detected (filled diamonds and filled squares, **Figure 5.29**, **A**). A low enantiomeric excess of the chiral starting material proves sufficient activity of the chemocatalyst, which performs the racemization of residual *(S)*-2-PeOH of chemo-enzymatic DKR. Discrepancies to the ideal case with a constant $ee_{(S)\text{-2-PeOH}} = 0$ % in this racemization step can be explained by the applied concentration of the Shvo catalyst (0.5 mol%), which is half of the concentration in the similar approach by *Mavrynsky et al. (2014)* [159]. In fact, determined enantiomeric excess values for *(S)*-2-PeOH and *(R)*-2-PeBu at the two investigated temperature differences ($\Delta T = 152 \pm 4$ °C and $\Delta T = 135$ °C) verified the simultaneous operation of spatially separated catalysts in the Soxhlet reactor setup. The main difference between the presented results is the observed increase in the analytical yield at $\Delta T = 135$ °C, which can be referred to a two-fold increase of the temperature at the position of NZ435 in the liquid line. With respect to the monitored temperatures at the position of NZ435, $T_{NZ435} = 57$ °C was present at $\Delta T = 135$ °C and for $\Delta T = 152 \pm 4$ °C it was $T_{NZ435} = 31 \pm 2$ °C. The temperature at the position of Shvo catalyst was almost the same in both cases ($T_{Shvo,mean} = 178 – 193$ °C). Although higher analytical yields might be explained by increased reaction velocity at increased temperatures according to Arrhenius law, further investigation is necessary to proof this observation at a reduced temperature differences ($\Delta T = 135$ °C).

Additionally, the chemo-enzymatic DKR was performed in two batch vessel experiments operating both catalysts at the same temperature without spatial separation (**Figure 5.29**, **B**). This corresponds to the state of the art procedure for chemo-enzymatic DKR [117] [122] [129]. Two different temperatures of T = 32 °C and T = 65 °C were selected to investigate the behavior of the enantiomeric excess of the starting material ($ee_{(S)\text{-2-PeOH}}$) and the formed product ($ee_{(R)\text{-2-PeBu}}$) against the yield (Y). The selected temperatures were similar to the temperatures at the position of NZ435 in the experiments with a temperature difference. At both selected temperatures, the enantiomeric excess of the reaction product *(R)*-2-PeBu revealed efficient performance of the KR step catalyzed by NZ435 due to constantly high values for $ee_{(R)\text{-2-PeBu}} > 96$ % up to $Y_{analytical} = 43.5$ % at T = 32 °C (open diamonds) and $Y_{analytical} = 58.5$ % at T = 65 °C (open squares). For the experiment with T = 65 °C, further increased yields up to $Y_{analytical} = 60.1$ % showed a decrease in $ee_{(R)\text{-2-PeBu}}$ to 86 %, which follows typical behavior of KR after total consumption of the faster reacting enantiomer. Similar behavior to KR is supported by an increase in the enantiomeric excess of residual *(S)*-2-PeOH up to $ee_{(S)\text{-2-PeOH}} = 50$ % at T = 32 °C and an analytical yield of 43.5 % (filled diamonds) as well as $ee_{(S)\text{-2-PeOH}} = 72$ % at T = 65 °C and $Y_{analytical} = 60.1$ % (filled squares).

According to the behavior of the enantiomeric excess, reduced reaction performance of the racemization step catalyzed by Shvo catalyst was present in both batch vessel experiments without a

temperature difference (**Figure 5.29**, **B**) compared to previously discussed results with a temperature difference between the catalysts (**Figure 5.29**, **A**). This observed reduction in the racemization step in batch vessel experiments can be explained by the drastically decreased operating temperature at the position of Shvo catalyst from T_{Shvo} = 183 ± 5 °C to T_{Shvo} = 32 °C as well as T = 65 °C. In fact, at least T = 80 °C are required to induce efficient racemization by Shvo catalyst [162].

With respect to the analytical yield, it is reduced to $Y_{analytical}$ = 24.3 ± 0.2 % at ΔT = 152 ± 4 °C and $Y_{analytical}$ = 41.5 % at ΔT = 135 °C in the experiments for the proof of principle of the chemo-enzymatic DKR with spatially separated catalysts (**Figure 5.29**, **A**) by considering only the desired reaction product *(R)*-2-PeBu. In contrast, no differences between the overall analytical yield and the analytical yield of *(R)*-2-PeBu occur in the batch vessel experiments with both catalysts operated at T = 32 °C as well as T = 65 °C (**Figure 5.29**, **B**). Therefore, this detection of low analytical yields for spatially separated catalysts was studied in detail for the two experiments with a temperature difference of ΔT = 152 ± 4 °C by taking a deeper look on the molar fractions (x_i) in the bottom of the Soxhlet reactor setup over the course of $Y_{analytical}$.

In **Figure 5.30**, **A**, the molar fractions (x_i) of the starting materials EtBu (triangles), *(R)*-2-PeOH (open diamonds) and *(S)*-2-PeOH (filled diamonds) as well as the solvent material *p*-xylene (crosses) are depicted.

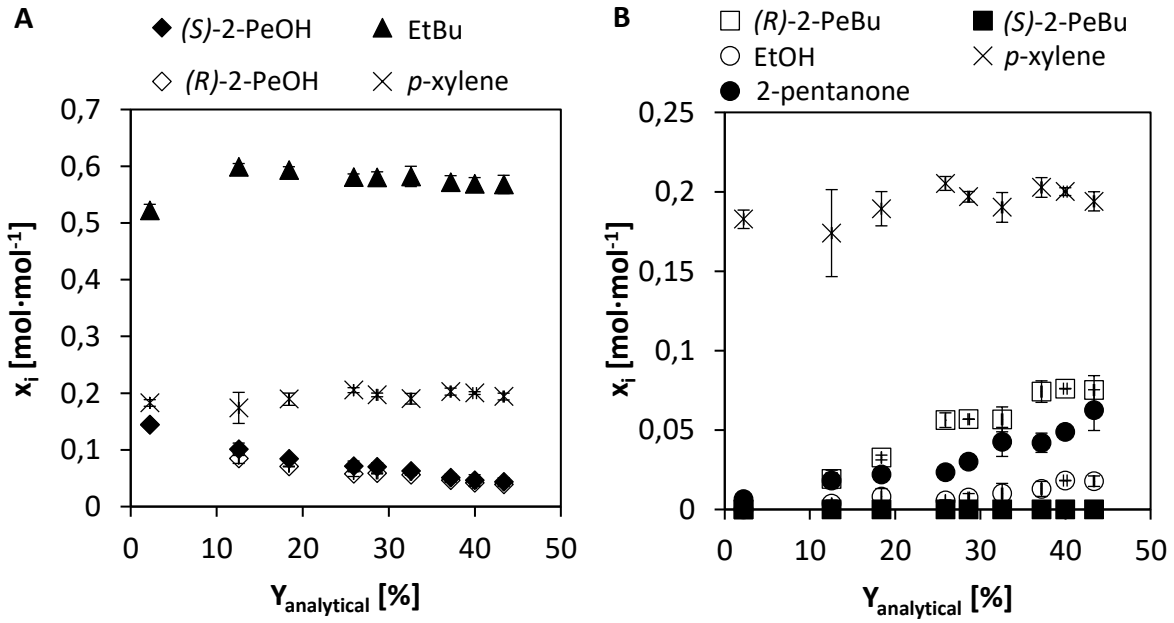

Figure 5.30: Profile of molar fractions (x_i) over yield (Y) in chemo-enzymatic DKR with spatially separated catalysts and a temperature difference of ΔT = 152 ± 4 °C in the Soxhlet reactor setup. **A**: starting materials, **B**: formed products and intermediates. *p*-xylene is present in both profiles. Operation conditions: p = 1013 mbar, x_{EtBu} = 0.54, $x_{(R/S)\text{-2-PeOH}}$ = 0.23, $x_{p\text{-xylene}}$ = 0.23, m_{NZ435} = 0.25 g, m_{Shvo} = 0.16 g, m_0 = 13.0 g (n = 2), position of Shvo catalyst: bottom of the setup, position of NZ435: lower part of liquid line in the setup

In **Figure 5.30**, **B**, formation of the reaction products *(R)*-2-PeBu (open squares), *(S)*-2-PeBu (filled squares) and EtOH (open circles), the intermediate product 2-pentanone (filled circles) and the solvent material *p*-xylene (crosses) is shown.

The expected behavior for *(R)*-2-PeOH and *(S)*-2-PeOH is observed by decreasing molar fractions from $x_{(R)\text{-},(S)\text{-2-PeOH}} = 0.14 \pm 0.01$ mol·mol^{-1} to 0.04 ± 0.01 mol·mol^{-1} over increased analytical yields of the successfully performed KR. Simultaneously, a selective formation of *(R)*-2-PeBu took place indicated by increased molar fractions from $x_{(R)\text{-2-PeBu}} = 0$ mol·mol^{-1} to 0.08 ± 0.01 mol·mol^{-1}. The absence of *(S)*-2-PeBu shows once more the enantioselective KR reaction of NZ435. In the data points of the molar fraction of EtBu in **Figure 5.30**, **A**, an initial step-like increase occurred followed by a slight decrease over the course of experiment. While this decrease corresponds to the consumption of EtBu during the enzymatic KR reaction, the initial step-like increased molar fraction can be explained by the initial evaporation of low boiling materials changing the composition of reactants in the bottom. In particular, the formed low boiling EtOH and residual *(R)*- as well as *(S)*-2-PeOH are causing this increase in the molar fraction of EtBu at the bottom due to high fractions in the vapor phase of these compounds. Lower molar fractions of EtOH were observed compared to the high boiling reaction product *(R)*-2-PeBu, which indicated that EtOH was mainly present in the vapor phase. Furthermore, the higher boiling solvent *p*-xylene stayed in the bottom and *(R)*-2-PeBu accumulated more and more over the course of the reaction. Additionally, a similar increase in the molar fraction of 2-pentanone was observed compared to the desired reaction product *(R)*-2-PeBu. Moreover, this determined molar fraction of 2-pentanone in the bottom might be further increased due to a part of it being present in the vapor phase of the setup according to its lower boiling point in comparison to the starting materials (**Figure 5.27**).

Therefore, reduced yields in the Soxhlet reactor setup occurred with respect to accumulation of the intermediate product 2-pentanone in the chemocatalyzed racemization step. With respect to the mechanism of Shvo catalyst described in literature, only the alcohol subunit is affected by oxidation [123]. In consequence, the enantiomeric excess of *(S)*-2-PeOH and the chiral reaction product *(R)*-2-PeBu was not affected by insufficient racemization. Only the yield of the desired product *(R)*-2-PeBu is reduced by the accumulation of 2-pentanone. In contrast, no formation of 2-pentanone was observed for the batch vessel experiments without a temperature difference (**Figure 5.30**, **B**) due to reaction temperatures below the activation temperature of Shvo's catalyst.

As a conclusion for the proof of concept study, desired constant low $ee_{(S)\text{-2-PeOH}}$ were successfully reached in the Soxhlet reactor setup, but low yields for *(R)*-2-PeBu compared to KR operation have to be optimized in future studies. In those investigations, further improved evacuation conditions of the Soxhlet reactor setup should be addressed to achieve more efficient racemization (i.e. operating under Argon atmosphere instead of N_2-atmospere). With respect to the achieved temperature difference up

to ΔT = 152 ± 4 °C, two different temperature zones allowed simultaneous performance of the chemo- and biocatalyst in the Soxhlet reactor setup, which even allows the operation of more sensitive biocatalysts with operating temperatures of T = 32 °C in the provided approach.

Concise summary of section 5.5.3:

- Simultaneous performance at spatially separated catalysts results in $ee_{(R)\text{-2-PeBu}} > 98$ %, $ee_{(S)\text{-2-PeOH}} < 13$ % and $Y \leq 65$ %
- Intermediate product 2-pentanone accumulates during the reaction

5.5.4. Interim Summary: Combination of Chemo- and Biocatalysts

- The performed proof of concept study shows the possibility to operate a chemo-enzymatic DKR with spatially separated catalysts in a Soxhlet reactor setup for a theoretically feasible starting material combination in RD (*(R/S)*-2-PeOH with EtBu)
- Temperatures of T = 32 °C for thermosensitive biocatalysts are feasible at simultaneously high temperatures of T = 183 - 193 °C for the chemocatalyst
- Intermediate product formation occurred, which should be prevented in an optimization process

6. OVERALL DISCUSSION & PERSPECTIVE

In the following section, all discussed results of this study are used to identify and discuss challenges and opportunities regarding the provided approach for *in situ* isolation of chiral molecules in an integrated biocatalytic batch reactive distillation setup (RD) as well as the applied combination of a bio- and a chemocatalyst in dynamic kinetic resolution (DKR).

6.1. Scope of Feasible Chiral Starting Materials and Biocatalysts for Biocatalytic Batch Reactive Distillation

Within the stage of selecting applicable reactions for biocatalytic RD (**section 5.1**), a preselection tool was developed and evaluated to identify feasible candidates for the synthesis of chiral molecules in RD with respect to available property data (Antoine parameters). This procedure mainly offers the opportunity to compare several starting material combinations on the basis of three implemented preselection criteria and to discard inacceptable combinations before experimental study. Thereby, biocatalytic RD can be taken into consideration for a known starting material as an alternative process strategy in the beginning of the process development phase. In contrast, recent literature on the application of biocatalysts in RD focuses on specific candidates without an option to compare different reactants [41] [45] [47]. However, as long as a starting material combination is theoretically feasible for biocatalytic RD, the generated theoretical operating windows should be verified by a detailed study on the phase change behavior and experimental data in any case. So far, the preselection tool comprises 120 kinetic resolution (KR) reactions with chiral secondary alcohols and non-chiral ester compounds catalyzed by CalB. But, changing the operating conditions in the column by variation of the column pressure (p_{RD}) could allow the identification of further reaction systems. Especially, reduced p_{RD} were promising due to simultaneously affected boiling points of the reactants (T_{boil}) to result in decreased T_{RD}. Within the discussed comparison between the feasible number of reactions (n_{Reac}) at p = 100 mbar (n_{Reac} = 7 at T = 60 °C) and p = 10 mbar (n_{Reac} = 44, T = 60 °C), 6.3 fold increased reactions were theoretically feasible concerning the implemented number of reactants to perform KR (**section 5.1**). Operating the column at reduced p_{RD} is the common strategy in this work as well as in the literature to be able to reduce the operating column temperature (T_{RD}) [42] [43] [45] [48]. By this design opportunity of reduced p_{RD}, lowered operating T_{RD} within the stability range of the biocatalyst become feasible due to decreased boiling temperatures and reduced biocatalyst deactivation.

Particularly, for the flexibility of selecting the biocatalyst, there are currently no competing candidates to lipases and especially CalB for the application in biocatalytic RD. In fact, thermal stability up to T = 80 °C (**section 5.2**) [37] [109] combined with a broad acceptance of starting materials [106] [107] underlines the outstanding position of this specific biocatalyst. The choice on CalB is confirmed by

previously published studies comprising the implementation of a biocatalyst in RD, which are all addressing CalB [42] [43] [45] [47] [48]. To ensure a feasible temperature range for CalB, a temperature criterion for the RD column between T_{RD} = 30 – 80 °C is predefined. Hence, the boiling points of the reactants are required to be in this temperature range, while they can be shifted by reduced operating pressures. For other candidates, either the accepted starting materials cannot be evaporated in the thermal stability range of the biocatalyst or thermal sensitive as well as expensive cofactors are required for catalyzing the reaction. A detailed overview on the classes of biocatalysts and their challenges towards biocatalytic RD is provided in **section 2.2.3**.

An additional challenge emerges regarding the feasibility of reactants with respect to required simultaneous evaporation of the starting materials and thermal separation of the reactants along the RD column. Based on **section 5.1**, a large temperature difference between the boiling points of the starting materials needs to be avoided. The resulting effects of an increased temperature difference between the starting materials of $\triangle T_{evaporation}$ = 24 - 31 °C (at p = 10 – 100 mbar) were in this work experimentally discussed on the applied KR of *(R/S)*-3-HEB with 1-PeOH, which demonstrated less availability of both starting materials in the packing height of the column setup (**section 5.2**). On the other hand, preselected candidates with a reduced temperature difference of $\triangle T_{evaporation}$ = 9 - 11 °C (at p = 80 – 100 mbar) comprising the two selected KR reactions of *(R/S)*-2-PeOH with PrBu and *(R/S)*-2-PeOH with EtBu showed feasible column performance in experiments (**section 5.3**)**.** Obtained feasibility for *(R/S)*-2-PeOH with EtBu can be supported by previously published data on its application in batch RD by *Heils et al. (2015)* [45]. Hence, the predefined criteria within the preselection phase comprising simultaneous evaporation of the starting materials (at $\triangle T_{evaporation} < 11$ °C) and thermal separation between the highest as well as lowest boiling components ($\triangle T_{separation} \geq 18$ °C, discussed in **section 5.1**), were successfully proven in experimental investigations to allow operation in batch biocatalytic RD. In fact, the proposed temperature differences serve as guiding values for the applied equipment in this work and will change with the column configuration as well as the applied column internals. Operating the column with additional feed streams for higher as well as lower boiling compounds will for example prevent the need for a temperature differences between the starting materials. This improved strategy for column operation is further discussed in **section 6.3**. On the other hand, an increase in the RD column height will offer an increase in the separation efficiency due to a substantially increased number of stages for the separation.

Although the application of biocatalytic RD clearly sticks to lipases, the application of an additional catalyst may become feasible by providing different temperature zones for an increase in flexibility of biocatalytic RD. Due to a detected temperature gradient, which decreases along the column height ($\triangle T_{max}$ = 30 °C comparing the temperature at the bottom and the top of RD in **section 5.3** and **section 5.4**), a catalyst requiring high temperatures can be placed in the bottom of the column setup. This

approach is proven by a proof of concept study on chemo-enzymatic DKR using CalB and Shvo catalyst, in which an additional chemocatalyzed racemization step is performed with spatially separated catalysts to achieve the enantiopure target compound *(R)*-2-PeBu (**section 5.5**). According to literature, the applied Shvo catalyst is activated at increased temperature, while for the biocatalyst lower temperatures are required to reduce the deactivation rate [124] [162]. At least, the experimentally implemented temperature difference of $\triangle T = 152 \pm 4$ °C for the selected starting materials *(R/S)*-2-PeOH and EtBu in the solvent *p*-xylene revealed theoretical feasible co-performance of both catalysts in a Soxhlet reactor setup with expected rather constant optical purities for the starting material as well as the formed product (**section 5.5**). However, the applied racemization catalyst currently shows side product formation due to inactivation by oxidizing species. Hence, spatial separation of catalysts in dynamic kinetic resolution is only efficiently feasible in future times, if side product formation is prevented or at least reduced to increase the yield of the desired target compound. Starting points for an improved performance are more efficient evacuation concepts or the substitution of the applied chemical catalyst by a more stable candidate. Experiments in a similar reactor setup by *Mavrynsky et al. (2014)* already demonstrated the feasibility of the application with chiral amines yielding high purities of the reaction product as well as excellent enantiomerix excess values [159]. Therefore, a combination of different catalysts in RD is in principle feasible.

6.2. Required Operation Conditions for *in situ* Isolation of a Chiral Target Compound in Batch Biocatalytic Reactive Distillation

Beside the provided scope of chiral target compounds in biocatalytic RD with one biocatalyst or a combination with an additional catalyst, the adjusted operation conditions should allow the *in situ* isolation of a chiral target compound at the top of the RD setup. Indeed, the *in situ* isolation by fractional distillation will be one big advantage of an integrated RD process compared to other reactor concepts like in STRs, which do not offer this possibility. However, in recent literature, only the reaction performance without isolation of the product in different RD concepts is available [39] [45] [48]. Therefore, the major aim of this study was to achieve *in situ* isolation at the top of the applied batch RD column and to identify influencing parameters to reach this aim.

On the basis of promising results by *Heils et al. (2015)* for KR of *(R/S)*-2-PeOH with EtBu implemented in a batch RD setup [45], an experimental comparison of two different non-chiral starting esters is done in batch RD to evaluate the possibility of *in situ* isolation of the chiral target compound *(S)*-2-PeOH. Basically, the results from **section 5.3** demonstrate the successful transfer of the previously selected chiral starting material *(R/S)*-2-PeOH with either EtBu or PrBu to the batch RD setup. In an initially performed experimental characterization phase (**section 5.2**), proper operation of CalB is confirmed

by determination of the initial activity, enantioselectivity and thermal stability at varied molar fractions of the starting materials. However, substitution of the ester compound from ethyl to propyl moiety resulted in a different boiling point order of the reactants, which substantially changes the behavior during column operation (**section 5.3**). While in the case of PrBu a higher boiling ester compared to the racemic starting alcohol *(R/S)*-2-PeOH is applied, a lower boiling point is present for starting with EtBu. In fact, the lower the boiling point of the desired target compound *(S)*-2-PeOH for the two investigated KR reactions with either EtBu or PrBu was, the faster it was accumulating at the top of the column due to thermal separation in the RD process. The desired *in situ* isolation of *(S)*-2-PeOH can be achieved by fractional distillation at the top of the column. Hence, the effect of a changed boiling point order significantly influences the isolation process in batch RD experiments. Using the previously discussed property data within the preselection tool (**section 5.1**), the boiling point order can already be identified at an early stage of the process development and finally predetermines the possibility for *in situ* isolation of the chiral target compound.

According to the impact factors of biocatalysts on RD in **section 2.2.3**, a second advantage will be the option to handle equilibrium limited reactions by shifting the equilibrium to the product side due to fractional distillation of low boiling compounds. In obtained results concerning the definition of equilibrium constants at different operating pressures, the need for an operation at reduced pressures and thereby a shift in the equilibrium was observed for *(R/S)*-2-PeOH and EtBu as well as PrBu in **section 5.2**. The detected equilibrium limitation was overcome by stripping low boiling product alcohol EtOH or 1-PrOH, which emphasizes the need for an integrated RD setup.

Within further investigations on parameters in the RD column setup, the composition of the starting molar fractions, the fractional distillation strategy and the implementation of the biocatalyst revealed a complex parameter set for achieving *in situ* isolation of a chiral target compound in batch RD (**section 5.4**). In the end, a narrowed operating window was obtained, in which all the parameters allow a full KR performance with high target compound specifications ($ee_{(S)\text{-2-PeOH,top}} > 99$ %, $x_{(S)\text{-2-PeOH,top}} = 0.95$ mol·mol^{-1}, $m_{(S)\text{-2-PeOH,top}} = 55.1$ g). Furthermore, the obtained productivity of a single batch RD run was 1.2 $kg_{(S)\text{-2-PeOH}}\cdot kg_{NZ435}^{-1}$, but considering the half-life time of NZ435 theoretically allows high productivities 104.4 $kg_{(S)\text{-2-PeOH}}\cdot kg_{NZ435}^{-1}$ within the industrial range of 50 - 100 $kg_{Product}\cdot kg_{Biocatalyst}^{-1}$ (**section 5.4**) [31]. The major reason for the reduced flexibility in the range of the operation window is the presence of an azeotropic mixture at the applied operating pressure of p = 80 mbar, T = 60.8 °C and $x_{(R/S)\text{-2-PeOH}} = 0.84$ mol·mol^{-1}regarding the starting materials *(R/S)*-2-PeOH and PrBu. Thereby, the reactant separation is restricted as long as both starting materials are present in the RD column and only after full conversion of the corresponding ester PrBu, high purity of the target compound can be reached. However, by careful adjustment of the discussed parameters (**section 5.4**), full KR in biocatalytic RD is demonstrated even for the case of dealing with an azeotrope. Specifically, as long as

the biocatalyst is provided along the whole packing height of the column, the presence of azeotropic mixture at upper column positions can be prevented or at least be reduced by the performed reaction (**section 5.4**). In addition to that, economic calculation already shows great potential of the process setup within the identified narrowed window of operation (**section 5.4**). Coming back to the second applied starting ester EtBu in a KR with *(R/S)*-2-PeOH with the knowledge gained by the KR with PrBu, high purity and *in situ* isolation of the target compound should even be possible for EtBu in batch biocatalytic RD. This will especially be feasible as long as the starting molar fractions of both starting materials are similar to the reactions performed with PrBu and full conversion of EtBu can be realized. Hence, the influence of the boiling point order becomes only beneficial for reactions without a formed azeotrope between the starting materials at the selected operation conditions, because a sufficient thermal separation along the column height can take place in those cases.
Finally, the following requirements can be derived for *in situ* isolation of a chiral target compound in batch biocatalytic RD with respect to the presented results for KR in this study:

- Preselection phase:
  1. Pure starting materials should provide a temperature difference of $\triangle T_{evaporation} < 11$ °C to allow availability of the starting materials for reaction along the RD column height
  2. For CalB, the column temperature should be in the range of $T_{RD} = 30 – 80$ °C (column pressure should be reduced to adjust the column temperature)
  3. Boiling point order: $T_{target\ compound} < T_{2nd\ starting\ material}$
- Experimental characterization phase in stirred tank reactors:
  1. Catalytic activity in the range of $x_{(R/S)\text{-substrate},0} \leq 0.66\ mol \cdot mol^{-1}$
  2. High enantioselectivity $E > 100$
  3. Reasonable catalyst stability at the desired column temperature (here: $\tau_{0.5} = 87 \pm 11$ d at 60°C)
  4. Equilibrium limited reaction ($K_{eq} < 1$) to emphasize the need for a reactor concept, which is able to overcome the limitation
- Experimental batch reactive distillation phase:
  1. Flexible NZ435 over the column height despite the bottom position (H = 0 m)
  2. Stepwise fractional distillation (a. Stripping of lowest boiling compound to shift equilibrium, b. Stripping of target compound with high $ee_{target\ compound}$)
  3. Starting molar fraction range between $0.6\ mol \cdot mol^{-1} < x_{(R/S)\text{-2-PeOH},0} < 0.67\ mol \cdot mol^{-1}$

6.3. Evaluation of the Chosen Batch Reactive Distillation Operation Mode

All experimental investigations in this work are carried out in a batch biocatalytic RD setup (**section 5.3**, **section 5.4**). In general, batch RD is the preferred setup compared to continuous RD in the case of required higher residence times due to low reaction rates [52]. However, the biocatalyst is placed along the height of the RD column to perform the reaction in the presented experiments, which is the same procedure in the continuous approach. The benefit of having no biocatalyst in the bottom of the column setup is given by obtained decreased temperatures in the packing height compared to the bottom of the column. Although less catalytic activity caused by mass transport limitations will be present, increased catalyst lifetimes can be achieved by placing the catalyst solely in the packing height. This is supported by long term activity measurements for the applied NZ435 resulting in a 4.6 fold increase in the half-life time from $\tau_{0.5}$ = 19 ± 3 d to $\tau_{0.5}$ = 87 ± 11 d by reducing the temperature from T = 80 °C to T = 60 °C (**section 5.2**) tested in a STR experiments, in which the shear stress by stirring also increase the deactivation compared to the use of the biocatalyst in catalytic packings in RD.

With respect to the position of the biocatalyst in the packing height, the investigated setup will allow the transfer to semi-continuous or continuous operation modes in future times. Comparing the different operation modes in RD, the major difference for the batch RD setup is to have a dynamic operation behavior, while the continuous setup is operated under steady-state conditions. Additionally, feed stages are not present in the applied batch RD setup. In contrast, continuous operation provides additional feed streams at different positions to the setup. Based on the investigated KR reactions without an additional feed to the RD setup, offering a feed strategy would behave as an important design opportunity. Thus, a constant feed of a higher boiling compound at increased column positions and simultaneous feeding of a low boiling reactant at lower column sections can increase the feasible spectra of reactions. Such a strategy will already become interesting for the characterized KR reaction of the chiral starting ester *(R/S)*-3-HEB with 1-PeOH (**section 5.2**). The major reason for excluding this reaction from successful batch RD column performance was the substantially higher boiling point of *(R/S)*-3-HEB compared to 1-PeOH, which may be overcome by feeding it into the column at a higher column position to increase the concentration in upper column parts for a sufficient reaction performance. Thereby, the criterion for the temperature difference between the starting materials implemented in the preselection tool can be avoided, which will allow a theoretically higher number of feasible reactions for the RD setup. This continuous operation is already introduced in literature by *Heils et al. (2014)* [41] as well as *Wierschem et al. (2018)* [48], which might be transferable to the investigated operation strategy with *in situ* isolation of chiral target compounds from this work.

Moreover, for the successfully implemented KR reaction of the chiral starting alcohol *(R/S)*-2-PeOH with PrBu, a different column setup may be beneficial as well. This is referred to the fact of being interested in the second lowest boiling compound (*(R/S)*-2-PeOH) beside the formed low boiling alcohol 1-PrOH during the reaction. Hence, it might be more efficient to operate this reaction in a divided wall column, in which a side stream can be generated of the desired target compound *(S)*-2-PeOH. A starting point for the application of a divided wall column can be the recently published study by *Egger et al. (2017)*, as they introduced this concept with the application of CalB, but at the current stage for non-chiral products [43].

Hence, successful characterization of the biocatalytic RD in the chosen batch RD setup was required to show the feasibility and discuss influencing parameters for the *in situ* isolation, while a further broadened scope of feasible starting materials should be addressed by adding feed or distillate stripping streams at flexible column stages in the next steps.

6.4. Perspective for Biocatalytic Reactive Distillation

According to the presented and discussed results, the following parameters should be addressed in future work to improve and broaden the feasibility of biocatalytic reactive distillation.

First of all, the implemented batch RD process can be further improved, especially with respect to the productivity of the desired chiral target compound obtained at the top of the column (kg target compound per kg biocatalyst). In detail, the applied amount of the catalyst should be varied and in best case be reduced to achieve an increase in the productivity of the batch RD process.

Within a second step, the suggested change in the operation mode from batch RD to at least additional feed or distillate streams (**section 6.3**) offers the possibility to broaden the scope of applicable starting material combinations in the integrated process. For example, the investigated chiral starting ester *(R/S)*-3-HEB and similar chiral ester candidates should be included within the investigations, because an experimental characterization of the KR reaction of *(R/S)*-3-HEB and 1-PeOH is already performed in this study. Moreover, the provided preselection tool can be extended to the use of feeding starting materials or an additional side stream in the column.

7. SUMMARY & CONCLUSION

Within this work, an approach for systematic incorporation of biocatalysts to evaluate the synthesis of chiral secondary alcohols in a reactive distillation setup is developed (**Figure 7.1**). The major aim of the approach is to offer a practicable strategy to achieve *in situ* isolation of a chiral target compound by simultaneously broadening the scope of reactive distillation to more valuable chiral products. Basically, it comprises theoretical preselection of feasible kinetic resolution reactions by available property data and their experimental characterization with respect to decisive parameters, their integration in a batch reactive distillation setup and experimental evaluation of generated data at varied operation conditions. Beside kinetic resolution of secondary alcohols, combined chemo-enzymatic catalysis is addressed in an integrated setup as an alternative type of reaction for reactive distillation. For this dynamic kinetic resolution concept involving the same chiral starting materials, spatial separation of both catalysts allows reaction performance at different temperature conditions and defines its advantaging and challenging aspects.

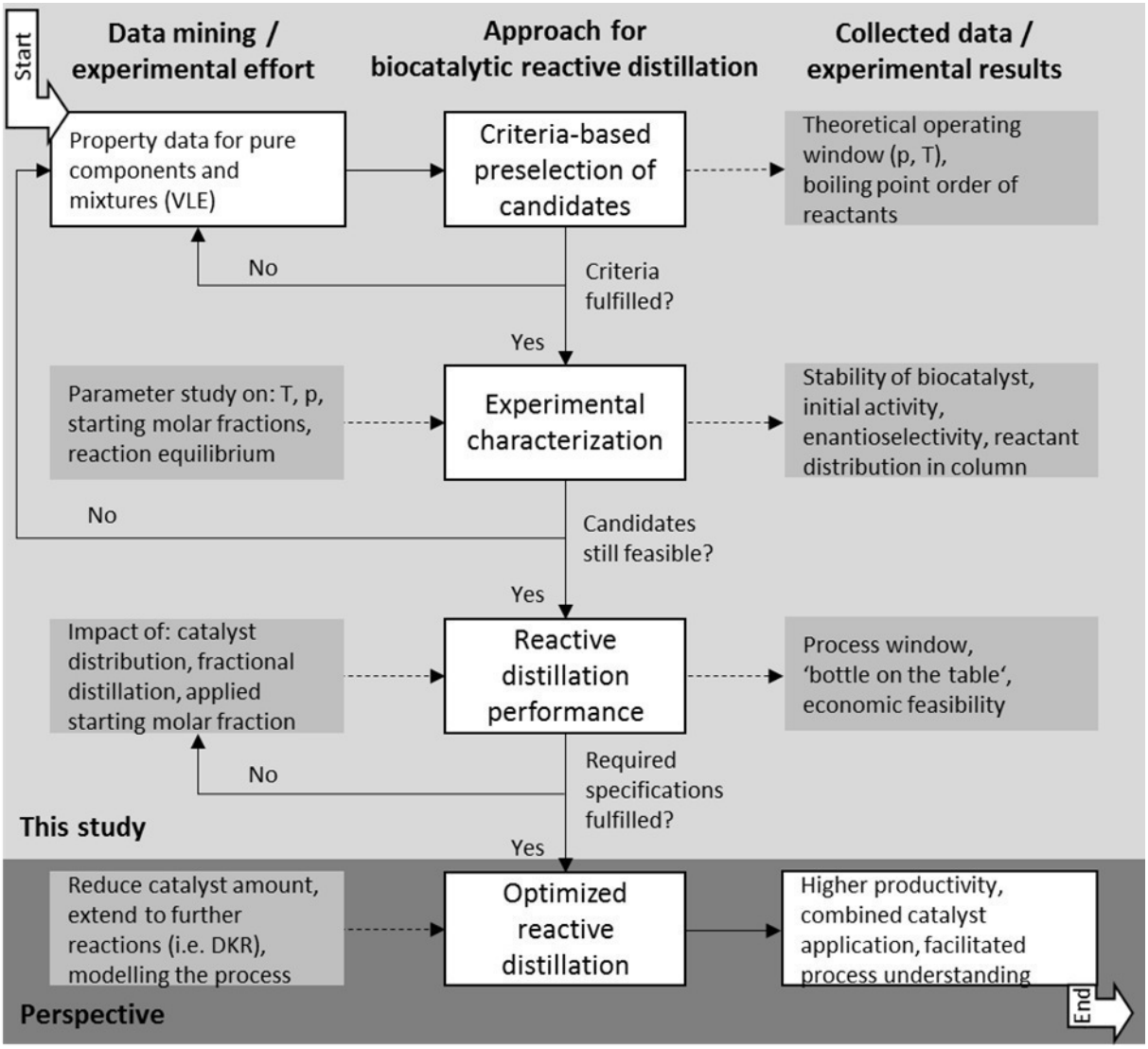

Figure 7.1: Proposed approach for the synthesis of chiral target compounds in biocatalytic reactive distillation

Finally, successful kinetic resolution performance with *in situ* separation of the optically pure chiral target compound *(S)*-2-PeOH ($ee_{(S)\text{-2-PeOH,top}}$ > 99 %, $x_{(S)\text{-2-PeOH}}$ = 0.95 mol·mol^{-1}, $m_{(S)\text{-2-PeOH,top}}$ = 55.1 g) at the top of the column setup is realized following the developed strategy. In the case of this CalB catalyzed kinetic resolution starting from *(R/S)*-2-PeOH with PrBu ($x_{(R/S)\text{-2-PeOH},0}$ = 0.65 mol·mol^{-1}, $x_{PrBu,0}$ = 0.35 mol·mol^{-1}), the profit per batch reactive distillation run already accounts for approximately 22.6 k€ within one day of operation (Productivity per batch RD run 1.2 kg·kg_{NZ435}^{-1}). This profit can even be substantially increased by feasible increased operation times of the applied catalyst preparation NZ435 of $\tau_{0.5}$ = 87 ± 11 d. Hence, the use of biocatalysts reveals great potential to obtain a 'bottle on the table' within reactive distillation processes, which is demonstrated for *(S)*-2-PeOH.

Conclusion 1:

The provided approach offers *in situ* isolation of chiral target compounds within biocatalytic reactive distillation with high purity and excellent enantiomeric excess

On the other hand, only a small process window allows efficient biocatalytic reactive distillation performance. This reduces flexibility of the integrated process compared to sequential connection of unit operations. In this work, multiple impact factors are detected throughout the different phases of reaction engineering to reach the finally adjusted operation conditions and to evaluate feasibility of an integrated operation. All of them should be considered for any biocatalytic reactive distillation process.

In the phase of preselection, criteria for evaporation and separation in the used column setup are fixed to temperature differences between the starting materials *(R/S)*-2-PeOH and PrBu of $\triangle T_{evaporation}$ = 9 °C and between the highest as well as lowest boiling components of $\triangle T_{separation} \geq$ 18 °C at p =80 mbar. Combined with a predetermined temperature range of the applied biocatalyst in RD (T_{RD} = 30 – 80 °C), the theoretical operating window for individual candidates is defined by providing a suitable column pressure. Practicability of the adjusted temperature differences are confirmed by successful operation of a second kinetic resolution performance (*(R/S)*-2-PeOH with EtBu: $\triangle T_{evaporation}$ = 10 °C, $\triangle T_{separation} \geq$ 26 °C, p = 100 mbar) and a negative control with temperature differences outside the recommended range (*(R/S)*-3-HEB with 1-PeOH: $\triangle T_{evaporation}$ = 24 °C, $\triangle T_{separation} \geq$ 48 °C, p = 10 mbar).

Conclusion 2:

The preselection tool allows an early stage decision by defining a theoretical operating window and identifying feasible candidates for kinetic resolution in biocatalytic batch reactive distillation

Experimental results are produced in the characterization phase to set up the fundamental data basis

for column experiments with respect to efficient catalytic activity of an appropriate catalyst configuration (v_0), long-term thermal catalyst stability ($\tau_{0.5}$) and high enantioselectivity (E) toward the selected candidates from the preselection phase. Furthermore, stationary batch RD column experiments without the presence of biocatalyst are conducted to define the region for placing the biocatalyst and to confirm the decisions made in the preselection phase by analyzing the distribution behavior over the column height. Obtained data involve the comparison of kinetic resolution performance starting either with a secondary alcohol (*(R/S)*-2-PeOH) or a chiral hydroxy ester (*(R/S)*-3-HEB). For the solvent-free kinetic resolution of *(R/S)*-2-PeOH with PrBu, RD column operation turns out to be feasible due to high enantioselectivity (E > 100) and the need for overcoming a strong equilibrium limitation (K_{eq} = 0.24 ± 0.04) by the application of reduced pressures (p = 80 mbar). On the contrary, solvent-free kinetic resolution of *(R/S)*-3-HEB with 1-PeOH is not recommended for reactive distillation performance. Although applying reduced pressures allows optically pure *(S)*-3-HEB for the less enantioselective reaction (E = 10 - 15), inadequate distribution in stationary column experiments prevents simultaneous accessibility of both starting materials. Referring to investigations on the selected biocatalyst preparation (Novozym435), optimal temperature conditions for column experiments are T = 60°C with displayed half-life times of $\tau_{0.5}$ = 87 ± 11 d. At the same time, Arrhenius dependency shows only a 1.2-fold increase in catalytic activity at $\triangle$T = 10°C in the operating temperature. Hence, further increase in temperature does not significantly change the reaction velocity within the column. With respect to thermal deactivation, incorporation of the biocatalyst should not be realized in the reboiler region of the column but in the column height. Otherwise, increased temperatures in the bottom of the column caused by accumulation of high boiling product (*(R)*-2-PeBu) during the reaction and constant heat induction leads to fast deactivation and frequent replacement of the biocatalyst. However, this procedure is a trade-off providing less thermal deactivation but simultaneously reduced catalytic activity compared to catalyst placement in the liquid phase of the bottom of the column (reboiler region) in consequence of mass transfer limitations. Finally, initial conditions for the transfer to batch reactive distillation are defined by the generated data.

Conclusion 3:

Experimental characterization of selected starting materials proves the criteria based theoretical preselection and predefines the starting conditions for reactive distillation experiments

In the phase of performing column experiments with biocatalyst, the main focus is on excellent optical purity (ideally ee_{top} = 100 %) and high molar fraction of the target compound (ideally x_{top} = 100 %). The most influencing parameters on the desired target compound specifications are stepwise fractional

distillation and the initial molar fraction of the starting material, while changes in catalyst distribution along the column height does not exhibit high impact on reaction performance. For fractional distillation, most efficient results are obtained with a temperature-controlled two-step strategy. In the first step, low boiling 1-PrOH is stripped until full kinetic resolution of *(R/S)*-2-PeOH with PrBu gives the residual enantiomer *(S)*-2-PeOH in high optical purity. A stepwise increased temperature for fractional distillation of optically pure *(S)*-2-PeOH results in rising target compound molar fractions ($x_{(S)\text{-2-PeOH,top}}$) in the second step. This method is applied at varied initial starting molar fractions ($x_{(R/S)\text{-2-PeOH,0}}$), which leads to considerably rising target compound molar fractions of $x_{(S)\text{-2-PeOH,top}} = 0.65\ mol \cdot mol^{-1}$ ($x_{(R/S)\text{-2-PeOH,0}} = 0.1\ mol \cdot mol^{-1}$) up to $x_{(S)\text{-2-PeOH,top}} = 0.95\ mol \cdot mol^{-1}$ ($x_{(S)\text{-2-PeOH,0}} = 0.65\ mol \cdot mol^{-1}$). Evaluation of the target compound molar fraction and the corresponding optical purity is depicted in an experimental process window for biocatalytic reactive distillation. Due to present azeotropic behavior within the investigated starting material combination of PrBu and *(R/S)*-2-PeOH, an excess of PrBu with respect to the faster reacting starting enantiomer (*(R)*-2-PeOH) should be prevented. Then, all of the applied PrBu reacts away and azeotrope formation can considerably be reduced. On the other hand, an excess of *(R)*-2-PeOH compared to PrBu in the beginning of the reaction prevents full kinetic resolution. Therefore, conditions in the range of $0.6\ mol \cdot mol^{-1} < x_{(R/S)\text{-2-PeOH,0}} < 0.67\ mol \cdot mol^{-1}$ should be applied for high target compound specifications.

Conclusion 4:

An operating window for high purity and enantiomeric excess is presented for biocatalytic batch reactive distillation experiments with fractional distillation at varied starting conditions

---

Among applying kinetic resolution in an integrated approach, a proof of concept study on dynamic kinetic resolution demonstrates simultaneous CalB catalyzed kinetic resolution with an additional chemocatalyzed racemization in a single apparatus. The special feature of this dynamic kinetic resolution performance is the operation of both catalysts at completely different temperatures ($135°C \leq \Delta T \leq 153°C$) by spatial separation in a Soxhlet reactor setup. Hence, beneficial conditions can be adjusted for thermal sensitive biocatalysts operated at T = 32 °C as well as thermally activated Shvo catalyst operated at T = 183 – 193 °C. In fact, this strategy provides typical behavior of rather constant optical purities for the reactants ($ee_{(R)\text{-2-PeBu}} > 98\ \%$, $ee_{(S)\text{-2-PeOH}} < 13\ \%$ at $Y < 65\ \%$).

Conclusion 5:

A proof of concept study demonstrates general application of two spatially separated catalysts operated at different temperature zones

---

All in all, performed investigations in this study contribute to the rising interest in successful application of biocatalysts in reactive distillation for the synthesis of chiral target molecules via biocatalytic kinetic resolution. Although the integrated concept is still in the development phase, several promising examples are presented comprising this study and current literature. Especially, gaining a valuable chiral target compound represented by *(S)*-2-PeOH within biocatalytic reactive distillation demonstrates the transfer of a classically chemical process setup to a new set of reactions and products in industry in future times.

APPENDIX

Additional information for extended understanding of presented data or discussed parameters are given in the following appendix sections. Cross references in the corresponding chapters are used to give further details on the topic within the appendix section.

A: CALCULATION

Figure A.1 and **Table A.1** represent additional information on the F-Factor calculation. The electric heating device was adjusted to the given values in **Figure A.1** (T_{heat}) and the time dependent temperature increase in the round bottom flask ($\triangle T \cdot t^{-1}$) of the reactive distillation setup was used to calculate $\dot{Q}_{heat}$ according to **Eq. 30**:

$$\dot{Q}_{heat} = m_0 \cdot c_p \cdot \frac{\Delta T_{bottom}}{t} \qquad \textbf{Eq. 30}$$

In **Eq. 30**, m_0 refers to the mass of water filled in the round bottom flask at the beginning of the experiment, while c_p represents the heating capacity of water. For calculation of $\dot{Q}_{heat}$ at a given temperature difference between the electric heating device and the temperature in the round bottom flask ($\triangle T$), the linear regression lines at the adjusted T_{heat} can be applied.

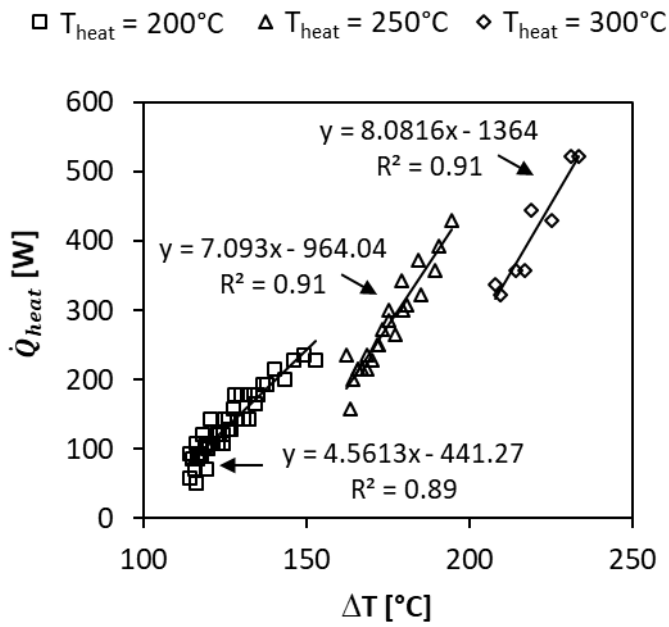

Figure A.1: Determination of $\dot{Q}_{heat}$ for F-factor calculation

The resulting estimated F-factors with respect to the conditions in the stationary column experiments (**section 5.2.4**) are summarized in **Table A.1**.

Table A.1: F-Factor calculation at varied temperature differences between the electric heating device and the temperature in the round bottom flask (*△T*). T_{heat} corresponds to the adjusted value at the heating device, h_V is calculated based on literature data (PrBu: [139], *(R/S)*-2-PeOH: [138]) and ρ_V is determined by assuming ideal gas behavior

			$x_{(R/S)\text{-2-PeOH}} : x_{PrBu}$ **60 : 40 mol%**			$x_{(R/S)\text{-2-PeOH}} : x_{PrBu}$ **40 : 60 mol%**		
T_{heat}[a] [°C]	$\triangle T$[b,c] [-]	$\dot{Q}_{heat}$[c] [W]	h_v [kJ·kg^{-1}]	ρ_V [kg·m^{-3}]	F[c] [Pa$^{0.5}$]	h_v [kJ·kg^{-1}]	ρ_V [kg·m^{-3}]	F[c] [Pa$^{0.5}$]
200	144 ± 10	216 ± 44		0.31	1.0 ± 0.2		0.33	0.9 ± 0.2
250	191 ± 8	392 ± 56	251.8	0.30	1.8 ± 0.2	224.6	0.33	1.7 ± 0.2
300	240 ± 5	572 ± 36		0.30	2.6 ± 0.1		0.33	2.5 ± 0.1

[a]adjusted temperature at heating device of RD column setup
[b]refers to △T of the electric heating device and the mean column temperature in stationary RD (**section 5.2.4**)
[c]standard deviation refers to fluctuations in the heating device at the adjusted T_{heat}

B: SELECTION OF APPLICABLE REACTIONS

Table B.1 represents the implemented starting materials in the preselection tool with their boiling temperatures at p = 1013 mbar and p = 100 mbar. The boiling temperatures were taken from the NIST database [140]. Feasible starting material combinations out of the 120 implemented possibilities at the given preselection criteria are summarized in **Table B.2** and **Table B.3**.

Table B.1: Implemented starting materials in the preselection tool

Chiral starting alcohol			**Non-chiral starting ester**		
Name *(R/S)*-	T_{boil} [°C] p = 1013 mbar	T_{boil} [°C] p = 100 mbar	Name	T_{boil} [°C] p = 1013 mbar	T_{boil} [°C] p = 100 mbar
2-butanol	99	49	ethyl isobutyrate	110	47
2-pentanol	119	65	propyl isobutyrate	133	68
3-hexanol	135	75	methyl butyrate	102	42
2-hexanol	139	82	ethyl butyrate	121	55
3-methyl-2-butanol	133	76	propyl butyrate	142	76
3-methyl-2-pentanol	133	76	ethyl acrylate	99	39
3,3-dimethyl-2-butanol	119	65	propyl acrylate	119	56
2-methyl-3-pentanol	124	69	methyl methacrylate	100	39
4-methyl-2-pentanol	131	72	ethyl methacrylate	117	51
2-methyl-1-butanol	130	75	propyl methacrylate	140	73
			methyl isovalerate	116	53
			ethyl isovalerate	134	69

Table B.2: Theoretically feasible n_{Reac} (+) at p = 10 mbar (T_{RD} = 60 – 80°C, $\Delta T_{separation}$ > 5 °C and $\Delta T_{evaporation}$ < 15 °C)

(R/S)-alcohol / Ester	2-BuOH	2-PeOH	3-HexOH	2-HexOH	3-methyl-2-BuOH	3-methyl-2-PeOH	3,3-dimethyl-2-BuOH	2-methyl-3-PeOH	4-methyl-2-PeOH	2-methyl-1-BuOH
Ethyl isobutyrate	+	-	-	-	-	-	-	-	-	-
Propyl isobutyrate	+	+	+	-	+	+	+	+	+	+
Methyl butyrate	+	-	-	-	-	-	-	-	-	-
Ethyl butyrate	+	-	-	-	+	-	-	-	+	-
Propyl butyrate	-	+	+	+	+	+	+	+	+	+
Ethyl acrylate	-	-	-	-	-	-	-	-	-	-
Propyl acrylate	-	-	-	-	-	-	-	-	-	-
Methyl methacrylate	-	-	-	-	-	-	-	-	-	-
Ethyl methacrylate	+	-	-	-	-	-	-	-	-	-
Propyl methacrylate	-	+	+	+	+	+	+	+	+	+
Methyl isovalerate	+	-	-	-	+	-	-	-	-	-
Ethyl isovalerate	+	+	+	-	+	+	+	+	+	+

Table B.3: Theoretically feasible n_{Reac} (+) at p = 100 mbar (T_{RD} = 80°C, $\Delta T_{separation}$ > 5 °C and $\Delta T_{evaporation}$ < 15 °C)

(R/S)-alcohol / Ester	2-BuOH	2-PeOH	3-HexOH	2-HexOH	3-methyl-2-BuOH	3-methyl-2-PeOH	3,3-dimethyl-2-BuOH	2-methyl-3-PeOH	4-methyl-2-PeOH	2-methyl-1-BuOH
Ethyl isobutyrate	+	-	-	-	+	-	-	-	-	-
Propyl isobutyrate	-	+	+	-	+	+	+	+	+	+
Methyl butyrate	+	-	-	-	-	-	-	-	-	-
Ethyl butyrate	+	+	-	-	+	-	+	+	-	-
Propyl butyrate	-	+	+	-	-	+	+	+	+	+
Ethyl acrylate	+	-	-	-	-	-	-	-	-	-
Propyl acrylate	-	+	-	-	+	-	+	+	-	-
Methyl methacrylate	+	-	-	-	-	-	-	-	-	-
Ethyl methacrylate	+	+	-	-	+	-	+	-	-	-
Propyl methacrylate	-	+	+	-	+	+	+	+	+	+
Methyl isovalerate	+	+	-	-	+	-	+	-	-	-
Ethyl isovalerate	-	+	+	-	+	+	+	+	+	+

Additional estimated VLE data at p = 80 mbar for the non-ideal binary behavior between 1-PrOH and *(R/S)*-2-PeOH (**Figure B.1, A**), 1-PrOH and *(R/S)*-2-PeBu (**Figure B.1, B**), *(R/S)*-2-PeOH and *(R/S)*-2-PeBu (**Figure B.1, C**) as well as PrBu and *(R/S)*-2-PeBu (**Figure B.1, D**) were estimated by the software Aspen properties V8.0 (Aspen Technology, Bedford, Massachusetts, USA).

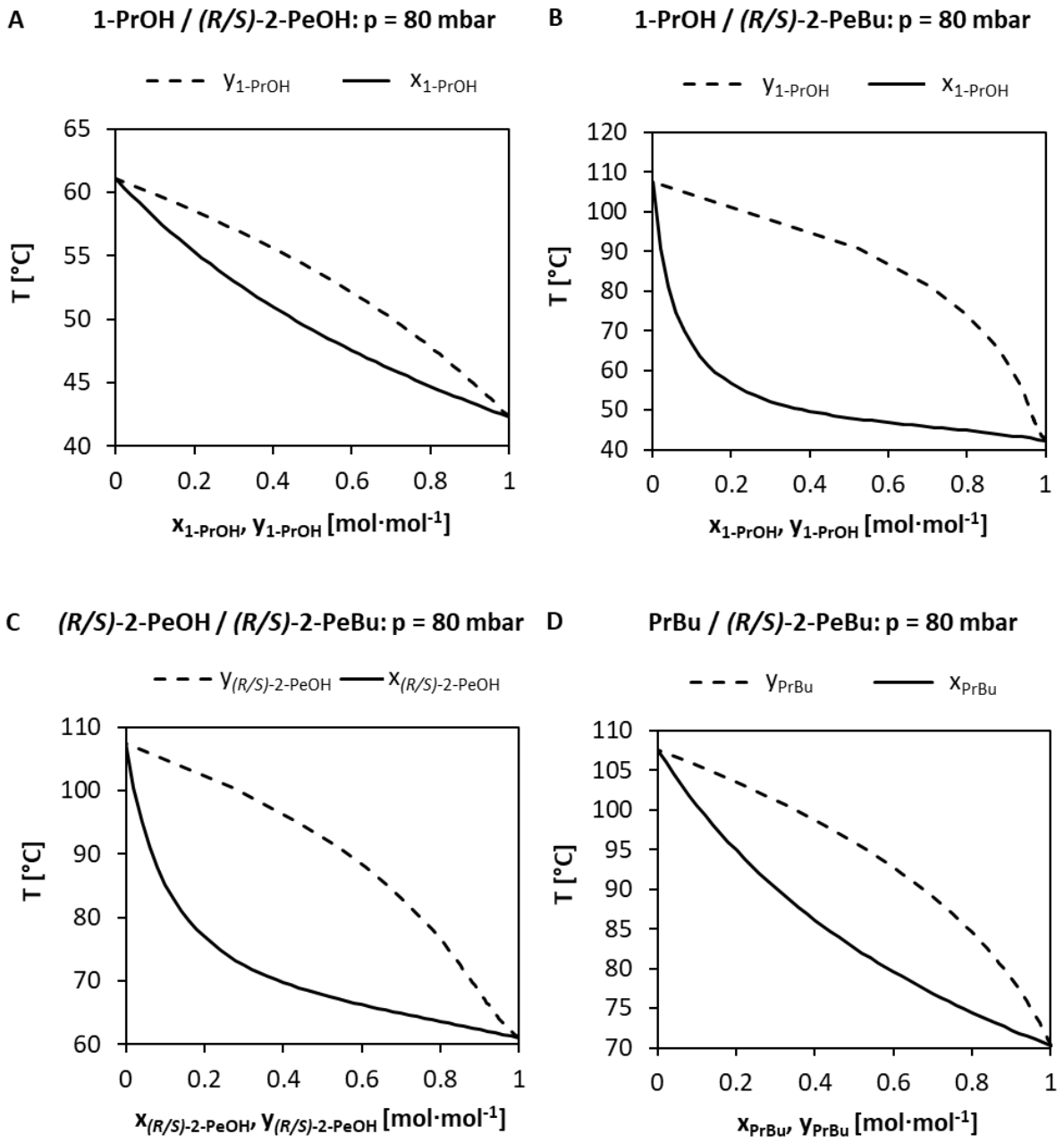

Figure B.1: Estimated vapor liquid equilibria (VLE) at p = 80 mbar by the software Aspen properties V8.0. **A**: 1-PrOH and *(R/S)*-2-PeOH, **B**: 1-PrOH and *(R/S)*-2-PeBu, **C**: *(R/S)*-2-PeOH and *(R/S)*-2-PeBu, **D**: PrBu and *(R/S)*-2-PeBu. Filled lines: liquid molar fraction (x_i), dashed lines: vapor molar fraction (y_i).

C: CHARACTERIZATION OF KINETIC RESOLUTION REACTIONS

Detailed numbers on the Arrhenius dependency (temperature T, initial activity v_0, activation energy E_A) are given in **Table C.1** (*(R/S)*-3-HEB with 1-PeOH) and **Table C.2** (*(R/S)*-2-PeOH with PrBu).

Table C.1: Arrhenius parameters for the kinetic resolution of *(R/S)*-3-HEB with 1-PeOH (*(R)*- and *(S)*-3-HPB). **Operation conditions**: $x_{(R/S)\text{-3-HEB},0}$ = 0.5 mol·mol^{-1}, $x_{1\text{-PeOH},0}$ = 0.5 mol·mol^{-1}, p = 1 bar, 400 rpm, c_{NZ435} = 7 mg·mL^{-1}, E_a determined by linear regression, SD refers to n=3.

		***(R)*-3-HPB**			***(S)*-3-HPB**		
T [°C]	**10^3/T [K^{-1}]**	v_0 [U·mg^{-1}]	ln (v_0)	E_a [kJ·mol^{-1}]	v_0 [U·mg^{-1}]	ln (v_0)	E_a [kJ·mol^{-1}]
30	**3.3**	1.02 ± 0.02	6.92 ± 0.14		0.05 ± 0.01	3.85 ± 0.12	
40	**3.2**	1.70± 0.09	7.44 ± 0.41		0.09 ± 0.01	4.45 ± 0.15	
50	**3.1**	1.99± 0.04	7.59 ± 0.16	18.1 ± 0.1	0.13 ± 0.01	4.89 ± 0.06	37.5 ± 0.1
60	**3.0**	2.22± 0.02	7.70 ± 0.07		0.18 ± 0.01	5.18 ± 0.09	
70	**2.9**	2.44 ± 0.02	7.80 ± 0.06		0.26 ± 0.01	5.54 ± 0.05	

Table C.2: Arrhenius parameters for the kinetic resolution of *(R/S)*-2-PeOH with PrBu (*(R)*-2-PeBu and *(S)*-2-PeBu). **Operation conditions**: $x_{(R/S)\text{-2-PeOH},0}$ = 0.5 mol·mol^{-1}, $x_{PrBu,0}$ = 0.5 mol·mol^{-1}, p = 1 bar, 400 rpm, c_{NZ435} = 7 mg·mL^{-1}, E_a determined by linear regression, SD refers to n=2.

		***(R)*-2-PeBu**			***(S)*-2-PeBu**		
T [°C]	**10^3/T [K^{-1}]**	v_0 [U·mg^{-1}]	ln (v_0)	E_a [kJ·mol^{-1}]	v_0 [U·mg^{-1}]	ln (v_0)	E_a [kJ·mol^{-1}]
40	**3.2**	1.91 ± 0.09	7.56 ± 0.35		0	-	
60	**3.0**	1.97 ± 0.04	7.59 ± 0.17	14.0 ± 0.1	0	-	-
80	**2.8**	3.55 ± 0.18	8.18 ± 0.42		0	-	

In **Figure C.1**, the experimental course of the enantiomeric excess ($ee_{(S)\text{-2-PeOH}}$, $ee_{(R)\text{-2-PeBu}}$) with rising conversion (X) is demonstrated for the kinetic resolution reaction by *(R/S)*-2-PeOH with PrBu at p = 1 bar. Presented lines refer to calculated behavior by Chen et al. (1982) [115].

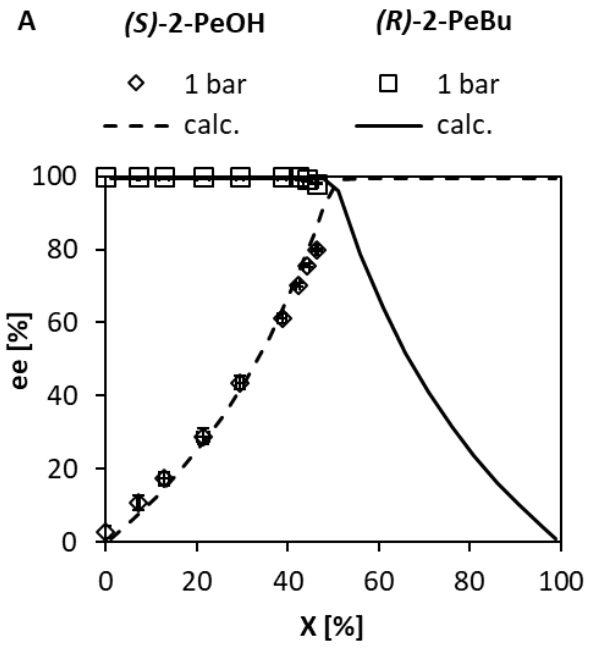

Figure C.1: Reaction performance of the kinetic resolution reaction by *(R/S)*-2-PeOH with PrBu, **Operation conditions**: $x_{(R/S)\text{-2-PeOH},0}$ = 0.1 mol·mol^{-1}, $x_{PrBu,0}$ = 0.9 mol·mol^{-1}, T = 60 °C, 400 rpm, c_{NZ435} = 7 mg·mL^{-1}, lines: calculated behavior at E = 100. SD refers to n=2.

D: IMPLEMENTATION OF SELECTED REACTIONS IN REACTIVE DISTILLATION

Additional courses of the molar fractions of all reactants (x_i) at the top of the batch reactive distillation column with rising conversions (X) are presented for initial starting molar fractions of $x_{(R/S)\text{-2-PeOH},0}$ = 0.1 mol·mol^{-1} and the starting ester EtBu ($x_{EtBu,0}$ = 0.9 mol·mol^{-1}) in **Figure D.1, A** as well as the starting ester PrBu ($x_{PrBu,0}$ = 0.9 mol·mol^{-1}) in **Figure D.1, B**. The courses at the bottom (**Figure D.1, C**) and at H1 (**Figure D.1, D**) of RD with PrBu are depicted as well. Manual fractional distillation in the case of EtBu and automated temperature controlled fractional distillation in the case of PrBu is indicated by grey boxes. The set temperature values for changes in fractional distillation in the experiment with PrBu are presented within the figures.

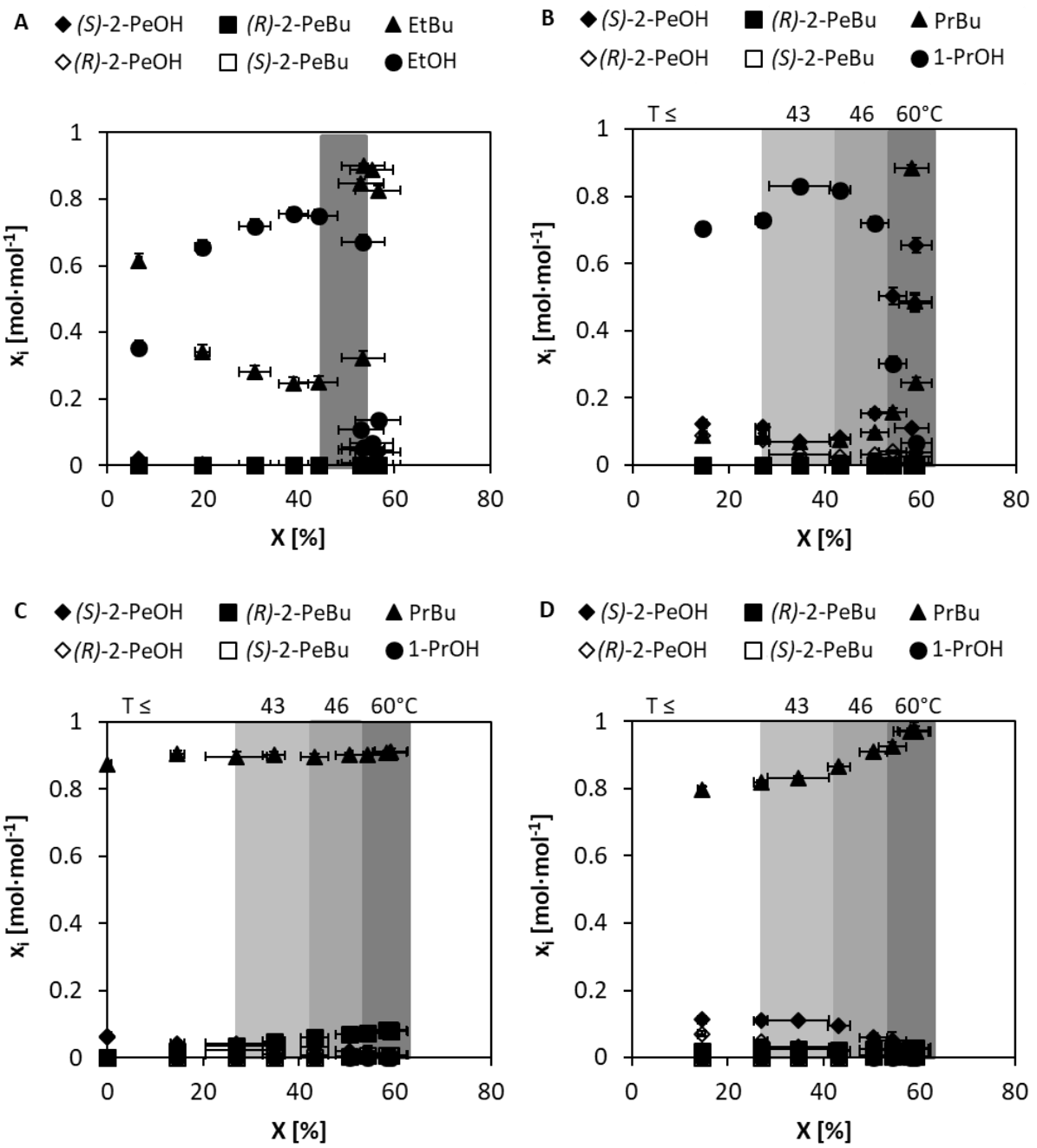

Figure D.1: Molar fractions (x_i) in biocatalytic batch reactive distillation for the kinetic resolution of *(R/S)*-2-PeOH ($x_{(R/S)\text{-2-PeOH},0}$ = 0.1 mol·mol^{-1}) with either EtBu ($x_{EtBu,0}$ = 0.9 mol·mol^{-1}) or PrBu ($x_{PrBu,0}$ = 0.9 mol·mol^{-1}) at different column heights. **A**: EtBu: top, **B**: PrBu: top, **C**: PrBu: bottom, **D**: PrBu, H1. **Operation conditions**: $m_{Bottom,0}$ = 800 g, SD: refers to maximum error estimation according to section 3.4. **EtBu**: p = 100 mbar, $m_{Bottom,0}$ = 800 g, grey box: area of manually adjusted fractional distillation with rr = 20, T_{Bottom} = 58 – 64 °C, m_{NZ435} = 6.5 g (c_{NZ435} = 104 mg·g$_{(R/S)\text{-2-PeOH},0}^{-1}$), **PrBu**: p = 80 mbar, $m_{Bottom,0}$ = 800 g, grey areas: automated temperature controlled fractional distillation (rr = 7.5), set temperature value: T ≤ 43 °C (lightest grey), T ≤ 46 °C (light grey), T ≤ 60 °C (dark grey), T_{Bottom} = 70 - 74°C, m_{NZ435} = 6.15 g (c_{NZ435} = 110 mg·g$_{(R/S)\text{-2-PeOH},0}^{-1}$). SD: refers to maximum error estimation according to **section 3.4**.

Moreover, the molar fraction profiles of all reactants (x_i) at the top of the column with rising conversions (X) are presented for initial starting molar fractions of $x_{(R/S)\text{-2-PeOH},0}$ = 0.1 mol·mol^{-1} and the

starting ester EtBu ($x_{EtBu,0}$ = 0.9 mol·mol^{-1}) at the bottom of the column (**Figure D.2, A**) as well as in height position H2 (**Figure D.2, B**), and position H3 (**Figure D.2, C**).

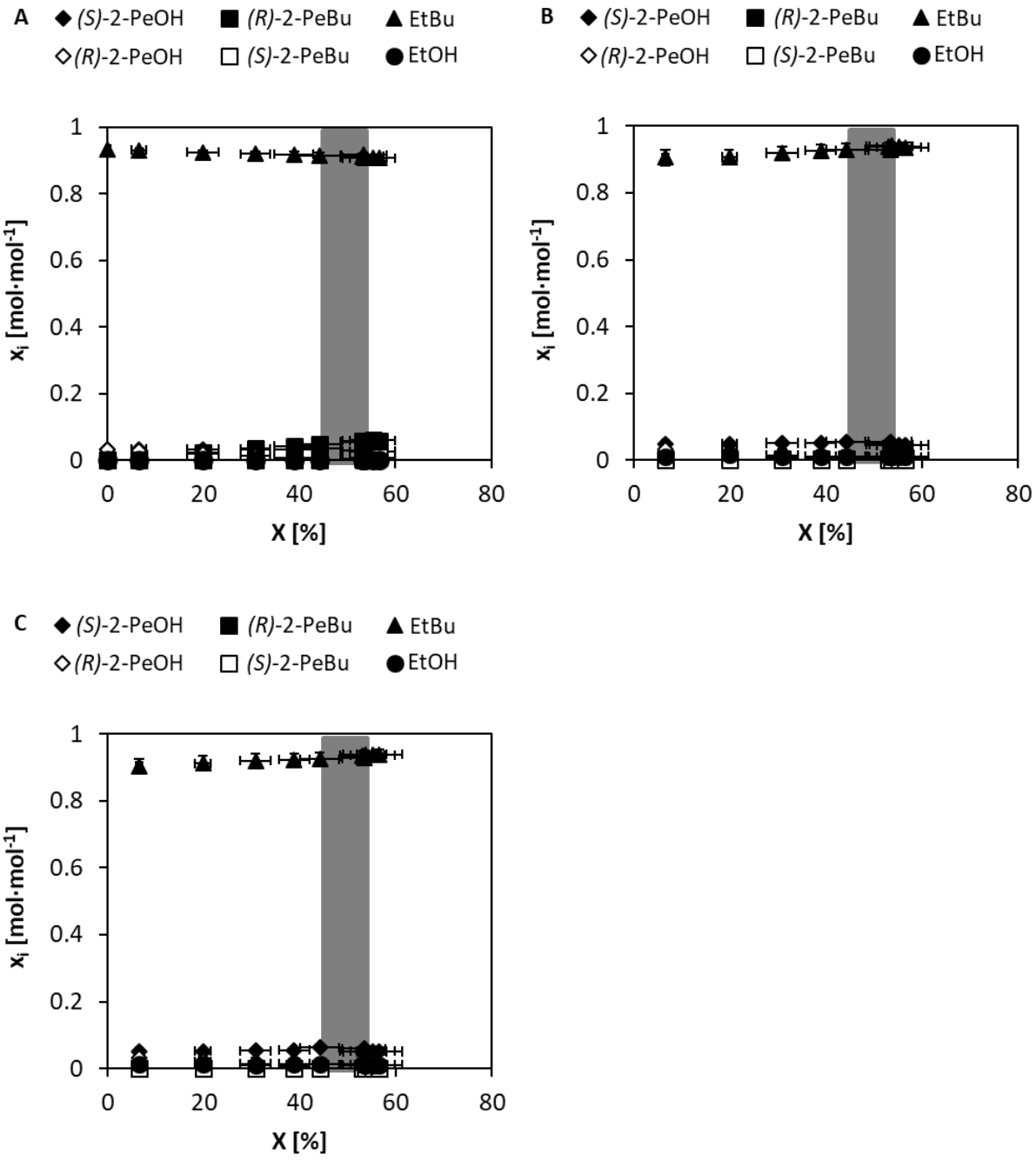

Figure D.2: Molar fractions (x_i) in biocatalytic batch reactive distillation for the kinetic resolution of *(R/S)*-2-PeOH ($x_{(R/S)\text{-2-PeOH},0}$ = 0.1 mol·mol^{-1}) with EtBu ($x_{EtBu,0}$ = 0.9 mol·mol^{-1}) at different column heights. **A**: bottom, **B**: H2, **C**: H3. **Operation conditions**: $m_{Bottom,0}$ = 800 g, p = 100 mbar, grey box: area of manually adjusted fractional distillation with rr = 20, T_{Bottom} = 58 – 64 °C, m_{NZ435} = 6.5 g (c_{NZ435} = 104 mg·g$_{(R/S)\text{-2-PeOH},0}^{-1}$), SD: refers to maximum error estimation according to **section 3.4**.

E: CHIRAL TARGET COMPOUND ISOLATION IN REACTIVE DISTILLATION

Figure E.1 shows spatially resolved $ee_{(S)\text{-2-PeOH}}$ at different column heights for two further conversion points (X = 24.1 ± 0.1 %, **Figure E.1, A**, X = 33.1 ± 0.7 %, **Figure E.1, B**) in the RD experiments with NZ435 in H1 - H4 (filled bars) and NZ435 in H1 - H2 (open bars). The data are add to support the discussed course in the result section by similar behavior of rather constant $ee_{(S)\text{-2-PeOH}}$ at different catalyst arrangement strategies in batch RD.

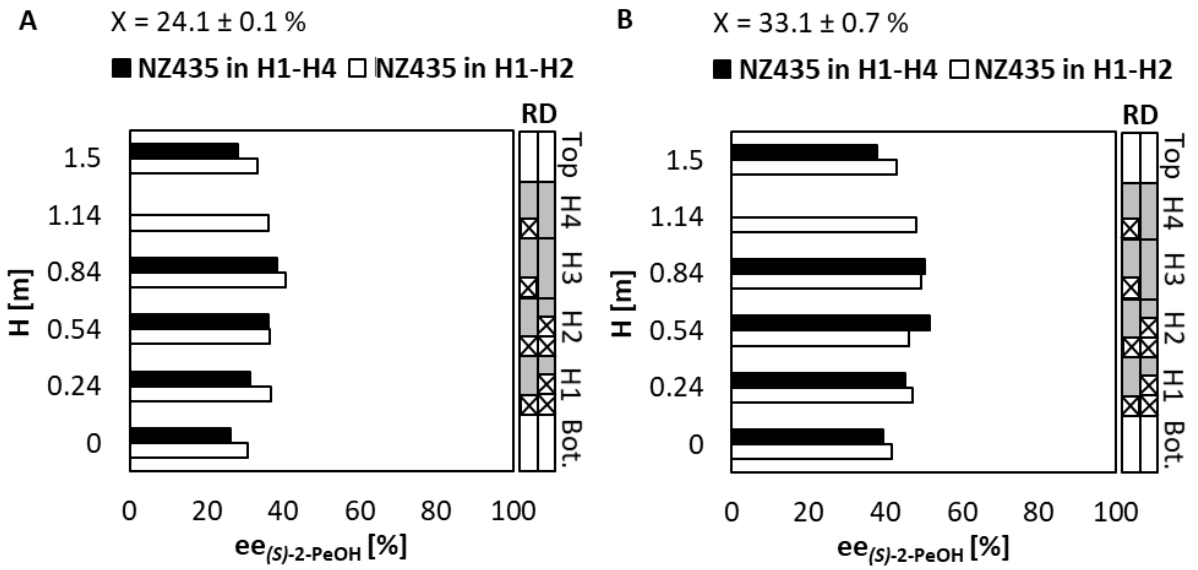

Figure E.1: Spatially-resolved enantiomeric excess ($ee_{(S)\text{-2-PeOH}}$) at similar conversion points (**A**: X = 24.1 ± 0.1 %, **B**: X = 33.1 ± 0.7 %) for NZ435 either distributed in H1 - H4 or in H1 - H2 in batch reactive distillation**. Operation conditions**: $x_{PrBu,0}$ = 0.4 mol·mol^{-1}, $x_{(R/S)\text{-2-PeOH},0}$ = 0.6 mol·mol^{-1}, p = 80 mbar, $m_{Bottom,0}$ = 800 g, m_{NZ435} = 30.36 g (c_{NZ435} = 75 mg·g$_{(R/S)\text{-2-PeOH},0}^{-1}$), SD of X is referred to mean values of compared conversions points in both RD experiments (n = 2).

For both batch RD experiments with a varied catalyst distribution strategy, pretty similar profiles were obtained during operation in **Figure E.2**, **A** – **E** and **Figure E.3**, **A** - **F**.

In **Figure E.2**, **A** - **E**, the obtained time-dependent batch RD profiles of the molar ratios (x_i) at the different column heights are depicted for the experiment with a distribution of NZ435 in H1 - H4. **A** refers to the bottom of the column, **B** to the top of the column and **C** to **E** to the sampling position within H1 - H3 (**C** = H1, **D** = H2, **E** = H3). Sampling at the different column heights was only possible in the given time-frames, whereas bottom and top samples were realized over the whole course of column operation (**A** and **B**).

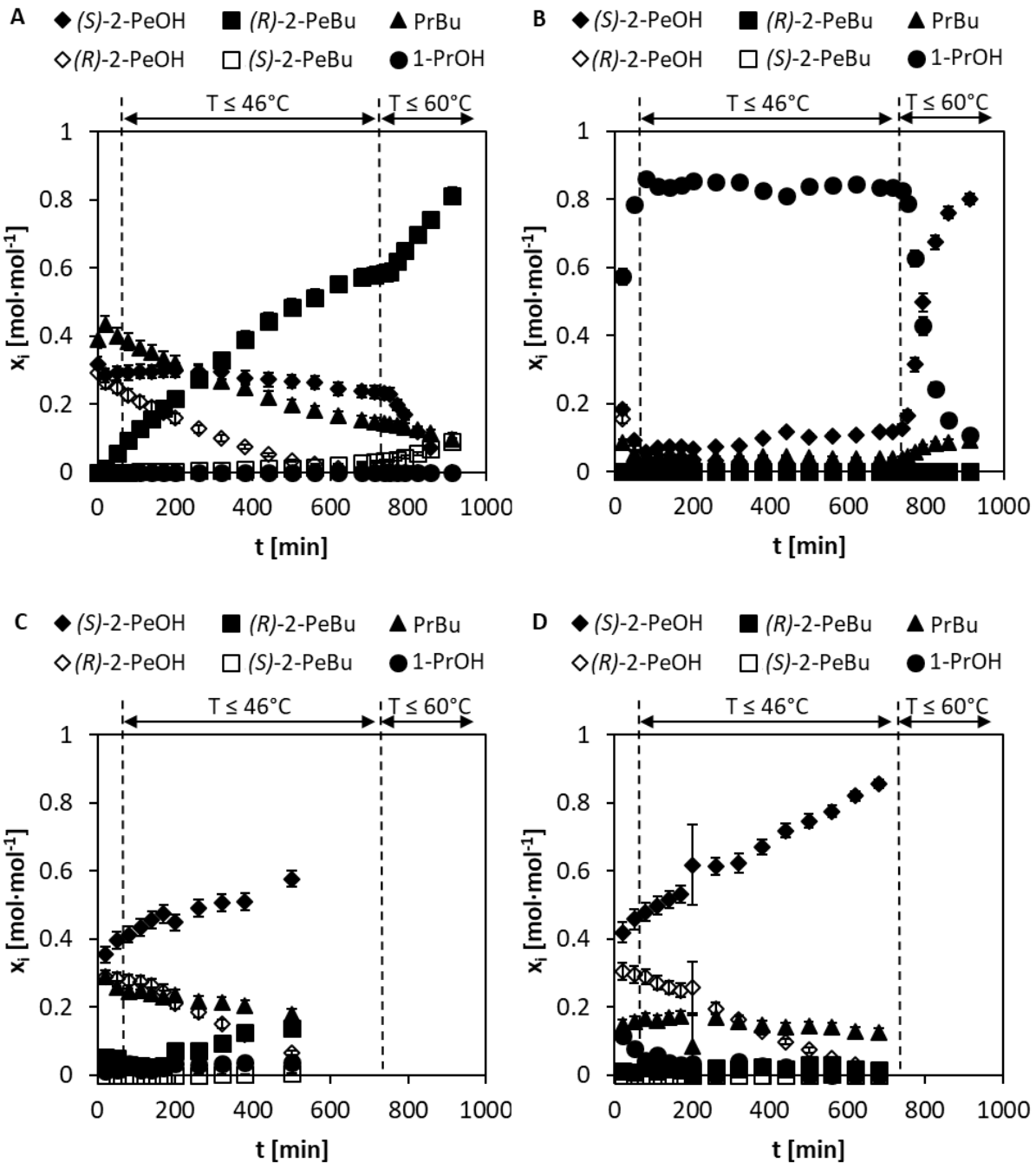
A
B
C
D
(S)-2-PeOH
(R)-2-PeBu
PrBu
(R)-2-PeOH
(S)-2-PeBu
1-PrOH
T ≤ 46°C
T ≤ 60°C
xi [mol·mol-1]
t [min]
0
0.2
0.4
0.6
0.8
1
0
200
400
600
800
1000

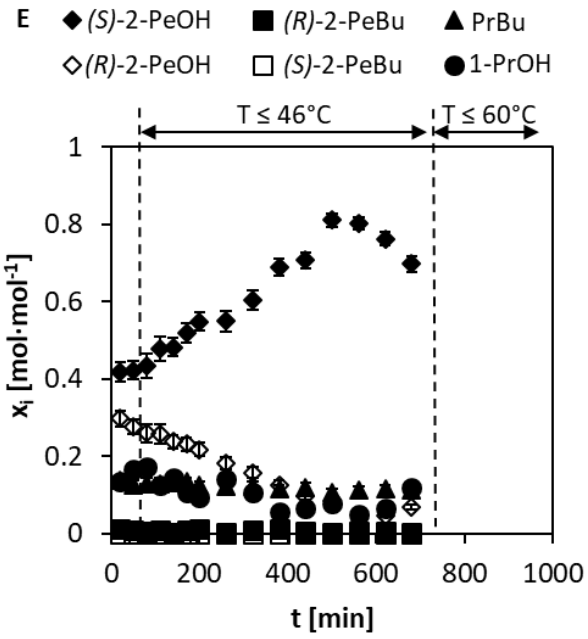

Figure E.2: Height-dependent profiles of molar fractions in batch reactive distillation for distribution of NZ435 in H1 - H4. **A:** Bottom, **B:** Top, **C:** H1, **D:** H2, **E:** H3. **Operation conditions**: $x_{PrBu,0}$ = 0.4 mol·mol^{-1}, $x_{(R/S)\text{-2-PeOH},0}$ = 0.6 mol·mol^{-1}, p = 80 mbar, $m_{Bottom,0}$ = 800 g, m_{NZ435} = 30.36 g (c_{NZ435} = 75 mg·g$_{(R/S)\text{-2-PeOH},0}^{-1}$), dashed line: calculated behavior of $ee_{(S)\text{-2-PeOH}}$, temperature induced fractional distillation at T ≤ 46 °C and T ≤ 60 °C: vertical lines and horizontal arrows (NZ435 in H1 - H4), SD: maximum error according to **section 3.4**.

In **Figure E.3**, **A** - **F**, the obtained time-dependent batch RD profiles of the molar ratios (x_i) at the different column heights are depicted for the experiment with a distribution of NZ435 in H1 - H2. **A** refers to the bottom of the column, **B** to the top of the column and **C** to **F** to the sampling position within H1 - H4 (**C** = H1, **D** = H2, **E** = H3, **F** = H4).

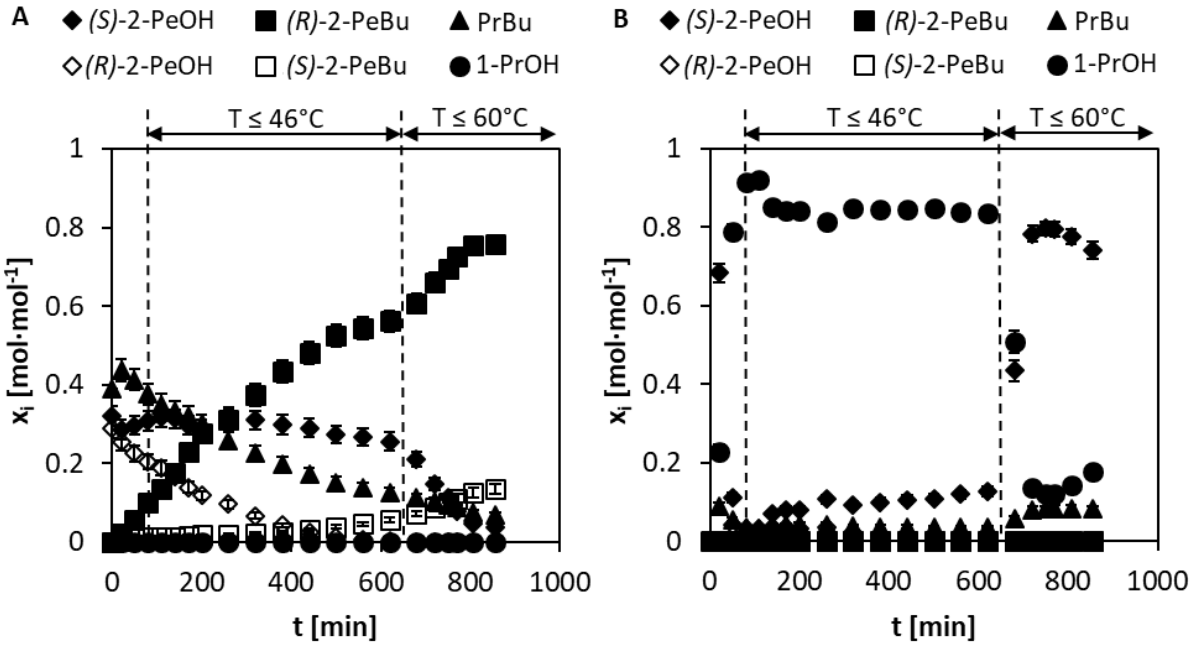

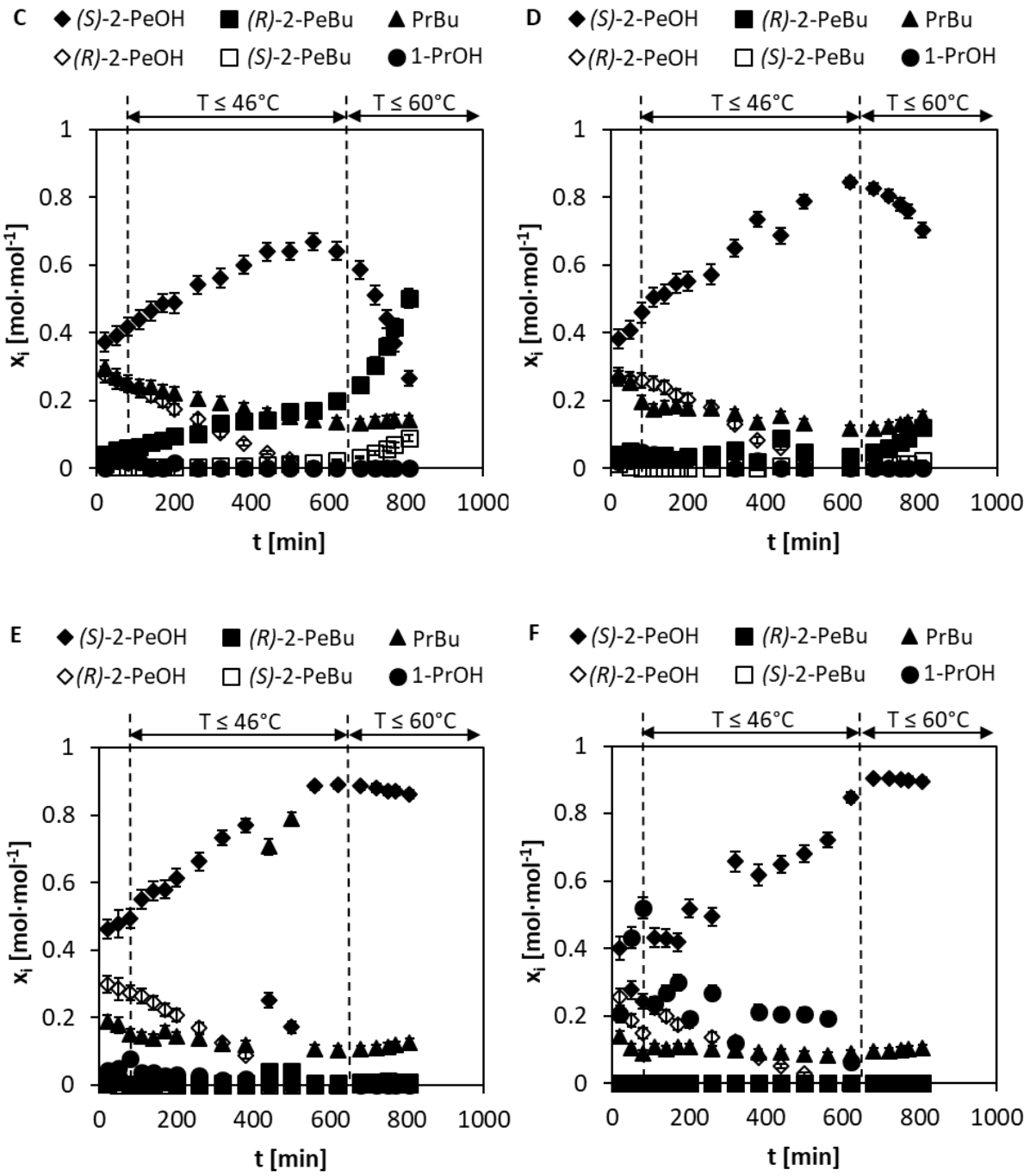

Figure E.3: Height-dependent profiles of molar fractions in batch reactive distillation for distribution of NZ435 in H1 - H2. **A:** Bottom, **B:** Top, **C:** H1, **D:** H2, **E:** H3, **F:** H4. **Operation conditions**: $x_{PrBu,0}$ = 0.4 mol·mol^{-1}, $x_{(R/S)\text{-}2\text{-}PeOH,0}$ = 0.6 mol·mol^{-1}, p = 80 mbar, $m_{Bottom,0}$ = 800 g, m_{NZ435} = 30.36 g (c_{NZ435} = 75 mg·g$_{(R/S)\text{-}2\text{-}PeOH,0}^{-1}$), dashed line: calculated behavior of $ee_{(S)\text{-}2\text{-}PeOH}$, temperature induced fractional distillation at T ≤ 46 °C and T ≤ 60 °C: vertical lines and horizontal arrows (NZ435 in H1 - H2), SD: maximum error according to **section 3.4**.

In **Figure E.4**, the molar fractions of all reactants in the top of the column for biocatalytic batch reactive distillation experiments with initial starting molar fractions of $x_{(R/S)\text{-}2\text{-}PeOH,0}$ = 0.67 mol·mol^{-1} (**Figure E.4**, **A**) and $x_{(R/S)\text{-}2\text{-}PeOH,0}$ = 0.65 mol·mol^{-1} (**Figure E.4**, **B**) are shown.

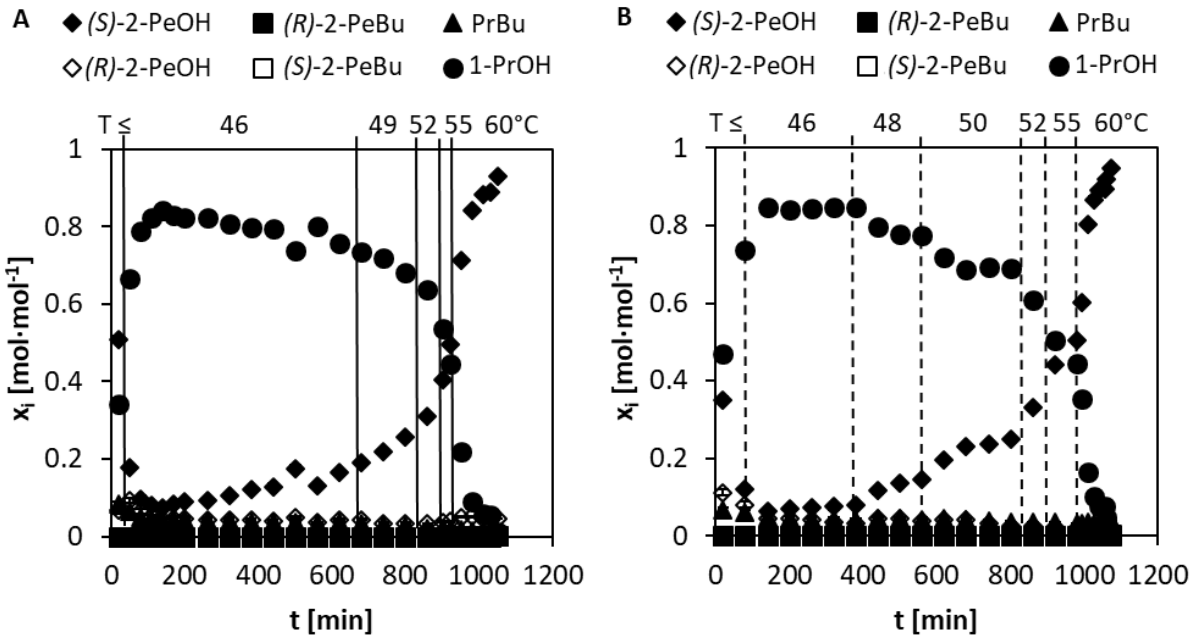

Figure E.4: Profiles of the molar fractions at the top of biocatalytic batch reactive distillation **A:** $x_{(R/S)\text{-2-PeOH},0}$ = 0.67 mol·mol^{-1}, **B:** $x_{(R/S)\text{-2-PeOH},0}$ = 0.65 mol·mol^{-1}. **Operation conditions**: p = 80 mbar, $m_{Bottom,0}$ = 800 g, m_{NZ435} = 45.3 g (c_{NZ435} = 98 - 104 mg·g$_{(R/S)\text{-2-PeOH},0}^{-1}$), rr = 9 (18 : 2) at t < 1035 min, rr = 0 at t > 1035 min, temperature induced fractional distillation at T ≤ 46 °C and T ≤ 60 °C: vertical lines, SD: maximum error according to **section 3.4**.

LIST OF SYMBOLS AND ABBREVIATIONS

Abbreviation	**Description**
CalB	Candida antarctica lipase B
CMC	Critical micellar concentration
DKR	Dynamic kinetic resolution
EtBu	Ethyl butyrate
EtOAC	Ethyl acetate
EtOH	Ethanol
GC	Gas chromatography
(R/S)-3-HEB	*(R/S)*-3-hydroxy ethyl butyrate
HETP	Height equivalent to a theoretical plate
(R/S)-3-HPB	*(R/S)*-3-hydroxy pentyl butyrate
ISTD	Internal standard material
KR	Kinetic Resolution
NADH	Reduced form of nicotinamide adenine dinucleotide
NADPH	Reduced form of nicotinamide adenine dinucleotide phosphate
NZ435	Novozym435
1-PeOH	1-pentanol
(R/S)-2-PeOH	*(R/S)*-2-pentanol
(R/S)-2-PeBu	*(R/S)*-2-pentyl butyrate
PIC	Pressure indicated control
PrBu	Propyl butyrate
1-PrOH	1-propanol
RD	Reactive Distillation
SD	Standard deviation
Shvo	Ruthenium catalyst for racemization
STR	Stirred tank reactor
TIC	Temperature indicated control
UNIFAC DMD	Universal Quasichemical Functional Group Activity Coefficients Dortmund
UNIQUAC	Universal Quasichemical
VLE	Vapor liquid equilibrium

Symbol	Description	Unit
α_{AB}	Relative volatility between the reactants A and B	[-]
a_i	Thermodynamic activity of reactant i	[-]
a_{spec}	Specific surface area	$[m^2 \cdot m^{-3}]$
c_i	Concentration of component or reactant i	$[mol \cdot L^{-1}]$ / $[g \cdot L^{-1}]$
d_i	Diameter of i	[mm]
E	Enantioselectivity	[-]
E_a	Activation energy	$[kJ \cdot mol^{-1}]$
ee_i	Enantiomeric excess of reactant i	[%]
F_v	F-Factor (vapor load)	$[Pa^{0.5}]$
γ	Thermodynamic activity coefficient	[-]
$\triangle G$	Difference in Gibbs free energies	[kJ]
$\triangle\triangle G$	Difference in Gibbs free energies of transition states	[kJ]
g^E	Free excess enthalpy to predict γ	$[kJ \cdot kg^{-1}]$
H_i / h_i	Height of i	[mm]
HETP	Height equivalent to a theoretical plate	[m]
h_V	Vaporization enthalpy	$[kJ \cdot kg^{-1}]$
k_0	Frequency factor for collision of molecules	[-]
k_d	Deactivation constant	$[s^{-1}]$
K_{eq}	Equilibrium constant	[-]
k_i	Reaction constant of reactant i	$[mol\ s^{-1}]$
λ	Wave length	[nm]
$m_{o,i}$	Initial mass of reactant i	[kg]
m_i	Mass of component or reactant i	[kg]
$\dot{m}_V$	Vapor mass flow	$[kg\ s^{-1}]$
n	Number of entities	[-]
n_i	Mole of reactant i	[mol]
p	Pressure	[bar]
$\dot{Q}_{Heat}$	Heat flow	[W]
ρ_i	Density of reactant i	$[kg\ m^{-3}]$
R	Ideal gas constant	$[J\ mol^{-1}\ K^{-1}]$
rr	Reflux ratio	[-]
$\overline{\sigma}$	Mean standard deviation	[%]
$\tau_{0.5}$	Half-life time	[d]
t	Time of reaction	[min]

Symbol	Description	Unit
$\triangle T_i$	Temperature difference between component or reactant i	[°C]
T_i	Temperature of component, reactant or position i	[°C]
$\dot{V}_i$	Vapor flow of component i	[$m^3\ s^{-1}$]
v_0	Specific initial reaction velocity	[U mg^{-1}]
v_i	Specific reaction velocity	[U mg^{-1}]
X	Conversion	[%]
$x_{0,i}$	Lnitial liquid molar fraction of reactant i	[mol mol^{-1}]
x_i	Liquid molar fraction of reactant i	[mol mol^{-1}]
Y	Yield	[%]
y_i	Vapor molar fraction of reactant i	[mol mol^{-1}]
$\triangle z$	Estimated maximum error	[%]

LIST OF FIGURES

LIST OF TABLES

LITERATURE

[1] European Commission *Energy, Transport and Environment Indicators*; Eurostat statistical books, first edition: Luxembourg, 2015.

[2] Segovia-Hernández; J. G., Hernández, S.; Petriciolet, A. B. Reactive Distillation: A Review of Optimal Design Using Deterministic and Stochastic Techniques. *Chem. Eng. Process.* **2015**, *97*, 134-143.

[3] Harmsen, G. J. Reactive Distillation: The Front-Runner of Industrial Process Intensification. *Chem. Eng. Process.* **2007**, *46*, 774-780.

[4] Keller, T. Reactive Distillation. *Distillation: Equipment and Processes* **2014,** 261-294.

[5] Ullmann *Reactive Distillation*, Wiley: Weinheim, 2012.

[6] Backhaus, A. A. Continuous Process for the Manufacture of Esters. U.S. Patent 1,400,849. Dec. 20, 1921.

[7] Backhaus, A. A. Apparatus for Producing High-Grade Esters." U.S. Patent 1,403,224. Jan. 10, 1922.

[8] Smith Jr, L. A. Catalyst System for Separating Isobutene from C4 Streams. U.S. Patent 4,215,011. Jul. 29, 1980.

[9] Agreda, V. H.; Partin, L. R. Reactive Distillation Process for the Production of Methyl Acetate. U.S. Patent 4,435,595. Mar. 6, 1984.

[10] Taylor, R.; Krishna, R. Modelling Reactive Distillation. *Chem. Eng. Sci.* **2000**, *55*, 5183-5229.

[11] Siirola, J. J. An Industrial Perspective on Process Synthesis. *AIChE Symp. Ser.* **1995**, *91*, 222-234.

[12] Doherty, M.F; Malone, M. F. Conceptual Design of Distillation Systems, first ed., McGraw-Hill: Boston, 2001.

[13] Rameshwar, S. H.; Bhate, N. V.; Mahajan, Y. S.; Mahajani, S. M., Industrial Applications of Reactive Distillation: Recent Trends. *Int. J. Chem. React. Eng.* **2004**, *2*, 1-52.

[14] Qi, W.; Malone, M. F. Operating Parameters and Selectivity in Batch Reactive Distillation, *Ind. Eng. Chem. Res.* **2010**, *49*, 11547-11556.

[15] Dejanovic, I.; Matijasevic, L.; Olujic, Z Dividing Wall Column—A Breakthrough Towards Sustainable Distilling. *Chem. Eng. Process.* **2010**, *49*, 559–580.

[16] Schembecker, G.; Tlatlik, S. Process Synthesis for Reactive Separations, *Chem. Eng. Process.* **2003**, *42*, 179-189.

[17] Okasinski, M. J.; Doherty, M. F. Simultaneous Kinetic Resolution of Chiral Propylene Oxide and Propylene Glycol in a Continuous Reactive Distillation Column. *Chem. Eng. Sci.* **2003**, *58*, 1289-1300.

[18] Schmid, A.; Dordick, J. S.; Hauer, B.; Kiener, A.; Wubbolts, M.; Witholt, B. Industrial Biocatalysis Today and Tomorrow. *Nat.* **2001**, *409*, 258-268.

[19] Gotor-Fernández, V.; Brieva, R.; Gotor, V. Lipases: Useful Biocatalysts for the Preparation of Pharmaceuticals. *J. Mol. Cat. B: Enzym.* **2006**, *40*, 111-120.

[20] Turner, N. J. Directed Evolution Drives the Next Generation of Biocatalysts. *Nat. Chem. Biol.* **2009**, *5*, 567.

[21] Bornscheuer, U. T.; Kazlauskas, R. J. *Hydrolases in Organic Synthesis: Regio-and Stereoselective Biotransformations*. John Wiley & Sons, 2006.

[22] Tsai, S. W. Enantiopreference of Candida Antarctica Lipase B Toward Carboxylic Acids: Substrate Models and Enantioselectivity Thereof. *J. Mol. Cat. B: Enzym.* **2016**, *127*, 98-116.

[23] Karl, U.; Simon, A BASF's ChiPros Chiral Building Blocks. *Chimica Oggi*, **2009**, *27*.

[24] Fox, R. J.; Davis, S. C.; Mundorff, E. C.; Newman, L. M.; Gavrilovic, V.; Steven, K. Ma.; Chung, L. M.; Ching, C.; Tam, S.; Muley, S.; Grate, J.; Gruber, J.; Whitman, J. C.; Sheldon, R. A.; Huisman, G. W. Improving Catalytic Function by ProSAR-Driven Enzyme Evolution. *Nat. Biotechnol.* **2007**, *25*, 338.

[25] Desai, A. A. Sitagliptin Manufacture: a Compelling Tale of Green Chemistry, Process Intensification, and Industrial Asymmetric Catalysis. *Ang. Chem. Int. Ed.* **2011**, *50*, 1974-1976.

[26] Greener Synthetic Pathways Award 2006, U.S. Environmental Protection Agency (accessed Feb 14, 2017)

[27] Hansen, K. B.; Balsells, J.; Dreher, S.; Hsiao, Y.; Kubryk, M.; Palucki, M.; Rivera, N.; Steinhuebel, D.; Armstrong, J. D.; Askin, D.; Grabowski, E. J. J. First Generation Process for the Preparation of the DPP-IV Inhibitor Sitagliptin. *Org. Process Res. Dev.* **2005**, *9*, 634-639.

[28] Hansen, K.B.; Hsiao, Y.; Xu, F.; Rivera, N.; Clausen, A.; Kubryk, M.; Krska, S.; Rosner, T.; Simmons, B.; Balsells, J.; Ikemoto, N.; Sun, Y.; Spindler, F.; Malan, C.; Grabowski E. J. J.; Armstrong, J. D. Highly Efficient Asymmetric Synthesis of Sitagliptin. *J. Am. Chem. Soc.* **2009**, *131*, 8798–8804.

[29] Savile, C. K.; Janey, J. M; Mundorff, E. C.; Moore, J. C.; Tam, S.; Jarvis, W. R.; Colbeck, J. C.; Krebber, A.; Fleitz, F. J.; Brands, J.; Devine, P. N.; Huisman, G. W.; Hughes, G. J. Biocatalytic Asymmetric Synthesis of Chiral Amines from Ketones Applied to Sitagliptin Manufacture. *Science* **2010**, *329*, 305-309.

[30] Bommarius, A. S. Biocatalysis: a Status Report. *Annu. Rev. Chem. Biomol. Eng.* **2015**, *6*, 319-345.

[31] Tufvesson, P.; Lima-Ramos, J.; Nordblad, M.; Woodley, J. M. Guidelines and Cost Analysis for Catalyst Production in Biocatalytic Processes. *Org. Process Res. Dev.* **2010**, *15*, 266-274.

[32] Liese, A.; Seelbach, K.; Wandrey, C. *Industrial Biotransformations*. Wiley: Weinheim, 2006.

[33] Haki, G. Developments in Industrially Important Thermostable Enzymes: a Review. *Bioresour. Technol.* **2003**, *89*, 17−34.

[34] Hills, G. A.; Macrae, A. R.; Poulina, R. R. Ester Preparation. EP 0383405 Feb 14, 1990.

[35] Bornscheuer, U. T. Immobilizing Enzymes: how to Create More Suitable Biocatalysts. *Ang. Chem. Int. Ed.* **2003**, *42*, 3336-3337.

[36] Liese, A.; Hilterhaus, L. Evaluation of Immobilized Enzymes for Industrial Applications. *Chem. Soc. Rev.* **2013**, *42*, 6236-6249.

[37] Poojari, Y.; Clarson, S. J. Thermal Stability of Candida Antarctica Lipase B Immobilized on Macroporous Acrylic Resin Particles in Organic Media. *Biocatal. Agric. Biotechnol.* **2013**, 2, 7−11.

[38] Salihu, A.; Alam, M. Z. Solvent Tolerant Lipases: A Review. *Process Biochem.* **2015**, 50, 86−96.

[39] Paiva, A. L.; van Rossum, D.; Malcata, F. X. Lipase-Catalyzed Synthesis of Butyl Butyrate by Alcoholysis in an Integrated Liquid-Vapor System. *Biotechnol. Prog.* **2003,** *19*, 750–754.

[40] Heils, R.; Sont, A.; Bubenheim, P.; Liese, A.; Smirnova, I. Integration of Enzymatic Catalysts in a Reactive Distillation Column with Structured Packings. *Ind. Eng. Chem. Res.* **2012,** *51*, 11482–11489.

[41] Heils, R.; Niesbach, A.; Wierschem, M.; Claus, D.; Soboll, S.; Lutze, P.; Smirnova, I. Integration of Enzymatic Catalysts in a Continuous Reactive Distillation Column: Reaction Kinetics and Process Simulation. *Ind. Eng. Chem. Res.* **2014,** *50*, 19612-19619

[42] Wierschem, M.; Schlimper, S.; Heils, R.; Smirnova, I.; Kiss, A. A.; Skiborowski, M.; Lutze, P. Pilot-Scale Validation of Enzymatic Reactive Distillation for Butyl Butyrate Production. *Chem. Eng. J.* **2017**, *312*, 106-117.

[43] Egger, T.; Fieg, G. Enzymatic Catalyzed Reactive Dividing Wall Column: Experiments and Model Validation. *AIChE J.* **2017**, *63*, 2198-2211.

[44] Au-Yeung, P. H.; Resnick, S. M.; Witt, P. M.; Frank, T. C.; Donate, F. A.; Robbins, L. A. Horizontal Reactive Distillation for Multicomponent Chiral Resolution. *AIChE J.* **2013,** *59*, 2603–2620.

[45] Heils, R.; Jensen, J.-H.; Wichert, S.; Behrens, N.; Fabuel-Ortega, M.; Liese, A.; Smirnova, I. Enzymatic Reactive Distillation: Kinetic Resolution of rac -2-Pentanol with Biocatalytic Coatings on Structured Packings. *Ind. Eng. Chem. Res.* **2015,** *54*, 9458–9467.

[46] Heils, R.; Hu, X.; Liese, A.; Smirnova, I. In Situ Production and Renewal of Biocatalytic Coatings for use in Enzymatic Reactive Distillation. *Chem. Eng. J.* **2016,** *306*, 992–1000.

[47] Wierschem, M.; Boll, S.; Lutze, P.; Górak, A. Evaluation of the Enzymatic Reactive Distillation for the Production of Chiral Compounds. *Chem. Ing. Tech.* **2016,** *88*, 147–157.

[48] Wierschem, M.; Langen, A. A.; Lins, J.; Spitzer, R.; Skiborowski, M. Model Validation for Enzymatic Reactive Distillation to Produce Chiral Compounds. *J. Chem. Technol. Biotechnol*. **2018,** *93*, 498-507.

[49] Moulijn, J.; Stankiewicz, A.; Grievink, J.; Gorak A. Process Intensification and Process Systems Engineering: A Friendly Symbiosis. *Comput. Chem. Eng.* **2008,** *32*; 3–11.

[50] Stankiewicz, A.;Moulijn, J. A. Process Intensification: Transforming Chemical Engineering. *Chem. Eng. Prog.* **2000**, *96*, 22-23.

[51] Holtbrügge, J.; Kunze, A. K.; Niesbach, A.; Schmidt, P.; Schulz, R.; Sudhoff, D.; Skiborowski, M. *Reactive and Membrane-Assisted Separations*. Walter de Gruyter GmbH & Co KG: Berlin, 2016.

[52] Schoenmakers, H.; Bessling, B. Reactive and Catalytic Distillation from an Industrial Perspective. *Chem. Eng. Process.* **2003**, *42*, 145–155.

[53] Kashani, N.; Siegert, M.; Sirch, T. Ein Sandwich zum Destillieren - Die Anstaupackung. *Chem. Ing. Tech.* **2004**, *76*, 929-933.

[54] Von Scala, C.; Wehrli, M.; Gaiser, G. Heat Transfer Measurements and Simulation of Katapak-M Catalyst Supports. *Chem. Eng. Sci.* **1999**, *54*, 1375-1381.

[55] Moulijn, J.A.; Kreutzer, M.T.; Nijhuis, T.A.; Kapteijn, F. Monolithic Catalysts and Reactors: High Precision with low Energy Consumption. *Adv. Catal.* **2011**, *54*, 249-327.

[56] Baerns, M.; Behr, A.; Brehm, A.; Gmehling, J.; Hinrichsen, K.-O.; Hofmann, H.; Palkovits, R.; Onken, U.; Renken, A. *Technische Chemie*. Wiley: Weinheim, 2013.

[57] Antoine, C. Vapor Pressure: a new Relationship Between Pressure and Temperature. C. R. Acad. Sci. **1888**, *107*, 681-684.

[58] McCabe, W. L.; Thiele, E. W. Graphical Design of Fractionating Columns. *Ind. Eng. Chem.* **1925**, *17*, 605-611.

[59] Fenske, M.; Quiggle, D.; Tongberg, C. O. Composition of Straight-run Pennsylvania Gasoline. *Ind. Eng. Chem.* **1932**, *24*, 408-418.

[60] Underwood, A. J. V. Fractional Distillation of Multicomponent Mixtures. *Ind. Eng. Chem.* **1949**, *41*, 2844-2847.

[61] Gilliland, E. R. Multicomponent Rectification Estimation of the Number of Theoretical Plates as a Function of the Reflux Ratio. *Ind. Eng. Chem.* **1940**, *32*, 1220-1223.

[62] Stichlmair, J. *Ullmann's Encyclopedia of industrial Chemistry (Distillation, 1. Fundamentals)* Wiley: Weinheim, 2012.

[63] Raoult, F. M. General Law of the Vapor Pressure of Solvents. *Comptes Rendus* **1887**, *104*, 1430

[64] Ewell, R. H.; Harrison, J. M.; Berg, L. Azeotropic Distillation. *Ind.Eng. Chem.* **1944**, *36*, 871-875.

[65] Lutze, P.; Górak, A. Reactive and Membrane-Assisted Distillation: Recent Developments and Perspective. *Chem. Eng. Res. Des*. **2013**, *91*, 1978-1997.

[66] Chalakova, M.; Kaur, R.; Freund, H.; Mahajani, S. DGMK *Tagungsber.* **2007**, *2*, 133.

[67] Baur, R.; Krishna, R. Hardware Selection and Design Aspects for Reactive Distillation Columns: a Case Study on Synthesis of TAME. *Chem. Eng. Process.* **2002**, *41*, 445-462.

[68] Ciric, A.R. Steady State Multiplicities in an Ethylene Glycol Reactive Distillation Column. *Ind. Eng. Chem. Res.* **1994**, *33*, 2738-2748.

[69] Siirola, J.J. Industrial Applications of chemical process synthesis. *Adv. Chem. Eng.* **1996**, *23*, 1-62.

[70] Terrill, D.L.; Sylvestre, L.F, Doherty, M.F. Separation of Closely Boiling Mixtures by Reactive Distillation. *Ind. Eng. Chem. Process. Des. Dev.***1985**, *24*, 1062-1071.

[71] Sakuth, M.; Reusch, D.; Janowsky, R. *Reactive Distillation. Ullmann's Encyclopedia of Industrial Chemistry*, Wiley: Weinheim, 2000.

[72] Bessling, B.; Löning, J.M.; Ohligschläger, A.; Schembecker, G.; Sundmacher, K. Investigations of the Production of Methyl Acetate by Heterogeneous Reactive Distillation. *Chem. Eng. Technol.* **1998**, *21*, 393–400.

[73] Song, W.; Doherty, M. F Discovery of a Reactive Azeotrope. *Nature* **1997**, *388*, 561–563.

[74] Jacobs, R.; Krishna, R. Multiple Solutions in Reactive Distillation for Methyl Tert-Butyl Ether Synthesis. *Ind. Eng. Chem. Res.* **1993**, *32*, 1706–1709.

[75] Mohl, K.-D.; Kienle, A.; Gilles, E.-D.; Rapmund, P.; Sundmacher, K.; Hoffmann, U. Steady-State Multiplicity in Reactive Distillation Columns for the Production of Fuel Ethers MTBE and TAME: Theoretical Analysis and Experimental Verification. *Chem. Eng. Sci.* **1999**, *54*, 1029–1043.

[76] Cooke, R.; Kuntz, I. D. The Properties of Water in Biological Systems. *Ann. Rev. Biophys. Bioeng.* **1974**, *3*, 95-126.

[77] Wolfenden, R.; Snider, M. J. The Depth of Chemical Time and the Power of Enzymes as Catalysts. *Acc. Chem. Res.* **2001**, *34*, 938-945.

[78] Menger, F. M. Enzyme Reactivity from an Organic Perspective. *Acc. Chem. Res.* **1993**, *26*, 206-212.

[79] Eyring, H. The Activated Complex in Chemical Reactions. *J. Chem. Phys.* **1935**, *3*, 107-115.

[80] Kraut, J. How do Enzymes Work? *Science* **1988**, *242*, 533.

[81] Sweers, H. M.; Wong, C. H. Enzyme-Catalyzed Regioselective Deacylation of Protected Sugars in Carbohydrate Synthesis. *J. Am. Chem. Soc.* **1986**, *108*, 6421-6422.

[82] Faber, K. *Biotransformations in Organic Chemistry: A Textbook*. 6th Edition, Springer: Heidelberg, 2011.

[83] Koshland, D. E. Application of a Theory of Enzyme Specificity to Protein Synthesis. *Proc. Natl. Acad. Sci.* **1958**, *44*(2), 98-104.

[84] Koshland Jr, D. E.; Neet, K. E. The Catalytic and Regulatory Properties of Enzymes. *Annu. Rev. Biochem.* **1968**, *37*(1), 359-411.

[85] Dewar, M. J. New Ideas About Enzyme Reactions. *Enzyme* **1986**, *36*, 8-20.

[86] Warshel, A.; Aqvist, J.; Creighton, S. Enzymes Work by Solvation Substitution Rather Than by Desolvation. *Proc. Natl. Acad. Sci.* **1989**, *86*, 5820-5824.

[87] Unsworth, L. D.; van der Oost, J.; Koutsopoulos, S. Hyperthermophilic Enzymes− Stability, Activity and Implementation Strategies for High Temperature Applications. *FEBS J.* **2007**, *274*, 4044-4056.

[88] Haki, G. D.; Rakshit, S. K. Developments in Industrially Important Thermostable Enzymes: a Review. *Bioresour. Technol.* **2003**, *89*, 17-34.

[89] Mateo, C.; Palomo, J. M.; Fernandez-Lorente, G.; Guisan, J. M.; Fernandez-Lafuente, R. Improvement of Enzyme Activity, Stability and Selectivity via Immobilization Techniques. *Enzyme Microb. Technol.* **2007**, *40*, 1451-1463.

[90] Klibanov, A. M. Asymmetric Transformations Catalyzed by Enzymes in Organic Solvents. *Acc. Chem. Res.* **1990**, *23*, 114-120.

[91] Yung-Chi, C.; Prusoff, W. H. Relationship Between the Inhibition Constant (Ki) and the Concentration of Inhibitor which Causes 50 per cent Inhibition (I50) of an Enzymatic Reaction. *Biochem. Pharmacol.* **1973**, *22*, 3099-3108.

[92] Cleland, W. W. The Kinetics of Enzyme-Catalyzed Reactions with two or more Substrates or Products: II. Inhibition: Nomenclature and Theory. *Biochim. Biophys. Acta* **1963**, *67*, 173-187.

[93] Janes, L. E.; Kazlauskas, R. J. Quick E. A fast Spectrophotometric Method to Measure the Enantioselectivity of Hydrolases. *J. Org. Chem.* **1997**, *62*, 4560-4561.

[94] Logan, S. R. The Origin and Status of the Arrhenius Equation. *J. Chem. Educ.* **1982**, *59*(4), 279.

[95] Wedler, G. *Lehrbuch der Physikalischen Chemie*, Wiley: Weinheim, 1987.

[96] Behr, A.; Agar, D. W.; Jörissen, J. *Einführung in die Technische Chemie.* Spektrum, Akad. Verlag: Heidelberg, 2010.

[97] Le Chatelier, H. L. On a General Expression of the Laws of Chemical Equilibrium *C. R. Acad. Sci.* **1884**, *99*, 786-789.

[98] Straathof, A. J.; Panke, S.; Schmid, A. The Production of Fine Chemicals by Biotransformations. *Curr. Opin. Biotechnol.* **2002**, *13*, 548-556.

[99] Desnuelle, P. The Lipases. *The Enzymes* **1972**, *7*, 575-616.

[100] Macrae, A. R. Lipase-Catalyzed Interesterification of Oils and Fats. *J. Am. Oil Chem. Soc.* **1983**, *60*, 291-294.

[101] Nielsen, T. Industrial Application Possibilities for Lipase. *Eur. J. Lipid Sci. Technol.* **1985**, *87*, 15-19.

[102] Aravindan, R.; Anbumathi, P.; Viruthagiri, T. Lipase Applications in Food Industry. *Indian J. Biotechnol.* **2007**, 141-158.

[103] Jaeger, K. E.; Reetz, M. T. Microbial Lipases form Versatile Tools for Biotechnology. *Trends Biotechnol.* **1998**, *16*, 396-403.

[104] Schmid, R. D.; Verger, R. Lipases: Interfacial Enzymes with Attractive Applications. *Ang. Chem. Int. Ed.* **1998**, *37*, 1608-1633.

[105] Solano, D. M.; Hoyos, P.; Hernáiz, M. J.; Alcántara, A. R.;Sánchez-Montero, J. M. Industrial Biotransformations in the Synthesis of Building Blocks Leading to Enantiopure Drugs. *Bioresour. Technol.* **2012**, *115*, 196-207.

[106] Uppenberg, J.; Patkar, S.; Bergfors, T.; Jones, T. A. Crystallization and Preliminary X-ray Studies of Lipase B from Candida Antarctica. *J. Mol. Biol.* **1994**, *235*, 790-792.

[107] De Zoete, M. C.; Van Rantwijk, F.; Sheldon, R. A. Lipase-Catalyzed Transformations with Unnatural Acyl Acceptors. *Catal. Today* **1994**, *22*, 563-590.

[108] Anderson, E. M.; Larsson, K. M.; Kirk, O. One Biocatalyst–Many Applications: the use of Candida Antarctica B-Lipase in Organic Synthesis. *Biocatal. Biotransform.* **1998**, *16*, 181-204.

[109] Kirk, O.; Christensen, M. W. Lipases from Candida Antarctica: Unique Biocatalysts from a Unique Origin. *Org. Process Res. Dev.* **2002**, *6*, 446-451.

[110] Martinelle, M.; Hult, K. Kinetics of Acyl Transfer Reactions in Organic Media Catalysed by Candida Antarctica Lipase B. *Biochim. Biophys. Acta* **1995**, *1251*, 191-197.

[111] Verger, R. Interfacial Activation of Lipases: Facts and Artifacts. *Trends Biotechnol.* **1997**, *15*, 32-38.

[112] Hilterhaus, L.; Thum, O.; Liese, A. Reactor Concept for Lipase-Catalyzed Solvent-Free Conversion of Highly Viscous Reactants Forming Two-Phase Systems. *Org. Process Res. Dev.* **2008**, *12*, 618-625.

[113] Santos, J. C.; Bueno, T.; Molgero, P. C.; Rós, D.; de Castro, H. F. Lipase-Catalyzed Synthesis of Butyl Esters by Direct Esterification in Solvent-Free System. *J. Chem. Technol. Biotechnol.* **2007**, *82*, 956-961.

[114] Kagan, H. B.; Fiaud, J. C. Kinetic Resolution. *Top. Stereochem.* **1988**, *18*, 21.

[115] Chen, C. S.; Fujimoto, Y.; Girdaukas, G.; Sih, C. J. Quantitative Analyses of Biochemical Kinetic Resolutions of Enantiomers. *J. Am. Chem. Soc.* **1982,** *104*, 7294–7299.

[116] Chen, C. S.; Wu, S. H.; Girdaukas, G.; Sih, C. J. Quantitative Analyses of Biochemical Kinetic Resolution of Enantiomers. 2. Enzyme-Catalyzed Esterifications in Water-Organic Solvent Biphasic Systems. *J. Am. Chem. Soc.* **1987**, *109*, 2812-2817.

[117] Pellissier, H. Recent Developments in Dynamic Kinetic Resolution. *Tetrahedron* **2011**, *67*, 3769-3802.

[118] Dinh, P. M.; Howarth, J. A.; Hudnott, A. R.; Williams, J. M.; Harris, W. Catalytic Racemisation of Alcohols: Applications to Enzymatic Resolution Reactions. *Tetrahedron Lett.* **1996**, *37*, 7623-7626.

[119] Larsson, A. L.; Persson, B. A.; Bäckvall, J. E. Enzymatic Resolution of Alcohols Coupled with Ruthenium-Catalyzed Racemization of the Substrate Alcohol. *Ang. Chem. Int. Ed.* **1997**, *36*, 1211-1212.

[120] Persson, B. A.; Larsson, A. L.; Le Ray, M.; Bäckvall, J. E. Ruthenium-and Enzyme-Catalyzed Dynamic Kinetic Resolution of Secondary Alcohols. *J. Am. Chem. Soc.* **1999**, *121*, 1645-1650.

[121] Koh, J. H.; Jeong, H. M.; Park, J. Efficient Catalytic Racemization of Secondary Alcohols. *Tetrahedron Lett.* **1998**, *39*, 5545-5548.

[122] Martín-Matute, B.; Bäckvall, J. E. Dynamic Kinetic Resolution Catalyzed by Enzymes and Metals. *Curr. Opin. Chem. Biol.* **2007**, *11*, 226-232.

[123] Menashe, N.; Shvo, Y. Catalytic Disproportionation of Aldehydes with Ruthenium Complexes. *Organometallics* **1991**, *10*, 3885-3891.

[124] Bogár, K.; Martín-Matute, B.; Bäckvall, J. E. Large-Scale Ruthenium-and Enzyme-Catalyzed Dynamic Kinetic Resolution of (rac)-1-Phenylethanol. *Beilstein J. Org. Chem.* **2007**, *3*, 50.

[125] Choi, J. H.; Kim, Y. H.; Nam, S. H.; Shin, S. T.; Kim, M. J.; Park, J. Aminocyclopentadienyl Ruthenium Chloride: Catalytic Racemization and Dynamic Kinetic Resolution of Alcohols at Ambient Temperature. *Ang. Chem.* **2002**, *114*, 2479-2482.

[126] Choi, J. H.; Choi, Y. K.; Kim, Y. H.; Park, E. S.; Kim, E. J.; Kim, M. J.; Park, J. Aminocyclopentadienyl Ruthenium Complexes as Racemization Catalysts for Dynamic Kinetic Resolution of Secondary Alcohols at Ambient Temperature. *J. Org. Chem.* **2004**, *69*, 1972-1977.

[127] Martín-Matute, B.; Edin, M.; Bogár, K.; Kaynak, F. B.; Bäckvall, J. E. Combined Ruthenium (II) and Lipase Catalysis for Efficient Dynamic Kinetic Resolution of Secondary Alcohols. Insight into the Racemization Mechanism. *J. Am. Chem. Soc.* **2005**, *127*, 8817-8825.

[128] Martín-Matute, B.; Edin, M.; Bogár, K.; Bäckvall, J. E. Highly Compatible Metal and Enzyme Catalysts for Efficient Dynamic Kinetic Resolution of Alcohols at Ambient Temperature. *Ang. Chem. Int. Ed.* **2004**, *43*, 6535-6539.

[129] Gustafson, K. P.; Guðmundsson, A.; Lewis, K.; Bäckvall, J. E. Chemoenzymatic Dynamic Kinetic Resolution of Secondary Alcohols Using an Air-and Moisture-Stable Iron Racemization Catalyst. *Chem. – Eur. J.* **2017**, *23*, 1048-1051.

[130] Shelden, R.; Stringaro, J.-P. Vorrichtung zur Durchführung Katalysierter Reaktionen. EP 0396650B1, 1995.

[131] Smirnova, I.; Fieg, G.; Hilterhaus, L.; Liese, A.; Bubenheim, P.; Sont, A. Ein in der Reaktivrektifikation einsetzbarer, einen Biokatalysator Aufweisende Kolonneneinbau und dessen Verwendung in der Reaktivrektifikation. DE 10 2010 028 788 A1, May 10, 2010.

[132] Reetz, M. T.; Zonta, A.; Simpelkamp, J. Efficient Immobilization of Lipases by Entrapment in Hydrophobic Sol-Gel Materials. *Biotechnol. Bioeng.* **1996**, *49*, 527-534.

[133] Reetz, M. T.; Zonta, A.; Simpelkamp, J.; Rufinska, A.; Tesche, B. Characterization of Hydrophobic Sol-Gel Materials Containing Entrapped Lipases. *J. Sol-Gel Sci. Technol.* **1996**, *7*, 35-43.

[134] Aferka, S.; Crine, M.; Saroha, A. K.; Toye, D.; Marchot, P. In situ Measurements of the Static Liquid Holdup in Katapak-SP12TM Packed Column Using X-ray Tomography. *Chem. Eng. Sci.* **2007**, *62*, 6076-6080.

[135] Bradford, M. M. A Rapid and Sensitive Method for the Quantitation of Microgram Quantities of Protein Utilizing the Principle of Protein-Dye Binding. *Anal. Biochem.* **1976,** *72*, 248-254.

[136] Knapp, Daniel R. *Handbook of analytical derivatization reactions*. John Wiley & Sons, 1979.

[137] Kühn, S.; Sluyter, G.; Christlieb, M. A.; Heils, R.; Stöbener, A.; Kleber, J.; Smirnova, I.; Liese, A. In Situ Separation of the Chiral Target Compound (S)-2-Pentanol in Biocatalytic Reactive Distillation. *Ind. Eng. Chem. Res.* **2017**, *56*(22), 6451-6461.

[138] Wilhoit, R.C.; Zwolinski, B.J. Physical and Thermodynamic Properties of Aliphatic Alcohols, *J. Phys. Chem. Ref. Data Suppl*. **1973**.

[139] Stephenson, R. M.; Malanowski, S.; *Handbook of the Thermodynamics of Organic Compounds*, Elsevier Science: New York, 1987.

[140] Brown, R. L.; Stein, S. E., Boiling Point Data. In NIST Chemistry WebBook, NIST Standard Reference Database Number 69; Linstrom, P. J., Mallard, W. G., Eds.; Gaithersburg, MD (accessed Feb 10, 2017)

[141] Fishman, A.; Eroshov, M.; Sheffer Dee-Noor, S.; Van Mil, J.; Cogan, U.; Effenberger, R. A Two-Step Enzymatic Resolution Process for Large-Scale Production of (S)-and (R)-Ethyl-3-Hydroxybutyrate. *Biotechnol. Bioeng.* **2001**, *74*, 256-263.

[142] Polling, B. E.; Prausnitz, J. M.; O'Connell, J. P. *The properties of gases and liquids.* McGraw-Hill: New York. 2001.

[143] Sigma Aldrich: Ethyl (S)-3-Hydroxybutyrate (accessed Feb 26, 2018)

[144] Thomas, L. H.; Meatyard, R. Viscosity and Molecular Association. Part IV. Association of Monohydric Alcohols and some Hindered Phenols. *J. Chem. Soc.* **1963,** 1986-1995.

[145] Schumann, O. Over Vapor Tension of Homologous Esters. *Ann. Phys.* **1881,** *12*, 40–65.

[146] Ambrose, D.; Sprake, C. H. S. Thermodynamic Properties of Organic Oxygen Compounds XXV. Vapour Pressures and Normal Boiling Temperatures of Aliphatic Alcohols. *J. Chem. Thermodyn.* **1970**, *2*, 631-645.

[147] Kretschmer, C. B.; Wiebe, R. Liquid-Vapor Equilibrium of Ethanol--Toluene Solutions. *J. Am. Chem. Soc.* **1949**, *71*, 1793-1797.

[148] Stull, D. R. Vapor Pressure of Pure Substances. Organic and Inorganic Compounds. *Ind. Eng. Chem.* **1947,** *39*, 517–540.

[149] Weast, R. C.; Grasselli, J. G. *Handbook of Data on Organic Compounds*, CRC Press: Boca Raton, Fla, 1989.

[150] Kemme, H. R.; Kreps, S. I. Vapor Pressure of Primary n-Alkyl Chlorides and Alcohols. *J. Chem. Eng. Data* **1969**, *14*, 98-102.

[151] González, C.; Ortega, J.; Hernández, P.; Galván, S. Experimental Determination of Densities and Isobaric Vapor−Liquid Equilibria of Binary Mixtures Formed by a Propyl Alkanoate (Methanoate to Butanoate) + An Alkan-2-ol (C 3 , C 4). *J. Chem. Eng. Data* **1999,** *44*, 772–783.

[152] Ortega, J.; Galvan, S. Vapor-Liquid Equilibria and Densities for Propyl Butanoate + Normal Alcohols at 101.32 kPa. *J. Chem. Eng. Data* **1995,** *40*, 699–703.

[153] Abrams, D. S.; Prausnitz, J. M. Statistical Thermodynamics of Liquid Mixtures: A new Expression for the Excess Gibbs Energy of Partly or Completely Miscible Systems. *AIChE J.* **1975,** *21*, 116–128.

[154] Weidlich, U., Gmehling, J. A Modified UNIFAC Model. 1. Prediction of VLE, hE, and. Gamma. Infin. *Ind. Eng. Chem. Res.* **1987,** *26*, 1372–1381.

[155] Orrenius, C.; Hbffner, F.; Rotticci, D.; Öhrner, N.; Norin, T.; Hult, K. Chiral Recognition of Alcohol Enantiomers in Acyl Transfer Reactions Catalysed by Candida Antarctica Lipase B. *Biocatal. Biotransform.* **1998**, *16*, 1-15.

[156] Chemtech, S. *Structured Packings for Distillation, Absorption and Reactive Distillation*. Switzerland: Winterthur, 2003.

[157] Montz, *High Performance Structured Packing* (accessed Feb 26, 2018).

[158] Sigma Aldrich: (R/S)-2-PeOH, NZ435 (accessed August 29, 2017).

[159] Mavrynsky, D.; Leino, R. An Approach to Chemoenzymatic DKR of Amines in Soxhlet Apparatus. *J. Organomet. Chem.* **2014**, *760*, 161-166.

[160] Collerson, R.R.; Counsell, J.F.; Handley, R.; Martin, J.F.; Sprake, C.H.S., Thermodynamic Properties of Organic Oxygen Compounds. Part XV. Purification and Vapour Pressures of Some Ketones and Ethers, *J. Chem. Soc.* **1965**, 3697-3700.

[161] Osborn, A. G.; Douslin, D. R. Vapor-Pressure Relations for 15 Hydrocarbons. *J. Chem. Eng. Data* **1974**, *19*, 114-117.

[162] Thorson, M. K.; Klinkel, K. L.; Wang, J.; Williams, T. J. Mechanism of Hydride Abstraction by Cyclopentadienone-Ligated Carbonylmetal Complexes (M= Ru, Fe). *Eur. J. Inorg. Chem.* **2009**, *2*, 295-302.

LEBENSLAUF

Persönliche Daten:

Name:	Kühn
Vorname:	Steffen
Staatsangehörigkeit:	deutsch
Geburtsdatum:	22.06.1987
Geburtsort, -land:	Marburg (Lahn), Deutschland

Ausbildungsdaten:

07/1997 – 06/2006:	Gymnasium Martin-Luther-Schule, Marburg (Lahn)
09/2006 – 07/2007:	Zivildienst, DRK Rettungsdienst Mittelhessen gemeinnützige GmbH, Marburg (Lahn)
10/2007 – 03/2012:	Studium an der Technischen Universität Dortmund Abschluss: Bachelor
04/2012 – 11/2013:	Studium an der Technischen Universität Dortmund Abschluss: Master
05/2014 – 09/2017:	Wissenschaftlicher Mitarbeiter an der Technischen Universität Hamburg am Institut für Technische Biokatalyse
03/2018 – 07/2018:	Wissenschaftlicher Mitarbeiter an der Technischen Universität Hamburg am Institut für Technische Biokatalyse
ab 08/2018:	Prozessingenieur bei Evonik in Hanau Abteilung: Bioprocess Technology, Bereich: Technology & Infrastructure